OPTICAL TECHNOLOGY
APOLLO EXTENSION SYSTEM
PART I

FINAL TECHNICAL REPORT

VOLUME I
(1of 2)

Section 1 - Introduction

Section 2 - Experiment Development

CONTRACT NAS 8-20256

SPACE DIVISION CHRYSLER CORPORATION

OPTICAL TECHNOLOGY
APOLLO EXTENSION SYSTEM
PART I

FINAL TECHNICAL REPORT

VOLUME I
(1 OF 2)

Section 1 - INTRODUCTION

Section 2 - EXPERIMENT DEVELOPMENT

CONTRACT NAS 8-20256
October 21, 1966

Approved by: William W Kloepfer
William W. Kloepfer
Program Manager

CHRYSLER CORPORATION SPACE DIVISION, MICHOUD ASSEMBLY FACILITY
P. O. BOX 29200, NEW ORLEANS, LA. 70129

2857A-10-21-66

PREFACE

The final report of the Optical Technology Apollo Extension System prepared for NASA/Marshall Space Flight Center under Contract Number NAS8-20256 is presented in three volumes. The study was a team effort by Chrysler Corporation Space Division (prime contractor), Kollsman Instrument Corporation, and Sylvania Electronics Systems.

Volume I contains the introduction, the proposed optical technology experiments, and the discarded experiments. CCSD was responsible for the following experiments:

- 4.13 Comparison of Isolation Techniques.
- 4.14 Interferometer System.
- 4.15 Segmented Optics.

CCSD discarded experiments:

- 5.1 Spectrograph Development.
- 5.2 Baffle Systems Comparison.
- 5.7 Cyrogenic Cooling.
- 5.8 Photo-Electro-Optical Experiment.
- 5.9 Mirror Coating.

SES was responsible for the following experiments:

- 4.1 Optical Heterodyne Detection on Earth.
- 4.2 Optical Heterodyne Detection on the Spacecraft.
- 4.3 Direct Detection Space to Ground.
- 4.4 Communication with 10 Megahertz Bandwidth.
- 4.8 Phase Correlation Measurements.
- 4.9 Pulse Distortions Measurements.

SES discarded experiments:

- 5.3 Atmospheric Absorption Spectroscopy.
- 5.4 Photon-Photon Scattering.

KIC was responsible for the following experiments:

- 4.5 Precision Tracking of a Ground Beacon.
- 4.6 Point Ahead and Space-to-Ground-to-Space Loop Closure.
- 4.7 Transfer Tracking from One Ground Station to Another.
- 4.10 Primary Mirror Figure Test and Correction.
- 4.11 Thin Mirror Nesting Principle and Erection and Alignment of Large Optics in Space.
- 4.12 Fine Guidance.

KIC discarded experiments:

5.5 Remote Manual Optical Alignment.
5.6 Visual Tracking Rating.

Volume II contains systems integration. CCSD prepared the sections on Experiment Grouping (7.0), OTAES Mission Development (10.0) except for Ground Stations Concepts (10.4) which was an SES effort, Supporting Spacecraft Subsystems (11.0), Experiment/Mission Time Phasing (12.0), and Typical OTAES Subsystem Component Summary (13.0). The section on the Stellar Oriented Experiment Group was prepared by CCSD and KIC. The section on the Optical Communication Experiment Group was prepared by SES (8.0 and 8.1) and KIC (8.2, 8.3 and 8.4). Volume III containing the Technology Development Plan was the responsibility of CCSD. Study recommendations appear in the separate summary volume.

The OTAES team gratefully acknowledges the help given by the NASA Ad Hoc working group during the course of this study.

MASTER

TABLE OF CONTENTS

Volume	Title
I	Section I - Introduction Section II - Experiment Development
II	Section III - Systems Integration
III	Section IV - Technology Development Plan

VOLUME I (1 of 2)*

TABLE OF CONTENTS

Section	Title	Page
I	INTRODUCTION	1-1
	1.0 Purpose	1-1
	2.0 Technical Approach	1-1
	3.0 Projected Optical Technology Needs	1-3
	3.1 Astronomy	1-3
	3.2 Meteorology	1-18
	3.3 Earth Remote Sensing	1-22
	3.4 Communication	1-31
	3.5 Commonality of Technology Needs	1-36
II	EXPERIMENTS	1-38
	4.0 Proposed OTAES Experiments	1-38
	4.1 Optical Heterodyne Detection on Earth	1-38
	4.2 Optical Heterodyne Detection on Spacecraft	1-123
	4.3 Direct Detection Space to Ground	1-135
	4.4 Communication with 10 Megahertz Bandwidth	1-201
	4.5 Precision Tracking of a Ground Beacon	1-221
	4.6 Point Ahead and Space-To-Ground-To-Space Loop Closure	1-249
	4.7 Transfer Tracking from One Ground Station to Another	1-282

***See Volume I (2 of 2) for Paragraphs 4.8 through 6.0.**

SECTION I

INTRODUCTION

1.0 PURPOSE

Success in future NASA space missions depends on technological development today. This implies the need for well planned research and development programs. Such programs need to have a broad scope because (a) although some of the problems are completely identified, more are only partially defined and most are probably not yet even known, (b) as technology advances, new problems are uncovered that require research.

The OPTICAL TECHNOLOGY APOLLO EXTENSION SYSTEM is one technological program. The purpose of OTAES is to identify the problems in the field of optical technology and develop alternative solutions in terms of development programs and space experiments. To achieve this, first the necessary technological requirements associated with the NASA objectives have to be identified. Then these requirements are compared to the technology state of the art. The gaps between the state of the art and the technological requirements dictate the problem areas that must be researched. Some of the alternative approaches to the problems can be finally evaluated on the ground; but to achieve complete evaluation for some of the solutions, the ground development program must culminate in space testing. To this end the OTAES study proposes a series of experiments to be performed in space. The successful completion of these experiments will make it possible to develop technology further and will give NASA a greater understanding of, and a wide range of solutions to some of the problems of space optics.

2.0 TECHNICAL APPROACH

The technical approach of this study proceeds logically step by step starting with future NASA objectives and ending with a development plan which, if followed, will lead to the ability to achieve these objectives.

The steps are:

a. Determine and document future NASA objectives in the application areas of astronomy, meteorology, earth remote sensing and communications. Scientific articles and industrial reports were the sources for the objectives. (This material appears in Vol I. section, 3.0)
b. Determine if it is possible to satisfy the objectives with present instruments. If it is not possible, determine the areas where optical technology development is required to improve present instruments or create new instruments which will satisfy the objectives. (This material appears in Vol I., section 5.0)
c. Develop space experiments which, if successful, will advance optical technology. (This material appears in Vol. I, section 4.0)

Justify each experiment on its own merits in terms of:

(1) Contribution and Need.
(2) Need for Space Testing.
(3) Feasibility.

Some experiments were considered and it was determined that they did not require space testing. However they are still important to the development of optical technology. The ground development program of these experiments and the reasons why they do not require space testing are discussed. (This material appears in Vol. I, section 5.0)

d. Consider possible future OTAES experiments, which were not extensively studied for this phase of the study. (This material appears in Vol. I, section 6.0)

e. Justifying each OTAES experiment in terms of feasibility implies a study of the experiment subsystems. This includes:

(1) Optical subsystems.
(2) Control subsystems.
(3) Laser subsystems.

(This material appears in Vol. II, sections 7.0, 8.0 and 9.0)

f. Consider each experiment in context with the other experiments and the entire OTAES system, for example, thermal control and power. This leads to evaluation of different means of operation and recommendation of preferred systems. (This material appears in Vol. II, sections 10.0, 11.0, 12.0 and 13.0)

g. The final step is the development of an overall technology plan which will start at the present day and end when the technology level satisfies the objectives of step a. Included in the plan are key development milestones in the earth based program, schedules for each individual experiment and master plan alternatives for overall OTAES. (This material appears in Vol. III)

3.0 PROJECTED OPTICAL TECHNOLOGY NEEDS

The beginning of a development program is the recognition of the technology needs. The needs may be identified only by considering future NASA applications. The beginning of this OTAES study was therefore directed toward considering future NASA applications. Four application areas were considered: astronomy, meteorology, earth remote sensing and interplanetary missions. Each application area was considered, first in terms of observational objectives and second in terms of technological needs to satisfy these objectives.

3.1 ASTRONOMY

"But it does move". Galileo said to himself after recanting his theory that the earth moves around the sun. Galileo was an empiricist. He had a theory and he tested it. He saw the moons of Jupiter move, he saw the phases of Venus, and knew that the Earth with its moon was not the center of the universe. For centuries before, men had looked at the stars, wondered, and then constructed vast theories far beyond the range of what they saw. They were disciples of Aristotle. Philosophy was the measure of truth and all speculations about the universe were judged by their philosophical coherence. But with Galileo and his telescope it became possible to verify a theory through observations. Astronomy was no longer speculation by itself.

Today the matching of theory to observation is the measure of acceptance, but speculation is still far ahead of observation. There are still vast theories that need to be tested. Observations are made and data collected but the quality of information is never quite good enough to prove one theory at the expense of another. Technology tries to keep pace by creating more advanced telescopes and instrumentation, but as the theories became more sophisticated, the atmosphere increasingly frustrated the attempts to verify the theories. Much information that the astronomer needs is contained in the parts of the spectrum blocked by the atmosphere. The information he needs is in the stars so distant that they are too faint to be seen without going beyond the Earth's sky fog and in the stars and galaxies packed so close together that the turbulence of the atmosphere prevents their resolution.

An astronomer and his telescope above the atmosphere -- this is a change in kind as radical as that when Galileo first saw the moons of Jupiter.

3.1.1 Observational Objectives

The end goal of astronomy is a constant. It is to understand the history of the universe -- what was in the beginning, the mechanism of evolution, and what will happen in the future. What is the stuff that stars are made of? And what is the dynamics of their change? With space astronomy the answers come closer.

Astronomers, fascinated by the potential of space, have been preparing for space astronomy long before the potential was close to becoming a reality. Leo Goldberg(1) says that his first encounter with space astronomy was in 1937 at the Harvard College Observatory when M. N. Saha described the advantages of solar observations from space. In articles over the years, astronomers have looked ahead and developed their ideas on what could be done with telescopes in space. Some of their ideas for observations are presented in tables 3.1.1-1. The list of observations is not intended to be or serve as a guide for an observational program but is intended to serve as a basis for indicating the technology needs of the coming space years. For each observation there is one or more figures of merit that characterize the observation. These are called performance parameters. As an example take the observation of the profile of the Lyman α absorption line of interstellar hydrogen.(2) The performance parameters for this observation are wavelength, spectral resolution and spatial resolution.(3) Each of the performance parameters has a value or value range necessary to complete the particular observation. Using the same example; the wavelength of the Lyman α absorption line is 1216 Å, the spectral resolution needed to obtain a good profile is 10^5 $(\lambda/\Delta\lambda)$ and the necessary spatial resolution is .1 arc seconds.(4)

The observations have been compiled from various scientific articles and industrial reports, and arranged into a chart by source. For each source there is the list of observations, extrapolated from the text, that the author considered important for space astronomy. For each observation the attendant performance parameters with their value range are listed, also as stated by the author. The chart is not complete. For some of the observations, there are no performance parameters or values; since the authors' intention was not necessarily the same as ours i.e., the neat lineup of observation, performance parameters and value range.

---

(1) Leo Goldberg, "The New Astronomies", International Science and Technology, pp. 18-28, August 1965.
(2) Orl Experiment Program, Volume B, Part XI. Astronomy/Astrophysics, p. 16-21, Feb. 1966, Federal System Division, International Business Machines Corp., Rockville, Maryland.
(3) Ibid.
(4) Ibid.

TABLE 3.1.1-1

ASTRONOMICAL OBSERVATION REQUIREMENTS

SOURCE: Applications in Astronomy Suitable for Study by means of Manned Orbiting Observations & Related Instrumentation & Operational Requirements, Edited by Lawrence W. Frederick NASA Grant No. NSG-480, Oct. 1963.

OBSERVATION	PERFORMANCE PARAMETER	VALUE RANGE
A size and shape catalog of faint galaxies.		
Resolution of binaries for determination of stellar mass.	Limiting magnitude Spatial resolution Wavelength	2000Å - 5000Å
Photometry of nebulae.	Wavelength Spatial resolution	1 sec of arc
High resolution photography and spectroscopy for study of planets, visual binaries and galactic structures.	Spatial resolution Wavelength	
Study of very cool stars with maximum radiation in IR, study of galactic nebulae and study of radio sources in IR.	Wavelength	1,1.5,3.5 microns
Measurement of stellar diameters.	Spatial resolution Wavelength	
Polarization studies-emission nebulae and interstellar dust. Investigation of Paschen Alpha Line, Cometary, Planetary and asteroidal polarmetry.	Spatial resolution Wavelength	Visual and IR especially, extended to UV
Search for small stellar companions with use of apodizer.	Spatial resolution Wavelength	

TABLE 3.1.1-1 (cont.)

SOURCE: "Stellar Astronomy from a Space Vehicle", Arthur D. Code, Washburn Observatory, University of Wisconsin, March 1960.

OBSERVATION	PERFORMANCE PARAMETERS	VALUE RANGE
Ultraviolet and Infrared survey studies.	Wavelength	1Å to 2700Å, infrared wavelengths
Stellar Energy Distribution	Wavelength	UV-beyond 504Å
	Photometric precision	Perhaps to 10 Å
Stellar Spectroscopy		
a. UV	Wavelength	3000Å to 1200Å
	Spectral resolution	better than 30A
b. X-ray	Wavelength	
	Spectral resolution	
c. Infrared	Wavelength	Absorption line of H_2O and CO_2
Photometry of Interstellar Medium Radiation	Spectral resolution	Better than 7Å
	Wavelength	to 30μ for UV
Photometry of extra-galactic nebulae.	Wavelength	Lyman α, x-rays, 1213Å, RF
High resolution studies of:		
a. Sub dwarfs	System resolution	Very high
b. White dwarfs	Wavelength	
c. SS Cygni stars	Limiting magnitude	Very high
Spectrophotometry reconnaisance		
Spectroscopy of bright stars for stellar and interstellar line profiles.	Spectral resolution	Very high
Spectrophotometry of diffuse and planetary nebulae for stellar energy distribution & emulsion line intensities	Spectral resolution	Very low

TABLE 3.1.1-1 (cont.)

SOURCE: A System Study of a Manned Orbital Telescope, Oct. 1965, Aerospace Group, The Boeing Co., Seattle, Washington.

OBSERVATION	PERFORMANCE PARAMETER	VALUE RANGE
Detection of quasars (Photometric)	Wavelength Limiting Magnitude	912-8000Å 28
High resolution studies of galaxies and nebulae (Photographic)	Limiting Magnitude Field of View Wavelength Spatial Resolution Spectral Resolution Guiding Accuracy Exposure time	22 ≈1 min 3000Å-8000Å 0.07 arc sec 2 Å 0.01 arc sec Up to 30 min
High resolution studies of galaxies and nebulae (Spectroscopic)	Wavelength Limiting Magnitude Exposure Time Guiding Accuracy Spectral Resolution	912Å - 3μ 16 800 min (max) 400 min (average) 0.01 - 0.02 arc sec 0.1Å
High resolution studies of galaxies and nebulae (photometric)	Wavelength Limiting Magnitude Exposure time	912Å - 3μ 27 800 minutes

SOURCE: Guido Munch, Mt. Wilson & Palomar Observatories, Missiles and Rockets, April 25, 1966.

To find the dimensions to quasi-stellar sources	Diffraction limited field of view Spatial resolution	20 arc sec 0.03 arc sec
To find the structure of nuclei of galaxies		
To resolve galaxies into stars to refine the distance scale.		
To study the faint end of population of clusters of galaxies and stars.		

TABLE 3.1.1-1 (cont.)

SOURCE: ORL Experiment Program, Vol. B, Part XI, Astronomy/Astrophysics, Feb. 1966.

OBSERVATION	PERFORMANCE PARAMETER	VALUE RANGE
Profile of the Lyman α absorption line of interstellar hydrogen (to find distibution of interstellar hydrogen- important to study of galactic structure)	Wavelength Spectral resolution Spatial resolution	1216Å 10^5 0.1 arc sec
Spectra and photographs in UV and visible of early type stars for stellar and planetary systems evolution.	Spatial resolution Spectral resolution Wavelength	10^{-3} - 10^{-5} 10^5 } 10^3 0.01A-3mu } 0.01-100m
Observe UV & IR of stars classified spectrally, map globular clusters to find UV & IR emission, then high resolution. To improve H-R diagram of globular clusters to find their evolutionary path. (Spectroscopic & Photometric)	Wavelength Spectral resolution Spatial resolution	.9mu - 3 mu 10^5 0.1 arc sec
UV spectra of stars. For better theoretical stellar models, extend H-R diagram, determine cosmic abundances. To understand cosmic processes. Will get improved values for total fluxes and profiles and equivalent widths of resonance lines in UV.	Wavelength Spectral resolution Spatial resolution	0.01Å - 15mu 10^4 0.1 arc sec
SOURCE: L. Goldberg, "Stellar and Interstellar Observations", Space Age Astronomy, 1962.		
Search for infrared sources.	Wavelength	0.7 to 30μ
Infrared interferometry		
Ultraviolet map of celestral sphere.	Field of view	5 to 6 degrees
Distribution, brightness size and red shifts of external galaxies	Limiting Magnitude	

TABLE 3.1.1-1 (cont.)

SOURCE: F. Zwickey, Space Age Astronomy, p. 234, 1962.

OBSERVATION	PERFORMANCE PARAMETERS	VALUE RANGE
Resolution of galactic nuclei	Wavelength Spatial resolution	10 <1000Å 0.1 arc sec

SOURCE: P. Swings, "Current Objectives of Astronomical Space Research", Space Age Astronomy.

Composition of interstellar gas; resonance absorption line of H, C, N, O, Mg & Fe	Wavelength	Down to 1008Å
High dispersion UV studies.	Spectral resolution Wavelength	0.2Å 913-3000Å
Composition of interstellar matter; infrared spectroscopy of radicals such as CH, NH, OH, CN, CH+	Wavelength	2.4μ to 85μ
Infrared Interferometry		
Observation of solar K & F Corona		
Search for stellar x-ray sources		

SOURCE: European Space Research Organization, "Report of the Working Group on the Large Astronomical Satellite", 1964.

1) Studies of stars in galactic clusters, distribution of interstellar matter in clusters.	Mean Resolution Fine pointing Wavelength	2' arc Few seconds arc 950-1050, 1300-1500, 1800-2200, 2330-2830, 2950-3050
2) Measurement of variable stars with very narrow bands (flare stars)	Color indices accuracy Limiting magnitude Time	± 0.03 10 2 minutes

TABLE 3.1.1-1 (cont.)

OBSERVATION	PERFORMANCE PARAMETERS	VALUE RANGE
3) Measurement of intense reddening produced by interstellar matter. (Stellar Photometry of Faint Stars)	Grating ruling	600-1200 l/mm
High resolution UV spectra of early type stars for information on stellar motion and rotation of galaxy. High resolution studies of brightest of other type stars. Interstellar lines and bands.	Spectral resolution Time Limiting magnitude	1Å 5 sec 6
Spectra of less bright stars and nebulae to extend knowledge of conventional spectral types and absolute luminosity classes; better data on chemical composition. More precise concept of population types.	Spectral resolution Time Limiting magnitude Bandwidth Limiting magnitude	10Å 50 sec 9 100Å 16
X-ray astronomy information on stellar, glactic, and extragalactic regions, orgin of high energy quanta and particles in space.	Wavelength Pointing accuracy Time	10Å 1 min arc hours
SOURCE: Report on the Optimization of the Manned Orbital Research Laboratory (MORL) System Concept, Vol. XXII, Douglas Aircraft Company, Inc. 1964.		
(Data Samples to be returned to Earth) 1. Stellar Spectra (emission) 2. Nebular Spectra (emission) 3. Stellar Spectra (absorption) 4. Planetary Albedos 5. Planetary Photographs 6. Earth Albedo 7. Earth Photographs 8. Sky Backgrounds	Spectral range Spectral resolution Wavelength Spatial resolution Fine Guidance accuracy Drift rate Grating resolving power Exposure (Single Scan)	1,000-10,000A 0.2Å 5,000Å 0.1125 arc sec 0.1 arc sec 0.07 sec/min 250,000 ≈10 min (≈ 1 hr)

TABLE 3.1.1-1 (cont.)

OBSERVATION	PERFORMANCE PARAMETERS	VALUE RANGE
To provide basic directional and spectral information concerning cosmis rays solar flare phenomena, galactic rays and neutron flux distribution	Electron Energy band Ray energy band Photon energy band	0.3-20 Mev 20 Mev 0.02-0.25, 0.25-1 1 Mev 8-16, 16-36, 36-90, 90-240 240 Mev
a. Charged particles & low energy α rays	Particles energy band Guiding accuracy	32-64, 64-150 150-360, 360-960 960 Mev 1°
b. High energy α rays	α ray energy band Guiding accuracy	100-1,000 Mev 1°
c. Neutrons	Guiding accuracy	1°
Study of Sun's corona	Aperture Exposure time Pointing accuracy Scattered light Solar radii	1.3 in 2 hrs 5 arc sec 10^{-9} 6
Stellar, planetary and solar observations in the vacuum UV and soft x-ray portion of the spectra.	Wavelength Guiding Accuracy	500-1200Å 0.1 arc sec

SOURCE: "Tasks for the Manned Orbital Telescope", Zdenek Kopal, Astronautics and Aeronautics, Dec. 1965.

1) Measurement of Stellar parallaxes and proper motions 2) Detection of stellar objects of masses less than .1 (Binary) 3) Measuring displacement of binary components, establishing elements of orbit, combined with parallax to determine absolute masses would extend mass-luminosity relation to very faint stars. 4) Photograph center of dense clusters to determine distribution of stars, relates to stellar masses to understand cluster dynamics (Narrow-field photography)	Field of view Exposure time Limiting magnitude Exposure time Limiting magnitude Spatial resolution	< 10' 40 min 22.5 400 min 23.8 0.06 arc sec

TABLE 3.1.1-1 (cont.)

OBSERVATION	PERFORMANCE PARAMETERS	VALUE RANGE
1) Search for faint but very hot stars (super nova remnants, blue subdwarfs or white dwarfs) 2) Search for nascent cool stars in IR (hayashi objects) 3) Search for extended nebular emissions in specific spectral lines requiring very narrow-pass band photography. (wide field photography)	Field of view Attitude stability Exposure time Limiting magnitude Exposure time Limiting magnitude Spatial resolution	$\approx .5°$ 0.01 sec 40 min 22.8 400 min 23.8 0.1 arc sec
1) Transient phenomena like explosive sources or flare stars, total-eclipsing systems. 2) Visual binaries to determine absolute masses. (High resolution) (Photometric)	Wavelength Aperture Spatial resolution Wavelength Aperture Spatial resolution	500Å 0.001 in 0.05 arc sec 10μ 0.02 in 1 arc sec
Variables at different phases, appearance of emission bands in explosive variables, hydrogen balmer of Lyman lines of eclipsing variables (High resolution spectroscopy)	Spectral resolution Limiting magnitude Dispersion Wavelength Grating ruling	0.1Å 16 3.67 to 4.05 Å/mm 4,000, 5,000, 6,000, 7,500 Å 600 l/mm
Extension of nebular counts by direct photography.	Limiting magnitude	27
Apparent magnitude of distant objects & measurements of the extent of general reddening of distant objects. Detection of quasistellar objects & distant stellar nebulae.	Limiting magnitude	29

TABLE 3.1.1-1 (cont.)

SOURCE: Space Research - Directions for the Future, Report of a Study by Space Science Board, Woods Hole, Mass., 1965.

OBSERVATION	PERFORMANCE PARAMETERS	VALUE RANGE
OPTICAL ASTRONOMY 1) Cosmic distance scale - measurement of brightness of individual objects, determination of the angular diameter of hydrogen emission regions (HII spheres) around early type stars. 2) Structure of nuclei of galaxies resolution of galaxies. 3) Distribution of molecular hyrogen - Observations in UV & IR to determine the spatial distribution of H_2 4) Detailed analysis of low-termperature objects - Dark interstellar clouds, globules, protoclusters, & protostars. Radiate around 100 microns, important to evoluation of stars & galaxies.	Wavelength Spatial resolution	800Å - 1 mm 0.03 arc sec
SOLAR ASTRONOMY Flare activity - to provide Ne, Te model of flares, surges, prominences time-history of spectrum during active events	Wavelength Spectral resolution Spatial resolution Exposure time	λ<20Å 10^2 $\lambda/\Delta\lambda$ High 1 min
Active Center model of distribution of Ne and Te in active chromosphere and corona and to study variations of the model with time	Wavelength Spatial resolution Exposure time	λ<20Å Low 10 sec
	Wavelength Spectral resolution Exposure time Spatial resolution	170<λ<360 10^3 $\lambda/\Delta\lambda$ Minutes to hours 10 sec
	Wavelength Spectral resolution Spatial resolution Exposure time	1<λ<20 10^2 $\lambda/\lambda\Delta$ 5 arc sec 1-150 sec

TABLE 3.1.1-1 (cont.)

OBSERVATION	PERFORMANCE PARAMETERS	VALUE RANGE
Quiet corona spectral & spectro-heliographic studies. To connect quiet corona with chromspheric network and spicule bushes to determine nature of chromosphere-corona interface.	Spectral resolution Wavelength Spatial resolution	$10^3 \lambda/\Delta\lambda$ $20 < \lambda < 500$ 2 - 5 arc sec
Quite Chromosphere especially lines HeII 304 and 256. Spectral observation of these lines to determine height variation of temperature and density of chromosphere as well as general structure.	Spectral resolution Spatial resolution Exposure time Wavelength	$\geq 10^3 \lambda/\Delta\lambda$ 1 - 5 arc sec 10 sec to 300 sec $\lambda < 500$
Spectrographic observation line profile measurements of emission lines from chromospheric and coronal structures.	Wavelength Spectral resolution Spatial resolution Guiding accuracy	$500 < \lambda < 1500$ $10^4 - 10^5 \lambda/\Delta\lambda$ 0.3 - 50 arc sec Few arc sec
Spectral Mapping	Wavelength Spectral resolution Scattered light	$1500 < \lambda < 3000$A $10^5 \lambda/\Delta\lambda$ 1% of continuum intensity
Spectroheliographic pictures in special lines to reveal coronal and chromospheric response to slow change in active regions.		
Spectrum of Selected regions	Guiding accuracy Spectral resolution	5 arc sec $10^5 \lambda/\Delta\lambda$
Lines Profiles - understanding of granulations, turbulent effects, spicules	Spatial resolution Spectral resolution Exposure time	0.1 sec $10^6 \lambda/\Delta\lambda$ High
Spectroheliogram studies	Spatial resolution Exposure time	0.1 - 5 arc sec 10-30 sec
Magnetometry - Zeeman splitting of spectral lines originating in chromosphere and lower corona		
Broadband features, spectroheliograms and spectrographic observation	Wavelength Spatial resolution Guiding accuracy	$\lambda > 3000$Å 0.1 arc sec 0.05

3.1.2 Technology Needs

Given the value range of the performance parameters and comparing this range with the current state of the art, it is then possible to determine the technology needs required for future space astronomy missions.

By inspecting table 3.1.1-1, it can be seen that the principal performance parameters are spatial resolution, spectral resolution, bandwidth sensitivity and limiting magnitude. Each of these performance parameters is, in turn, dependent on a number of interrelated parameters. For example, many future space astronomy applications are heavily dependent on the ability to achieve high spatial resolution as indicated in table 3.1.2-1.

TABLE 3.1.2-1

ASTRONOMY OBSERVATIONS REQUIRING HIGH SPATIAL RESOLUTION

OBSERVATION

a. Angular diameter of hydrogen emission regions around early type stars.
b. Structure of nuclei of galaxies.
c. Resolution of quasi-stellar radio sources.
d. Photometric measurements of faint end of galaxy and star clusters.
e. UV images of early type stars.
f. Resolution of binaries.
g. Search for small stellar companions.

The estimated required spatial resolution to achieve these observations ranges from 1 arc second to .03 arc second. This spatial resolution is, in turn, dependent on several design parameters as shown in figure 3.1.2-1 which is a system resolution implication diagram.

In this implication diagram the errors contributing to resolution degradation are placed into four catagories. By considering each of these in turn it is possible to isolate the technology needs for a high resolution application.

The optical system degrades the resolution due to the usual aberrations, (coma, astigmatism, etc.) diffraction (1.22 λ/D) and mirror figure distortion. The error due to diffraction can be improved by decreasing λ or increasing D. The former can be achieved by developing a detector which is sensitive only in the ultraviolet. An increased telescope diameter inplies the need for light weight mirror materials to avoid excessive weight penalties.

Two areas of technological development are implied by the need to maintain mirror figure. These are: improved passive thermal control and mirror figure control. In the latter case, there are several competing techniques which must be evaluated, as for example, thermal actuation, mechanical actuation, and segmented optics.

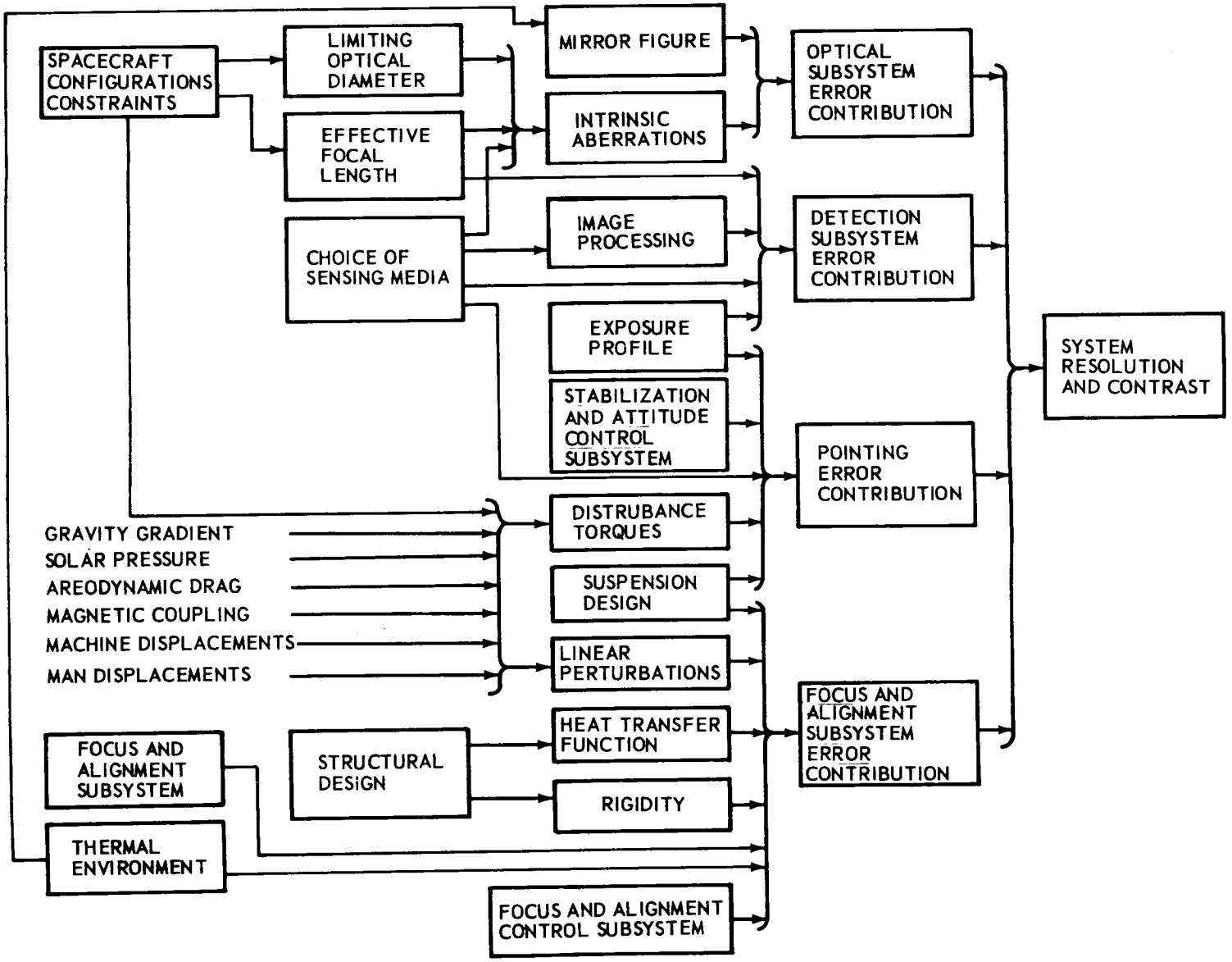

Figure 3.1.2-1. System Resolution Implication Diagram

Detection error contribution requires improved photographic and photoelectric resolution. However, this improvement must be consistent with low sensitivity requirements. A dry development emulsion with high resolution capability is a technology need which will eliminate the weight penalty associated with development liquids. Furthermore, the high resolution detectors, whether photographic or photoelectric, should be compatible with ultraviolet detection requirements.

The pointing error contribution can be minimized by development of control and stabilization subsystems. The major areas requiring development are the fine error sensors and the fine beam deflectors. The fine error sensors must be compatible with various means of detection (spectroscopy, photometry, imagery, etc.) and the beam deflectors should be compatible with ultraviolet detection (non-refractive). Associated with the improvement and control and stabilization subsystem is the development of isolation systems which would isolate gimballed telescopes from disturbances generated in the spacecraft. This problem is more acute for manned missions.

The technology needs implied by improved focus and alignment capability includes the development of small displacement actuators (0.0001 inch increments over dynamic ranges up to 0.5 inches), small displacement sensors, defocusing sensors and improved passive thermal control. Each of these areas involves the evaluation of materials, fabrication and integration into the telescope system.

In summary, the technology needs implied by improving the spatial resolution of present telescope systems are:

a. Detectors sensitive only in the ultraviolet.
b. Lightweight primary mirrors.
c. Mirror figure control.
d. Improved passive thermal control.
e. Photographic resolution.
f. Photoelectric resolution.
g. Fine error sensors.
h. Fine beam deflectors.
i. Isolation techniques.
j. Small displacement actuators.
k. Alignment and focus sensors.

The above listed needs apply specifically to the performance parameter, spatial resolution. Further technology needs arise from other performance parameters such as bandwidth sensitivity, spectral resolution, etc.

Improved spectral resolution is dependent on development in fine pointing, high resolution sensors, mechanical support to survive launch, improved thermal control, and high density diffraction gratings.

Bandwidth requirements impose the need to develop detectors sensitive from 100 microns to approximately 900 angstroms. These in turn require development in cryogenic cooling (0.25 to 4 degrees Kelvin), multi-layer interference reflection filters for far ultraviolet detection, broadband photoelectric detectors, and for infrared detectors between 20 and 100 microns.

In addition there is considerable technology development implied by specific observations. For example optical interferometry establishes the need for long stable beams (up to 50 feet) and fine positioning actuators (.0001 inches).

A summary of the technology needs to support specific astronomy observations are presented in table 3.1.2-2.

3.2 METEOROLOGY

The first goal of meteorology is to understand the atmosphere and its variable products. The final goal of meteorology is to control or create the products. The goals of meteorology are social -- with the understanding of the atmosphere, it will be possible to predict the weather and protect people from approaching disasters; with the control of the atmosphere, it will not only be possible to eliminate such disasters but also improve the efficiency of production.

For an astronomer, the atmosphere is a hindrance and in space he turns his instrument away from Earth and toward the stars. The meteorologist above the atmosphere turns his instrument towards Earth for a comprehensive and detailed examination of the atmosphere. To fully exploit the advantages of being above the atmosphere, the meteorologist, as well as the astronomer, needs better tools.

3.2.1 Observational Objectives

The nation's overall goals in meteorology are indicated by the results of a recent study conducted for the Interdepartmental Committee on Atmospheric Science of the Federal Council for Science and Technology by the U. S. Weather Bureau and the Rand Corporation(1). The three overall national objectives for meteorology as determined by this study are:

a. Protection of life and property.
b. Preservation of health, promotion of safety and contribution to convenience and general well being.
c. Increased efficiency in the production of goods and services.

These three overall socio-economic national objectives have been translated into four specific technical objectives by seven Federal agencies (Departments of Commerce, Defense, HEW, Interior, and State, plus NASA and NSF) to define a national research program in meteorology.(2)

(1) Referred to in the NASA-ORL Experiment Program, Vol. B, Part V, Atmospheric Science and Technology, IBM, Feb. 1966, p. V-3.
(2) Ibid, pp. V-3 and V-5.

TABLE 3.1.2-2

ASTRONOMY TECHNOLOGICAL NEEDS

TECHNOLOGY	High Resolution	Spectroscopy	Photometry	Interferometry	Wide Angle Surveys	Solar Observation	Astronometric
SPACE TELESCOPE TECHNOLOGY							
Mirror Surface Degradation	*	*	*		*	*	
Mirror Figure Control	*	o	o	o	o	o	o
Alignment & Focusing	*	*	o	*	o	*	o
Thermal Compensation	*	*	o	*	o	o	o
Beam Stability	*	*	o	*	o	o	o
Precision Deployment	*			*		*	
Baffles	o	o	o	o	o	*	o
Launch Isolation	*	*	o	*	o	*	o
Small Displacement Actuators	*	*	*	*	o	*	*
CONTROL AND STABILIZATION							
Fine Error Sensors	*	*	*	o		o	
Fine Beam Deflectors	*	*	*	o		o	
Isolation Techniques	*	*	o	o	o	*	*
Acquisition	*	*	*	*	*	*	*
DETECTORS							
High Resolution Image Tubes	*	*		o		*	
Low Level Image Tubes	*	*	*		*		
Broadband Photoelectric Detectors			*				
Large Area Photocathodes	*						
Far Infrared Detectors		*	*		*	*	
Dry Emulsions	*	*	*	*	*	*	*
High Data Capacity Photographic Recording	*	o			*	o	
X/UV Sensitive Photographic Emulsions	*	*			*	o	
AUXILIARY DEVICES							
Dissector		*					
Objective Grating Mosaic					*		
Michelson Interferometer				*			o
Fabry Perot Interferometer				*			o
Phosphor Camera					*		
UV Coronagraph						*	
Slit Spectrograph		*				*	

( ) WEAK RELATIONSHIP * MAJOR REQUIREMENT o SIGNIFICANT RELATIONSHIP

a. Accurate warning of meteorological disasters.
b. Improved length and accuracy of weather forecasts.
c. Weather and climate modification and, ultimately, control.
d. Prediction, modification and control of atmospheric pollution.

Fulfillment of each of these four technical objectives requires an expansion of knowledge of phenomena in the atmosphere and space. This is our most pressing problem in meteorology.

It is generally agreed by meteorologists that the ideal weather observation system should provide measurement of cloud and surface fog, vertical and horizontal wind, jet stream temperature, pressure, tropopause and water vapor content, as well as measurement of the heat budget and the concentration of the principal abosrbers and emitters of radiation (CO_2, H_2O, and O_3), on a global grid of about 250 to 300 kilometers from the surface up to 100 kilometers. Conventional surface and upper-air balloon meteorological observations provide adequate coverage over less than 10 percent of the Earth's surface, and only up to 30 kilometers. This coverage could be expanded somewhat, but economic and physical limitations prohibit adequate global measurements with the conventional techniques. The solution to this problem awaited recent developments in space technology.

The Tiros series of experiments, now complete, and the Nimbus series, still in progress, have enabled the U.S. to loft two currently operational meteorological satellites, dubbed ESSA-1 and ESSA-2.

ESSA-1 and ESSA-2, and their successors, will provide near-synoptic day and night coverage of the visible and infrared parts of the spectrum over the entire globe from near polar, sun-synchronous, circular orbits at altitudes of about 800 miles. For example, ESSA-1 is now in a sun-synchronous orbit which allows the vidicon camera system to tape a virtually continuous picture of clouds in the late afternoon (local sun time) over the entire globe. ESSA-2 follows close behind to transmit a live TV picture to properly equipped ground stations. ESSA-1 and ESSA-2 vidicon camera systems operate only in the visible part of the spectrum.

Continuing research and development in the Nimbus series will also provide infrared sensor systems which will measure the temperature of earth or cloud surfaces as well as the mean temperature over certain layers in the atmosphere.

The next generation of meteorological satellites will carry at least these four measuring systems as noted:

a. Advanced Vidicon Camera System (AVCS)
   Three cameras jointly covering 105°
   ½ mile resolution at picture center
   Data recorded and later transmitted to ground receiving station

b. Automatic Picture Transmission (APT) System
Two-Camera, Cross-strapped
System, 108° field
Transmits live TV picture to ground receivers. Resolution 2 miles at picture center. Each picture roughly 800 miles square.

c. High Resolution Infrared Radiometer (HRIR)
Operates at wavelengths of 3.4 to 4.2 microns in the infrared spectrum. Provides resolution of 5 miles at picture center.
Measure temperatures differences of 2 deg. F.

d. Medium Range Infrared Radiometer (MRIR)
Measures heat balance of the entire 200 million square miles of the earth's surface each. Resolution about 30 mi from 690 and altitude of miles
MRIR operates in five spectral bands, as follows:

(1)	6.5 - 7.0 microns	water vapor absorption	temperature & relative humidity profile
(2)	10 - 11 microns	atmosphere in transparent	earth's profile, low atmosphere radiation, & cloud cover.
(3)	14 - 16 microns	emission from the CO_2 abosrption band	Stratospheric temperature
(4)	7 - 30 microns	thermal emissions from earth	energy budget of earth
(5)	0.2 - 4 microns	earth's albedo	solar energy reflected by earth and its atmosphere.

Additional details concerning instrumentation which is now on the ESSA-1 and ESSA-2 satellites or which is expected to be carried as part of the continuing Nimbus series of experiments are listed in the following tabulation below.

TIROS-ESSA SERIES

TV Pictures

	Wide Angle 105°	Medium Angle 78°	Narrow Angle 12°	APT 105°
Area (miles)	700 X 700	420 X 420	70 X 70	800 X 800
Number of lines	500	500	500	800
Resolution mi/line	1.5	0.8	0.15	1.0

NIMBUS SERIES

AVCS	HRIR	MRIR
3 cameras		
105°	3.4 - 4.2 microns	
Resolution 0.5 mi.	5 miles	30 miles
	2 deg.F	0.2 - 4 microns
	1000 ft. cld ht	6.5 - 70 microns
		10.0 - 11.0 microns
		14.0 - 16.0 microns
		7 - 30 microns

Near synoptic coverage, as now provided by ESSA-1 and ESSA-2, and ultimately, by their successors is sufficient for most meteorological purposes. However in the case of certain short-lived or rapidly occuring meteorological events continuous surveilliance may be required. For example a severe thunderstorm with a tornado or tornadoes could build to maturity and dissipate between successive passes of a polar orbiting satellite or a hurricane could develop between passes.

3.2.2 Technology Needs

Continuous surveillance requires a satellite in equatorial synchronous orbit. Assuming that the ground resolution requirements are not relaxed the angular resolution requirements are considerably more severe than they are for the satellites in 800 mile orbit.

Table 3.2.2-1 indicates ephemeral meterological phenomena which require continuous surveillance from an equatorial synchronous satellite. Measurables and their sensing requirements are shown. The linear resolution requirements are the same for the synchronous orbit as for the lower orbit; thus the angular resolution requirements are thus more severe.

The technology needs associated with these high resolution requirements are essentially similar to those associated with high resolution astronomy observations. There are, however, additional or different needs. For instance, non synchronous earth orbit missions will require image motion compensation. Furthermore the error sensor may be different as it may be necessary to track an extended source rather than a point source. The meteorology technology needs are presented in table 3.2.2-2.

3.3 EARTH REMOTE SENSING

To maintain the United States and world economies at their present level requires continued discovery and development of new resources. The supply problem is compounded by rapid growth in population and by the rise in per capita consumption of raw materials and energy. For example, the U. S. will

TABLE 3.2.2-1

SUMMARY OF THOSE SELECTED KNOWLEDGE REQUIREMENT FOR ATMOSPHERIC SCIENCE AND TECHNOLOGY FOR WHICH INDICATIVE PHENOMENA ARE EPHEMERAL IN NATURE (NASA-ORL EXP. PROGRAMS, VOL. B, PART V, IBM, FEBRUARY, 1966)

Selected Knowledge Requirements	Indicative Phenomena	Spectral Band (microns)	Resolution	
			Linear on Ground (FT)	Angular at Synchronous Altitudes (arc. sec.)
1. Characteristics of Individual Clouds or Cloud Systems	Shape-Size	0.3 - 0.9	50	.01
	Percent of Area Covered	0.3 - 0.9	500	0.1
	Extent of pattern	0.3 - 0.9	500	0.1
2. Characteristics of Storm Systems, Severe Storms, Thunderstorms, Tornadoes, Hurricanes	Cloud system pattern	0.3 - 0.9	500	0.1
	Storm system position	0.3 - 0.9	500	0.1
	Storm wind velocity	0.3 - 0.9	500	0.1
	Storm system velocity	0.3 - 0.9	500	0.1
3. Atmospheric Circulation	Horizontal wind			
	Wave activity	0.3 - 0.9	50	0.1
	Water wave pattern	0.3 - 0.9	1 to 50	0.002 - .01
4. Pollutant Characteristics	Color Contrast	0.3 - 0.9	100 - 5000	0.02 - 1.0
	Observation	0.3 - 0.9	100 - 5000	0.02 - 1.0
	Earth Contrast Reduction	0.3 - 0.9	10 - 500	0.002 - 0.1
5. Clear Air Turbulence	Star occultation	0.3 - 0.9		
	Scattering	0.3 - 0.9		

TABLE 3.2.2-1

METEOROLOGY TECHNOLOGICAL NEEDS

SPACE TELESCOPE TECHNOLOGY	High Resolution Imagery	Distribution of Constituents	Cloud Top & Aerosol Altitude	Vertical Temperature Profile	Point-to-Point Turbulence	Point-to-Point Scattering
Mirror Surface Degradation	*	*°	°	*°	°	°
Mirror Figure Control	*	°	°	°	°	°
Alignment & Focusing	*	*°	°	*°	°	°
Thermal Compensation	*	°	°		°	
Beam Stability	*					
Precision Deployment	*					
Launch Isolation	*	*°	°	°	°	°
Small Displacement Actuators	*					
CONTROL & STABILIZATION						
Image Motion Compensation	*	*	*	*		
Fine Error Sensors	*					
Fine Beam Deflectors	*					
Isolation Techniques	*					
Acquisition	*	*	*	*	*	*
DETECTORS						
High Resolution Image Tubes	*					
Large Area Photocathodes	*					
Far Infrared Detectors	*	*		*		
Dry Emulsions	*	°	°			
UV Photography		°				
Mechanical Image Scanning	*					
LASERS						
Direct Detection			*		*	*
Heterodyne Detection			*		*	*
Atmospheric Transfer Function		°	°	°	*	*
Scattering & Absorption			*		*	*

∩ WEAK RELATIONSHIP * MAJOR REQUIREMENT ° SIGNIFICANT RELATIONSHIP

double its present consumption of most minerals within 15-25 years; it is a particularly vulnerable position, as its consumption rate is high and it depends heavily upon materials from many areas of the world.

NASA has begun a "Natural Resources Program" to utilize sensors in space for the discovery, inventory, evaluation, development, and conservation of natural and cultural resources. Resources which can be studied in this manner include minerals, soils, crops, timber, water, housing, and transportation networks. Instruments appropriate to this work in earth orbital spacecraft possess a number of distinct advantages - rapidity and continuity of observation, greater freedom from weather disturbances, synoptic views for regional syntheses, reduced data-acquisition times, reduced costs, and better quality data of several types.

3.3.1 Observational Objectives

In the past few years, imaging sensors in unmanned and manned spacecraft have been employed to provide the first true synoptic coverage of the lithosphere, hydrosphere and atmosphere. It has been demonstrated by Tiros, Nimbus, and Gemini that certain phenomena related to the earth can be understood only when viewed from a great distance. These programs have also demonstrated that, for the first time, man has the ability to survey large sections of the earth and its environment within a very limited time frame.

The amount of detail required and the extent to which it is economically practical to conduct such sensing from space has not yet been determined. The obvious need for such determinations provides the rationale for the Natural Resources Program. To date four broad areas related to the earth's resources have been identified as potentially suitable for the application of space technology:

a. Agriculture and Forestry.
b. Geography and Cartography.
c. Geology and Hydrology.
d. Oceanography and Marine Technology.

The Tiros, Nimbus and Gemini experiments have demonstrated the potential use of photographs and TV pictures in the visible and infrared as a means of analyzing geophysical and geographical features.

The currently operational ESSA-1 and ESSA-2 provide a quai-synoptic global coverage of geophysical and geographical features of the earth's surface.

Successors to ESSA-1 and ESSA-2 will provide these four measurements as already described in section 3.2.1. Meteorology observational objectives.

a. Advanced Vidicon Camera System (AVCS).
b. Automatic Picture Transmission (APT) System.

c. High Resolution Infrared Radiometer (HRIR).
d. Medium Range Infrared Radiometer (MRIR).

Most requirements for measurements in each of the four broad areas will be met by instrumentations now extant or under development. As with the Meteorology measurement the polar orbiting satellite will not detect ephemeral events which occur between passes of the satellites. Examples of such ephemeral occurrences are given in the following tabulation from three of the four broad "Natural Resource" areas. There are evidently no ephemeral events of interest within the Geography/Cartography area. As with astronomy there will be a need to develop space qualified detectors in the infrared region. Table 3.3.1-1 summarizes the technology required to support these earth remote sensing objectives.

The table gives indicative phenomena for each measurement which may be ephemeral in nature, as well as the desired spectral band or bands. Ground linear resolution requirements and angular resolution requirements at synchronous altitude are also noted.

3.3.2 Technology Needs

Continuous surveillance requires a satellite in equatorial synchronous orbit. Assuming that the ground resolution requirements are not relaxed, the angular resolution requirements at the synchronous altitude (22,300 miles) will be considerably more severe than they are for satellites in an 800 mile orbit.

Table 3.3.2-1 indicates ephemeral or rapidly changing phenomena on or below the earth's surface which require continuous surveillance from an equatorial synchronous satellite. Measurables and their indication phenomena are shown. The linear resolution requirements on the ground are the same as that for the 800 mile orbit; then the angular resolution requirements are considerably more severe.

The technology needs associated with these requirements for high resolution are essentially the same as those associated with the high-resolution astronomical and meteorological observations.

Table 3.3.2-2 lists the technology needs association with specific earth remote sensing observations.

TABLE 3.3.1-1

SUMMARY OF THOSE SELECTED KNOWLEDGE REQUIREMENTS FCR EARTH REMOTE SENSING FOR WHICH INDICATIVE PHENOMENA MAY BE EPHEMERAL IN NATURE, (NASA-ORL EXPERIMENT PROGRAM, VOL. B, IBM FEB. 1966)

Selected Knowledge Requirements	Indicative Phenomena	Spectral Band (microns)	Resolution	
			Linear on Ground (FT)	Angular at Synchronous Altitudes (arc.sec.)
Geology/Hydrology				
1. Igneous Activity	Deformation of mountain systems	0.4 - 9.0	1000 - 10,000	2.0 - 20.0
	Temperature discontinuities	3.0 - 14.0	1000 - 10,000	2.0 - 20.0
2. Volcania Eruptions	Lava Flow ash formation	0.4 - 14.0	100 - 1,000	0.2 - 2.0
	Damage to cultural features	0.4 - 0.9	1 - 25	
	Surface deformation	0.4 - 0.9	10 - 100	0.02 - 0.2
3. Flood	Coverage	0.4 - 0.9		
	Destruction of cultural	0.4 - 0.9		
	Erosion & setting pattern	3.0 - 14.0		
4. Snow	Area coverage	0.4 - 0.9 3.0 - 14.0	100 - 500	0.2 - 1.0
	Color	0.4 - 3.0	100 - 500	0.2 - 1.0
	Temp Contrast	3.0 - 14.0	100 - 500	0.2 - 1.0
5. Water flow	Color & patterns of land forms	0.4 - 3.0	10 - 100	0.02 - 0.2
	Area & tropography	0.4 - 0.9	10 --100	0.02 - 0.2
6. Sea Ice	Areal extent	0.4 - 0.9 3.0 - 14.0	10 - 100	0.02 - 0.2
	Pattern	0.4 - 0.9 3.0 - 14.0	10 - 100	0.02 - 0.2
	Distribution	0.4 - 14.0 3.0 - 14.0	500 - 5000	1.0 - 10.0
	Temperature	3.0 - 14.0	500	1.0

TABLE 3.3.2-1

SUMMARY OF SELECTED KNOWLEDGE REQUIREMENTS FOR EARTH REMOTE SENSING (NASA ORL EXPERIMENT PROGRAM, VOL. B, IBM, FEB. 1966)

Selected Knowledge Requirements	Indicative Phenomena	Spectral Band (microns)	Resolution	
			Linear on Ground (FT)	Angular at Synchronous Altitudes (arc. sec.)
Agriculture Forestry				
1. Location, identification, type and migration of wildlife, animal pests and insects	Color & Pattern Thermal	0.4 - 14	5	0.01
2. Identify and locate forest fires	Color, Fire Smoke Thermal Pattern	0.4 - 3 3.0 - 14.0 3.0 - 14.0	100 100 500	0.2 0.2 1.0

TABLE 3.3.2-1

SUMMARY OF SELECTED KNOWLEDGE REQUIREMENTS FOR EARTH REMOTE SENSING
(NASA-ORL EXPERIMENT PROGRAM, VOL. B., IBM, FEBRUARY, 1966)

Selected Knowledge Requirements	Indicative Phenomena	Spectral Band (microns)	Resolution	
			Linear on Ground (FT)	Angular at Synchronous Altitudes (arc. sec.)
Oceanography/Marine Technology				
1. Movement of fish	Color & pattern	0.4 - 3.0	50 - 200	0.1 - 0.4
	Bioluminescence	0.4 - 0.9	50 - 1000	0.1 - 2.0
	Predators	0.4 - 0.9	5 - 100	0.01 - 0.2
		3.0 - 14.0	5 - 100	0.01 - 0.2
2. Hazards	Sea Ice	0.4 - 0.9	100 - 1000	0.2 - 2.0
	Sea state	3.0 - 14.0	100 - 1000	0.2 - 2.0
	Sea state	0.4 - 0.9	100 - 1000	0.2 - 2.0
3. Damage Assesment		0.4 - 0.9	1 - 10	0.002 - 0.02

TABLE 3.3.2-2

EARTH REMOTE SENSING TECHNOLOGICAL NEEDS

SPACE TELESCOPE TECHNOLOGY	High Resolution Imagery	Contour Mapping	Thermal Mapping
Mirror Surface Degradation	*	°	°
Mirror Figure Control	*	°	°
Alignment & Focusing	*	°	°
Thermal Compensation	*	°	°
Beam Stability	*	°	°
Precision Deployment	*		
Launch Isolation	*		
Small Displacement Actuators	*		
CONTROL & STABILIZATION			
Image Motion Compensation	*		
Fine Error Sensors	*	*	*
Fine Beam Deflectors	*		
Isolation Techniques	*		
Acquisition	*	*	°
DETECTORS			
High Resolution Image Tubes	*		
Large Area Photocathodes	*		
Far Infrared Detectors	*	*	*
Dry Emulsions	*	*	
UV Photography	*	*	°
Mechanical Image Scanning	*	*	*
LASERS			
Direct Detection		*	
Heterodyne Detection			
Atmospheric Transfer Function		*	
Scattering & Absorption		*	
Range/Rate		*	

□ WEAK RELATIONSHIP * MAJOR REQUIREMENT ° SIGNIFICANT RELATIONSHIP

3.4 INTERPLANETARY MISSIONS

Interplanetary missions play a prominent role in future NASA plans. The Mariner and Voyager programs are well established in NASA planning. Beyond these lies the possibility of Manned Mars Missions.(1) (2) As a result there will be a continuing evolution of optical needs to satisfy these missions.

These needs can be classified into two groups; first, observation of planetary surfaces and atmospheres and second, the technology associated with optical communications. The technology needs associated with observations are generally similar to the technology needs presented in preceeding sections 3.2 Meteorology and 3.3 Earth Remote Sensing. This section will therefore be directed toward a discussion of the optical needs which arise from optical communication objectives.

3.4.1 Communication Objectives

A principle technological need in interplanetary missions is the transmission of high data rates over interplanetary distances. It was recently stated(3) that near future (1970-1980) requirements in interplanetary communications would necessitate the need to develop information capacities up to 5 times 10^7 bits/second. This frequently expressed need (4) for real time television bandwidth deep space-to-earth data links suggests the use of a wide bandwidth laser communication system in which all the short wavelength optical energy can be concentrated into a very narrow diffraction-limited beam.

In fact, the development of laser communication systems was referred to by the National Academy of Sciences. (5)

Given the potential need for interplanetary optical communication links, it is then necessary to determine the required technology to implement such capability.

---

(1) Statement of Dr. D. F. Horning, Director, Office of Science & Technology, before Senate Committee on Aeronautical & Space Sciences, Aug. 24, 1965.

(2) Statement by Dr. Harry Hess, Chairman of the Nat'l Academy of Sciences, before the Senate Committee on Aeronautical and Space Sciences, Aug. 25, 1965.

(3) Hearings before the Committee on Aeronautical and Space Sciences, U. S. Senate, Aug., 1965.

(4) Adams, M. C. Hearings before the Committee on Science and Astronautics, U. S. House of Representatives, 89th Congress, Feb. 23, 24, 25 & 28 thru March 1, 2, 3, 7, and 8, 1966, Part 4, p. 97.
Kelley, A. J., "Nasa's New Electronic Res. Ctr", Astronautics & Aeronautics, Vol. 3, NO. 5, May 1965, pp. 58-63. Newell, H. E., Hearings before the Committee on Aeronautical & Space Sciences, U. S. Eighty-ninth Congress, March 22, 23, 24, 25 & 30, 1965.

(5) Space Research Directions for the Future, National Academy of Sciences - National Research Council, Woods Hole, Mass., Publication 1403, 1965, pp. 8, 61 and 242.

3.4.2 Technology Needs

The first basis for determining optical communication technology needs is to compare optical communication with microwave communication in order to establish bounds on the required systems as for example, telescope aperture.

Taking the ratio of the well-known Friss transmission expressions for optical and microwave communication gives:

$$\frac{\left(\frac{S}{N}\right)_o}{\left(\frac{S}{N}\right)_m} = \frac{\xi_{ot}}{\xi_m} \frac{A_{to}}{A_{tm}} \frac{\lambda_m^2}{\lambda_o^2} \frac{A_{ro}}{A_{rm}} \frac{kT}{\gamma/q}$$

In table 3.4.2-1 the various terms of this relation are evaluated for the view point of microwave optimism (e.g., a 100 meter, X-band receiving aperture on the Earth; a 20 meter X-band transmitter on the spacecraft; a 100Å receiver noise temperature; a 50 per cent, X-band transmitter efficiency, etc.). These assumed characteristics are contrasted with 0.6328 micron laser communication (Helium-Neon components which could be fabricated today. The noise, receiving aperture and transmitter efficiency ratios (23.5 + 20.0 + 20.5 = 64.0 decibels) are inherently advantageous to the microwave technology. Only the wavelength (93.5 decibels) term favors the optical technique. Thus a favorable comparison of optical communication with microwave communication requires a telescope aperture of one meter or greater.

A one meter 0.6328 micron aperture will give a diffraction limited bandwidth of 0.14 arc seconds posing pointing accuracy requirements in the order of 0.1 arc seconds. This pointing precision is less than the Bradley effect which can be expected at planetary ranges. Therefore such a precision pointing system must be capable of compensation a pointing ahead.

Table 3.4.2-1 is an analytical comparison between microwave and laser communications. There is considerable uncertainty in this analysis since the effects of the atmosphere on a coherent light beam are not known. Therefore spaceborne optical communications data is necessary before there can be a real comparison between laser and radio frequency communications.

Other technological development is implied. For instance, competing techniques of detection must be developed and evaluated. It is necessary therefore to compare the efficiency of optical direct detection and optical heterodyne detection. Since the laser communication offers ultimate advantages at extreme ranges, verification of this potential, and attendant developmental experiments, should be considered in a planetary mission context. A typical mission is the Mars orbiter/lander case depicted in figure 3.4.2-1. For the foreseeable future, such probes will follow minimum energy trajectories. Launch could be initiated about four months before opposition.

TABLE 3.4.2 - 1

OPTICAL/MICROWAVE COMPARISON PARAMETERS

	$\frac{K_T}{h\ \gamma/q}$	$\frac{A_{ro}}{A_{rm}}$	$\frac{\xi_o}{\xi_m}$	$\frac{\lambda_m}{\lambda_o}$	$\frac{Ato}{A_{tm}}$
OPTICAL	A_t 6328Å $h\gamma = 3.12 \times 10^{-19}$ Joules $q = 0.05$	D = 10 Meter $A_{ro} = 78.5 M^2$	0.0045	$\lambda_o{}^2 = 4 \times 10^{-13}$ m^2	D = 1 Meter 0.785 M^2
MICRO-WAVE	AT 100°K 1.38×10^{-21} Joules	D = 100m $A_{rm} - 785 m^2$	0.5	$\lambda_m{}^2 = 9 \times 10^{-4} m^2$	D = 30 Meters $A_{rm} = 706 m^2$
db:	+23.5	+20	+20.5	-93.5	+29.5

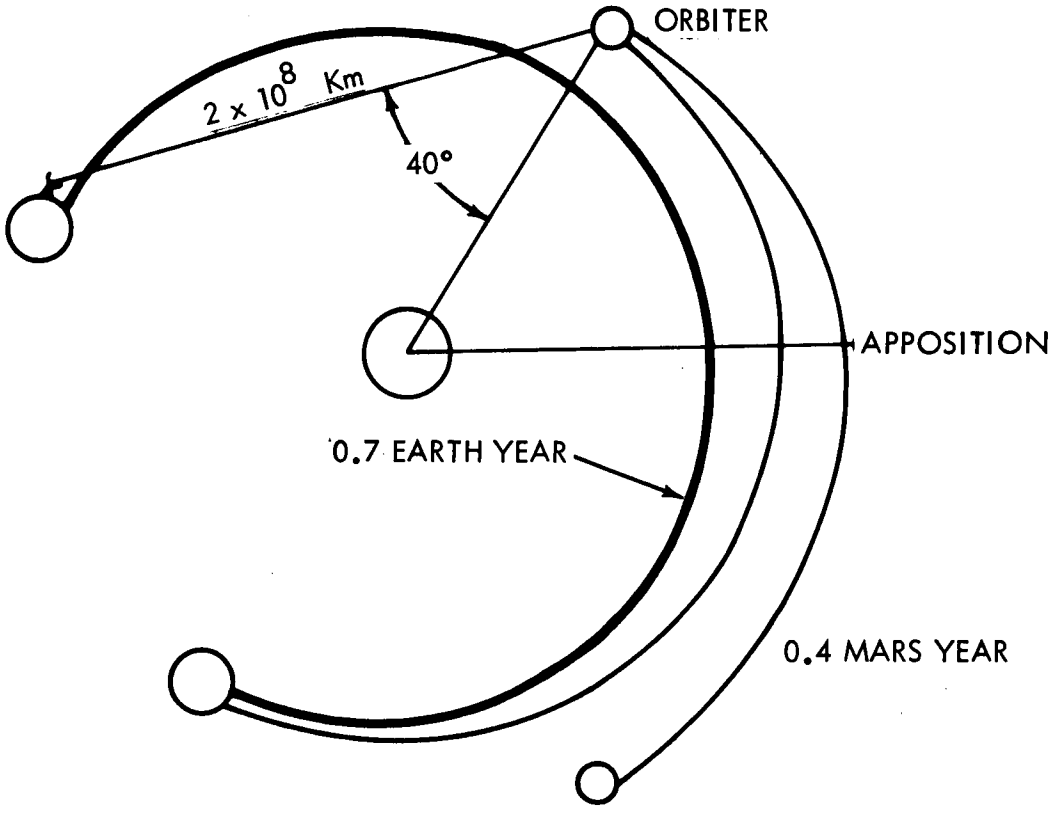

Figure 3.4.2-1. Typical Mars/Earth Communications Geometry

Since Mars takes almost twice as long in its travel around the Sun as the Earth does, Earth will pass and proceed well ahead of Mars during the flight time of probe. When the probe reaches the vicinity of Mars, the two planets will be separated by a distance of about 2 times 10^8 kilometers, and the line-of-sight from Earth to Mars will be only about 40 degrees from the Mars-Sun line. Thus, at Mars intersection, the portion of that planet viewed from the Earth will be almost fully sunlit. At optical communication frequencies this means that the probe will be executing its primary mission tasks with an unavoidable high noise background.

Furthermore, during much of the viewing time each day, the receiver must be in a daylight ambient noise environment, and as time progresses, the line-of-sight will pass closer to the sun admitting more energy directly from this intense noise source.

While it might appear that viewing could take place during the twilight hours, atmospheric effects place a 20 degree lower limit on elevation angle. The conclusions to be drawn from planetary geometry are straightforward. Any practical optical communication link must be capable of operating with a daylight sky background. For this reason, direct detection will require a very narrow filter, and heterodyne detection is attractive.

In addition to detection several modulation schemes must be evaluated and compared. In many cases this can be done preliminarily by analytical techniques and ground tests. The technology need is nevertheless real.

It is interesting to note that the simpler, space-to-ground communication system concepts are fundamentally inseparable from the atmospheric perturbations. Knowledge of the atmosphere is then essential to the communication link designer. Conversely, to measure properties of the whole atmosphere requires the establishment of an earth orbit propagation link. It is only with the addition of system complexity, such as an orbit-relay-station system concept, that it is possible to divorce the atmospheric physics problems from communication system problems.

In summary, therefore, the optical needs associated with interplanetary optical communications include:

a. Diffraction limited telescope of at least one meter aperture.

b. Pointing capability in the order of 0.1 arc second combined with point ahead.

c. Space qualified lasers, modulators and receivers.

d. Comparative evaluation of modulation and detection techniques.

e. Thorough understanding of atmospheric effects on optical propagation.

3.5 COMMONALITY OF TECHNOLOGY NEEDS

It is apparent from the preceding material on technology needs associated with each application that technology development to support one application will in many cases satisfy the needs generated by other applications. This is due to the commonality of technology needs. This commonality is easily recognized by developing a matrix which display needs versus application. Such a matrix is presented as figure 3.5-1. Commonality is indicated by comparing the needs across a horizontal row.

It can be seen from inspection that high resolution applications have the greatest correlation in commonality. For instance, mirror figure control will directly benefit astronomy, meteorology, earth remote sensing and laser communication applications.

Due to this element of commonality, technology development can be expected to generate increased needs in the never ending cycle of supply and demand.

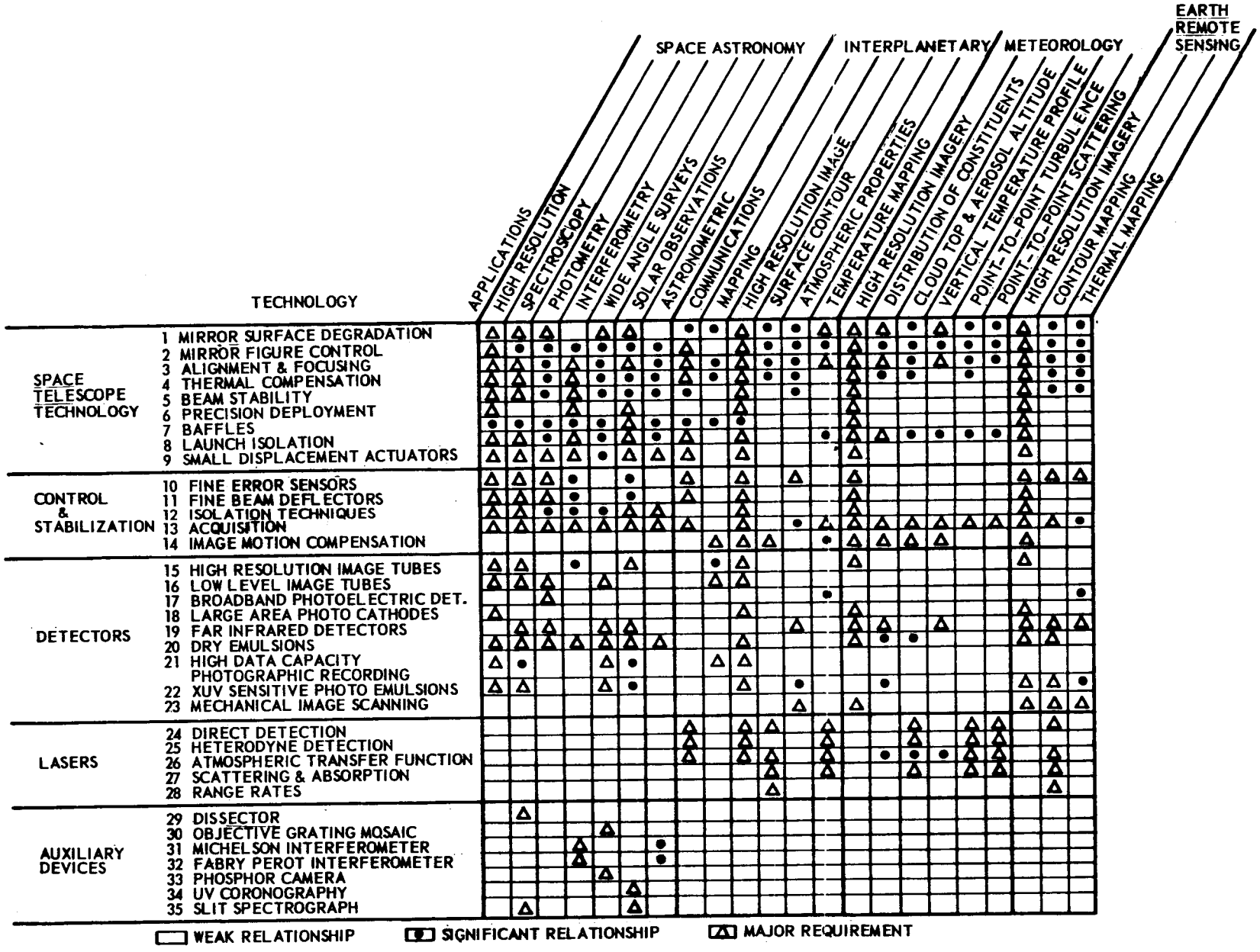

Figure 3.5-1. Commonality of Required Optical Technology

SECTION II

4.0 PROPOSED OTAES EXPERIMENT

The OTAES study considered four space science application areas. Preceding sections have described these application areas from the viewpoint of their optical technology needs. The sections which follow present space experiments relating to particular aspects of these needs and which, if successful, will advance optical technology and thus constitute partial fulfullment of important future space objectives.

4.1 OPTICAL HETERODYNE DETECTION ON EARTH

4.1.1 Summary

The atmosphere has been studied for centuries from Earth-bound observatories using the non-coherent light from stars. Rockets and satellites now permit remote measurements of the Earth and its atmosphere. Over the past decade, the national space program has accumulated many such data--and a large portion of these data were measured in the ultraviolet, visible, and infrared. To make optimum use of remotely sensed data, more must be known about the physics of the atmosphere and the effect of the atmosphere on signals passing through it. As a tool to advance our knowledge in these areas, the laser possesses two highly useful properties: spatial and temporal coherence. A laser transmitter can emit an extremely narrow, intense beam of monochromatic light. Furthermore, since it operates at frequencies sensitive to atmospheric absorption, scattering, and variations in the index of refraction, the laser is the most promising instrument for obtaining a better understanding of the turbulent structure of the atmosphere.

To study the physics of the atmosphere using a space-borne light source is to study the character of a space-ground transmission path. The establishment of such a path is tantamount to establishing an optical communication link. Indeed, the most promising operational application for lasers is wideband communication over extremely long distances. By providing sufficient data transfer rates, the laser may make exploration of the remote planets feasible--and may thus assist in setting the post-Apollo national goals in space. But, before such vistas open, a foundation of space-borne optical communication engineering data must be obtained. The propagation experiments, singly and as a group, are advanced as a means for studying the Earth's atmosphere and for the development of alternatives in the field of communication.

Alternatives are developed at several levels. Collectively, the space-to-ground communication experiments provide a comparison of the two fundamental communication techniques: direct detection and heterodyne detection. Furthermore, the heterodyne experiment discussed here has been formulated on a scale sufficient to allow comparison between laser and radio frequency communication.

Within the experiment (figure 4.1-1), provision is made for combining various signal forms, coding and modulation methods for test under atmospheric constraints. Such tests require a space-borne transmitter. From the communication viewpoint, it is necessary to determine the capacity of the transmission medium. Statistical data must be gathered over periods of many hours and repeated for many days. Signal distortion measurements must be made through the entire sensible atmosphere, and results must be correlated with observable meteorological parameters. The atmospheric physics content of this experiment is predicated on near-zenith elevation angles.

Tests over horizontal paths on Earth and from high level balloons are prerequisite to the proposed space-borne experiment--but in themselves would be inadequate. Aircraft tests are not possible because the turbulence local to a lifting body would mask the effects to be measured and because of the aircraft vibration environment. Balloon testing eliminates the upper atmosphere from the transmission medium--an element which is critical to both

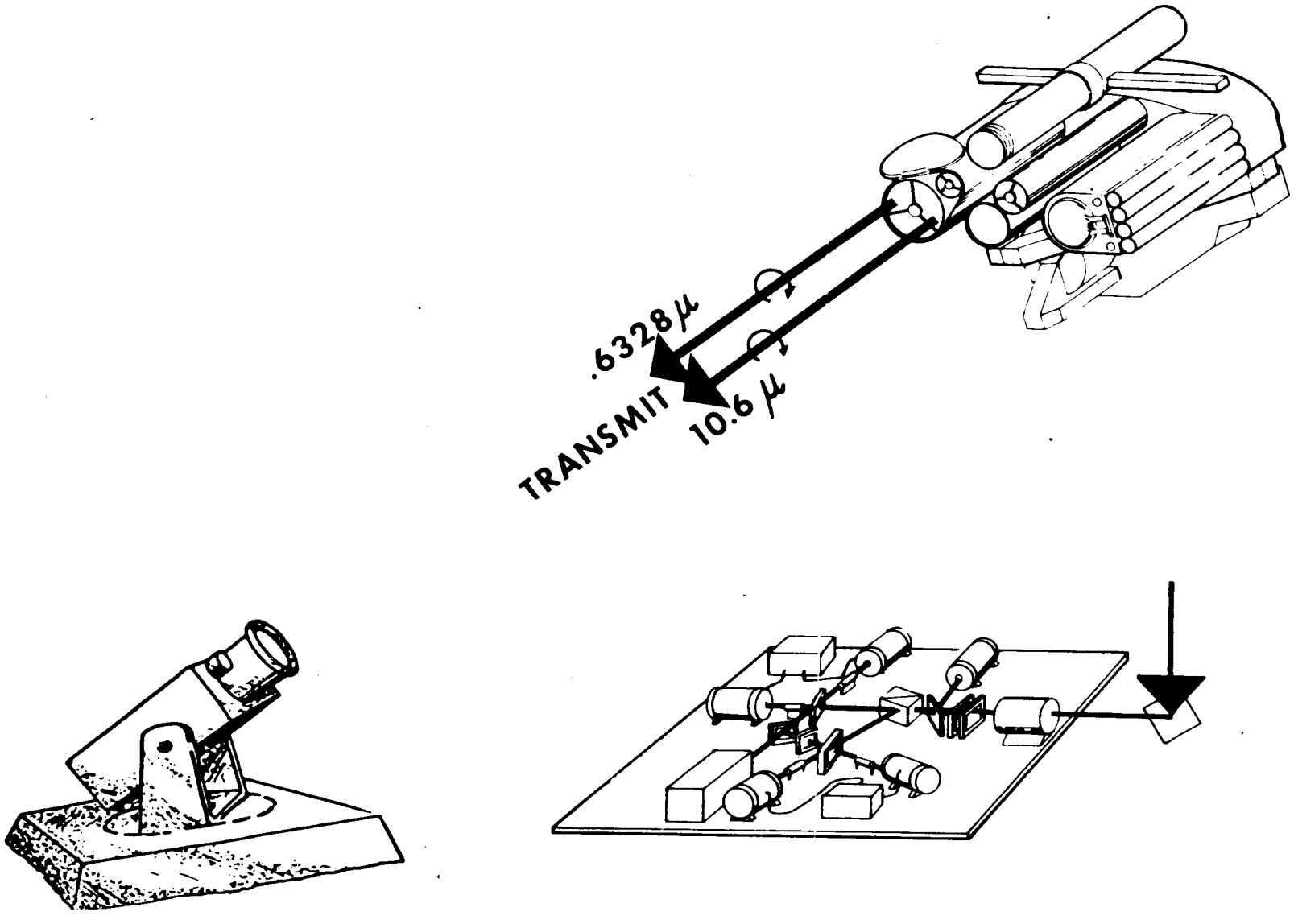

Figure 4.1-1. Heterodyne Detection on the Earth

the atmospheric physics purposes, in which upper air effects and turbulences constitute a primary class of unknowns, and to the communication theorist who seeks to reduce the total transmission medium to verify or refine the postulates in his simulations. Simulation of the space-to-Earth medium (and rigorous correlation of Earth-based test results) can not be fully credible until the empirical data to be derived from this Optical Heterodyne Detection on Earth experiment become available.

4.1.2 Experiment Objective

The objective of this experiment is to establish a heterodyne link from spacecraft to ground to permit: (a) measurements of the degradation of heterodyne signal strength and bandwidth capability caused by the atmosphere at several wavelengths simultaneously; and (b) comparison of potential forms of wideband planetary communication.

4.1.3 Experiment Justification

4.1.3.1 Contribution and Need

Manned exploration of the planets must be preceded by a significant increase in communication capability. A single voice channel requires a data rate of 10^4 bits per second, which now appears possible at Mars ranges using RF techniques.(1) However, it was recently stated that, to meet near future (1970-1980) interplanetary communications requirements, it would be necessary to develop information capacities greater than 10^7 bits per second.(1) In seeking such large advances in capability, it is well to pursue all promising technologies. In this way it is possible to guard against excessive cost and risk; and, hopefully, to provide options for the mission designer.

The most promising operational application for lasers is planetary communication. Because of its high radiant intensity, a laser communication system can achieve wide information bandwidths at great range. Since these ultimate advantages apply at extreme ranges, the potential of laser communication, and attendant developmental experiments, should be considered and evaluated in a planetary mission context. Clearly, it is desirable to conduct tests in Earth orbit which can be interpreted in the context of planetary mission applications.

For an Optical Heterodyne Communication System, the transmission equation is

$$\frac{S}{N} \times \Delta f = \frac{\eta q}{h\nu}\left(P_s\right) = \frac{\eta q}{h\nu}\left(\frac{D_r^2\, T_A T_o}{R^2\, \theta_t^2}\right)\left(P_t\right)$$

(1) M. C. Adams, Hearings before the Committee on Science and Astronautics, United States House of Representatives, Eighty-ninth Congress, February 23, 24, 25, and 28 through March 1, 2, 3, 7, and 8, 1966, Part 4, p. 97.

A. J. Kelley, "NASA's New Electronic Research Center," Astronautics and Aeronautics, May 1965, Vol. 3, No. 5, pp. 58-63.

H. E. Newell, Hearings before the Committee on Aeronautical and Space Sciences, United States Eighty-ninth Congress, March 22, 23, 24, 25, and 30, 1965.

Space Research Directions for the Future, Space Science Board, National Academy of Sciences, National Research Council, Part I Planetary and Lunar Exploration, Dec. 1965, c.f. p. 6, Deep Space Information Transfer; p. 59, Laser Communication Ibid, Part II Optical Astronomy, Jan. 1966, p. 96, Recommendation 11 of the Radio and Radar Astronomy Working Group.

where the local oscillator power is large, and the local oscillator beam fills the same solid angle as the receiving aperture diffraction-limited field of view. For practical reasons, it may become necessary to enlarge the local oscillator beam; and then the equation for the enlarged field heterodyne receiver is:

$$\frac{S}{N} \times \Delta f = \frac{\eta q}{h\nu k^2} \left(\frac{D_r^2 \; T_A T_o}{R^2 \; \theta_t^2} \right) \left(P_t \right)$$

where k = ratio of the actual field of view to the diffraction-limited field of view.

Using these expressions, a series of curves can be prepared to show the relationship of the Figure of Merit $\frac{S}{N} \Delta f$ to the spacecraft prime power required at earth synchronous orbit and at maximum Mars Distance, for a given set of assumptions. These assumptions are tabulated in table 4.1-1 for two important examples: the helium-neon wavelength of 0.6328 microns and the N_2-CO_2 wavelength of 10.6 microns.

Figure 4.1-2 compares the performance at the helium-neon wavelength for the Heterodyne System with the local oscillator beam sized to match the diffraction-limited field of view and for an enlarged field of view local oscillator beam. Figure 4.1-3 makes a similar comparison at 10.6 microns wavelength for the same sized transmitter aperture on the spacecraft. The performance of optical heterodyne communication links cannot be accurately predicted when the receiver is immersed in the Earth's atmosphere. The atmospheric effects are more severe than for a direct detection system, and they are not known for a long, high angle, slant path through the entire atmosphere.

TABLE 4.1-1

ASSUMED VALUES FOR OPTICAL HETERODYNE LINK CALCULATIONS

Parameters	Assumed Values		Units
Wavelength	0.6328	10.6	microns
D_t^*	100	100	cm
D_r	15	150	cm
θ_t	6.33×10^{-7}	1.06×10^{-5}	rad
θ_r	4.2×10^{-6}	7.1×10^{-6}	rad
T_A	0.5	0.5	--
T_o	0.5	0.5	--
$\Delta\lambda$	2×10^{-4}	40×10^{-4}	microns
k^2	1.2×10^{3}	400	--
ηq	5×10^{-2}	1×10^{-1}	--
η_t	8×10^{-4}	8×10^{-2}	--

*Transmitter Diameter

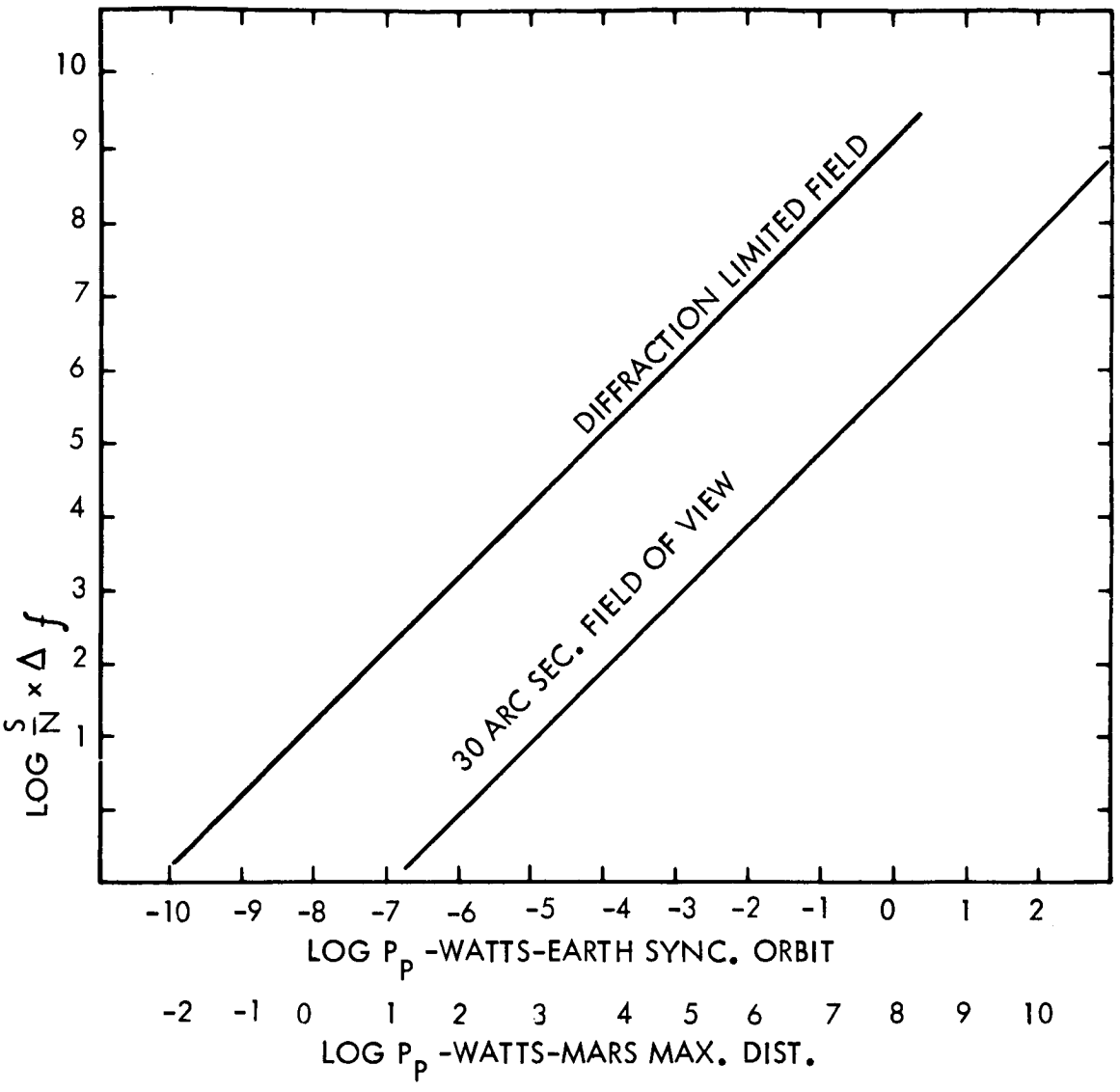

CONDITIONS:

PHOTOTUBE EFFICIENCY = 5×10^{-2}

TRANSM. APERTURE = 1.0 m

LASER EFFICIENCY = 8×10^{-4}

RECEIVING APERTURE = 0.15 m DIA

NARROW FIELD = .87 ARC SEC

ENLARGED FIELD = 30 ARC SEC

EARTH SYNC ORBIT = 3.6×10^{7} m

MARS MAXIMUM DISTANCE = 3.8×10^{11} m

Figure 4.1-2. Heterodyne Communication at 0.6328 μ

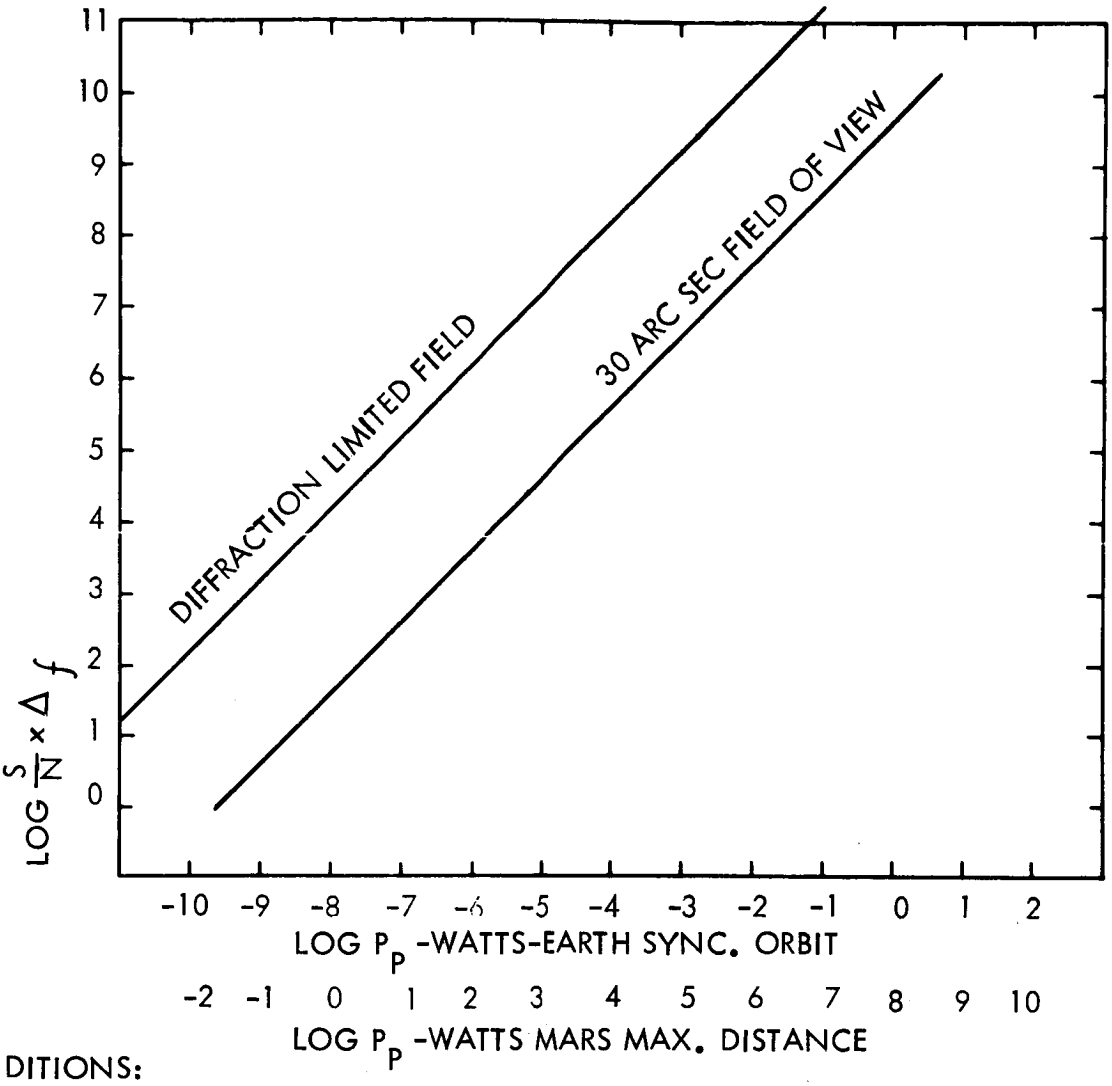

CONDITIONS:

DETECTOR EFFICIENCY = 1×10^{-1}

TRANSMITTER APERTURE = 1.0 m

LASER EFFICIENCY 8×10^{-2}

RECEIVING APERTURE 1.5 m DIA

NARROW FIELD =

ENLARGED FIELD = 30 ARC SEC.

EARTH SYNC. ORBIT = 3.6×10^{7} m

MARS MAXIMUM DISTANCE = 3.8×10^{11} m

Figure 4.1-3. Heterodyne Communication at 10.6 μ

The maximum useful size of a ground-based coherent receiver aperture depends strongly on these variables, and the measurements made with this link will give results that are extremely hard to predict theoretically. If large coherent collector apertures can be used at 10.6 microns, the efficacy of the highly efficient N_2-CO_2 laser is established. Fluctuations in angle of arrival can be measured and separated from scintillation in order to determine the effects of each. Measurements of pulse distortion and polarization fluctuation can be made. In addition, the optical phase noise over a long vertical path can be determined if sufficient frequency stability of transmitter and local oscillator lasers can be obtained. These effects will be established as functions of weather conditions and wavelength.

4.1.3.2 Need for Space Testing

The laser space-to-ground tests proposed for the OTAES vehicle must ultimately be done in space. One of the important objectives of the OTAES is to develop optical technology for space communication that is really relevant to future space mission design. If the mission designer is to have a set of viable alternate approaches to his communication link problems, OTAES must advance the optical technology to the point where it is technically and economically competitive with microwave or millimeter wave technology. Only then will a laser link become a real system alternative, worthy of serious consideration. As will be described in section 4.1.4.1 (Experiment Design), this requires that the optical technology be advanced to the point where at least a one-meter diameter transmitting telescope can be effectively utilized on board the spacecraft. Smaller apertures will not break even with projected microwave systems at interplanetary distances.

To measure the performance of a space-to-ground link using a one-meter transmitting aperture, as is proposed for OTAES, it is necessary that the ground receiver be located in the far field of the transmitting telescope. Taking the Rayleigh criterion, this Fraunhoffer region occurs at a range of approximately

$$R_f = \frac{2D_t^2}{\lambda} ,$$

where D_t is the transmitter aperture diameter and λ is the wavelength. For OTAES, this range is about 1000 kilometers. The amount of power transferred from the transmitter to a receiver in the near field is a complicated function and varies rapidly with angle and range. The effects of near-field focusing or defocusing as the vehicle changes position with respect to the ground station would complicate or mask the atmospheric variables to be measured.

For this reason, a synchronous orbit is desirable; it is well beyond the near-field limit for a one-meter transmitting telescope.

It is necessary to propagate optical frequencies through the whole atmosphere to measure its effect on heterodyne link performance. A distorted wavefront will have random displacements which will appear as a phase perturbation to any aperture parallel to the "average" phase front. For a sufficiently small aperture, the entire wavefront will arrive at an angle θ which will cause motion of the entire image in the focal plane of the lens. When the magnitude of this angle subtends a significant fraction of a wavelength across the receiving aperture, the advantages of the heterodyne technique are compromised. From measurements made by astronomers, θ has been found to be up to 3 arc seconds ($\approx 15 \times 10^{-6}$ radians) with the wavefront correlated up to a distance of 6 inches (15 cm), or more, under conditions of great image motion.

With these numbers assumed, a short calculation shows that the phase perturbation at any point:

$$\frac{2\pi\rho\theta}{\lambda} = \frac{2\pi \ .15 \ 15 \times 10^{-6}}{.6328 \times 10^{-6}} \quad 2\pi \ (3.5) \text{ radians}$$

which is greater than an optical wavelength. Because these phase jumps can occur in $\frac{1}{10}$ second intervals or less, frequency shifts of greater than 30 cycles per second can be expected under rather ordinary conditions. It is known, for example, that winds at 20,000 to 40,000 ft. contribute to the stellar scintillation observed on the ground and can be expected to affect the coherence of laser radiation as well. However, there is no conclusive proof that the total effect is introduced at these altitudes. From the viewpoint of space-to-earth propagation, the total effect is of primary importance, including increments derived from the stratosphere. Once bounded, it is then amenable to detailed empirical analysis.

Because it is desirable to have the aperture parallel to the average wavefront, the technique of tracking the source in angle was examined. Assuming that it was desirable to keep the tracking noise down to say $\frac{1}{10}$ of the expected phase deviation to be measured would require, for a one-meter aperture, tracking accuracy of better than .25 micro-radians $\left(\approx \frac{1}{20} \text{ sec}\right)$ which is nearly the goal for the spaceborne precision tracking experiment and does not seem to be a reasonable objective for ground-based instrumentation.

The effects of the atmosphere in a long vertical path cannot be adequately predicted by the results of laser propagation tests on long horizontal paths in the lower atmosphere. The structure and scale of turbulence is very different along the two paths, and present theory is not yet able to predict all of the effects observed on a horizontal path. A nearly stationary Earth synchronous satellite vehicle is desired for this experiment. This will allow measurements to be made over a sufficiently long time to obtain statistically meaningful data, as well as to monitor minute-by-minute changes in atmospheric conditions with a fixed line-of-sight. Measurement from lower altitude vehicles would be complicated by large angular tracking rates. This produces sources of excess phase noise, due to both the physical motion and vibration of the tracking pedestal, and to the movement of the optical line-of-sight through the atmosphere. Correcting for these effects is difficult or impossible, masking the true properties of a stationary LOS.

High-altitude balloon tests could give useful results, within the dynamic constraints of this type of vehicle, for lower atmosphere ($< 60{,}000$ ft.) effects. Aircraft tests are not possible because the turbulence local to a lifting body would mask the effects to be measured and the high vibration environment aboard the aircraft will destroy the frequency stability of the lasers on board. A realistic test in a space environment will be necessary to obtain data directly applicable to an assortment of eventual operational feasibility.

4.1.3.3 Feasibility

The 10.6-micron link represents the highest degree of technical risk in this experiment. No element of such a link has been space tested. Present detectors such as gold or mercury-doped germanium operate, at cryogenic temperatures, with bandwidths less than one MHz. Modulators for this wavelength are just now emerging, although 100 kHz frequency modulation of the laser itself is possible using piezoelectric crystals to drive the end mirrors. Very few transmission materials are available and those refractive elements which have been tested have proven difficult to fabricate. Although the 10.6 micron link has the greatest

potential for deep space application, from the standpoint of reliability, the Heterodyne Detection on Earth experiment has been designed to rely most heavily on the 0.6328-micron link.

Thus, from an experiment viewpoint the critical element is the Helium-Neon link. At 0.6328 microns all necessary components and their coatings are adequately developed and, in the case of optical elements and beam splitters, have already been proven in space. Optical heterodyne links have been demonstrated under field conditions on earth.[2] Only the laser, the modulator and the heterodyne technique itself now require space testing.

A technology plan is advocated herein which would test these components, and a rudimentary heterodyne space-to-ground link, in an early, piggyback experiment. Such a procedure, and the preceding development efforts which it implies, would serve to eliminate much of the risk associated with the 0.6328 micron portion of this experiment. It appears that the highest element of risk may be the frequency stability of the lasers in both transmitter and receiver, a deficiency which could be partially solved through acoustic decoupling from their surroundings.

4.1.4 Implementation

4.1.4.1 Experiment Design

A space-to-ground link will be established. The ground-based receiver will use both optical heterodyne and direct detection of the signal transmitted from the spacecraft. The spacecraft may transmit several laser wavelengths simultaneously, and they will all be processed through the same ground receiving telescope aperture.

Several parameters will be measured at each receiver. They are:

(a) amplitude fluctuation of the heterodyne signals;

(b) intensity fluctuation of the direct signals (total received energy fluctuation);

(c) frequency (or phase) fluctuations in the heterodyne signals;

(d) receiving aperture size and field of view;

(e) atmospheric conditions such as temperature profile, winds aloft, haze conditions.

These parameters can be combined to give further results:

(a) heterodyne mixing efficiency: the degradation of heterodyne efficiency can be found by normalizing the instantaneous heterodyne signal to the total received power level;

(b) polarization fluctuation: since each direct and each heterodyne receiver is sensitive to orthogonal polarizations, any differential treatment by the atmosphere can be detected.

The block diagram of the equipment required for the Optical Heterodyne Detection on Earth experiment is shown in figure 4.1-4. The spacecraft transmitter will be made up of the following subsystems: 1) single frequency laser with its power supply, mode stabilization

(2) R. F. Lucy, C. J. Peters, E. J. McGann, and K. T. Lang, "Precision Laser Automatic Tracking System," Applied Optics, April 1966, Vol. 5, pp. 517-524.

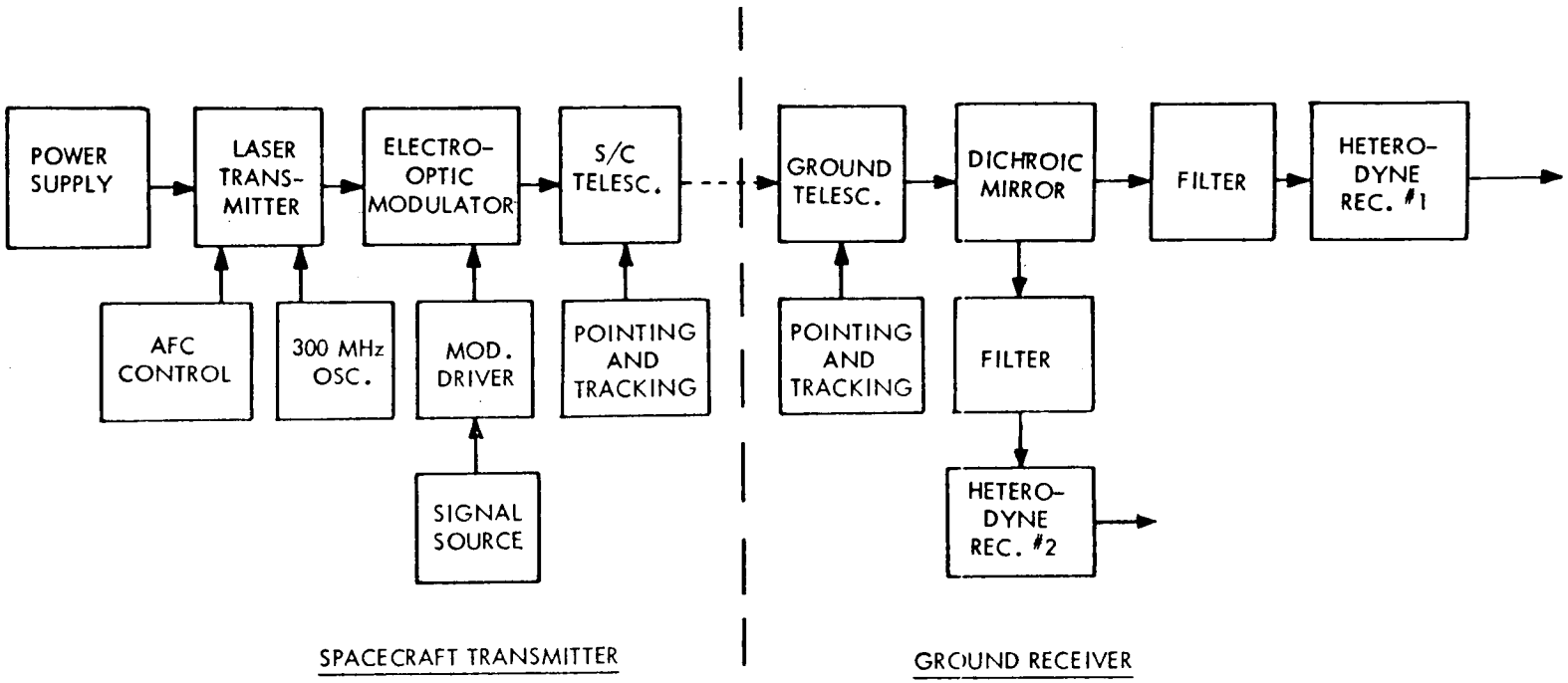

Figure 4.1-4. Block Diagram of Heterodyne Detection on Earth Experiment - 0.6328 μ

controls, and automatic frequency control; 2) electro-optic modulator with the modulator driver, power supply, and signal source; and 3) telescope, including secondary optics, beam deflection subsystem, and pointing and tracking controls. The ground receiver will be made up of the following subsystems: 1) ground telescope, including its secondary optics, beam deflection subsystem, and pointing and tracking controls; 2) dichroic mirror; 3) optical filter; and 4) duplex heterodyne receiver.

The single frequency laser configuration is shown in figure 4.1-5. The cavity length will be 50 centimeters, giving a spacing between axial modes of about 300 MHz. The current-regulated power supply for the discharge tube will operate at about 1500 volts and provide 20 ma of current. The phase modulator will be driven by an oscillator operating at slightly higher frequency than 300 MHz to provide energy coupling between the modes of the laser. The interferometer mirror is spaced from the end mirror by about one millimeter to form a Fabry-Perot etalon output coupler that will be tuned to transmit only the selected frequency occurring near the center of the resonance band. The automatic frequency control drives the moveable mirror to adjust the cavity length so that the single mode output occurs near the center of the resonant band and may also be used to control the etalon. The output of the laser will be a single wavelength, plane polarized and centered in the fluorescence band of the excited gas.

Referring again to figure 4.1-4, the electro-optic modulator contains an electro-optic crystal and quarter-wave plates arranged so that the application of the modulation signal alters the optical properties of the crystal. The output of the modulator will be plane-polarized light. The output may be amplitude modulated or polarization modulated. The modulation bandwidth will be in excess of 10 MHz.

The one-meter diameter telescope will contain the necessary secondary optics to circularly polarize and position the beam and to diverge it to fill the primary mirror. This will form a collimated beam, diverging at the diffraction-limited rate.

The need for a one-meter, diffraction-limited aperture on the spacecraft is derived from the second objective of this experiment: to demonstrate a potential form of wideband planetary communication. Taking the ratio of the well-known Friis transmission expressions for optical and microwave communication gives:

$$\frac{\left(\frac{S}{N}\right)_o}{\left(\frac{S}{N}\right)_m} = \frac{\epsilon_{ot} A_{to} \lambda_m^2 A_{ro} kT}{\epsilon_m A_{tm} \lambda_o^2 A_{rm} h\nu/q}$$

In table 4.1-2 the various terms of this relation are evaluated from the viewpoint of microwave optimism (e.g., a 100-meter, X-band receiving aperture on the Earth; a 30-meter X-band transmitter on the spacecraft; a 100° receiver noise temperature; a 50%, X-band transmitter efficiency, etc.). These assumed characteristics are contrasted with 0.6328-micron laser communication components which could be fabricated today. The noise, receiving aperture, and transmitter efficiency ratios (23.5 + 20.0 + 20.5 = 64.0 dB) are inherently advantageous to the microwave technology. Only the wavelength (93.5 dB) term favors the optical technique. Thus, a favorable comparison of optical communication with microwave communication cannot be made with apertures less than one meter, and this choice imposes the 0.1 arc second pointing requirement. The Helium-Neon, single frequency laser, the one-meter diffraction-limited aperture and the 0.1 arc second pointing system combined in a single earth orbital test, will make a significant basis for comparison between microwave and optical techniques for wideband planetary communication.

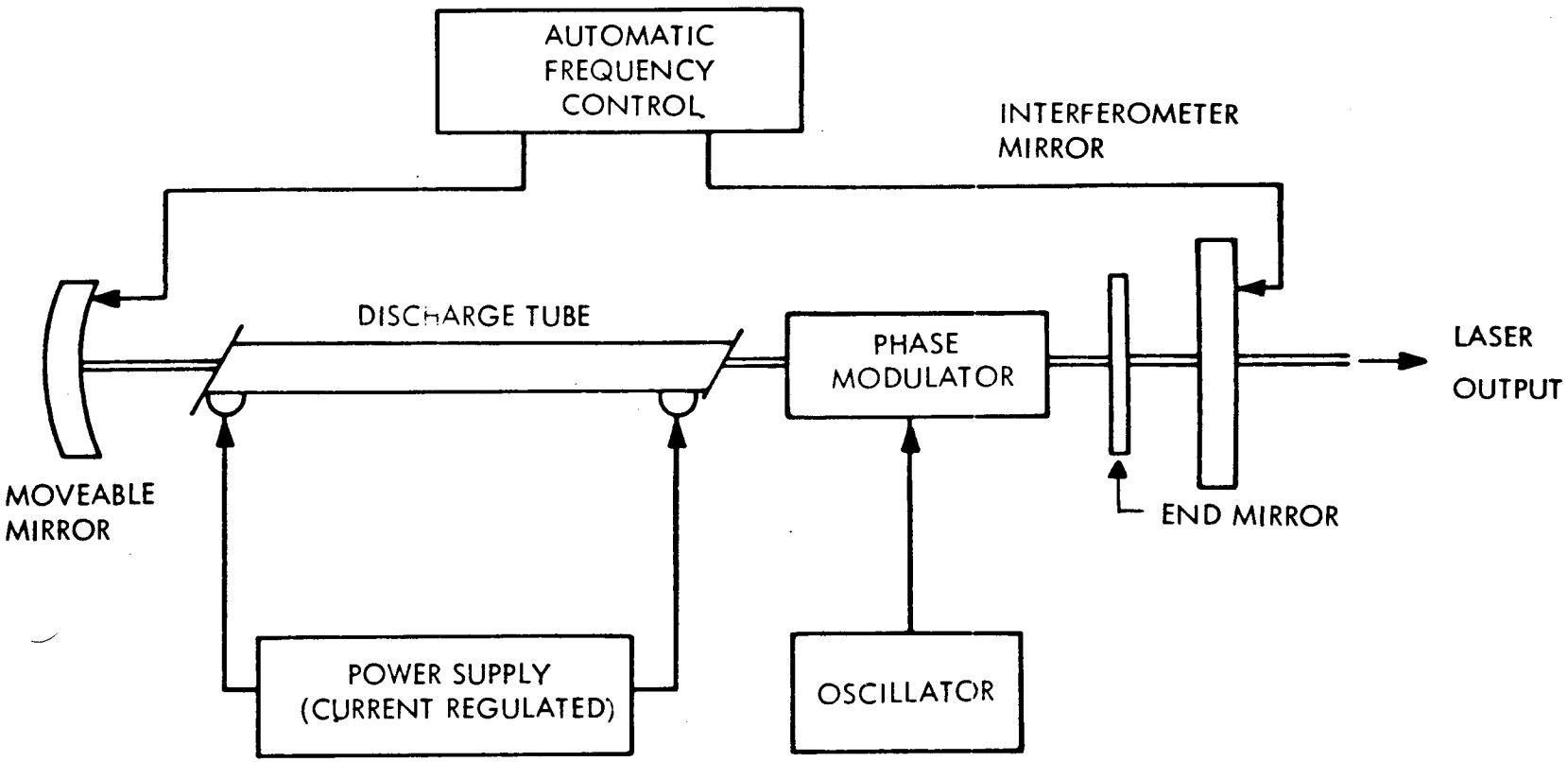

Figure 4.1-5. Super-Mode Laser - 0.6328 μ

TABLE 4.1-2

COMPARISON PARAMETERS

	$\frac{K_T}{h\nu/q}$	$\frac{A_{ro}}{A_{rm}}$	$\frac{\epsilon_o}{\epsilon_m}$	$\frac{\lambda_m}{\lambda_o}$	$\frac{A_{to}}{A_{tm}}$
OPTICAL	A_t 6328Å $h\nu = 3.12 \times 10^{-19}$ Joules $q = 0.05$	D = 10 Meters $A_{ro} = 78.5 m^2$	0.0045	$\frac{\lambda_o^2}{m^2} = 4 \times 10^{-13}$	D = 1 Meter 0.785 m^2
MICROWAVE	AT 100°K 1.38×10^{-21} Joules	D = 100 Meters $A_{rm} = 785 m^2$	0.5	$\frac{\lambda_m^2}{m^2} = 9 \times 10^{-4}$	D = 30 Meters $A_{rm} = 706 m^2$
dB:	+23.5	+20	+20.5	-93.5	+29.5

ϵ = transmitter efficiency

A = Aperture area

λ = wavelength

k = Boltzmann constant

h = Planck's constant

ν = frequency

q = quantum efficiency

T = receiver noise temperature

r = receiver

t = transmitter

o = optical

m = microwave

The receiving telescope will have a diameter larger than the largest coherence diameter expected in the atmosphere. The aperture will be variable to permit matching of it to the coherence diameter of the atmosphere. The dichroic mirror will be used to pass the energy at wavelength #1 to receiver #1 and reflect energy at wavelength #2 to receiver #2. Figure 4.1-6 is an optical schematic of the duplex heterodyne receiver. The filter is used to eliminate most of the background radiation which might otherwise overload the detectors under high background levels. The filter passband will be in the order of 40 Angstroms wide. The quarter-wave plate will convert the circularly polarized light to plane-polarized light. The light entering the polarization analyzer will contain horizontally and vertically polarized light. The analyzer will separate the two planes of polarization, transmitting the vertically polarized light and reflecting the horizontally polarized light. The detection for each plane of polarization is identical. The light falls on a beam splitter that will transmit and reflect equally. The energy from the local oscillator will also be divided by the beam splitter. The light energy then will fall on the photodetectors, and the difference frequency will be produced at the photodetector output. The photodetectors and the output processing to the summing point must be balanced so that the output will be an accurate sum of the duplexed signal. Since the light energy undergoes a 180^{o} phase shift when reflected from the beam splitter, a compensating 180^{o} phase shift is introduced before summing takes place. The duplexing technique makes total use of the incoming signal, providing improved signal-to-noise performance.

The major equipment necessary for this experiment (figure 4.1-7) is listed below:

Spaceborne Equipment:

Single-frequency laser transmitters operating at 0.6328 and 10.6 microns with minimum power outputs of 10 milliwatts and 10 watts, respectively.

3 High-voltage DC power supplies, one for each laser

3 Cavity tuning control and stabilization circuits for mode-lock or single-frequency operation

1 In-cavity modulator for mode-locked operation at 0.6328 microns

1 Modulator driver amplifiers for mode-locked operation

2 On-board video detectors and preamplifiers for 0.6328 and 3.39 microns

2 Output power monitor detectors, one for each wavelength

2 Video modulators for 10 MHz communication

2 Transmitting telescopes: 1 meter diameter at 0.6328 microns, 0.3 meter diameter at 10.6 microns

Ground-Based Equipment:

1 Tracking telescope of nominal one-meter aperture, having all reflective optics. Tracking and fine pointing to $\pm$ 5 microradian capability

2 Heterodyne receivers, mounted on the telescope

3 Single-frequency laser local oscillators, operating at 0.6328 and 10.6 microns

3 High-voltage DC-laser power supplies for each laser
(Cavity control and stabilization circuits for each laser)

4 High-speed photodetectors for each wavelength
(Amplifiers and signal processing circuits for each channel)

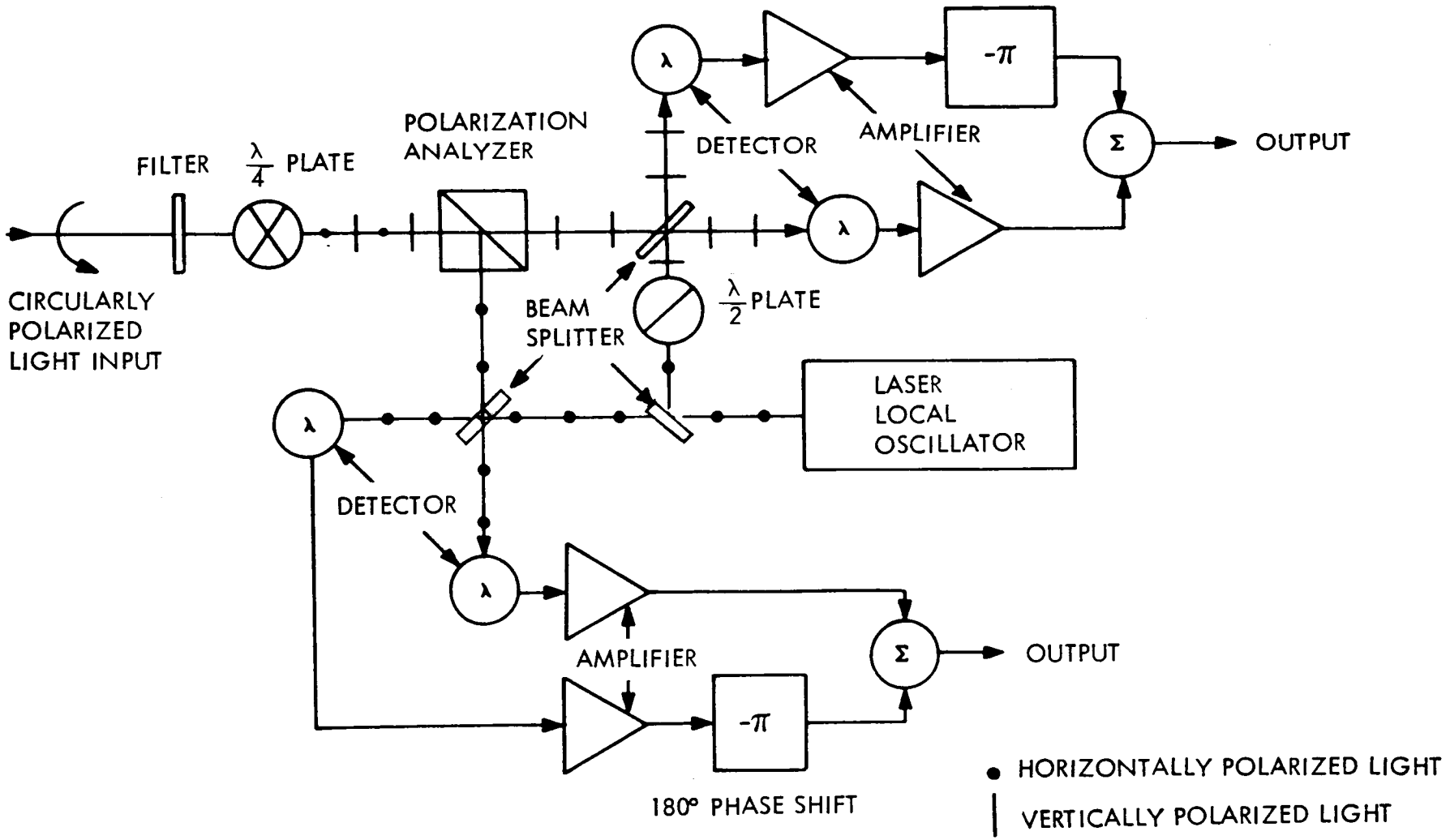

Figure 4.1-6. Optical Schematic Duplex Heterodyne Receiver

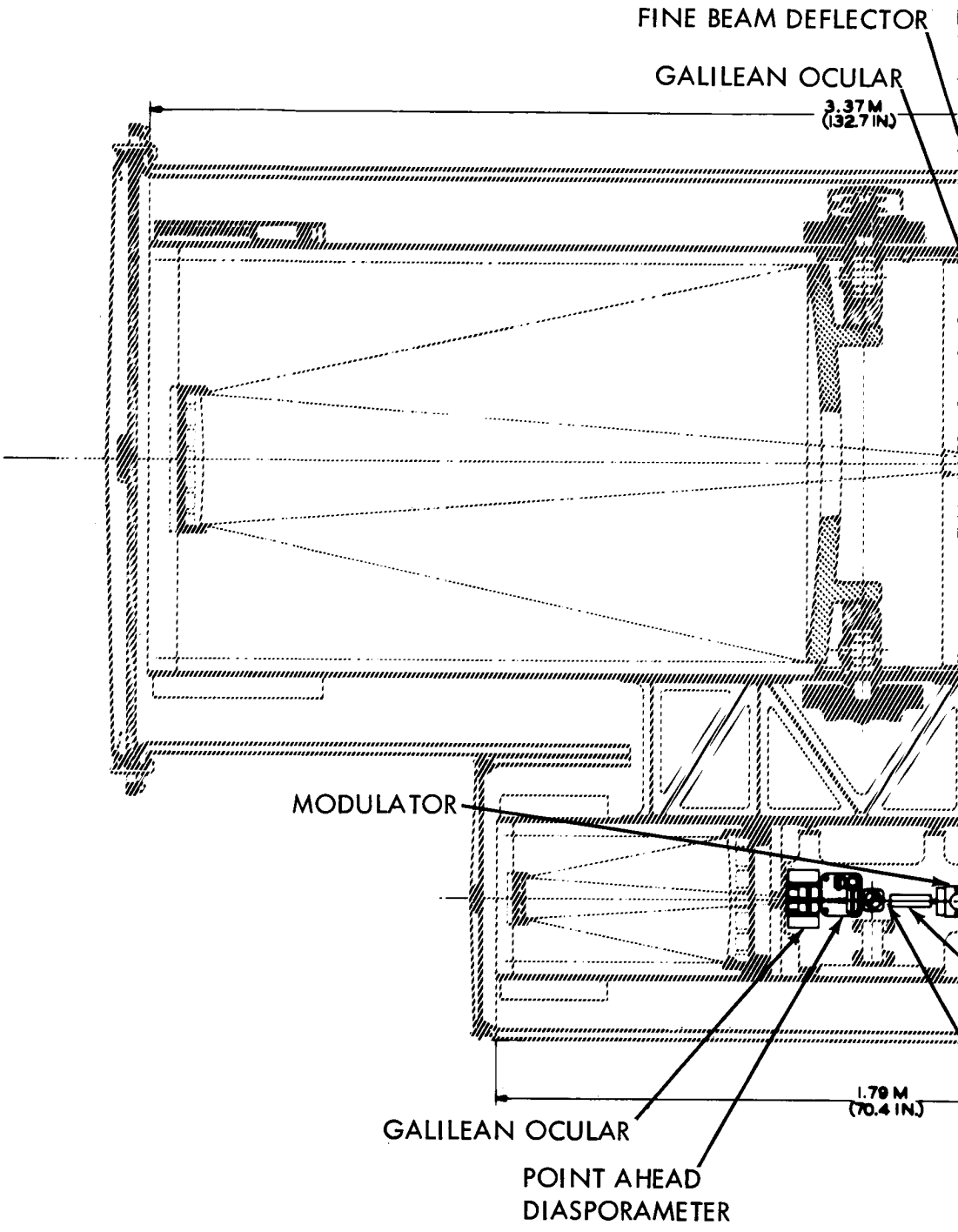
FINE BEAM DEFLECTOR
GALILEAN OCULAR
3.37 M
(132.7 IN.)
MODULATOR
1.79 M
(70.4 IN.)
GALILEAN OCULAR
POINT AHEAD
DIASPORAMETER

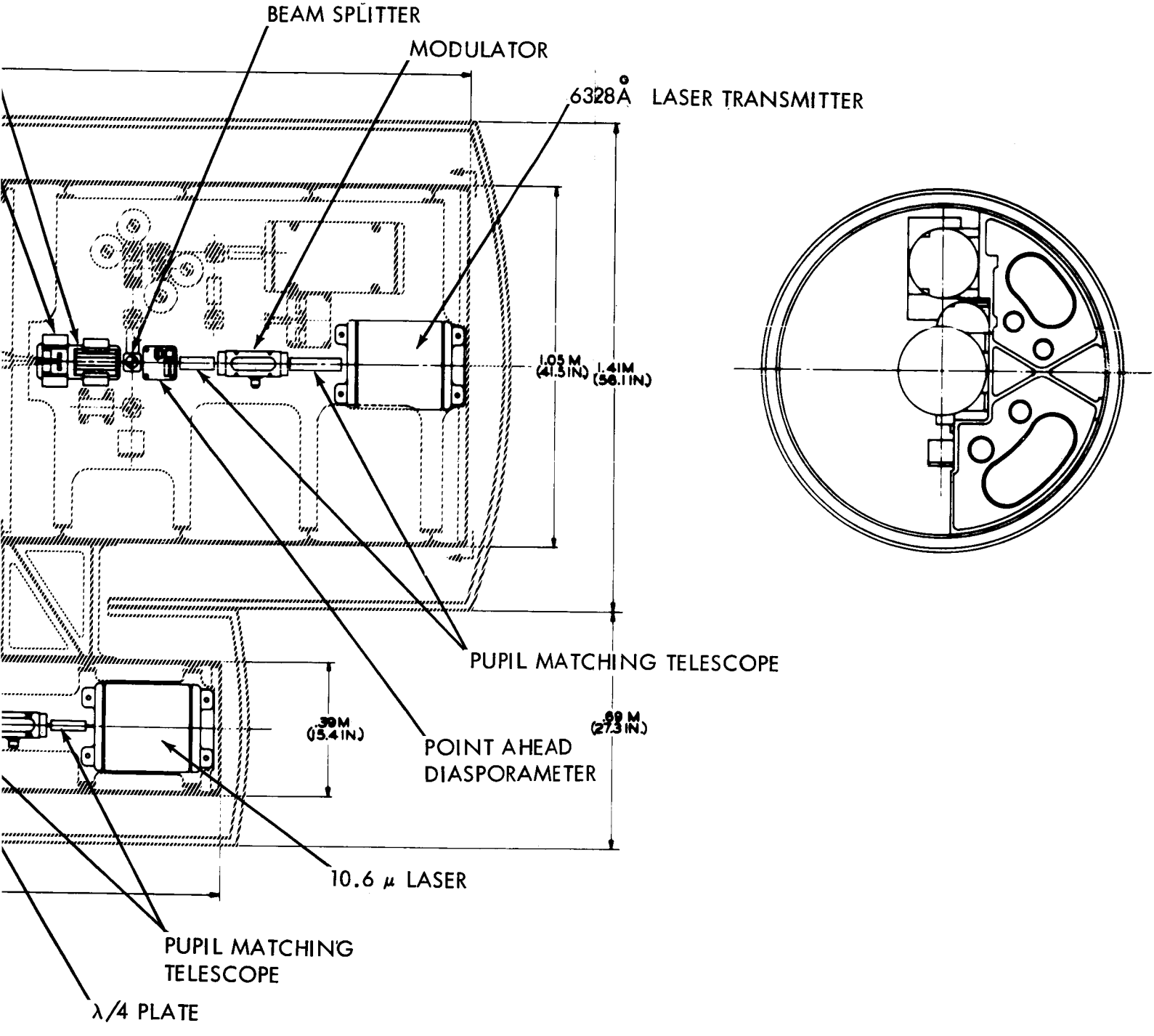

Figure 4.1-7. Telescope Numbers 1 and 2

4.1.4.2 Operational Procedure

Tasks:

(1) Begin recording atmospheric conditions above ground site.

(2) Turn on spacecraft lasers, allow to come to thermal equilibrium with telescope and spacecraft. (Est. 4 hours.)

(3) Turn on ground-based laser local oscillators for warm-up. (Est. 2 hours.)

(4) Turn on in-cavity modulators, allow to come to thermal equilibrium. (Est. 1/2 hour.)

(5) Turn on video modulator(s) for thermal equilibrium (Est. 1/2 hour) if 10 MHz communication experiment is to be performed. (All thermal delay times depend strongly on spacecraft package design. It may be preferable to leave the lasers running all the time, if possible.)

(6) Select the combination of beams to be transmitted. (10 seconds.)

(7) Orient spacecraft telescope(s) toward the Earth, acquire ground beacon, begin fine tracking. Acquire and track at the ground station. Reduce the spacecraft angular rates as close as possible to the tracking rates so that no corrections are needed from vibration-producing thrusters (see timeline).

(8) Turn on laser cavity AFC control. (10 milliseconds.)

(9) Turn on laser mode-lock and single-frequency control circuits. (10 milliseconds.)

(10) Select (tune) operating frequency of each laser. (One minute.)

(11) Begin recording of data from ground-based receivers. (Up to 24 hours, as indicated in timeline, see figure 4.1-8.)

4.1.5 Supporting Analyses

4.1.5.1 Optical Propagation Measurements

The development of experiments involving the propagation of electromagnetic energy at optical wavelengths is logically followed by an evaluation of means for performing the experiments. During the concept stage, the feasibility of performing the experiment was considered, and a cursory estimate was made of the equipment required. To advance an experiment to Level II, it is necessary to determine the experimental equipment that will be needed and to develop an overall system concept for the implementation of experiments. The following sections record the extent of these studies.

The need for a laser source is inherent to several of these experiments. These needs have been reduced to performance characteristics. Several laser types have been evaluated, and recommendations have been made for their application. The tentatively selected laser wavelengths cover a frequency spectrum of over 4 octaves.

For purposes of comparative evaluation, the Heterodyne Detection Communication System has been defined, based on the assumption of a 1.0 meter primary mirror on the spacecraft, and a somewhat smaller primary mirror on the ground, for space-to-ground communication. The useful size of the ground mirror is limited by the atmospheric effects on the spatial coherence of the communication beam. For ground-to-space heterodyne communication, a 1.0

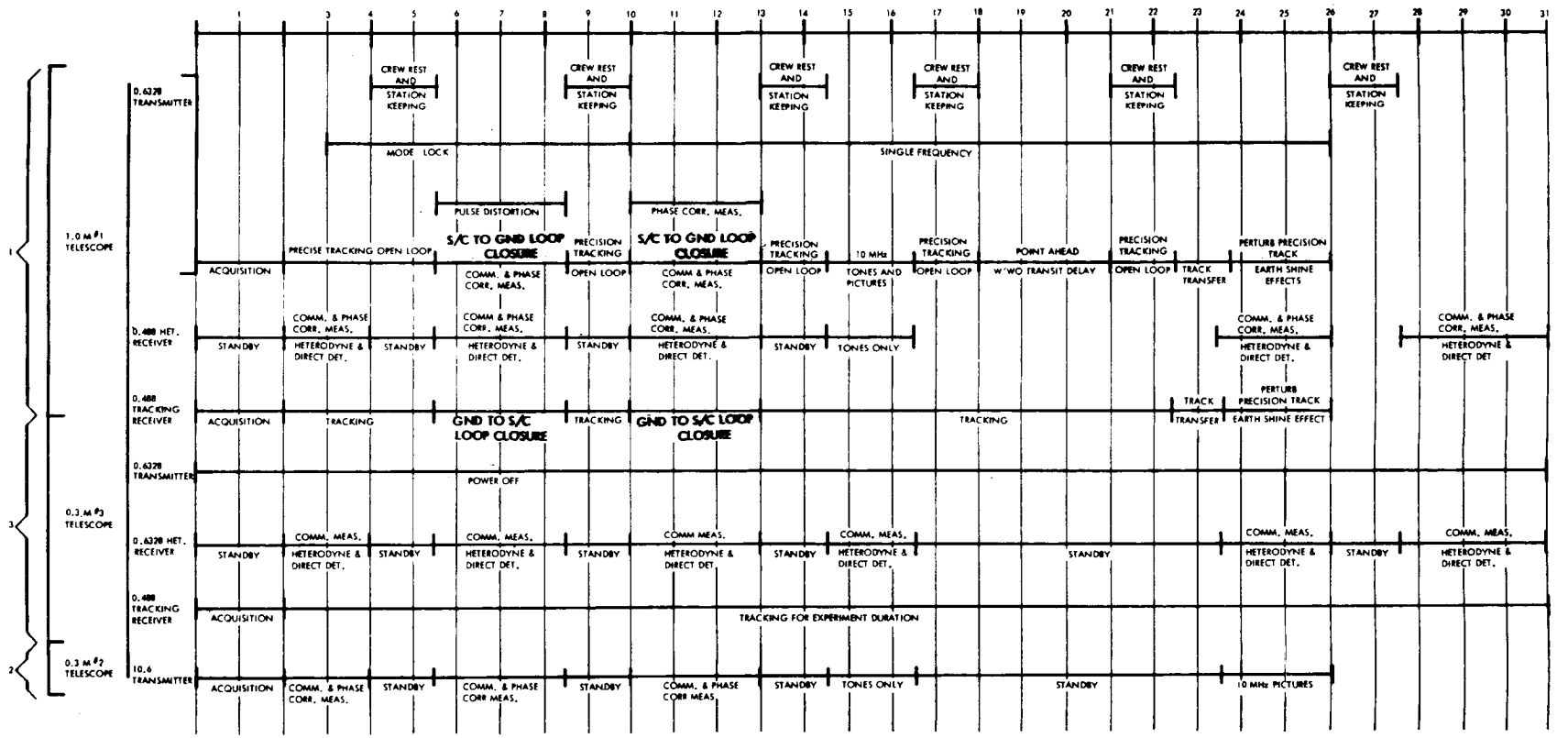

Figure 4.1-8. Activity Timeline During Optical Communication Telescope Experiments.

meter mirror should be adequate for the transmitter on the ground if the same 1.0 meter spacecraft down-link mirror will be used for the receiver. It is planned to implement the receivers with duplex polarization detectors to provide the capability needed to measure atmospheric effects on propagation.

The Direct Detection System has been developed primarily for the space-to-ground link. This will use the spacecraft transmitter for the Heterodyne System although the Direct Detection System transmitter requirement is not as stringent as the heterodyne requirement. The ground receiver will, typically, use an 8-meter diameter collector. It will be a crude optical system made up of a number of identical segments which can be aligned to provide a circle of confusion of about 5 millimeters. Performance of the Direct Detection System during Earth Orbit experiments will be significantly better than the heterodyne system, when the background is negligible.

4.1.5.1.1 Optical Communication Analyses

The performance of the Heterodyne and Direct systems can be compared by using a normalizing Figure of Merit: the product of "Bandwidth" Δf and "Signal-to-Noise" (S/N). This Figure of Merit is particularly useful since it can be derived directly from system requirements.

Heterodyne detection at optical frequencies is possible only with laser radiation, and uses a second laser at the receiver to act as a local oscillator, in exactly the way that heterodyne receivers at lower RF frequencies are operated. AM or FM modulation on the light is converted to the same modulation on an intermediate frequency carrier, and processed by conventional electronic techniques.

In direct, or energy detection, AM modulation on the light beam is detected directly by a photocell that is sensitive to changes in input beam power. This is analogous, in the RF spectrum, to the early crystal sets.

The heterodyne technique has all of the advantages at optical frequencies that it does at RF: higher sensitivity and selectivity than direct detection, but it is also limited in performance because of atmospheric turbulence effects, which is not true of direct detection systems.

The choice of which technique to use depends on several factors, such as:

a) required channel bandwidth

b) background radiance levels

c) wavelength of operation

d) atmospheric turbulence.

It will be shown where these factors affect the choices to be made.

4.1.5.1.2 Achievable S/N x Δf for Various Systems

4.1.5.1.2.1 Case 1, Direct Detection

As Case 1, the S/N ratio for an optical communication link using Direct Detection is given by

$$\frac{S}{N} = \frac{1/2\left(\eta_q e/h\nu\right)^2 P_s^2 M^2 R_{eq}}{kT\Delta f + 2e\Delta f\left(\eta_q e/h\nu\right)\left[P_s + P_b\right] M^2 R_{eq}}$$

where

η_q = detector quantum efficiency, charge carriers released per incident photon

e = electron charge (coulombs)

$h\nu$ = energy of a photon of frequency ν (joules)

P_s = received signal power at the detector (watts)

M = detector multiplication gain, if any

R_{eq} = detector equivalent output resistance (ohms)

k = Boltzmann's constant (joule/degree Kelvin)

T = absolute temperature of the detector, including its equivalent output resistance

Δf = information bandwidth (hertz)

P_B = received optical background power (watts)

The product of S/N and Δf will be used as a Figure of Merit for the link.

It can be shown that the thermal noise term in the denominator can be neglected, to get:

$$\frac{S}{N} \times \Delta f = \frac{\eta_q}{4h\nu} \frac{P_s^2}{\left(P_s + P_B\right)}$$

P_s is related to the transmitted optical power, P_t, by geometry and losses in the atmosphere and the receiving optical system

$$P_s = P_t \times \frac{D_r^2 \, T_A T_o}{R^2 \, \theta_t^2}$$

where

D_r = diameter of the receiving aperture (cm)

T_A = atmospheric transmission

T_o = optical system transmission, including filters

R = range from transmitter to receiver (cm)

θ_t = transmitted beam angle; the full cone angle between half power points (radians).

While P_B is a function of background radiance and receiver "throughput," which is the product of collector area and solid angle:

$$P_B = \frac{\pi^2}{16} D_r^2 \theta_r^2 N_\lambda \Delta\lambda$$

where

θ_r = receiver angular field of view (radians)

N_λ = background spectral radiance (watts/cm^2-ster-$\mathring{A}$)

$\Delta\lambda$ = receiver optical filter bandwidth ($\mathring{A}$)

So that the expression for S/N x Δf becomes

$$\frac{S}{N} \times \Delta f = \frac{\eta_q D_r^4 T_A^2 T_o^2 P_t^2}{4h\nu R^4 \theta_t^4 \left[\frac{D_r^2 P_t T_A T_o}{R^2 \theta_t^2} + \frac{\pi^2}{16} \theta_r^2 N_\lambda \Delta\lambda \right]}$$

This complicated expression can be viewed rather simply. There are two alternative "modes" of operation for such a direct detection system: (a) background light dominates the noise, so that the first term in the brackets of the denominator can be neglected; or (b) the signal energy itself is the source of the limiting noise in the system, and the second denominator term is negligible. The region where received signal and background power levels are nearly equal is a smooth transition between two extremes.

For case (a), large background or small signal powers, S/N x Δf is given by

$$\frac{S}{N} \times \Delta f = \left(\frac{\eta_q}{4h\nu} \right) \left(\frac{D_r^2 T_A T_o}{\theta_t^2 R^2} \right) \left(\frac{T_A T_o}{\theta_t^2 R^2} \right) \left(\frac{P_t^2}{\frac{\pi^2}{16} \theta_r^2 N_\lambda \Delta\lambda} \right)$$

For case (b), small background or large signal powers, S/N x Δf is given by

$$\frac{S}{N} \times \Delta f = \frac{\eta_q D_r^2 T_A T_o}{4h\nu R^2 \theta_t^2}$$

which is independent of receiver field of view, θ_r, as expected. These relations are plotted in figure 4.1-9 showing Log S/N x Δf vs log P_t for various background power levels. The units are arbitrary, and the figure is intended only to show the form of the dependence.

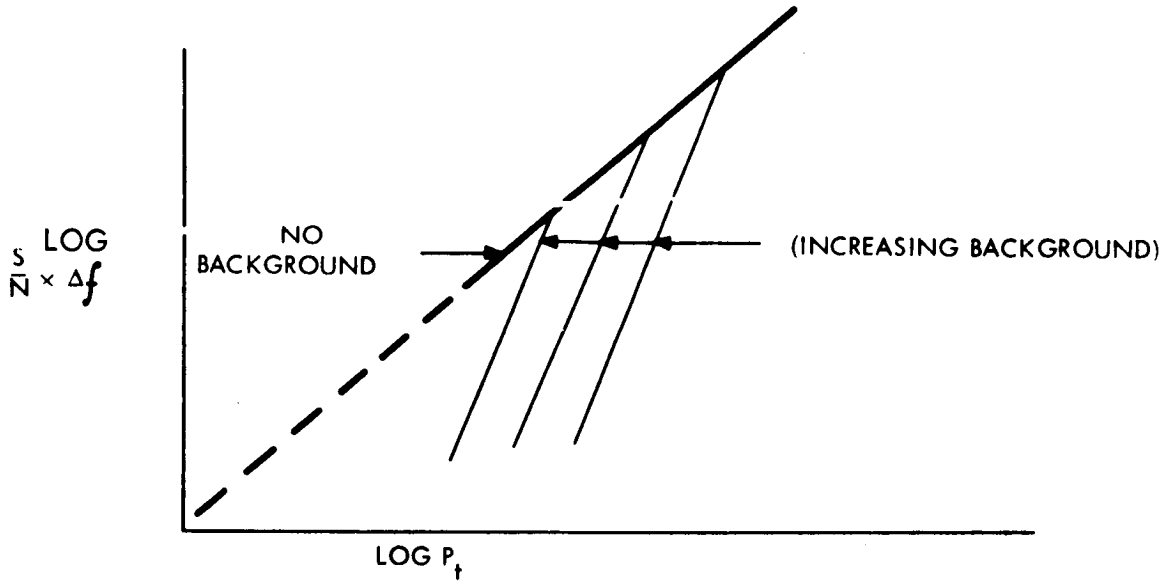

Figure 4.1-9. Log S/N Δf vs. Log P_t for Various Background Power Levels

4.1.5.1.2.2 Case 2, Heterodyne Detection

For Case 2 the same type of analysis is done for a link using Heterodyne Detection. The general expression for S/N is:

$$\frac{S}{N} = \frac{\left(\eta_q e/h\nu\right)^2 \, 2P_s \, P_{LO} \, M^2 \, R_{eq}}{kT\,\Delta f + 2e\Delta f\left(\eta e_q/h\nu\right)\left[P_s + P_B + P_{LO}\right] \, M^2 \, R_{eq}}$$

where P_{LO} is the optical local oscillator power incident on the detector (watts).

As before we may neglect the kT noise term to obtain the S/N x Δf product as

$$\frac{S}{N} \times \Delta f = \frac{\eta_q \, P_s \, P_{LO}}{h\nu\left(P_s + P_B + P_{LO}\right)}$$

When P_{LO} is large compared to the other terms in the denominator, which is the only case of interest in heterodyne detection, the expression reduces to

$$\frac{S}{N} \times \Delta f = \frac{\eta_q}{h\nu} P_s$$

or, in terms of the link geometry,

$$\frac{S}{N} \times \Delta f = \frac{\eta_q \, D_r^2 \, T_A T_o \, P_t}{h\nu \, R^2 \, \theta_t^2}$$

It should be noted that this result is very nearly the same as the low-background case for direct detection.

The result above assumes that the receiving aperture is fully utilized, i.e., that the arriving laser signal beam is concentrated into a spot on the detector that is as small as the diffraction limit for the receiving aperture, and, further, that all of the laser local oscillator light is concentrated in the same spot and mixed with the signal with full efficiency. These conditions can never be met in practice for a receiving system immersed in the Earth's atmosphere. Fluctuations in atmospheric density and index of refraction cause variations in the phase coherence between points only a few centimeters apart. The receiving system sees the result as fluctuations in mixing efficiency, due to either momentary phase cancellation between different sections of the beam or changes in the angle of arrival.

The field of view of an ideal diffraction-limited heterodyne receiver is equal to the limit of resolution of the collecting optical system, and this becomes impractically small if the aperture diameter is more than a few centimeters. It is, however, possible to enlarge the field of view by spreading the local oscillator beam so that it fills a solid angle

larger than the diffraction limit of the aperture. This technique allows the receiver to operate reliably with reduced sensitivity, and largely eliminate the susceptibility to angle of arrival fluctuations. Only a fraction of the local oscillator light will mix with the signal at any one time.

The S/N x Δf achievable under these conditions is given by

$$\frac{S}{N} \times \Delta f = \frac{1}{k^2} \frac{\eta_q}{h\nu} P_s$$

where k is the ratio of the actual field of view to the diffraction-limited field of view.

Figure 4.1-10 shows the relation between log S/N x Δf and log P_t for the ideal heterodyne and enlarged field heterodyne receivers. It is seen that there is no dependence on background radiance as would be expected, and which is one of the great advantages of heterodyne detection.

4.1.5.1.3 Comparison of Direct and Heterodyne Detection

The table below summarizes the results obtained so far:

Case 1 No Background Diffraction Limited Operation	$\frac{S}{N} \Delta f = \frac{\eta_q}{h\nu} \frac{D_r^2 T_A T_o}{R^2 \theta_t^2} P_t$	$\frac{S}{N} \Delta f = \frac{\eta_q}{4h\nu} \frac{D_r^2 T_A T_o}{R^2 \theta_t^2} P_t$
Case 2 No Background Enlarged Field of View	$\frac{S}{N} \Delta f = \frac{\eta_q}{h\nu k^2} \frac{D_r^2 T_A T_o}{R^2 \theta_t^2} P_t$	Same as above
Case 3 High Background Diffraction Limited Operation	$\frac{S}{N} \Delta f = \frac{\eta_q}{h\nu} \frac{D_r^2 T_A T_o}{R^2 \theta_t^2} P_t$	$\frac{S}{N} \Delta f = \frac{\eta_q D_r^2 T_A^2 T_o^2 P_t^2}{4h\nu R^4 \theta_t^4 \frac{\pi^2}{16} \theta_r^2 N_\lambda \Delta\lambda}$
Case 4 High Background Spread LO for Wider Field	$\frac{S}{N} \Delta f = \frac{\eta_q}{h\nu k^2} \frac{D_r^2 T_A T_o}{R^2 \theta_t^2} P_t$	Same as above

Table of Operating Modes

There are three important conclusions that come out of this comparison. They are:

a. The difference in performance between direct and heterodyne receivers is small whenever the S/N x Δf requirement for the link is large. That is, in these cases the arriving signal power is larger than the total collected background power, and the background problem disappears for the direct as well as the heterodyne system. This can be seen in the following sections where the curves for large P_t or large S/N x Δf differ by only 6 dB. The system to be implemented should be the simplest, most reliable, and cheapest, which points to a large aperture direct detection system.

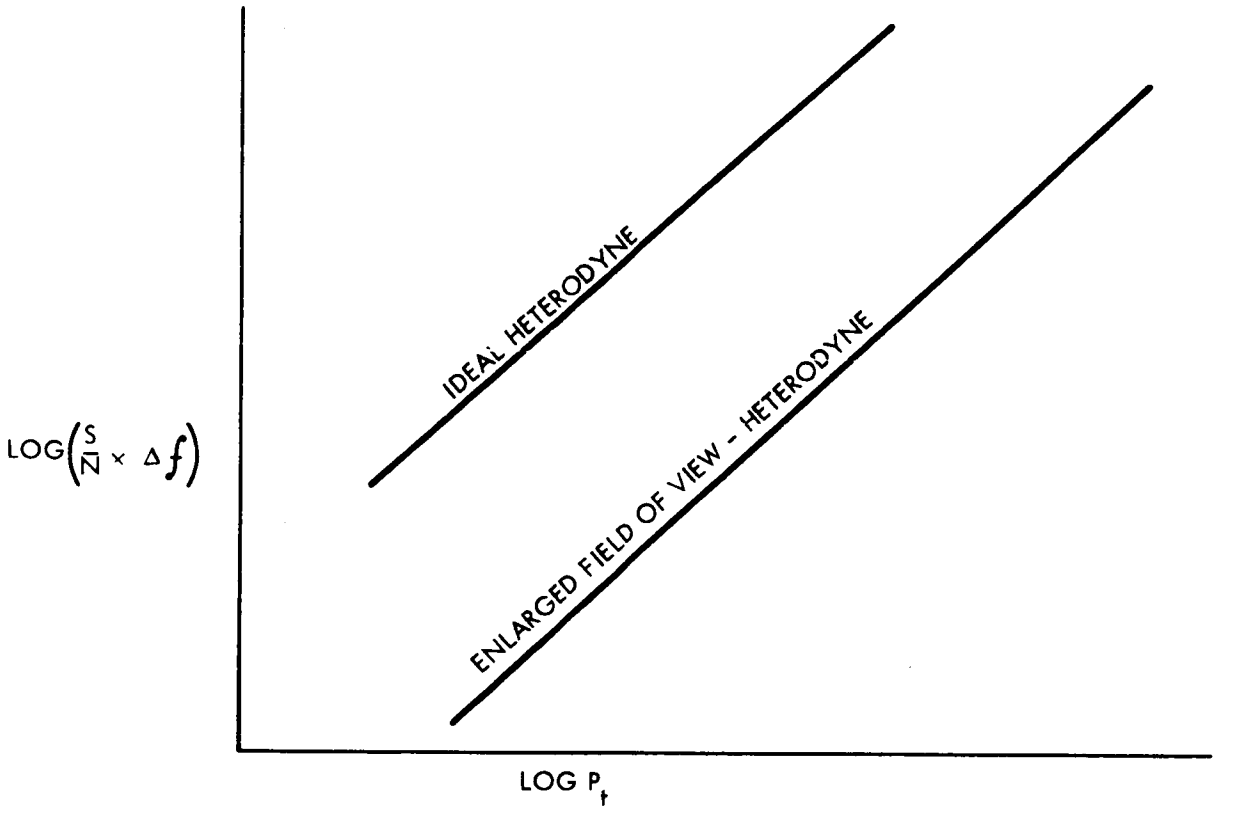

Figure 4.1-10. Log S/N x Δf vs. Log P_t for the Ideal Heterodyne and Enlarged Field Heterodyne Receivers.

b. The heterodyne detection receiver outperforms the direct system whenever S/N x Δf requirements on the link are low, and background levels are not negligible. This indicates that a heterodyne system would be best used for beacon tracking in the presence of Earthshine, or for low data-rate command, control, and telemetry signals.

c. The performance of either kind of optical communications link depends very strongly upon the choice of operating wavelength. An inspection of the equations for signal-to-noise and bandwidth product show that almost every parameter is wavelength dependent, quantum efficiency, optical frequency, transmitted solid angle, and most especially the laser transmitter efficiency. It will be shown that operation at a far infrared wavelength of approximately 10 microns will provide better link performance than will the visible laser system. This is due primarily to the fact that the 10 micron lasers, which have been recently developed, have efficiencies that are on the order of 100 to 1000 times larger than previous lasers in the visible spectrum.

   In the case of heterodyne reception, the diameter of the receiving aperture becomes dependent on wavelength, in that the atmospheric transverse coherence diameter depends on the wavelength. Perturbations caused by the atmosphere are less significant at longer wavelengths and, consequently, a larger collecting aperture can be used at longer wavelengths with good efficiency. It is important to note that the actual atmospheric transverse coherence diameter has not yet been measured in the 10 micron region. It can safely be assumed, however, that the diameter will increase approximately a factor of ten over that available in the visible region.

Comparisons between laser communications links operating at different wavelengths are best made using prime power required from the spacecraft as a basic parameter. Let the transmitted optical power be related to the spacecraft power by $P_t = \eta_t P_p$; where P_p is the spacecraft prime power requirement, and η_t is the laser transmitter efficiency. The signal-to-noise bandwidth product obtainable with different systems at different wavelengths can be compared by taking the ratio of the two quantities.

4.1.5.1.3.1 Comparison of Heterodyne Links

The ratio of signal-to-noise bandwidth products for heterodyne systems operating at different wavelengths is given by

$$\frac{(S/N \times \Delta f)_1}{(S/N \times \Delta f)_2} = \frac{\eta_{q1} \lambda_1 D_{r1}^2 T_{A1} T_{o1} \theta_{t2}^2 \eta_{t1} P_{p1}}{\eta_{q2} \lambda_2 D_{r2}^2 T_{A2} T_{o2} \theta_{t1}^2 \eta_{t2} P_{p2}}$$

Assume that T_A and T_o are the same for each wavelength; and assume also that the transmitter aperture diameter, D_t, is constant for either system. For equal spacecraft power P_p, the ratio becomes

$$\frac{(S/N \times \Delta f)_1}{(S/N \times \Delta f)_2} = \frac{\eta_{q1} \lambda_2 D_{r1}^2 \eta_{t1}}{\eta_{q2} \lambda_1 D_{r2}^2 \eta_{t2}}$$

It is seen here that the receiver diameter D_r is a wavelength dependent quantity because of atmospheric turbulence limitations.

4.1.5.1.3.2 Direct Detection

For the signal-shot-noise-limited region, the ratio of signal-to-noise bandwidth product for the two systems is as given for the heterodyne case. But for the background-noise-limited region, the ratio becomes

$$\frac{(S/N \times \Delta f)_1}{(S/N \times \Delta f)_2} = \frac{\eta_{q1}\,\lambda_1\,D_{r1}^2\,\theta_{t2}^4\,\theta_{r2}^2\,N_{\lambda 2}\,\Delta\lambda_2\,\eta_{t2}^2\,P_{p1}^2}{\eta_{q2}\,\lambda_2\,D_{r2}^2\,\theta_{t1}^4\,\theta_{r1}^2\,N_{\lambda 1}\,\Delta\lambda_1\,\eta_{t2}^2\,P_{p2}^2}$$

Assume a large receiver aperture equal in both cases, a large field of view equal for both cases, and for equal spacecraft power, the expression becomes:

$$\frac{(S/N \times \Delta f)_1}{(S/N \times \Delta f)_2} = \frac{\eta_{q1}}{\eta_{q2}}\left(\frac{\lambda_2}{\lambda_1}\right)^3 \frac{N_{\lambda 2}\,\Delta\lambda_2}{N_{\lambda 1}\,\Delta\lambda_1}\left(\frac{\eta_{t1}}{\eta_{t2}}\right)^2$$

4.1.5.1.4 Calculations for OTAES Links

This section assumes values for the important parameters shown in the previous section, and the performance of space-to-ground OTAES links is calculated for the 0.6328 and 10.6 micron wavelengths. Link assumptions are given in table 4.1-3.

TABLE 4.1-3

ASSUMED VALUES FOR OPTICAL LINK CALCULATIONS

	Heterodyne Detection		Direct Detection		Units
Wavelength	0.6328	10.6	0.6328	10.6	microns
η_q	5×10^{-2}	1×10^{-1}	5×10^{-2}	1×10^{-1}	--
D_t	100	100	100	100	cm
D_r	15	150	1000	1000	cm
θ_t	6.33×10^{-7}	1.06×10^{-5}	6.33×10^{-7}	1.06×10^{-5}	rad
θ_r	4.2×10^{-6}	7.1×10^{-6}	1×10^{-3}	1×10^{-3}	rad
T_A	0.5	0.5	0.5	0.5	--
T_o	0.5	0.5	0.5	0.5	--
N_λ	--	--	2.6×10^{-7}	8.0×10^{-9}	watts/cm^2-ster-A
$\Delta\lambda$	2	40	2	40	A
k^2	1.2×10^3	400			--
η_t	8×10^{-4}	8×10^{-2}	8×10^{-4}	8×10^{-2}	--

Development of System Parameters

Assume R = 3.6×10^9 cm--earth synchronous orbit

$R^2 = 1.3 \times 10^{19}$ cm^2

D_t - 1 meter, nominal, at all transmitted wavelengths

Take $\theta_t = \frac{\lambda}{D_t}$; neglecting the usual factor of 1.2, then the transmitted angles and solid angles are, for various λ's:

Wavelength (m)	θ_T (rad)	Arc/Sec	θ_T^2 (rad^2)
0.6328×10^{-6}	6.33×10^{-7}	0.131	4.0×10^{-13}
10.6×10^{-6}	1.06×10^{-5}	2.2	1.1×10^{-10}

For atmospheric transmission, take:

$T_A = 1/2$

For receiver optical system, take:

$T_o = 1/2$

Background: clear blue sky, 31° elevation, sun 110° left, 11° high, Mt. Wilson, California, 5650 ft.(3)

λ	N_λ	Δλ	$N_\lambda \Delta\lambda$
Wavelength (m)	(W/cm^2-ster-A)	(A)	(W/cm^2-ster)
0.6328×10^{-6}	9.6×10^{-8}	2.0	1.9×10^{-7} day only
10.6×10^{-6}	1.5×10^{-8}	40	6.0×10^{-7} day and night

For the visible spectrum, let the ground receiver aperture be:

D_r = 15 cm, restricted by "transverse coherence length"

$D_r^2 = 2.25 \times 10^2$ cm^2 in the visible.

The diffraction-limited half-power beamwidth, θ_r, is then, for these calculations:

$\theta_r = \frac{\lambda}{D_r}$

(3) Aerojet General Report No. 798, "Final Engineering Report on Target and Background Studies for the Development of Infrared Homing Equipment," Vol. I, May 1954, Contract No. NOAS-53-424, ASTIA #AD-47464.

Wavelength (m)	θ_r(rad)	Arc/Sec	θ_r^2(rad^2)
0.6328×10^{-6}	4.2×10^{-6}	0.87	1.8×10^{-11}

However, let D_r = 150 cm for 10.6-micron radiation because of reduced atmospheric perturbations:

$$D_r^2 = 2.25 \times 10^4 \text{ cm}^2$$

$$\theta_r^2 = 7.1 \times 10^{-6} \text{ rad. (1.5 arc/sec)}$$

$$\theta_r^2 = 5.0 \times 10^{-11} \text{ rad}^2$$

Values for $h\nu$ (joules) are: 3.1×10^{-19} at 0.6328×10^{-6}m

1.9×10^{-20} at 10.6×10^{-6}m

Quantum Efficiencies of Detectors:

S-20 Phototube

$\eta_q = 5.0 \times 10^{-2}$ at 0.6328×10^{-6}m

Doped Ge Photoconductor

$\eta_q = 10^{-1}$ at 10.6 μ

Conversion Efficiencies of Lasers:

$\eta_t = 8 \times 10^{-4}$ at 0.6328×10^{-6}m

8×10^{-2} at 10.6×10^{-6}m

Development of System Performance

In this section are developed the system relationships using the parameters developed in the preceding section. For simplicity, γ is substituted for S/N x Δf.

Direct Detection--Large Signal

For the Direct Detection System where the signal shot noise is dominant:

$$\gamma = \frac{\eta_q}{4h\nu} \frac{D_r^2 T_A T_o}{R^2 \theta_t^2} P_t = \frac{\eta_q}{4h\nu} \frac{D_r^2 T_A T_o}{R^2 \theta_t^2} \eta_t P_p$$

$\gamma = 4.4 \times 10^{11} P_t$ at 6328 A (15 cm rcvr)

$= 3.5 \times 10^8 P_p$ at 6328 A

$= 5.2 \times 10^{12} P_t$ at 10.6 μ (150 cm rcvr)

$= 4.2 \times 10^{11} P_p$ at 10.6 μ.

Direct Detection--Small Signal

For the Direct Detection System where the background is dominant:

$$\gamma = \frac{\eta_q}{4h\nu} \frac{D_r^2 T_A T_o}{R^2 \theta_t^2} \frac{T_A T_o}{R^2 \theta_t^2} \frac{16}{\pi^2 \theta^2 N_\lambda \Delta\lambda} P_t^2$$

$$= (. . . . . .) \eta_t^2 P_p$$

$$= 9.95 \times 10^{21} P_t^2 \text{ at } .6328 \mu \text{ (15 cm rcvr)}$$

$$= 6.35 \times 10^{15} P_p^2$$

$$= 4.9 \times 10^{19} P_t^2 \text{ at } 10.6 \mu \text{ (150 cm rcvr)}$$

$$= 3.14 \times 10^{17} P_p^2 .$$

Heterodyne Detection--Diffraction-Limited Local Oscillator Field

For the Heterodyne System where the local oscillator beam size is equal to the diffraction-limited signal image size:

$$\gamma = \frac{\eta_q}{h\nu} \frac{D_r^2 T_A T_o}{R^2 \theta_t^2} P_t = \frac{\eta_q}{h\nu} \frac{D_r^2 T_A T_o}{R^2 \theta_t^2} \eta_t P_p$$

$$= 1.8 \times 10^{12} P_t \text{ at } .6328 \mu \text{ (15 cm rcvr)}$$

$$= 1.4 \times 10^{9} P_p \text{ at } .6328 \mu$$

$$= 2.0 \times 10^{13} P_t \text{ at } 10.6 \mu \text{ (150 cm rcvr)}$$

$$= 1.6 \times 10^{12} P_p \text{ at } 10.6 \mu .$$

Heterodyne Detection--Spoiled Local Oscillator Field

For the Heterodyne System where the local oscillator beam size is larger than the diffraction-limited signal image size:

γ	θ_r	λ	k	k^2
$1.4 \times 10^{10} P_t$	for 10 arc/sec	at .6328 μ	11.5	1.3×10^2
$1.5 \times 10^{9} P_t$	30 sec		34.5	1.2×10^3
$4.5 \times 10^{11} P_t$	for 10 arc/sec	at 10.6 μ	6.7	45
$5.0 \times 10^{10} P_t$	30 sec		20	400

Direct Detection--Large Receiving Aperture

For the 10-meter diameter receiving aperture to be used for direct detection, the attainable γ is determined as follows:

For all wavelengths:

$$D_r = 10^3 \text{ cm}$$

$$D_r^2 = 10^6 \text{ cm}^2$$

Assume a field of view: $\theta_r = 10^{-3}$ rad

$$\theta_r^2 = 10^{-6} \text{ rad}^2$$

Then for signal shot noise dominant:

$$\gamma = 2.0 \times 10^{15} P_t \text{ at } .6328 \mu$$

$$= 1.6 \times 10^{12} P_p \text{ at } .6328 \mu$$

$$= 2.3 \times 10^{14} P_t \text{ at } 10.6 \mu$$

$$= 1.8 \times 10^{13} P_p \text{ at } 10.6 \mu$$

For background shot noise dominant:

$$\gamma = 8.0 \times 10^{20} P_t^2 \text{ at } .6328 \mu$$

$$= 5.1 \times 10^{14} P_p^2 \text{ at } .6328 \mu$$

$$= 1.1 \times 10^{17} P_t^2 \text{ at } 10.6 \mu$$

$$= 7.0 \times 10^{14} P_p^2 \text{ at } 10.6 \mu$$

System Characteristic Curves

Using the data developed in the preceding sections, characteristic curves have been plotted for comparison of the Heterodyne Systems and comparison of the Direct Detection Systems. Figure 4.1-11 shows the relationship between the Heterodyne diffraction-limited local oscillator field-of-view system (A) and the spoiled local oscillator field-of-view system (B) for 0.6328-micron and 10.6-micron wavelengths. Figure 4.1-12 shows the relationships for the Direct Detection System for three aperture sizes used at two wavelengths. The 10-meter aperture is shown for 10.6 microns (Curve A) and 0.6328 microns (Curve B). An aperture of 1.5 meters is shown for 10.6 microns (Curve C), and an aperture of 15 centimeters is shown for 0.6328 microns (Curve D). The unusual performance shown by Curve C is explained by the fact that it is a diffraction-limited collector where the 10-meter aperture in Curves A and B is not.

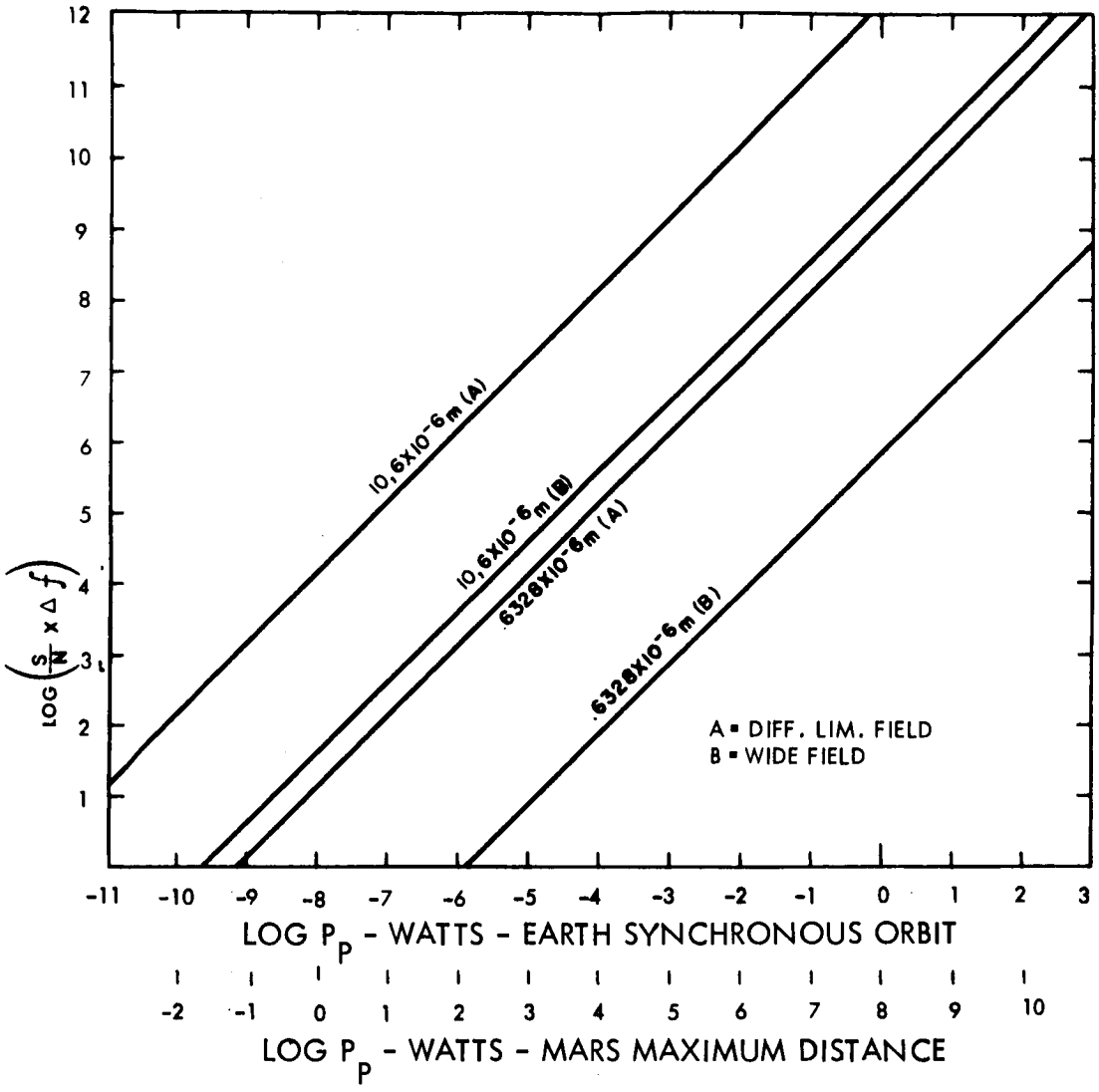

CONDITIONS:
TRANSMITTING APERTURE 1.0 M

AT $.6328 \times 10^{-6}$M

D_r = 15 cm.
$n_q = 5 \times 10^{-2}$
$n_t = 8 \times 10^{-4}$
DIFF. LIM. FIELD .87 ARC SECS
WIDE FIELD = 30 ARC SECS

AT 10.6×10^{-6} m

D_r = 150 cm
$n_q = 1 \times 10^{-1}$
$n_t = 8 \times 10^{-2}$
DIFF LIM FIELD = 1.5 ARC SECS
WIDE FIELD = 30 ARC SECS

Figure 4.1-11. Heterodyne Detection System

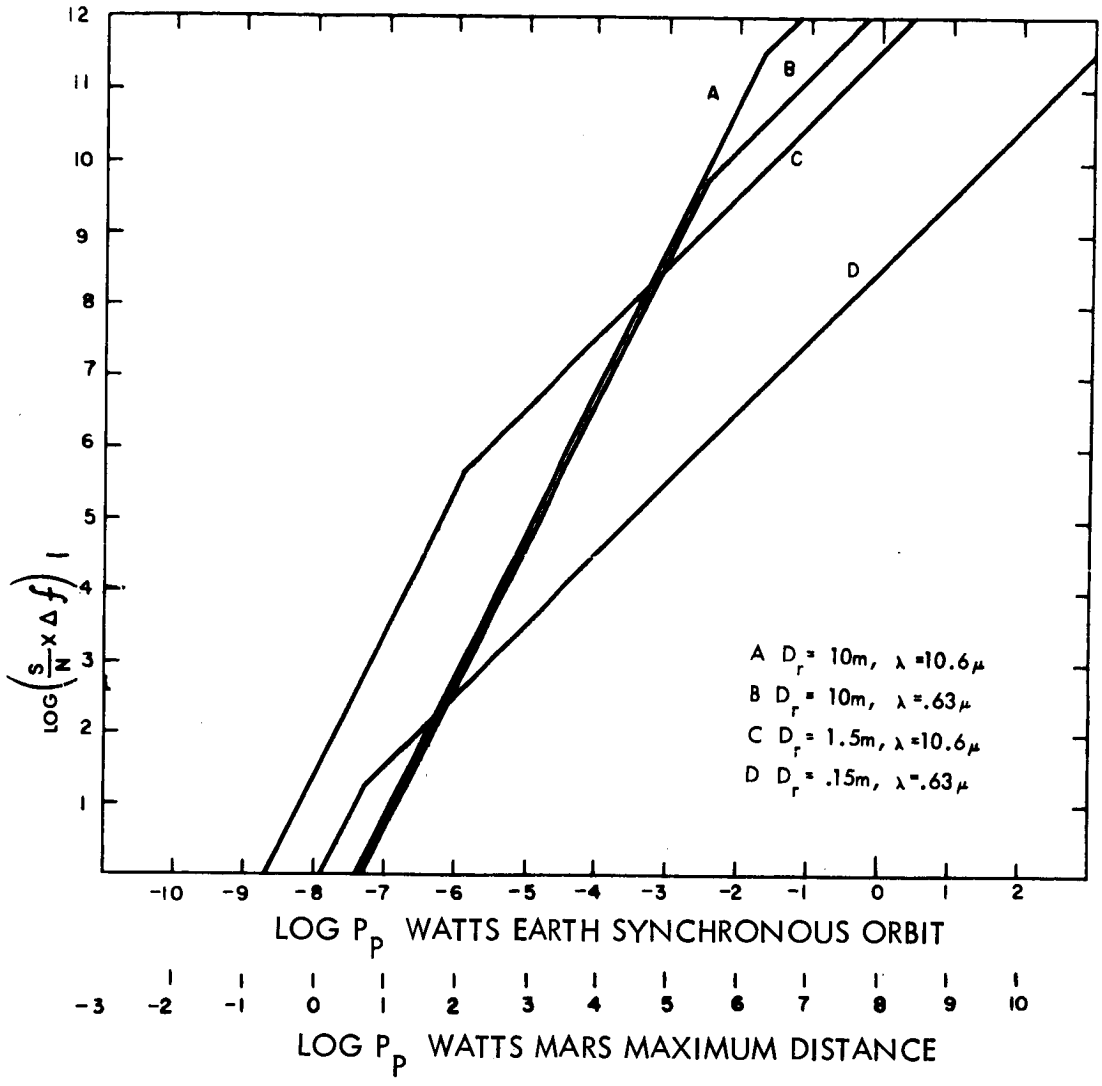

CONDITIONS:
TRANSMITTING APERTURE 1.0M

At $.6328 \times 10^{-6}$m	At 10.6×10^{-6}m
$n_q = 5 \times 10^{-2}$	$n_q = 1 \times 10^{-1}$
$n_t = 8 \times 10^{-4}$	$n_t = 8 \times 10^{-2}$

Figure 4.1-12. Direct System

4.1.5.2 Laser Evaluation

The design requirements for the OTAES spacecraft and ground-based lasers have been compared with the performance and theoretical capabilities of existing laser forms. These laser forms have been analyzed and catalogued; they provide a variety of wavelengths for use as: a) transmitter supermode single frequency light generators, b) receiver single frequency local oscillators, c) transmitter multimode oscillators for direct detection applications, and d) signal sources for physical measurement systems.

4.1.5.2.1 Requirements

Transmitter lasers for the optical heterodyne detection experiments must provide high power in a single narrow beam at a single frequency. The spatial coherence required for forming the narrow beam is achieved by designing the cavity for TEM_{00} oscillation. For lasers where the fluorescent line is narrow in comparison to the spacing of the cavity modes, single frequency operation is obtained by tuning the cavity to the fluorescent line. For lasers where the fluorescent line is broad, supermode operation will be used to impose temporal coherence on the oscillation within the cavity and provide maximum output at single frequency.

Local oscillators for the optical heterodyne detection experiments must have a single frequency output and a coherent phase front that can be matched to the phase front of the received signal at the surface of the detector. These requirements are fulfilled by using a short laser of small bore so that the gain exceeds the loss at only one cavity resonance. The mode separation increases as the length is decreased and the small bore discriminates against higher order TEM_{mn} modes. The cavity length is adjusted so this resonance has a frequency well within the fluorescence line. This cavity length adjustment will require servo control to maintain constant frequency or to track the carrier frequency of the transmitter.

In some instances, it may be necessary or desirable to use the supermode technique for local oscillator lasers. Consideration is being given to high sensitivity optical receiver systems using 10 by 10 arrays of 12.5-cm aperture heterodyne detectors on a gimbal mount (the maximum size of each aperture is limited by the coherence diameter of the signal phase front after passing through the atmosphere). Each detector requires about 0.1 mW of local oscillator power, and the local oscillator frequencies for all of the detectors must be controlled to track the incoming signal frequency. It is much more practical, therefore, to use one local oscillator, dividing its power among the detectors, rather than use separate local oscillators for each of the detectors. The required total local oscillator power, which exceeds that attainable from the short single frequency generating lasers, could be obtained from a supermode single frequency laser.

The transmitters for the direct detection experiments do not require single frequency carriers, but do require the spatial coherence achieved when the laser operates in one or more TEM_{00} modes.

For all of the OTAES lasers, except beacon light sources, maximum spatial coherence is required so that diffraction-limited performance can be approached for both transmitters and heterodyne receivers. The transmitter lasers should provide output beams that are collimated and of a diameter of about 1.0 mm to match the requirements of the electro-optic modulators. All of the OTAES lasers must incorporate polarizing devices to orient the output beam in the prescribed plane of polarization. The output of all lasers must be steady and free from hum, spiking, and pumping noise.

In terms of mission performance, the laser must be started and stopped by remote switching, operate continuously for extended periods of time, and restart after long periods of shutdown. Turn-on and stabilization must be accomplished in not more than one hour after long

duration shutdown at any temperature in the range of -50°C to +50°C. During operation, the external temperature of exposed surfaces of the laser package will not exceed 50°C.

The availability of prime power on the spacecraft is limited and requires that input power of the laser be coordinated with operating periods of other lasers and equipment so that power consumption will not exceed the limits shown below:

a. 200 W - Continuous.

b. 1000 W - Maximum of 60 minutes per 24-hour period.

c. 2000 W - Maximum of 20 minutes per 24-hour period.

Provision must be made to obtain and maintain alignment of the beam with the optical system. As is customary for spacecraft equipment, the weight and volume must be minimized; however, for the OTAES, volume reduction is the more important of the two.

In order to operate reliably, each laser in the spacecraft must have a system that will maintain the mirror alignment automatically. The differential thermal expansion of the laser interferometer will be enough to produce misalignment. Also, a search-for-alignment mode must be available when the laser is turned on.

The range of motion for the mirror alignment controls that would be required depends on many factors. The structure of the laser interferometer is very significant as it determines the rigidity of the mirror alignment and the response to vibration and acceleration. Changes of mirror alignment with changes in temperature on passing from the laser-off to the laser-on condition will depend strongly on the symmetry of this structure. A good approximation to axial symmetry of heat producing, heat storing, and heat conducting elements is desirable so that rising temperature causes the structure to expand without bending.

To estimate the ranges required on the alignment controls, a thick walled aluminum pipe, 0.5 m long and 0.1 m diameter, was taken as the model for the interferometer. This shell was assumed to be cooled by conduction through a close fitting collar that is in intimate contact with a constant temperature bulkhead. For a laser dissipation of 20 watts and a coefficient of expansion of $23 \times 10^{-6}/°C$, the mean temperature rise of the shell would be about 4°C and the length would increase by 46×10^{-6} meters, on warming from the bulkhead temperature to the equilibrium operating temperature.

If the laser and interferometer were axially symmetrical, no misalignment would result even though the expansion is some 70 wavelengths (or 140 cavity modes). If the laser cathode were off-axis, or the contact of the collar to the shell were imperfect and non-symmetrical, the expansion of the interferometer would be uneven. One side would expand somewhat more than 46×10^{-6} meters, while the other side would expand somewhat less. Thus, the differential expansion might be about 10 percent of the total, or about 5×10^{-6} meters. During operation, the differential expansion and contraction would be even less because a period of time has been allotted for warm-up. Thus an alignment mechanism with 5 to 10 $\times 10^{-6}$ meters movement would safely control the differential expansion. For comparison, the differential expansion range over which such a laser would lase is estimated as 2×10^{-6} meters.

During the operation of the laser, thermal changes will probably be the main cause of misalignment. Since the thermal changes are slow, the response time of the transducer may be slow, less than a cycle per second. A slow mirror alignment system is an advantage if another servo system is used for fast automatic frequency control.

Moving the mirror to maintain alignment will change the laser frequency. The frequency changes can be minimized, but probably cannot be avoided. These changes must be so slow that the automatic frequency control can easily handle them. A suitable mirror actuator is a differential screw driven by a small (0.8-inch diameter) servo motor. Two axes of adjustment are required.

When the actuators are used in the search mode, the time required to complete a search pattern is determined by the actuator speed. Conversely, the time allowed for the search (and also the pattern of the search) determines how fast the actuators must go. If one second is required to close the servo loop when lasing occurs and the sweep is 3 times the lasing range, then one axis will sweep across and back in six seconds while the second axis will make one sweep in 18 seconds. The sweep would take about 200 seconds if the pattern must be 10 times the lasing range in each dimension.

Figure 4.1-13 is a schematic diagram of the servo and search loops that keep the laser aligned. Only one axis is shown. If the laser is not lasing, the switch is in the search position. When lasing occurs, the signal from the photo cell is also fed to the phase sensitive detector. The linear actuator controls the tilt of the laser mirror. The dither signal from the oscillator causes the linear actuator to make a small oscillation in the laser alignment. The presence and phase of the dither signal on the laser beam contains the necessary information about the alignment of the laser. This information is processed in the phase sensitive detector, and the resulting signal is fed to the linear actuator to correct any misalignment. In the search mode, the contactor with hysteresis provides a signal that causes the linear actuator to sweep the mirror through the entire search angle. When the limit is reached, the sign of the signal from the contactor is reversed and the sweep of the mirror is reversed.

4.1.5.2.2 Environmental Factors

Storage of up to six months may occur after final tests have been performed and the equipment is awaiting assembly to the launch vehicles. The storage temperature will be in the range of $0^{o}C$ to $30^{o}C$ at controlled low humidity. The lasers must perform within specification limits following this storage period.

During transportation and launch, the equipment will be subject to noise, vibration, shock, and acceleration that will not exceed the limits shown in table 4.1-4.

The lasers will be designed to withstand these forces or will use special mountings to isolate them from critical frequencies.

Energetic particle exposure of the spacecraft will be a function of orbit parameters. In near earth equatorial orbit (500-mile altitude), electron intensity for energies in excess of 500 keV will be about 1×10^{5} electrons/cm^2/s. The proton intensity for energies greater than 40 MeV will be about 1×10^{2} protons per cm^2/s. For synchronous equatorial orbit electron intensities, there will be about 5×10^{4} electrons/ cm^2/s, with energies above 500 keV; and proton intensities will be negligible. For highly elliptical orbits, electron intensities may reach peaks of 2×10^{8} electrons/cm^2/s; and proton intensities will be as high as 2×10^{4} protons/cm^2/s.

The laser exposure to energetic particles will be altered by the presence of the surrounding walls of the telescope well. The lasers are not to experience any degradation during a one-to-two-year period of exposure to the above levels of radiation.

During ground checkout, the lasers will be operated in air at atmospheric pressure. In orbit, the lasers will be operated in vacuum at pressures below 1×10^{-6} torr. The lasers must be able to operate at both pressure extremes without manual readjustment during a one-to-two-year period.

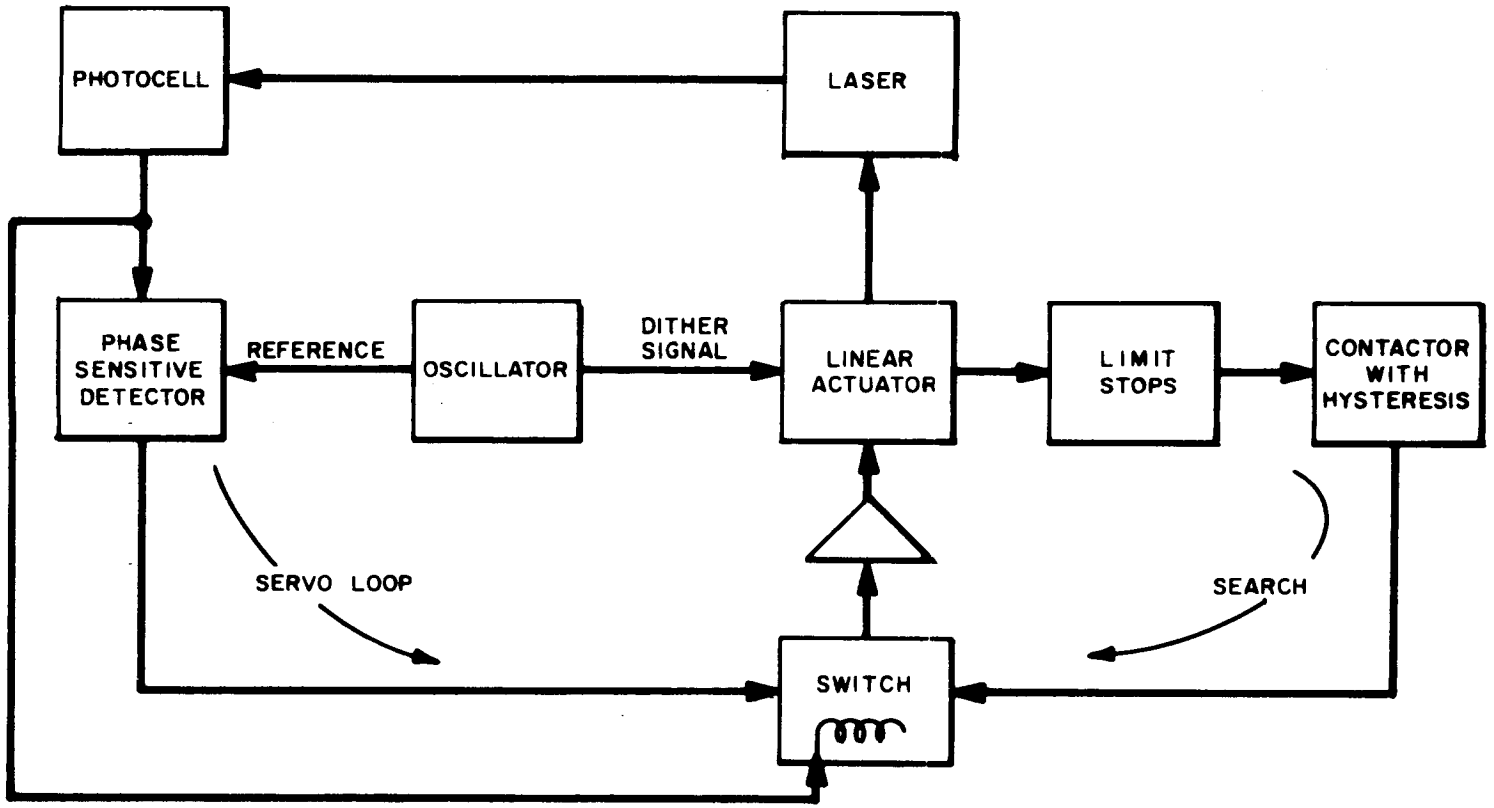

Figure 4.1-13. Servo and Search Loops (Maintain Laser in Alignment; Only One Axis Shown).

TABLE 4.1-4

LAUNCH ENVIRONMENT

a. Noise (Any Direction) Relative to 2×10^{-5} N/m^2

Overall External Sound Pressure Level: 175 dB

b. Random Vibration (Any Direction):

20 c/s - 200 c/s at 2.0 dB per octave
200 c/s - 700 c/s at 0.65 g^2 per c/s
700 c/s - 900 c/s at 0.18 dB per octave
900 c/s - 2000 c/s at 0.15 g^2 per c/s

c. Sinusoidal Vibration (Any Direction):

5 c/s - 33 c/s at 3.5 mm double amplitude displacement
33 c/s - 140 c/s at 8.0 G's peak
140 c/s - 240 c/s at 0.2 mm double amplitude displacement
240 c/s - 2000 c/s at 24 G's peak

d. Shock (Any Direction):

20 G's peak at half sine pulse of 10 milliseconds

e. Acceleration:

5.1 G's in longitudinal direction of vehicle
1.5 G's in lateral direction of vehicle
0.04 rad/sec^2 rotational acceleration in all directions

4.1.5.2.3 Evaluation Basis

The discussion of the last two subsections has covered a wide variety of factors involved in the selection of laser forms and conceptual designs for the OTAES. The importance of these factors in selecting lasers for the various specific OTAES applications will be discussed in this section.

The first and foremost requirement for every laser now under consideration for use in the OTAES is that it has already been shown to be capable of achieving continuous operation as a laser oscillator. This requirement will cause several developmental laser forms to be rejected at this time. However, these lasers could be reconsidered in later phases of this program if CW operation is obtained and if they offer distinct advantages over selected laser devices.

Proposed OTAES experiments will be designed for operation at a variety of optical wavelengths to provide comparisons of the effectiveness of these wavelengths for various applications, including optical communications, meteorological measurements, space astronomy, and optical navigation and tracking. Therefore, lasers of comparable wavelengths will be compared for use in specific portions of the spectrum; but lasers of widely different wavelengths will not compete with each other since active consideration of a variety of wavelengths must continue during the evaluation of optical technology experiments.

Table 4.1-5 identifies the significantly strong and the major relationships between the laser characteristics and the OTAES applications. Various important output, drive, and physical characteristics are listed in rows. Lasers for heterodyne experiments, direct detection experiments, beacon use, and other spaceborne applications are listed as column headings.

TABLE 4.1-5

EVALUATION BASIS FOR OTAES LASERS

	Heterodyne Experiment				Direct Detection Experiment			
	Ground Xmtr.	Ground L.O.	Space Xmtr.	Space L.O.	Ground Xmtr.	Space Xmtr.	Beacon Laser	Other Space Applications
Output Characteristics								
Spatial Coherence	Δ	Δ	Δ	Δ	Δ	Δ		Δ
Beam Axis Stability	Δ	Δ	Δ	Δ	Δ	Δ		Δ
Intensity Stability	Δ	Δ	Δ	Δ	Δ	Δ	0	Δ
Low Atmosph. Atten.	Δ	Δ	Δ	Δ	Δ	Δ	Δ	0
Output Power	Δ		Δ		Δ	Δ	Δ	
Temporal Coherence	Δ	Δ	Δ	Δ				0
Detectability	Δ	0	0	Δ	Δ	0	Δ	
Operational Life	0	0	Δ	Δ	0	Δ	0	Δ
Shelf Life	0	0	Δ	Δ	0	Δ	0	Δ
Warm-up Time			Δ	0		Δ		Δ
Drive Characteristics								
Efficiency	0		Δ	Δ	0	Δ	0	Δ
Operating Temp.			Δ	Δ		Δ		Δ
Dissipation Capacity			Δ	Δ		Δ		
Input Power			Δ	0		Δ		0
Conduction Cooled			0	0		0		0
Physical Characteristics								
Weight			Δ	Δ		Δ		Δ
Length			Δ	0		Δ		0
C-S Dimensions			0	0		0		0

Weak Relationship ☐ Significant Relationship 0 Major Requirement Δ

The strongest evaluation bases are four output characteristics of importance to all but the beacon laser applications. These are:

a. Spatial coherence, needed to achieve the principal advantage of the laser for long distance propagation.

b. Beam axis stability, without which the narrow laser beam would be useless.

c. Intensity stability, essential to wideband transmission of information.

d. Low atmospheric attenuation at the output wavelength.

High output power is of importance for transmitter and beacon lasers but not for nonpropagation applications, such as local oscillator uses and telescope figure measurements. Temporal coherence is a strong requirement for all lasers used in heterodyne experiments and unimportant for the other lasers. Detectability refers to the achievement of quantum noise limited signal thresholds with uncooled 10-MHz bandwidth detectors. Since cryogenically cooled detectors that are required at the longer wavelengths cannot be provided for the spacecraft receiver, except with a severe weight or power penalty, detectability of the wavelength becomes important in the selection of the ground-based transmitter lasers. Operational life becomes a major factor when it is not extremely large compared with the total duration of the spacecraft laser experiments (for spacecraft lasers), or large compared with the duration of individual experiments (for ground-based lasers). Similar remarks apply to shelf life, which, in general, must be large compared with the duration of the spacecraft mission. Short warm-up time is important for spacecraft lasers, particularly at high power levels, and where long operational life is difficult to achieve.

The laser drive and physical characteristics are of importance principally for spaceborne lasers. High laser efficiency, low operating temperature of the laser package, and good dissipation capacity for extracting laser pumping heat by conduction offer a basis of comparison for laser constructional techniques as well as different laser forms. The lasing threshold and pumping efficiency must permit operation from a level of input power that can be obtained from solar cells and storage batteries on the spacecraft. Weight is an important basis of comparison only for those lasers for which very heavy power supplies, magnets, or cooling systems are needed. For the present concept of the spacecraft laser, length is at a premium; but it is easy to accommodate the cross-sectional (C-S) dimensions of existing lasers.

4.1.5.2.4 Laser Characteristics

In this subsection, the characteristics of present laser forms are described; and significant factors in the use of lasers for various OTAES applications are discussed.

The laser characteristics achievable for ground-based operation are listed in table 4.1-6 for convenient comparison. This table covers lasers best suited to applications for which no severe environmental constraints are imposed or limited on weight, volume, and length. A more restricted listing is presented in table 4.1-7 applicable to lasers for possible use on-board the spacecraft. For all of the lasers listed, operation is in the lowest order transverse mode (TEM_{00}).

Some of the lasers provide simultaneous outputs at several close-spaced frequencies within one fluorescence line. These lasers, designated by footnote (1) in the tables, can provide their output at a single frequency through the use of the supermode technique. These supermode single frequency lasers would be used as transmitter lasers or as receiver local oscillators for driving arrays of heterodyne detectors. The supermode operation would not be needed for laser transmitters involved in direct detection experiments. Single heterodyne detectors for use on the spacecraft would use small single frequency lasers, designated by footnote (2) in the tables.

TABLE 4.1-6

LASER CHARACTERISTICS ACHIEVABLE FOR GROUND-BASED OPERATION

	He-Ne(1)	He-Ne(2)	Argon(1)	N_2-CO_2(2)	YAG:Nd
Wavelength (μ)	0.6328	0.6328	0.4880	10.6	1.065
Power Output (mW)	100	0.2	1000	10	500
Length (cm)	200	12	100	20	20
Width (cm)	15	6	30	10	20
Height (cm)	15	6	30	10	20
Weight (kg)	50	2	50	5	3
Power Input (W)	112	8	11,000	11	2,200
Discharge (V)	2000	1000	200	1500	-
(A)	0.05	0.004	30	0.005	-
Cathode (V)	12.6	6	15	6	-
(A)	1.0	0.7	40	0.7	-
Solenoid (V)	-	-	35	-	-
(A)	-	-	125	-	-
Lamp (V)	-	-	-	-	110
(A)	-	-	-	-	20
Coolant Flow Water (gal/min)	-	-	5	5	2

(1) Multiple Frequency

(2) Single Frequency

TABLE 4.1-7

LASER CHARACTERISTICS ACHIEVABLE FOR SPACEBORNE OPERATION

Type	He-Ne(1)	He-Ne(2)	Argon(1)	Argon(2)	N_2-CO_2	YAG:Nd
Wavelength (μ)	0.6328	0.6328	0.4880	0.4880	10.6	1.065
Power Output (mW)	10	0.2	100	0.1	10,000	500
Length (cm)	50	12	50	30	50	20(3)
Width (cm)	10	4	15	5	10	20(3)
Height (cm)	10	4	15	10	10	20(3)
Weight (kg)	15	1	25	1	15	3(3)
Power Input (W)	30	4	500	225	200	500(4)
Discharge (kV)	1.5	1.0	r.f.	0.3	2	--
(ma)	20	4	27 MHz	500	100	--
Cathode (V)	12	6	--	6	6	--
(A)	1	0.7	--	4	4	--
Solenoid (V)	--	--	--	--	--	--
(A)	--	--	--	--	--	--
Lamp (V)	--	--	--	--	--	--
(A)	--	--	--	--	--	--
Coolant Flow (gal/min)	--	--	1	1	2	1

(1) Multiple frequency.
(2) Single frequency.
(3) Laser cell only, not including sun pump mirror and mount.
(4) From 1.0 meter sun pump mirror.

Helium neon lasers, in addition to characteristics listed in the tables, have operating life of 100-1000 hours and extended shelf life. The 0.6328-micron wavelength is in the visible and in the range of photocathode detectors, such as photomultiplier and traveling-wave tube photodetectors. Modification of 0.6328-micron lasers, by change of mirrors, gives outputs at 1.153 microns or 3.39 microns. Modification of the laser to suppress the 0.6328-micron oscillation, by the use of a dispersive element such as a prism in the cavity, gives lasers that have outputs at 0.6118 micron or other visible wavelengths with reduced efficiency.

Failure modes include loss of gas, mirror misalignment, mirror damage, electrical failure, and cathode failure. Several configurations of helium neon lasers are being considered for use in both ground-based and spacecraft operation because of the advanced development of this laser device and proven operation in various configurations, including single frequency, high output, and supermode oscillation.

The argon laser has a high threshold input power requirement but a high power output capability. The ground-based transmitter would provide high signal power for a wideband uncooled detector on the spacecraft. The interest in using heterodyne detection at this wavelength (0.4880 micron) on the spacecraft has required that an estimate be made of characteristics achievable in a low output laser for the local oscillator. Therefore, there has been listed a spaceborne argon local oscillator laser that appears practical from the point of view of providing adequate output power from a limited input power. However, this input power is not only unusually high for a local oscillator, but is high in terms of available power aboard the spacecraft, suggesting a need for developmental effort. In addition to the He-Ne failure modes, argon lasers can fail from disrupted cooling and loss of magnetic field.

The nitrogen carbon-dioxide (N_2-CO_2) laser is a new form showing great promise because of its high power and efficiency and favorable wavelength for operation in the atmosphere. Significant advances in detection and modulation devices will be required before this laser can be applied in wideband systems. Threshold of oscillation is about one-tenth that of argon lasers of comparable power. For the proposed optical heterodyne detection experiment at a long optical wavelength, the transmitter is aboard the spacecraft and the receiver is at the ground station, where it is practical to use cryogenically cooled detectors. The width of the fluorescent line compared to the mode spacing of the resonator is much less than for the visible lasers of comparable dimensions so single frequency operation of transmitter lasers would probably not require the phase locking modulator of supermode lasers. Additional space may be required for nitrogen and carbon dioxide reservoirs.

The local oscillators for the receivers will have a low threshold so that adequate output can be obtained with 1-watt input. Because of the longer wavelength, the tuning and alignment problems are less severe than for the helium neon local oscillator. However, the output will have to be maintained at specified frequency in a single TEM_{00} mode. Nitrogen nitrous oxide lasers have similar characteristics except that the wavelength is 10.9 microns, and the efficiency is somewhat lower.

The types of lasers listed in tables 4.1-6 and 4.1-7 do not exhaust the possibly useful types for OTAES. The pulsed lasers and giant-pulse lasers (ruby, neodymium-glass) are not listed because they are not suitable for the experiments that are being considered for inclusion in the OTAES. There are a number of solid-state lasers (CaF_2:Dy, YAG, Nd:Cr) that have been operated continuously, and some (ruby) have been used in resonators that give TEM_{00} output. The YAG:Nd laser is listed because its reported characteristics are representative of solid-state lasers. In some respects its characteristics are more suitable than those reported for other lasers, especially with respect to the absence of spiking, low power input for reaching the threshold of oscillation, and the ability to operate at

temperatures as high as 20°C. A number of ion lasers have been reported, but the argon laser has been more fully developed as a high power laser source for visible output. Loss of the gas is a problem even with argon, and would be presumably more of a problem with more reactive gases.

The semiconductor lasers, such as GaAs, have not been listed because of the cryogenics problem in CW operation and the relatively poor collimation of the laser output. Liquid lasers have been excluded because of low temperature requirements and unsatisfactory CW operation.

4.1.5.2.5 Application Recommendations

In this section is presented a list of specific lasers for the proposed OTAES experiments and a discussion of problems involved in their application to OTAES. These lasers cover the requirements for the heterodyne and direct detection communication experiments presently under consideration and other applications, such as illuminators for spacecraft telescope figure measurements and as ground beacons for optical tracking tests. These lasers were described in detail in subsection 4.1.5.2.4.

The set of candidate lasers is presented in table 4.1-8. This set includes lasers at 1.06 microns which could be employed if further study defines a need for an intermediate wavelength. Laser forms specifically being rejected at this time are listed in table 4.1-9 along with the principal reasons for their rejection.

The laser mounting should determine the position and direction of the laser beam to close tolerances. The aperture of the modulator is only 1 to 2 mm in diameter; the laser beam, which will be of nearly the same diameter, must pass through this aperture before being expanded to the 1-meter diameter of the transmitting telescope. Laser resonators will be constructed with a plane exit mirror, and the direction of the beam axis will be constrained to be normal to this mirror and thus fixed with respect to the mounting. By using a limiting aperture in the laser resonator of such a diameter as to permit oscillation only in TEM_{00} modes, and by rigidly mounting this aperture the position of the beam axis will be approximately fixed with respect to the mounting.

Only to the degree that the diffraction losses introduced by the internal aperture predominate over other losses will the aperture determine the location of the resonator mode. Therefore, to assure single frequency operation along a prescribed axis, a high degree of uniformity is required to laser mirror losses, window transmissions, and reflection losses of any internal modulators. Laser construction will be such that the orientation of the exit plane mirror and the position of the limiting aperture are rigidly determined by the attachment of the laser package to the primary support for the package and ultimately to the other fixed components of the optical train.

The outer shell of each laser package must be of good thermal conductivity and mounted to a support plate that conducts the heat from the shell to the heat sink. These shells must function as a structural element as well as functioning to prevent undesirable transfer of radiation into the telescope well, which would otherwise produce thermal distortions of the optical surfaces and their support structures. The shell will provide the support for the laser, rigid alignment for the output mirror, and rigid positioning of the limiting aperture within the resonator cavity. Such construction is illustrated in figure 4.1-14.

For those lasers that have low power dissipation, the shell will serve as the principal means for removing heat from the laser package without the surface temperature and the temperature gradient rising to intolerable levels. For higher power dissipation, inner shells may be used to surround the discharge tube or other dissipative element. These shells would conduct the major portion of the heat to the mounting plate through a short span of the outer shell with a minimum temperature rise on the outer shell. For lasers

TABLE 4.1-8

CANDIDATE OTAES LASERS

Item	Function	Experiment	Location	λ	Type	Po	Pi
1	L.O.	Heterodyne(1)	S-C	0.6328 μ	He-Ne Single Frequency	0.2 mW	4 W
2	L.O.	Heterodyne	Ground	0.6328 μ	He-Ne Single Frequency	0.2 mW	4 W
3	Xmtr.	Direct(1)	S-C	0.6328 μ	He-Ne	10 mW	20 W
4	Xmtr.	Heterodyne	S-C	0.6328 μ	He-Ne Supermode	10 mW	20 W
5	Xmtr.	Heterodyne	Ground	0.6328 μ	He-Ne Supermode	100 mW	200 W
6	Xmtr.	Direct(2)	Ground	0.4880 μ	Argon Ion	1 W	10 kW
7	Xmtr.	Heterodyne	Ground	0.4880 μ	Argon Ion Supermode	1 W	10 kW
8	L.O.	Heterodyne	S-C	0.4880 μ	Argon Ion Single Freq.	0.1 mW	225 W(3)
9	Xmtr.	Heterodyne	S-C	10.6 μ	N_2-CO_2 Single Frequency	10 W	100 W
10	L.O.	Heterodyne	Ground	10.6 μ	N_2-CO_2 Single Frequency	10 mW	1 W
11	Xmtr.	Direct	S-C	1.06 μ	YAG:Nd Solar Pumped	500 mW	(4) (5)
12	Xmtr.	Direct	Ground	1.06 μ	YAG:Nd Tungsten Lamp	500 mW	2.2 kW(5)

(1) Also recommended for on-board spacecraft optical measurements

(2) Also recommended as ground beacon for tracking experiments

(3) Estimated

(4) Thermal input from 30-inch mirror

(5) Possible improvement using YAG:Nd:Cr

TABLE 4.1-9

REJECTED LASER FORMS

(Reported CW Operation)

Type	λ	Location	Reasons for Rejecting
He-Ne, 100 mW Output	0.6328 μ	S-C	Tube too long for telescope well
Argon, High Power	0.4880 μ	S-C	Too much power and weight
He-Ne	1.15 μ	All	Not competitive with YAG:Nd; strong absorption by water vapor
He-Xe	3.508 μ	All	Strong atmospheric absorption
N_2-CO_2	10.6 μ	GND	Requires cryogenic cooling of detector on spacecraft
YAG:Nd Tungsten Lamp	1.06 μ	S-C	Too much electrical input power
Ruby	0.6943 μ	All	Spiking, high threshold, low power
Glass:Nd	1.06 μ	All	Spiking, higher threshold than YAG:Nd
CaF_2:Dy	2.36 μ	All	Low temperature operation, spiking
$CaWO_4$:Nd	1.065 μ	All	High threshold
GaAs	0.843 μ	All	Poor spatial coherence, low temperature operation
InAs	3.11 μ	All	Poor spatial coherence, low temperature operation
Europium Chelate Liquid	1.61 μ	All	Low temperature operation
HeNe	3.39 μ	All	Strong atmospheric absorption

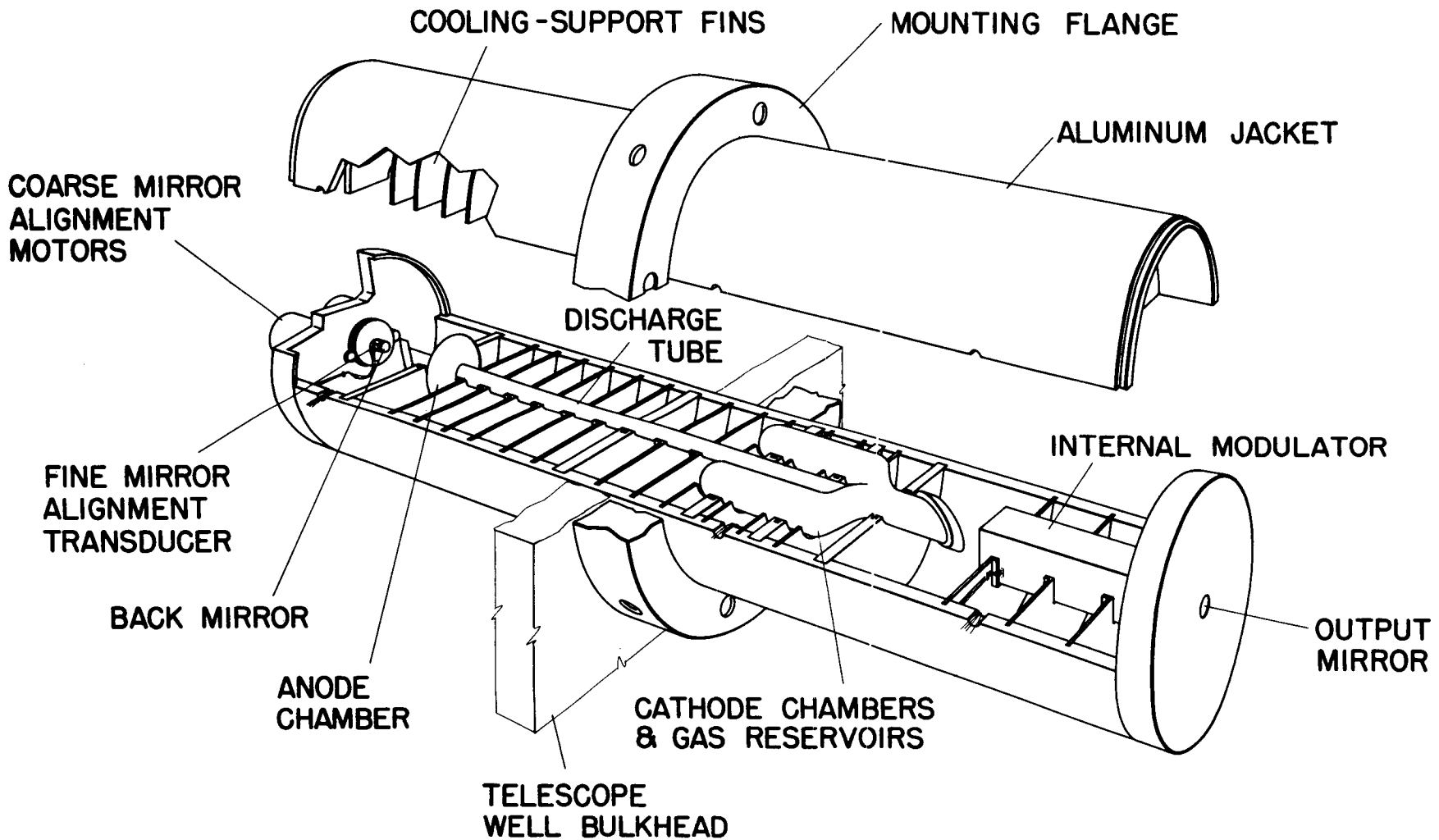

Figure 4.1-14. Spacecraft Laser Package

that have dissipations in the hundreds of watts or kilowatts range, cooling by circulating liquid would be required to prevent internal temperatures from rising to destructive levels. In these cases, conductive heat transfer to the liquid coolant would occur within the package. The line for the liquid coolant would be required to pass from the package through the shell at a point near its attachment to the support plate to minimize mechanical strains from the coolant lines.

The nearly isothermal shell of the laser package will serve as the principal structural element in determining the dimensions of the resonator cavity. The mirror spacing is the determining factor in tuning of the cavity mode to the desired wavelength. It is generally near the center of the fluorescent line of the laser medium. The fundamental frequency of a half-meter cavity is 300 MHz, and an expansion of these multiwavelength cavities by as little as one-half wavelength of the fluorescent line center brings the oscillating modes to new frequencies that are lower by almost 300 MHz. The tuning rates df/dL for the modes of a half-meter cavity are given in table 4.1-10. Approximate values of the doppler width of the respective fluorescent lines are also given. It is to be recognized that the gain for a given mode is high when near the center of the line and low near either edge, and that changes in the cavity length will result in modulation of the gain.

Lasers for use in heterodyne detection experiments must have constant length to avoid rapid changes of frequency that would be difficult to track. The dimensional stability requirement is more severe at shorter wavelengths because of the higher tuning rate. On the other hand, the doppler width is much narrower for the longer wavelengths; a small change in length will cause the oscillation to stop. This does not occur at the shorter wavelength, where expansion that takes one mode out of oscillation brings the next higher frequency mode in. For the lengths under consideration, expansion of metal or quartz mirror spaces will greatly exceed tolerable limits during warm-up. Therefore, length compensation under servo control will be required of single frequency lasers even if long warm-up periods are allowed.

Several techniques are available for tuning an oscillating cavity mode to a frequency near the center of the fluorescent line. These techniques vary in precision and complexity. For spacecraft transmitter lasers, it may be sufficient to have a servo system that adjusts the cavity length to maintain a maximum laser output and use automatic frequency control to make the heterodyne local oscillator laser track the carrier of the received signal.

TABLE 4.1-10

LASER TUNING RATES AND DOPPLER WIDTHS

Wavelength μ	df/dL MHz/μ	Doppler Width MHz
Ne 0.6328	970	1500
Ne 1.153	520	750
Ne 3.39	180	250
CO_2 10.6	180	80
A^+ 0.4880	56	3500

In the past few years several frequency stabilized lasers have been constructed. A variety of methods are now suitable for the development of a frequency stabilized local oscillator laser to be used in the spacecraft.[4,5,6,7,8] The most common laser is the short single frequency laser with about 0.25 mW output at 0.6328 micron. Multi-mode lasers may also be stabilized.[9] Typically line widths of about 2 parts in 10^{10} or 0.1 MHz are ordinarily obtained.[5,8] The methods which employ a frequency dither will have a residual FM modulation that can be about 5 MHz.[4,5]

4.1.5.2.6 Recent Technological Advances

Advances in laser technology continue to be reported at a rapid rate. The developments that are bringing the ion lasers and molecular lasers to higher levels of power clearly extend the range of distances over which laser communications in space will be possible. A liquid laser[10] having high efficiency and low threshold has been operated in the pulsed mode; if it can be developed as a CW laser it would make the power levels and efficiencies that are now available at 10 microns also available at the 1-micron wavelength. This would be of immediate advantage as the wideband photoelectric detectors can be used at this shorter wavelength.

4.1.5.3 Heterodyne Detection OTAES Link

Experiments to be conducted with the heterodyne system will include communication at wide bandwidths, and measurements to determine thepolarization, scintillation, and phase effects introduced by the atmosphere. To this end, statistical data will be gathered over periods of time and correlated with atmospheric conditions. The system parameters to be recorded will include transmitted power, received power, bandwidth, and signal-to-noise ratio. These experiments will be made using several wavelengths of light energy to evaluate system performance over as much of the optical spectrum as is feasible.

(4) W. R. C. Rowley and D. C. Wilson, "Wavelength Stabilization of an Optical Laser," Nature 200, 745 (1963).

(5) Koichi Shimoda, "Frequency Stabilization of the He-Ne Laser," IEEE Trans. on Instrumentation and Measurement.

(6) A. D. White, E. I. Gordon and E. F. Labuda, "Frequency Stabilization of Single Mode Gas Laser," Appl. Phys. Letters 5, 97 (1964).

(7) M. S. Lipsett and P. H. Lee, "Laser Wavelength Stabilization with a Passive Interferometer," Appl. Optics 5, 823 (1965).

(8) A. D. White, "A Two-Channel Laser Frequency Control System," IEEE J. of Quantum Electronics (Correspondence), QE-1, 322 (1965).

(9) S. E. Harris, M. K. Oshman, B. J. McMurtry, and E. O. Ommann, "Proposed Frequency Stabilization of the FM Laser," Appl. Phys. Letters 7, 185 (1965).

(10) Adam Heller, "A High-Gain Room-Temperature Liquid Laser: Trivalent Neodymium in Selenium Oxychloride," Appl. Physics Letters, (New York, August 1, 1966).

Alexander Lempicki and Adam Heller, "Characteristics of the $Nd^{+3}SeOCl_2$ Liquid Laser," ibid.

The heterodyne technique provides a unique signal detection capability under conditions of high background illumination. Thus, a heterodyne detection optical communication system will be particularly valuable where the transmitter may be located in a high radiance background. The transmitter signal is modulated with the information to be communicated. In the receiver this composite signal is compared with a local oscillator operating at the transmitter frequency. The difference frequency is a reconstruction of the modulated information. For this reason the transmitter laser must operate at a single frequency. The development of the super-mode laser technique is essential for this capability. Its output will be spatially and temporally coherent and linearly polarized.

The heterodyne detection system recommended for OTAES will be composed of two communication links: space-to-ground and ground-to-space. The spaceborne transmitter will have a single frequency laser (super-mode), a wide bandwidth modulator, secondary optics, and a primary mirror to form the transmitted beam. The modulator must be capable of wide bandwidth performance and must not distort the spatial coherence of the beam. The output optics must be diffraction-limited in their performance to assure that the output energy density will be maximum.

The ground-based receiver will consist of a receiving aperture, secondary optics, and a duplex heterodyne detector. The energy received will be polarized light. The duplex receiver will provide a capability for detecting both vertically and horizontally polarized light. The super-mode local oscillator laser beam will be mixed with the incoming signal and be detected, in accordance with the transmitter frequency, by either photomultipliers or cooled semiconductor detectors. The detector output will be a function of the difference frequency.

The performance of this space-to-ground system is affected not only by the efficiency of the transmitting lasers, but also by the efficiency of the detectors on the ground. In the visible wavelengths, photomultipliers will provide reasonable efficiency plus gain through the multiplier sections, raising the output level above the thermal noise level of the electronic system. In the infrared region, photomultipliers are not available, and diode detection or photoconduction detectors will be required. The output of these detectors will not have the benefit of photomultiplication, and their output level may be considerably lower than the thermal noise level at the input of the electronics.

The ground-to-space link will be similar in performance requirements except that the ground receiving aperture may be considerably larger than the ground transmitting aperture, and will be about one meter in diameter. The transmitted beams will be received on the spacecraft by the 1.0-meter and the 0.3-meter receiving apertures. It is planned that the transmitting aperture for the down-link will be one of the receiving apertures for the up-link. Detection on the spacecraft will be accomplished by a duplex receiver similar to the one on the ground.

Input power on the spacecraft is limited, and this will limit the maximum output power for some types of lasers. The expected laser output power that can be obtained in the spacecraft will be in the order of 100 milliwatts. It is planned to use several wavelengths in the spacecraft transmitter. These will be helium neon at 0.6328 micron and N_2-CO_2 at 10.6 microns. All power not transmitted will be dissipated as heat. Provision will be made for the conduction or radiation of this heat from the exterior surface of the laser assembly to the exterior of the spacecraft for radiation to space.

The principal environmental hazards to the operation of the heterodyne link are atmosphere and vibration. Although the heterodyne system is not affected by background illumination, the transmitter and receiver apertures must not be pointed to within 10° of the sun since the solar energy collected will create a temperature in excess of $500^{\circ}C$ at the focal point of the 15-cm. aperture.

For a heterodyne system, transmission of the optical beam through the atmosphere is of special concern. Lateral spatial coherence of the beam is restricted to approximately 15 to 25 centimeters under normal conditions, due to turbulence in the atmosphere. Use of the receiving aperture larger than this coherence diameter will cause a reduction in the total received signal because of destructive interference between out-of-phase components. Furthermore, atmospheric constituents and impurities will attenuate the signal. Measurement of the system performance will be correlated with the atmospheric conditions to determine the proportion of signal degradation due to each separable characteristic.

The requirement for a temporal and spatial coherence of the beam places serious constraints on the allowable magnitude of vibration in the spacecraft. The structural assembly and alignment of components must be adequate to assure diffraction-limited performance of the beam while the necessary attitude control devices are operating. The spaceborne receiver will be particularly sensitive to on-board disturbances because of the extremely precise alignment requirements for the duplex receiver. The elements of the receiver must be aligned to within fractions of minutes of arc to assure effecient heterodyne detection. In fact, all of the system electro-optical and secondary optical elements will require rigid or stiff mounting relative to their respective primary optics to maintain alignment for diffraction-limited performance throughout the system. It must be emphasized that the diffraction-limited performance requirement is imposed to obtain a maximum energy density in the transmitted or received beam. Any disturbances such as vibration or shock that will cause optical misalignment will reduce the energy density of the beam.

The operation of the spaceborne equipment will be remote-controlled, and will consist of turning on and turning off appropriate lasers and the associated frequency stabilization circuitry, turning on and off the modulator, and selecting the several signal sources to be used with the modulator. Control of the transmitting optics will be handled through the telescope control. Although the laser will be designed to be automatically tuned and adjusted, remote adjustment of the laser cavity may be required.

4.1.5.3.1 Spaceborne Transmitter

The requirements for spaceborne transmitters in the heterodyne detection case are more severe than for the direct detection case. A heterodyne receiver with its narrow inherent bandwidth must have a single-frequency transmitter, or it must use only one of the several frequencies that a transmitter laser may be generating as its signal source. In addition, the frequency stability of the transmitter laser is most important, whether it be a multimode or a single-frequency laser.

The spaceborne transmitter system, which will consist of single-frequency laser transmitters at 0.6328, and 10.6 microns, will be capable of broadcasting at these two optical frequencies simultaneously, so that comparison of the effects of the atmosphere on these two wavelengths could be made simultaneously at the ground receiver station. The selection of radiating wavelengths and their frequency offset from line center in the case of the mode-coupled single-frequency laser will be controlled by a radio command from the ground station.

Circularly polarized radiation will be transmitted to allow any atmospheric depolarizing effects to be detected.

Each of the spacecraft transmitter lasers can be expected to drift in frequency at rates of a few megacycles per minute because of thermal changes alone. These slow drifts are caused by expansion or contraction in the supports that separate the cavity mirrors. Good mechanical and thermal design can minimize, but can never eliminate, these motions in the presence of diurnal heat input fluctuations and the turning on and off of other equipment.

In addition, there are more rapid disturbances to be contended with because of acoustic vibrations carried to the laser structure from other parts of the spacecraft. Mechanical actuators, gyros, reaction jet valves, transformers, etc. all can generate disturbances at audio and ultrasonic frequencies, causing frequency jitter in the transmitter lasers if they are not compensated.

For these reasons, various laser stabilization techniques must be used. In the case of the helium-neon laser at 0.6328 micron, the FM laser-supermode laser technique can be used to convert the output of a multimode laser to a single frequency, and simultaneously to stabilize the output frequency to a point near the laser line center.[11,12] In the case of the carbon dioxide laser at 10.6 microns the inherent linewidth of the carbon dioxide fluorescence is only about 50 MHz, and the laser will operate at a single frequency without the necessity for mode-coupling schemes. It will, however, need to be stabilized near line center to keep the output at full power, and to keep acoustically-induced frequency jitter in the transmitter from showing up as a spurious signal in a heterodyne ground receiver.

The optical configuration of a frequency-stabilized, multimode, single-frequency output laser is shown in figure 4.1-15. The resonant cavity of the laser system is formed by an opaque mirror at one end and two highly reflective mirrors at the other end, which together act as a frequency selective output coupler. The two mirrors form a Fabry-Perot etalon, which will pass only a very narrow band of frequencies. Inside the cavity formed by the mirrors is a laser tube that provides gain, and a phase modulator that is made of a material such as KDP, which has a high electro-optic coefficient. When the phase modulator is driven with a frequency that is very near to the frequency spacing between the axial modes of the laser itself, the modes become coupled together and are converted from independent free-running oscillations into mutually-dependent coupled oscillations at nearly the same optical frequencies. The amplitude and phase of each of the previously independent oscillations is altered by the presence of significant coupling between the modes, so that the laser modes become sidebands of a single, coherent signal. Both AM and FM coupling have been observed.[13,14]

The Fabry-Perot etalon output coupler at one end of the cavity can then be tuned by varying the spacing between the two mirrors in the etalon to select only one of the oscillating frequencies in the laser. Power extracted at any one frequency acts as a power drain on all of the oscillations going on within the laser cavity. It is thus possible to obtain essentially all of the power of the multimode laser in a single-frequency output.

(11) S. E. Harris, M. K. Oshman, B. J. McMurtry, E. O. Ammann, "Proposed Frequency Stabilization of the FM Laser," Applied Physics Letters, October 1, 1965, Vol. 7, No. 7, p. 185.

(12) S. E. Harris, and B. J. McMurtry, "Frequency Selective Coupling to the FM Laser," Applied Physics Letters, November 15, 1964, Vol. 7, No. 10.

(13) S. E. Harris, and O. P. McDuff, "FM Laser Oscillation--Theory," Applied Physics Letters, November 15, 1964, Vol. 5, No. 10.

(14) E. O. Ammann, B. J. McMurtry, and M. K. Oshman, "Detailed Experiments on He-Ne FM Lasers," Journal Quantum Electronics, September 1965, Vol. QE-1, No. 6.

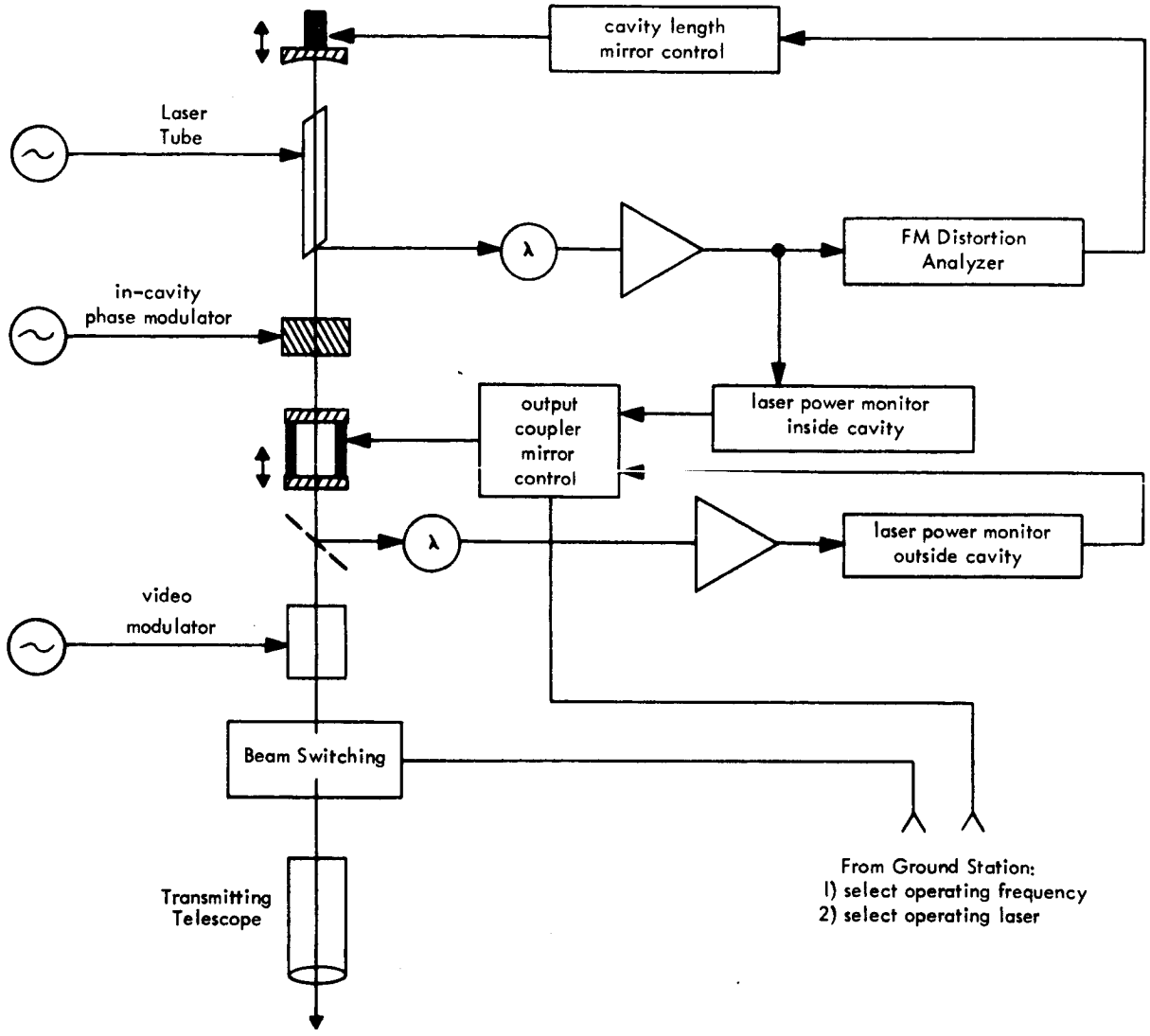

Figure 4.1-15. Single Frequency Spacecraft Transmitter

This passive etalon output coupling system will work with either AM or FM coupled multimode lasers. The FM mode coupled, or "FM laser", has an additional advantage, however: the light inside the cavity is effectively frequency-modulated at a rate controlled by the intra-cavity phase modulator, and the amount of AM distortion on this signal strongly depends on the optical frequency difference between the center of the FM mode pattern and the center of the fluorescence line. This dependence can be used to measure the absolute frequency drift of the mode pattern, and thus the drift in the cavity mirror separation, and to provide an error signal to correct drift or jitter as it occurs. An FM laser can thus be stabilized and deliver its full power into a single frequency simultaneously.

Two feedback control systems are needed in order to operate the laser in this way. They are:

a. The Laser AFC Subsystem. This subsystem monitors the AM distortion on the FM light within the laser cavity and adjusts the cavity length to the correct value. This is accomplished by moving one end mirror (the single end mirror) with a piezoelectric transducer. In this fashion the spectrum of oscillating modes can be placed on the center of the resonance fluorescence line of the laser.

b. The Selective Output Coupling Subsystem. This subsystem monitors the output power. The Fabry-Perot selective output coupler is then tuned to take power out at one of the oscillating frequencies. Tuning is again accomplished by moving one of the etalon mirrors through a small distance by use of a piezoelectric transducer.

It is not necessary to couple power from the multimode FM laser at the frequency of the oscillation that is nearest to line center. The power can be coupled out at any one of the oscillating frequencies that may be spaced, in the case of the helium-neon laser, as far away as 500 to 800 MHz from line center. In this way some simulation of or correction for a vehicle Doppler shift can be accomplished in increments of 300 MHz.

4.1.5.3.2 Ground Receiver

The heterodyne ground receiver system will have its useful collecting aperture diameter limited by atmospheric turbulence effects.(15,16) The atmosphere produces random phase variations on the order of $\pi/2$ or more between optical paths separated from each other by no more than a few inches, during usual clear weather conditions. For this reason, a 0.6328-micron heterodyne receiver immersed in the atmosphere will have a useful collector only 15 to 25 centimeters in diameter. It is anticipated that a larger diameter could be used in the far infrared at the 10-micron band, and this remains to be experimentally verified.

(15) Goldstein, Chabot, and Miles, "Heterodyne Measurements of Light Propagation through Atmospheric Turbulence," Proc. IEEE, September 1965, Vol. 53, No. 9, pp. 1172-1180.

(16) D. L. Fried, "Optical Heterodyne Detection of an Atmospherically Distorted Signal Wave Front," Proceedings of the Conference on Atmospheric Limitations to Optical Propagation, 1965, National Bureau of Standards, Boulder, Colorado.

The ground heterodyne receiver system would consist of a collecting aperture, which, for purposes of finding the dependence of receiver diameter on atmospheric conditions, would be on the order of 1.0 meter in diameter. The full aperture of this system would not be effectively used at short wavelengths or perhaps under poor conditions, but it will provide an aperture large enough to make tests of the atmospheric turbulence wavelength dependence. A set of two laser heterodyne receivers will be mounted near the focus of the optical system, and a set of dichroic mirrors or prisms will be used to separate the incoming wavelengths and direct them to their respective heterodyne receivers. The operating wavelengths will be at 0.6328 micron and 10.6 microns. The instantaneous field of view of each receiver system could be as small as the diffraction limit of the receiver aperture, which, for the case of visible radiation, is on the order of 0.2 second of arc, but this narrow a field of view would not be usable in general because of the atmospherically induced variations in angle of arrival of the signal as seen by the receiver.

The receiver must either: (a) track the incoming signal in angle; or (b) operate with a larger instantaneous field of view and operate with some sacrifice in sensitivity. The latter method will be used. The field of view can be increased over the diffraction limit by deliberately spreading the local oscillator beam so that mixing takes place over a larger angle. This is fully equivalent to masking the aperture size down to that having an equal diffraction-limited angular resolution.

The heterodyne receiver configuration is shown in figure 4.1-16. The received circularly-polarized energy is divided by dichroic beam splitters and sent to the appropriate receiver units. Within each unit, the received energy is pre-filtered and then analyzed by a quarter-wave plate, which converts right- or left-circularly-polarized input radiation into orthogonal plane polarized beams. These are then separated by a polarization-sensitive prism and sent to one of two basic heterodyne receivers. Both basic receivers are fed by the same laser local oscillator, but are sensitive to opposite polarizations. This configuration is called a polarization diversity optical heterodyne receiver. It is capable of processing the two polarization channels simultaneously. The local oscillator's power is divided equally by a beam splitter between the two channels. The beams are superimposed at the two mixer beam splitters. Their directions and phase fronts are matched so that they will beat coherently to produce a signal at their difference frequency at the output of the detector. This is then amplified by the IF amplifiers.

Each of the polarization channels uses two detectors in a balanced mixer configuration. The signals from the two detectors are out of phase because of the phase reversal produced on the light by reflection at the beam splitter. One of the legs of the circuit has an inverter that restores the signal to its correct polarity. Then it is added to the signal from the other leg, and a heterodyne signal of full amplitude is obtained without wasting any of the incoming signal light or any of the local oscillator power. This basic configuration is used for heterodyne reception at each wavelength. The details of the implementation will differ, particularly in the case of the detectors that at longer wavelengths require cooling and the attendant cooling equipment.

The frequency of the laser local oscillator must be stabilized to a fixed frequency offset from the frequency of the optical signal being received. The difference frequency to be detected must lie within the bandpass of the photodetector. In the visible and near infrared spectrum, there are available broadband detectors[17,18] that permit the laser local oscillator to operate as far as 3 GHz away from the frequency of the incoming signal. A second electronic conversion with a tracking local oscillator can always move the signal to a convenient intermediate frequency. At 10.6 microns, the available detectors have bandwidths of only about 1 MHz, thus requiring the laser local oscillator to track the

(17) M. B. Fisher, "A Multiplier Travelling Wave Phototube," Presented at the Conference on Electron Device Research, University of Illinois, Urbana, Illinois, June 23, 1965 (to be published).

(18) L. K. Anderson, L. A. D'Asaro, and A. Goetzberger, "Microwave Photodiodes Exhibiting Microplasma--Free Carrier Multiplication," Applied Physics Letters, Vol. 6, No. 4, February 15, 1965.

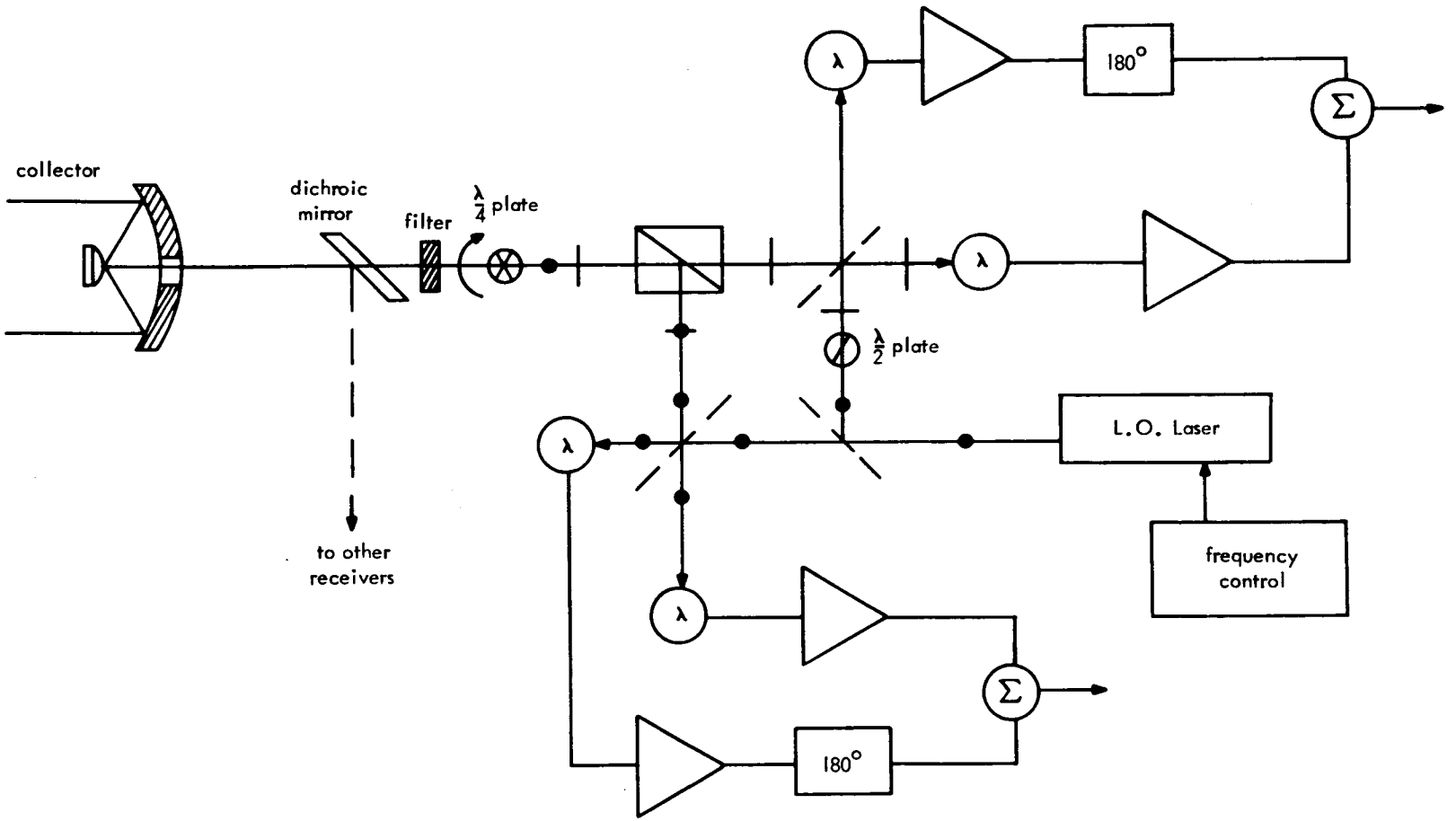

Figure 4.1-16. OTAES Polarization Diversity Heterodyne Receiver - Ground Based

signal. It is necessary that the length of the laser cavity be adjusted with a piezoelectric mirror control.

A block diagram of the signal processing system following the photodetectors is shown in figure 4.1-17. The IF signal from each balanced photomixer pair is amplified at the IF frequency. An AGC circuit compensates for large changes in received signal strength. The IF signals from the two channels are processed in several ways, depending on the type of experiment being performed:

a. A limiter-discriminator combination is sensitive to optical frequency modulation, and is also used to control the frequency of the laser local oscillator to the desired fixed offset. The frequency offsets due to Doppler effects aboard the OTAES will not be large compared to those obtained on an inter-planetary mission. It is therefore very difficult to simulate them on a stationary satellite-to-ground-station experiment. The ground receiver, however, should be capable of tracking Doppler shifts over a bandwidth well above that required so that experiments with different orbit configurations could be carried out.

b. A set of gated second detectors followed by a PCM demultiplexing system is used for digital transmission tests. It should be noted that if alternate pulses of right- and left-circularly polarized light are used, the received pulse will always be present in one channel or the other.

c. A set of video bandwidth AM detectors for analog AM transmission tests and beat amplitude scintillation measurements. The heterodyne receiver can also be used for angle-of-arrival fluctuation measurements.

The receiver packages will be small and light enough to be mounted aboard the tracking telescope. The helium-neon receiver package is estimated to weigh 13.6 kilograms and have dimensions of 25 x 12 x 7 centimeters. The CO_2 receiver package will be bulkier because the detectors must be cooled to 30° Kelvin or less, and dewars for liquid hydrogen become part of the package. The weight and size become about 20 kilograms and 25 x 12 x 15 centimeters.

4.1.5.3.3 Experiments

Several important kinds of experiments can be carried out with the optical heterodyne receivers in the satellite and on the ground. They are:

a. Atmospheric effects measurements. This group of experiments is designed to determine the atmosphere properties that significantly affect space-to-ground laser communication links. These are experiments that can only be made from a satellite vehicle that is well above the Earth's atmosphere and moving at angular rates slow enough to simulate those that will be encountered on interplanetary probe missions. The objective is to determine experimentally the types and rates of modulation that the atmosphere will support. Heterodyne receivers at the spacecraft will measure:

(1) Scintillation in received signal amplitude. Predictions have been made[19] that the power spectra of amplitude scintillation observed from a satellite will be larger and peaked at higher frequencies than that observed at the ground. Verification of theoretical predictions will establish the useful bounds on fade rates for an optical up-link.

(19) R. J. Munick, "Turbulence-Produced Irradiance Fluctuations in Ground-to-Satellite Light Beams," NAA--Space & Information Systems Division, Report No. SID 64-2222, December 28, 1964.

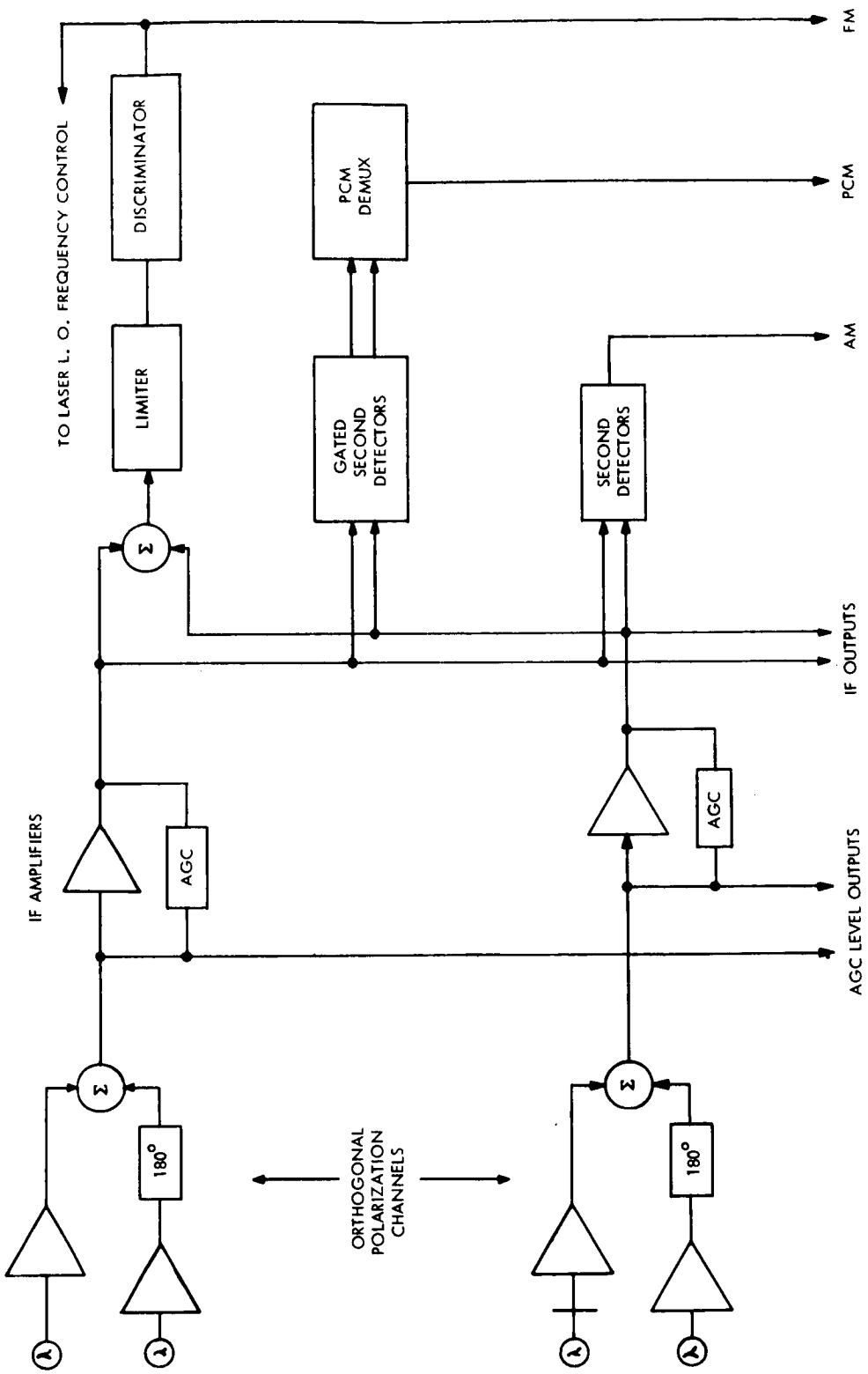

Figure 4.1-17. Heterodyne Receiver Electronic System

(2) Fluctuations in optical phase on a coherent signal passing through the entire atmosphere. The magnitude and rate of such phase fluctuations will establish the usefulness of optical FM modulation for communication. The frequency, or phase stability of the spacecraft local oscillator, may not be good enough to permit definitive measurements to be made except when acoustic disturbances aboard the vehicle are absent.

(3) Polarization fluctuation. The spacecraft heterodyne receivers can detect any differential in amplitude or phase fluctuations between orthogonally polarized input beams. Correlation between any of the fluctuations in the two channels will allow estimates of atmospheric depolarizing effects to be made.

Each of these measurements can be carried out in the visible and in the infrared regions to obtain the wavelength dependence of these effects.

Heterodyne receivers on the ground will measure:

(1) Angle-of-arrival fluctuations. The extremely narrow beamwidth of a heterodyne receiver makes it useful for detecting small changes in angle-of-arrival of a signal from the spacecraft. The fluctuations in receiver output due to angle-of-arrival cannot be separated from those due to amplitude scintillation. A second detector with a wider field of view is necessary to separate the effects. When this is done, the fade rates for ground-based heterodyne systems of varying beamwidths can be measured.

(2) Phase fluctuations on the received signal. The phase noise generated by the atmosphere on the down-link can be measured when both the spacecraft transmitter and the local oscillator on the ground are undisturbed by external vibrations.

(3) Polarization fluctuations. These ground-based measurements will be made in the same way as done aboard the spacecraft.

(4) Wavelength dependence of receiver diameter. The effective collecting area of an optical heterodyne receiver can be measured as a function of wavelength over the range from visible (0.6328 micron) to the far infrared (10.6 microns). These experiments will determine whether the gain in system performance that is predicted for the infrared system can be achieved.

b. Optical communications experiments. This group of experiments will test alternative modulation techniques, with the objective of testing their capability for communication with 10-MHz bandwidths over a space-to-ground link.

4.1.5.4 Optical Modulation

Implementation of pulse code type modulation methods requires the optical modulator and modulation driver to be capable of much wider bandwidths than the suggested ultimate analog bandwidth of 10 MHz. A study has been concluded which shows the feasibility of a 100-MHz bandwidth modulator and driver that is applicable. During the past several years, several optical modulators have been developed. The first was a traveling-wave phase modulator[20] with a bandwidth of about 1.0 GHz, requiring 50 watts to achieve a modulation index of unity. The next type was a traveling wave amplitude modulator[21] which has a bandwidth of 1.0 GHz and produces 100% modulation with a drive of 50 watts. This modulator is shown in figure 4.1-18.

The optical design principles developed in connection with this 1.0-GHz bandwidth modulator were applied to the design of a video bandwidth modulator[22] shown in figure 4.1-19. This video modulator is optically efficient, rugged, and simple to operate. It has been used in the transmission of TV over long paths through the atmosphere.

These three modulators are the products of a continuing research and development program. In this program, which includes the investigation of all the available electro-optic materials, it has been determined that the optimum choice of material depends not only upon its electro-optic coefficient but also upon its electrical, thermal, and mechanical properties.

There have been developed thermal design techniques that minimize the effect of internal losses upon the deflection and decollimation of the beam. Optical finishing techniques that produce high optical efficiency have been developed. All these factors are directly applicable to the development of a 100-MHz bandwidth modulator.

4.1.5.1 Modulator Design Approach

Two design approaches have been investigated for the 100-MHz bandwidth optical modulator. One approach applies the traveling-wave techniques used in the construction of the 1.0-GHz bandwidth modulators. This approach was modified by the inclusion of loading coils in the modulator transmission line structure to increase the characteristic impedance of the modulator. By increasing the characteristic impedance of the transmission line structure, the drive power requirement is reduced significantly while still retaining velocity match between the modulation and the light.

In the second approach, the modulator is treated as a lumped circuit element with a capacitive reactance. Measurements on the video bandwidth modulator have proved that this approximation is valid up into the GHz frequency range. The frequency response of the modulator and modulator driver is extended in this approach by paralleling the capacitor with an inductance so that the circuit is resonant near the upper frequency limit of the modulator. Comparison of the modulator design resulting from the two approaches indicates

---

(20) "Gigacycle Bandwidth Coherent Light Traveling-Wave Phase Modulator," Proceedings of the IEEE-Special Issue on Quantum Electronics, January 1963, vol. 51, no. 1, pp. 147-153.

(21) "Gigacycle-Bandwidth Coherent Light Traveling-Wave Amplitude Modulator," Proceedings of the IEEE, May 1965, vol. 53, no. 5, pp. 455-460.

(22) Peters, C. J., et al, "Laser-Television System Developed with Off-the-Shelf Equipment," Electronics, February 8, 1965, pp. 75-78.

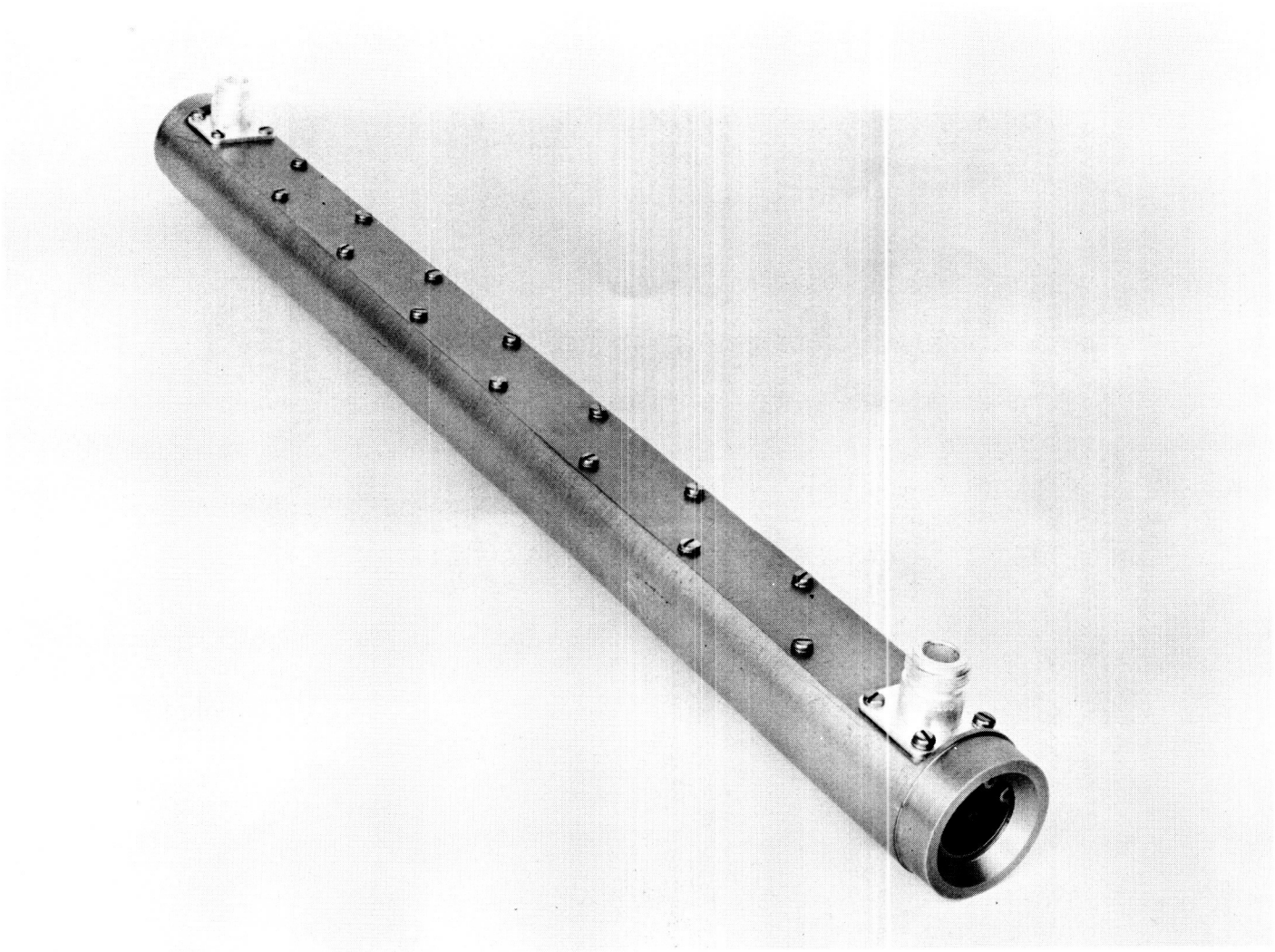

Figure 4.1-18. Traveling - Wave Amplitude Modulation

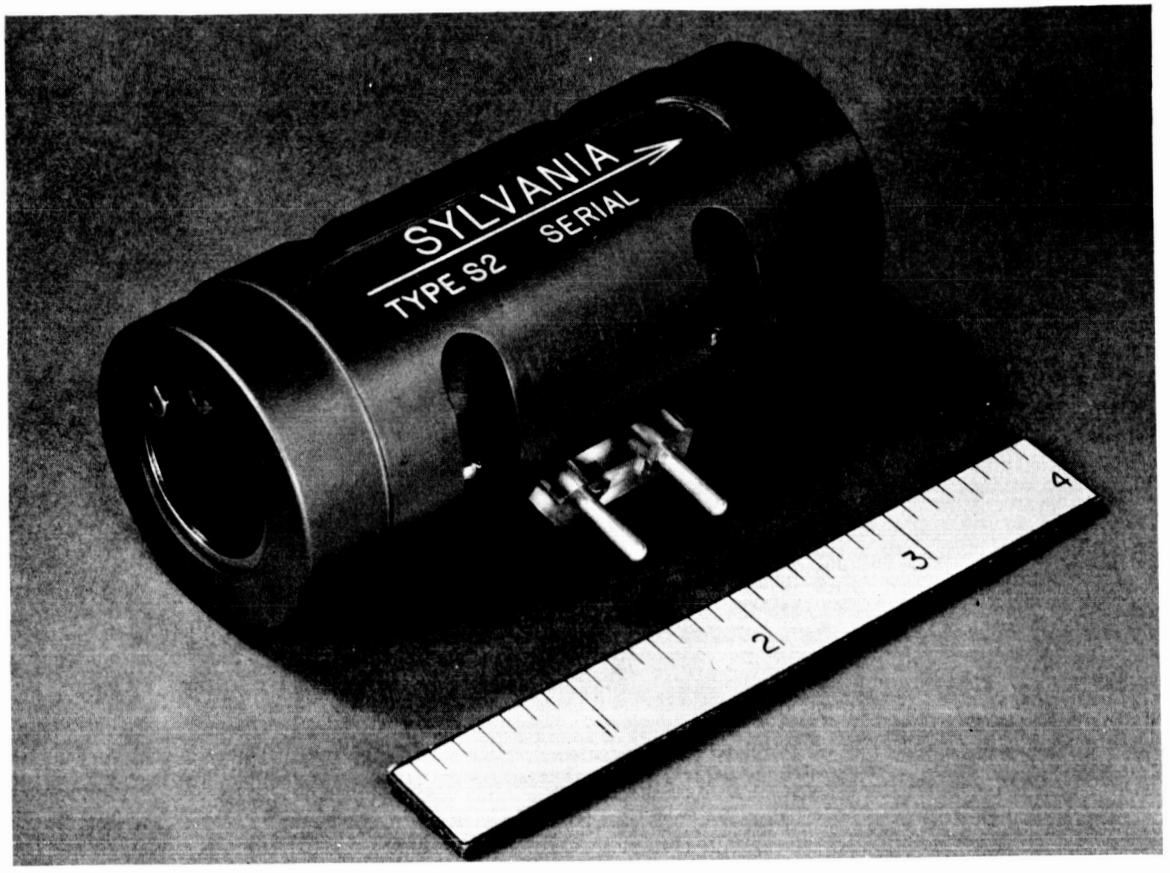

Figure 4.1-19. S2A Video Bandwidth Modulation

that the second approach yields a more economical modulator design. Although a description of the traveling-wave approach is not directly useful, it is significant in that it indicates that the transit time considerations for the light and the modulation through the modulator are adequately fulfilled. A description of the traveling-wave approach is given in section 4.1.5.4.1.4.

To obtain an optimum system design it is necessary to tailor the modulator drive circuitry to the modulator. This is important to ensure that the stray capacity is minimized. It is also important to match the output impedance of the drive amplifier to the capacitance of the modulator to obtain the desired cutoff frequency. Both the modulator design and drive design are discussed in the following section.

4.1.5.4.1.1 Electrical Design

In this design approach the modulator forms the capacitive element in a peaking circuit, as those used in a cascade video amplifier. The frequency response of this peaking circuit is determined by the parameter[23],

$$\frac{RC}{\sqrt{LC}} . \qquad (1)$$

When this parameter is set equal to 1.6, a flat frequency response without overshoot is obtained. Under these circumstances, the RC product should equal:

$$RC = \tau_R , \qquad (2)$$

where:

$\tau_R = 2.56 \times 10^{-9}$ s for the 100-MHz bandwidth case.

The circuit power required to drive the modulator is given by:

$$P = \frac{V^2}{R} , \qquad (3)$$

where the voltage across the modulator can be related to the material properties and dimensions of the crystals by the expression:

$$V = \frac{Mb*}{\ell} , \qquad (4)$$

(23) A. V. Bedford, G. L. Fredendall, "Transient Response of Multi-stage Video-Frequency Amplifier," Proc. I.R.E., 27 April 1939.

* Derived from Eq. (3) of Reference (21).

where:

b = the thickness of the electro-optical material
ℓ = the length of the active portion of the modulator
V = the applied voltage

$$M = \frac{\lambda}{2\sqrt{2}\ n^3 r_{63}}$$

λ = the wavelength of light
n = the index of refraction
r_{63} = the electro-optic coefficient

From the figure of merit for the peaking circuit

$$R = \frac{\tau_R}{C} = \frac{\tau_R}{\epsilon\epsilon_o \ell} \tag{5}$$

Substituting Eq. (4) and Eq. (5) into the expression for drive power:

$$P = \frac{M^2 b^2 \epsilon\epsilon_o}{\ell \tau_R}\ , \tag{6}$$

which is solved for the length of the modulator:

$$\ell = \frac{M^2 \epsilon\epsilon_o}{P\tau_R}\ b^2\ . \tag{7}$$

The object of the design is to minimize the length of the modulator ℓ. By minimizing the length of the modulator, a minimum optical loss is obtained, and the sensitivity of longitudinal temperature gradients to angular misalignment, plus internal heating, is reduced. Each of these factors has an important effect on the overall performance of the modulator[21], as can be seen from Eq. (7). The length of the modulator can be reduced by using a small cross sectional dimension and by using a material that has a minimum value for M.

A survey of electro-optic materials was made. This survey included a careful review of the literature and a measurement of those properties not reported in the literature. These material properties are given in table 4.1-11.

Using these data we have computed the modulator length using Eq. (7) for each of these materials. The results of this computation are given in table 4.1-12.

This table shows that the best material to be used for the 100-MHz bandwidth modulator is RDA (rubidium dihydrogen arsenate). The length of the active portion of this modulator is slightly less than five inches. It will have an input impedance of approximately 120 ohms, which makes it adaptable to the impedance level encountered in wide bandwidth transistor circuitry.

TABLE 4.1-11

ELECTRO-OPTIC MATERIAL PROPERTIES

Property	KDP	KDA	ADP	ADA	RDP (RbH_2PO_4)	RDA ($R_bH_2A_sO_2$)	KD*P
r_{63} M/Vx10^{12}	10.3[24]	10.9[24]	4.9[27]	5.5[27]	11.[27]	13.[27]	26.4
n_o	1.512[24]	1.5707[24]	1.525[25]	1.5766[27]	1.52*	1.559[24]	1.512*
n_e	1.47[24]	1.5206[24]	1.479[25]	1.5217[27]		1.520[24]	
	20.2	21.0[26]	14.3	14.0[27]	15.[27]	19.	50.
tan δx10^4	5.	10.	5.	10.		10.	
Thermal Conductivity watts/^oC cm	0.0021[28]	0.0081	0.0071[28]	0.0043		0.0082	
Thermal Birefringence Coefficient x 10^5 ^oC	1.1	2.6	4.7				
Thermal Refraction Index Coefficient x 10^5 ^oC	-1.5	-3.1					

* Estimated

(24) J. H. Ott, T. R. Sliker, Journal of the Optical Society of America, vol. 54, no. 12, December 1964, pp. 1442-1444.

(25) Handbook of Chemistry and Physics, 31st edition, Chemical Rubber Publishing Company.

(26) D. A. Berlincourt, D. R. Curran, and H. Jaffe, Physical Acoustics, edited by W. P. Mason, Academic Press, Inc., New York, 1964.

(27) W. R. Cook, Jr., E. H. Jaffe, Reference Data on Linear Electro-optic Effects in KY_2PO_4 Type Crystals, a publication of the Clevite Corporation, October 15, 1962.

(28) D. A. McCarthy, S. S. Ballard, Journal of the Optical Society of America, vol. 41, 1951, pp. 1062-1063.

TABLE 4.1-12

MODULATOR DESIGN

Material	Length (meters)	Voltage (volts)	Capacity ($\mu\mu$f)	Resistance (ohms)
KDP	0.25	24	44	58
KDA	0.18	27	34	74
ADP	0.73	17	90	28
ADA	0.47	21	59	43
RDP	0.16	35	21	120
RDA	0.12	35	21	120
KD*P	0.095	25	42	61
KTN	0.055	24	490	5.2

A smaller model could be made using deuterated potassium dihydrogen phosphate (KD*P) or KTN. The KD*P modulator would be only about four inches long. However, the optical absorption in KD*P is much higher[29] than that encountered in other electro-optic materials. This higher absorption more than offsets the gain of the shorter length.

KTN could be used for this modulator. The active portion of the modulator would be two inches in length. However, KTN gives a low circuit impedance, which requires a transformer between the circuitry and the modulator. Also, the dielectric and electro-optic coefficients of KTN are sensitive functions of temperature, so that satisfactory operation may be difficult to achieve over even a modest temperature range. Although measurements of the optical absorption of KTN have not been reported, it is likely that because of its high index of refraction and because of its domain structure there is considerable scattering within the KTN crystal and hence high optical absorption.

From these considerations it is concluded that the best material to be used in the 100-MHz bandwidth modulator is RDA.

4.1.5.1.2 Optical Design

The first element in the modulator is a telescope that has an input window of 4mm, so that the modulator will accept a 4mm beam. This telescope reduces the beam diameter from 4mm to 1mm. It has an optical efficiency of 90%, and the wavefront of the exit beam is distorted less than 0.1 wavelength.

The basic configuration of the active portion of the modulator, consisting of the electro-optic crystals and half-wave plates, is described in Reference (21).

---

(29) T. R. Sliker, S. R. Burlage, "Some Dielectric and Optical Properties of KD_2PO_4," Journal of Applied Physics, July 1963, vol. 34, no. 7, pp. 1837-1840.

The half-wave plates balance the natural birefringence of one part of the modulator against the birefringence of the other part. In this modulator we plan to use two half-wave plates that will divide the modulator in effect into four parts. By this means the sensitivity of the modulator to longitudinal temperature gradients is reduced.

The electro-optic crystals will be RDA, 1x1x15mm. They will be equal in length to within one-quarter wavelength. The faces will be flat to 1/10 wavelength and parallel to within two seconds.

Following the active portion of the modulator is a quarter-wave plate and a polarizer to develop the amplitude modulation.

4.1.5.4.1.3 Driver Design

The design of the modulator driver is developed on the requirement that it have an output capability of 10 watts into a load impedance of 120 ohms with a bandwidth of 100 MHz. There are vacuum tube amplifiers that can supply this output requirement. However, for space applications, the necessity to conserve prime power dictates that a solid-state amplifier be used for this purpose. Such solid-state amplifiers are not commercially available. Because of the space application, the driver amplifier will be developed using solid-state techniques.

There are available a number of transistors that have adequate frequency response for this application. However, no single unit has adequate power capabilities. To obtain the desired power level, it is necessary to parallel a number of transistors. The distributed amplifier is a common technique for paralleling a number of elements to obtain both wide bandwidth and power capability.

A block diagram of a distributed amplifier is shown in figure 4.1-20. The input of this distributed amplifier is a lumped element transmission line. The output circuit for the distributive amplifier is also a lumped element transmission line. These two transmission lines are connected by means of active gain elements spanning between the nodal points of the two transmission lines. Either vacuum tubes or transistors can be used for these active gain elements. The problems facing the designer using transistors for these active elements are that the transistor is not a unilateral element, so that coupling exists from the output transistor line back to the input. If this inverse coupling is not neutralized, there is a possibility that the amplifier will oscillate. A second major problem is that the input impedance of the transistor has a substantial resistive component so that attenuation exists along the input lumped element transmission line.

For a first-order analysis, the resistive parts of the input circuits are neglected, and a constant-k characteristic is assumed for both the input and the output lines. The voltage gain is given by:

$$A_v = \frac{V_o}{V_{in}} = \left(\frac{n}{4}\, g'_m\right) Z_o \ ,$$

where:

$$g'_m = \frac{1}{r'_e} \ ,$$

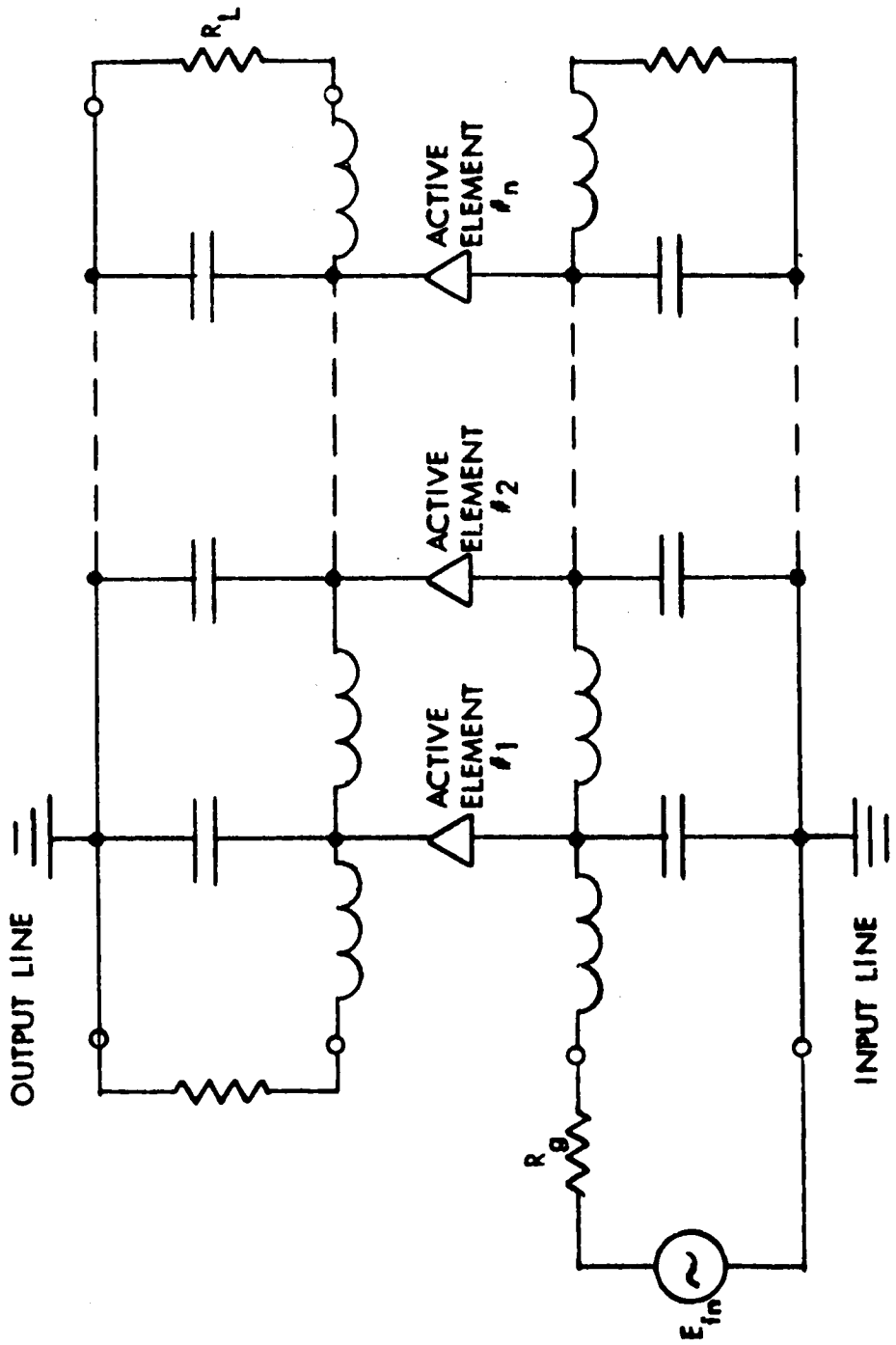

Figure 4.1-20. Distributed Amplifier with n Active Elements

and:

$$Z_o = \left(Z_o\right)_b = \left(Z_o\right)_c = \sqrt{\frac{L}{C}} \ .$$

The bandwidth is given approximately by the cutoff frequency of the line:

$$BW \cong \omega_c = \sqrt{\frac{2}{LC}} \ ,$$

and the voltage gain-bandwidth product of the idealized model is:

$$GBW = \frac{1}{2} n\omega_T \ .$$

The above results cannot be obtained in practice since the idealized model used in the analysis neglects the presence of the series resistance r_b', which is an important factor in the actual design of transistor distributed amplifiers. The resistance r_b' introduces loss along the base-emitter line, and thus decreases the gain-bandwidth product in the common-emitter distributed amplifiers.

Various design approaches may be used when r_b' is taken into account. One approach is to consider a constant-resistance characteristic for both the base and the collector lines. This is the simplest since it avoids mismatching problems. A better approach is to use a constant-resistance base line and a constant-k collector line. This is shown schematically in figure 4.1-21. In this case $r_b' = \left(Z_o\right)_b$ has been selected. This is by no means the only choice. For example, $r_b' = \left(Z_o\right)_b/3$ may be chosen; then a flat-delay characteristic will be obtained for the base line.

The gain of the transistor distributed amplifier is:

$$A_v(0) = \frac{V_o}{V_{in}} = \frac{1}{2}\left(\frac{ng_m'}{2}\right)\left(R_o\right)_c = \frac{n}{4}\frac{\left(R_o\right)_c}{r_e'} \ .$$

When the loss in the base line is included, the 3-dB bandwidth can no longer be approximated by ω_c as is done for the idealized model. The reduction of bandwidth with n is quite severe for both the constant-resistance and flat-delay cases. For example, with the constant-resistance base line, the 3-dB bandwidth is only one quarter of ω_c for n = 5.

Based upon the foregoing discussion, a preliminary design of a transistor distributed amplifier has been made that satisfies the specified performance requirements. A schematic diagram of this amplifier is shown in figure 4.1-22, and its design is described in the following paragraphs.

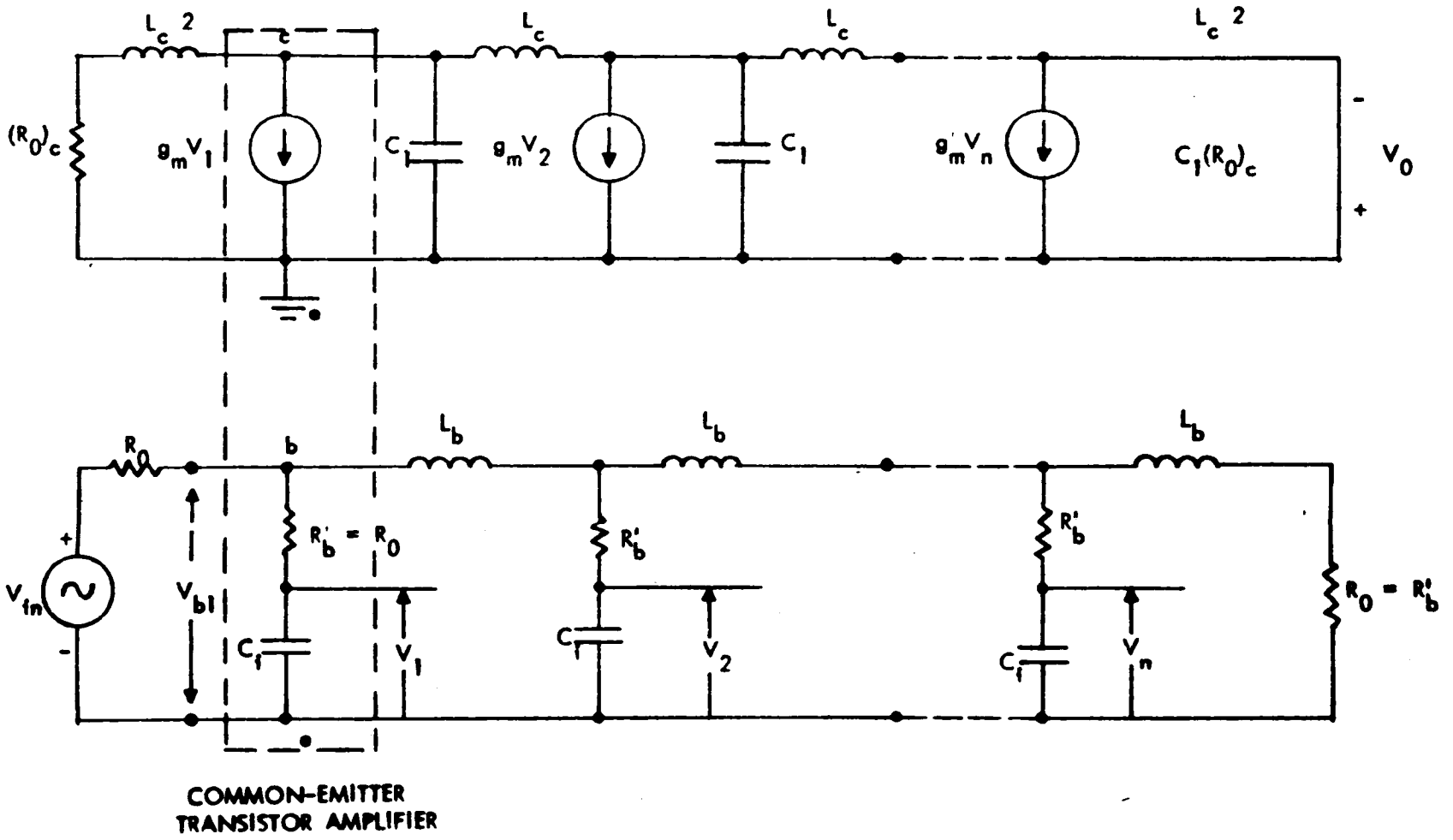

Figure 4.1-21. Complete Transistor Distributed Amplifier with Constant - Resistance Base Line and Constant - K Collector Line

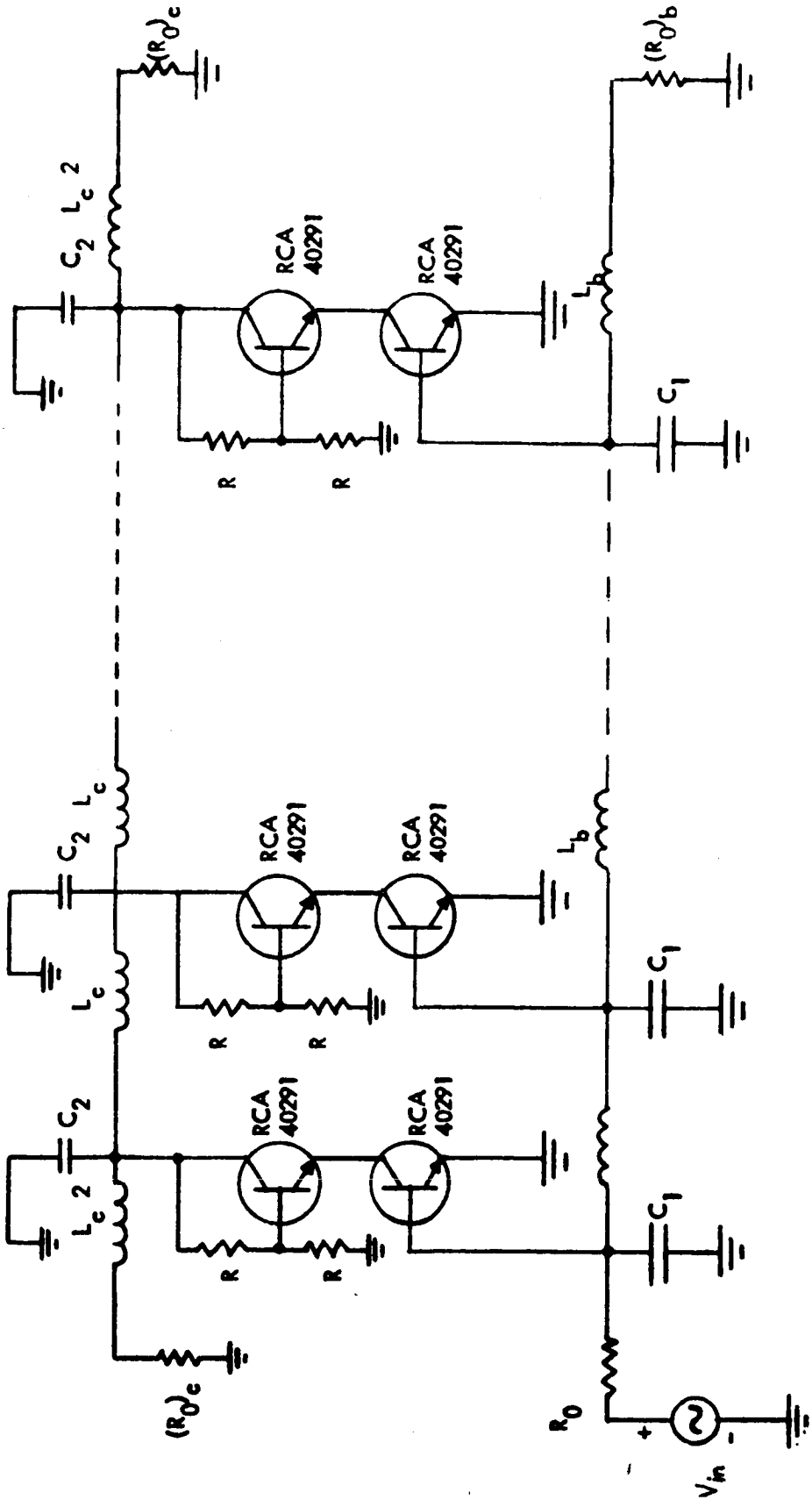

Figure 4.1-22. Preliminary Design of a Distributed Amplifier Using RCA 40291 Transistors.

A cascaded RC-coupled transistor amplifier, such as those manufactured by C-Cor Electronics, may be used as the preamplifier stage for the distributed amplifier. The preamplifier provides approximately 2V rms across a 50-ohm output resistance over a bandwidth of 150 MHz.

Several high frequency transistors such as the 2N706, 2N753, or the more recent Fairchild 2N2884 and RCA 40291 may be used. The preliminary design is based on the RCA 40291 silicon high-power transistors having a breakdown collector-to-emitter voltage, BVces, of 90 volts. For the modulator impedance of 120 ohms and 10-watt output power, an rms output voltage is required:

$$\frac{V_o^2}{120} = 10 ,$$

or

$$V_o = \sqrt{1200} \cong 35 \text{ volts.}$$

Thus the required peak-to-peak output voltage swing is $(2\sqrt{2})x(35)$, which is approximately 100 volts. To satisfy this requirement on the output capability, the amplifier has been designed using two 40291 transistors operating in series to obtain the required voltage swing. This is shown in figure 4.1-22

The bandwidth and the power gain requirements are now considered in order to find the number of transistors needed in the amplifier. The RCA 40291 transistor has a $f_T = \omega_T/2\pi$ of 500 MHz and a maximum collector dissipation, P_c, of 11.6 watts with infinite heat sink.

For the bandwidth consideration, a reference bandwidth of the line to be f_T of the transistor is chosen, i.e., $\omega_c = \omega_T = 2\pi(500 \times 10^6)$, and the base line is designed to have a characteristic impedance of $(R_o)_b = 120$ ohms. Assuming a base spreading resistance $r_b' = 120$ ohms, the base line is designed to have a constant resistance characteristic (see figure 4.1-20). To provide a 3-dB bandwidth of 100 MHz, we need an n of 10 (each consists of two RCA 40291 transistors as shown in figure 4.1-21).

The required gain of the distributed amplifier can be calculated as follows: from the preamplifier an output of 2.2 V rms across 50 ohms is available and the required output from the distributed amplifier is 35 V rms across a 120-ohm output. Thus the required gain is:

$$\frac{35}{2}\sqrt{\frac{50}{120}} = \left(\frac{17.5}{1.55}\right) = 11.3 ,$$

where the collector line is designed to have a characteristic impedance of:

$$(R_o)_c = 120 \text{ ohms.}$$

The transistor transconductance, g'_m, is given by:

$$g'_m \cong \frac{1}{r'_e} = \frac{2}{120} = \frac{1}{60} .$$

Using the gain expression presented previously:

$$A_o(o) = \frac{V_o}{V_{in}} = \frac{1}{2}\left(\frac{ng'_m}{2}\right)(R_o)_c = \frac{1}{2}\left(\frac{n}{2}\right)\left(\frac{1}{60}\right) 120 = 11.3 \text{ (required)}.$$

or

$$n = 2 \times 11.3 \cong 23.$$

Therefore, for the required voltage gain, an n of approximately 23 is needed. However, the actual distributed amplifier can be built as a cascade of several stages, each of which consists of a number of sections. Since the same characteristic impedance has been chosen for both the base and collector lines, no impedance transformer is needed in cascading the stages. The total number of transistors needed will be reduced.

The distributed amplifiers in cascade are now considered. The complete amplifier consists of several stages connected in cascade, i.e., the output end of the collector line of one amplifier is coupled into the input end of the base line of the succeeding amplifier. For simplicity, consider the case where $(R_o)_b = (R_o)_c$, and denote the following quantities:

n = number of sections in a stage
m = number of stages in cascade
N = total number of transistor sections
A = gain of a section
A_v = gain of a stage
G_v = total gain of the amplifier.

Then:

$$N = nm,$$
$$A_v = n\left[\frac{1}{4} g'_m (R_o)_c\right] = nA,$$

and

$$G_v = (A_v)^m = (nA)^m = \left[\frac{n}{4} g'_m (R_o)_c\right]^m .$$

From the last equation for the total gain:

$$n = \frac{1}{A}(G_v)^{1/m} .$$

Thus:

$$N = nm = \frac{m\left(G_v\right)^{1/m}}{A} .$$

The minimum total number of transistors can be found by setting the derivative dN/dm = 0. The result is that N is a minimum when:

$$m = \log_e\left(G_v\right) ,$$

and the corresponding minimum N is:

$$N = n \log_e\left(G_v\right) .$$

That is, the gain of each stage must be

$$A_v = nA = \epsilon = 2.71 \ (8.7 \text{ dB}) .$$

This minimization represents a method of dividing transistors into identical stages, so that a given overall gain is achieved using the smallest number of transistors. It is noted, however, that there is a reduction of the overall bandwidth because of the shrinkage of cascaded stages. Thus, this must be taken into account by designing the individual stages to have a bandwidth exceeding the required 100 MHz.

Applying these results on cascading stages to the design of the complete amplifier, it is noted first that the overall gain required is 20 log (11.3) = 21 dB. Since the optimum gain of each stage, as shown above, is 8.7 dB, the number of stages is chosen to be m = 3. Then the number of sections to provide the 8.7 dB gain can be calculated.

We have:

$$\frac{n}{4} g_m'\left(R_o\right)_c = 2.71 ,$$

or

$$n = 5.42 \cong 6 .$$

This yields a total of N = nm = 18 transistors. The bandwidth of each stage should be around 200 MHz to compensate for the shrinkage due to the cascading of three identical stages. In addition, alternative design is possible using cascade stages that are not identical in the number of sections. The bandwidth of the overall amplifier must, however, be calculated to satisfy the required specification.

Finally, for the power handling capabilities of the transistors, it can be assumed that a 30% efficiency can be obtained, and that each transistor section (consisting of two RCA 40291 transistors) will provide a minimum of one or two watts with the required output voltage swing. Then the final amplifier stage with a total of six transistor sections having a total of 12 transistors will be adequate as far as power handling capability is concerned.

4.1.5.4.1.4 Traveling-Wave 100-MHz Modulator Design

In the design of the 1.0-GHz-bandwidth phase[30] and amplitude[31] modulators, the dimensions of the modulator structure are chosen to obtain a match between the velocity of the light in the crystals and the phase velocity of the modulation in the transmission line. In these very wide bandwidth modulators, the electrodes are the conductors of a distributed element transmission line. These modulators typically require 50 watts drive to obtain 100% amplitude modulation, and have a characteristic impedance on the order of 27 ohms.

The design of the 100-MHz bandwidth, 10 watt amplifier will also be predicated on obtaining an adequate match in velocity of the light through the crystal and the modulation on the electrode structure. However, in order to obtain the higher characteristic impedance and thus reduce the drive power requirement, a lumped-element structure will be used.

The analysis of this lumped element modulator will proceed by first defining the velocity matching requirements. These velocity matching requirements are expressed in terms of the difference between the transit time of the light through the modulator and the transit time of the modulation at 100 MHz. This modulation transit time will be computed from the expressions from the phase shift per section for the filter section.

Tchebycheff, Butterworth, Bessel function, and constant K filters have been investigated, and it was found that the constant K filter is adequate for this work, and is indeed superior to the other more sophisticated filter designs. An expression will then be written for the drive power requirement for the modulator in terms of the material properties of the electro-optic material and the characteristic impedance of the modulator. Combining these expressions, the transit time inequality is written in terms of the length and width of the electro-optic material, the drive power, and the electro-optic material properties.

Using the design equations above, we have examined each of the available electro-optic materials for this application. The most promising material is RDA $\left(RbH_2A_sO_2\right)$.

From Eq. (12) of Reference (31) an equation is obtained for the permissible difference in velocity between the modulation and the light. This expression is obtained by setting M in Eq. (12) of Reference (31) equal to 0.7 and solving for the argument of the sine function. This results in:

$$\omega\left(\frac{\ell}{V_L} - \frac{\ell}{V_m}\right) = \pm 1.4 \ , \qquad (8)$$

(30) "Gigacycle Bandwidth Coherent Light Traveling Wave Phase Modulator," Proc. IEEE, January 1963, vol. 51, no. 1, pp. 147-153.

(31) "Gigacycle Bandwidth Coherent Light Traveling Wave Amplitude Modulator," Proc. IEEE, May 1965, vol. 53, no. 5, pp. 455-460.

where

ℓ = the length of the modulator
V_L = the velocity of light
V_m = the velocity of modulation.

Recognizing that ℓ/V_m is the transit time of the modulation, Eq. (8) can be rewritten in the form:

$$t_m \leq \pm \frac{1.4}{\omega} + t_L = \frac{1.4}{\omega} + \frac{n}{V_L} = \frac{1.4}{2\pi \times 10^8} + \frac{\ell \times 1.54\ s}{3 \times 10^8 m} = 2.2 \times 10^{-9} + 5.1 \times 10^{-9} \ell\ , \quad (9)$$

where:

t_m = the transit time for modulation
t_L = the transit time for the light.

Evaluating this equation for $\omega = 2\pi \times 10^8$/second gives the curve shown in figure 4.1-23.

For a constant K filter the phase constant per section is:

$$\beta = 2 \sin^{-1} \frac{\omega}{\omega_c}\ . \quad (10)$$

The transit time through a modulator composed of N sections would then be:

$$t_m = \frac{N}{\omega} = \frac{2N}{\omega} \sin^{-1} \frac{\omega}{\omega_c}\ , \quad (11)$$

where:

$$\omega_c = \frac{1}{\sqrt{LC}}\ ,$$

N = the number of sections in the filter.

From the expression for the drive power for the modulator, N can be eliminated from Eq. (11). The drive power is given by:

$$P = \frac{V^2}{z}\ , \quad (12)$$

where

V = the voltage on the modulator
z = the characteristic impedance.

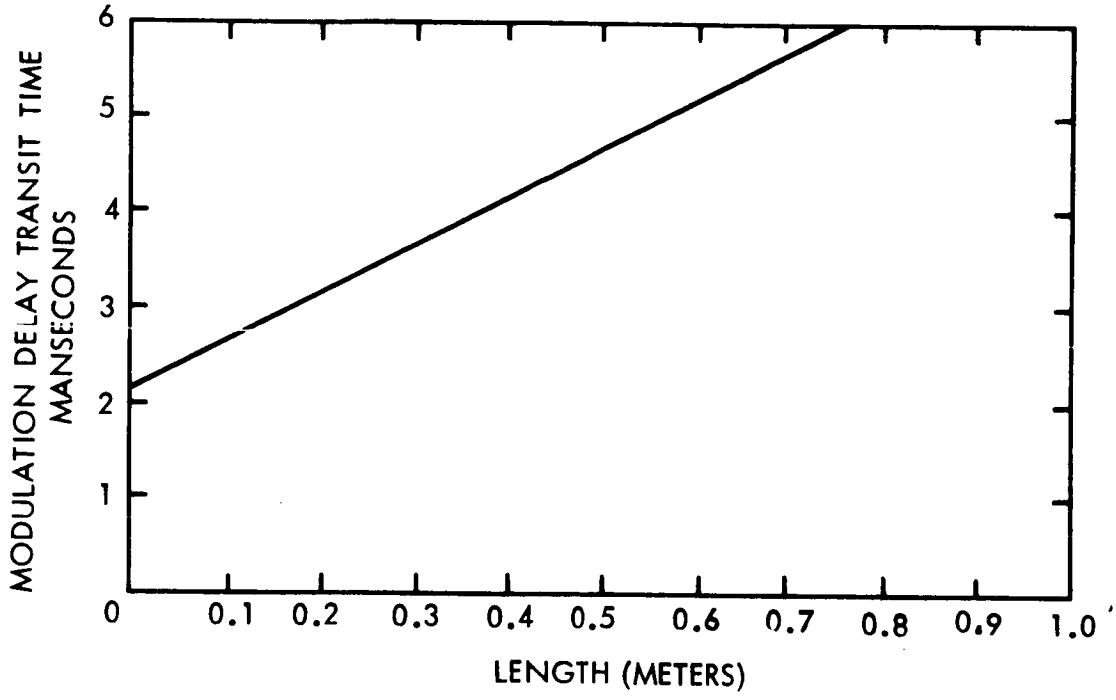

Figure 4.1-23. Plot of Maximum Allowable Modulation Delay Time at 100 MHz as a Function of Modulator Length

The voltage on the modulator is expressed in terms of the electro-optic properties of the material and the modulator dimensions by:

$$V = \frac{\lambda b}{2\sqrt{2}n^3 r_{63}\, \ell} \tag{13}$$

where:

λ = the wavelength of light
b = the cross sectional dimension of the electro-optic crystals
n = the index of refraction
r_{63} = the electro-optic coefficient
ℓ = the length of the modulator.

For convenience, let M:

$$\frac{\lambda}{2\sqrt{2}n^3 r_{63}}\,, \tag{14}$$

so that:

$$V = M\,\frac{b}{\ell}\,. \tag{15}$$

The characteristic impedance of the modulator is given by:

$$z = \sqrt{\frac{L}{C}} = \frac{1}{\omega_c C} = \frac{N}{\omega_c C_T}\,, \tag{16}$$

where:

C_T = the total capacity of the modulator
c = the capacity/section.

The total capacity of the modulator can be expressed as:

$$C_T = c\ell\,,$$

where:

$$c = \epsilon\epsilon_o\,,$$

so that rewriting the characteristic impedance of the modulator we get:

$$z = \frac{N}{\omega_c c_1 \ell} . \tag{17}$$

This expression for the characteristic impedance and the expression for the voltage in Eq. (15) are substituted into Eq. (12), and the result solved for N yields:

$$N = \frac{M^2 b^2}{P\ell} \omega_c c . \tag{18}$$

This expression and the number of filter sections in the modulator are substituted into the equation for the modulator transit function given in Eq. (11) to give:

$$t_m = \frac{2M^2 b^2 \omega_c c}{P\ell\omega} \sin^{-1} \frac{\omega}{\omega_c} \tag{19}$$

Thus the design inequality for the modulator is:

$$\frac{(c_o + s1)P\ell}{2M^2 b^2 c} \geq \frac{\omega_c}{\omega} \sin^{-1} \frac{\omega}{\omega_c} . \tag{20}$$

Satisfying this inequality will assure that the difference between the transit time for the modulation and the transit time for the light is adequately small. The right-hand side is a normalized expression for the actual transit time through the modulator. The left-hand side is an expression for the maximum allowable transit time through the modulator. Figure 4.1-24 is a plot of the right side of Eq. (20) showing that, for small values of ω/ω_c, this expression is substantially equal to unity. The left side of Eq. (20) contains all the material properties of the electro-optic material. These material properties can be lumped together as:

$$P(t_o + s\ell) \frac{1}{b^2} ,$$

so that the quantity $p = P/2M^2 c$.

Table 4.1-11 lists p for each of the available electro-optic materials. The most attractive material will have the highest value of p. Thus from examination of this table it can be seen that the material RDA is markedly most suited to this application. It is almost twice as good as KDP and 50% better than KDA.

By inserting various values for b and ℓ into Eq. (20) satisfactory dimensions are determined for the RDA modulator: a crystal cross-section of 1 mm and an optical material length of 20 cm. The characteristic impedance of this modulator will be 50 ohms; there will be

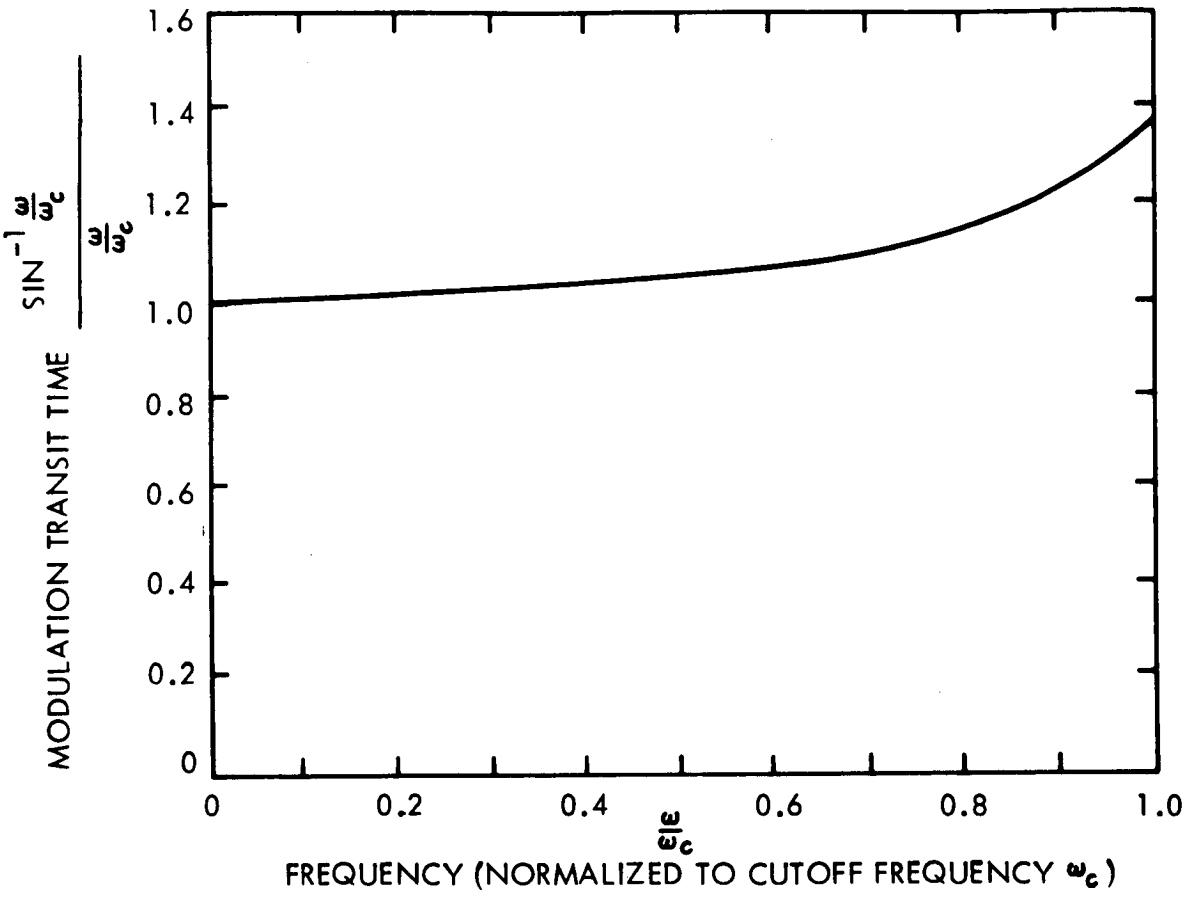

Figure 4.1-24. Modulation Transit Time as a Function of Frequency

10 filter sections within the modulator; and 20 volts will be required to obtain 100% amplitude modulation.

4.1.6 Required Technology Development Schedule

FY 1967:

Begin 24-month development of video modulators for use at 10.6 microns.

Study and experimentally evaluate those modulation techniques and materials that can be used at the CO_2 laser wavelength of 10.6 microns. Optical AM, FM, PM, and Pol M should be considered. Electro-optic and acousto-optic techniques should be examined. The objective will be the fabrication and delivery of a suitable modulator, meeting the following operating specifications;

a. instantaneous bandwidth capability shall be at least 10 MHz.
b. optical insertion loss of no more than 6 dB.
c. materials must be able to withstand launching shocks and prolonged exposure to high vacuum.
d. the lowest drive power requirement for a given modulation index consistent with the above.

(Developments in tunable optical parametric oscillators may make it possible to overcome the Doppler shift encountered on interplanetary missions if a good video bandwidth detector is available at 10.6 microns.)

Begin development of stable 0.6328-micron and 10.6-micron lasers (now underway NASA Contract No. NAS8-20631) with emphasis on ruggedization.

The development of a laser package suitable for spacecraft use will be analyzed under the following topics: Gas Discharge, Optical Resonator, Cooling System, Control System, and Integrated Package.

a. Gas Discharge: The lasers now being considered for OTAES are gas lasers. From laboratory versions of these lasers, one has information on the gas composition and pressure, current densities, and bore diameters that are suitable for lasers. The problem is one of devising a gas discharge tube that has long life in both the operating and the on-the-shelf condition.

b. Optical Resonator: The mathematical treatment of the problem of the optical resonators suitable for lasers has been developed thoroughly. The technical methods for making the laser cavities to the high degree of precision on mechanical and optical tolerances have been perfected so that laboratory lasers have the characteristics predicted by the mathematical models. The problem is to devise rugged structures that are resistant to environmental factors such as shock and vibration. In addition to ruggedization, compensation for unavoidable changes will probably have to be provided by servo systems to obtain anything that approaches optimum performance.

c. Cooling System: One of the significant differences between the environment of laboratory lasers and spacecraft lasers is the loss of convection cooling. In some cases there will be no air cooling simply because of a vacuum environment. Even if the laser is in a pressurized environment, convection cooling would not be effective because of the free-fall condition of the spacecraft. Radiation of heat from the surface of the laser package must be restricted because such radiation would give rise to undesirable thermal expansion of associated elements of the optical system. For low power lasers

a shell that has good thermal conductivity may absorb the radiant heat from the laser and conduct it to a bulkhead or other heat sink. For high power lasers conduction cooling will probably have to be supplemented by some form of forced-flow liquid cooling.

d. Control System: The inaccessibility of the spacecraft laser for manual adjustment requires that automatic or remotely operated controls should be devised that are capable of getting the laser into operation and for switching it on and off as the experimental program requires.

e. Integrated Package: In the spacecraft it is necessary to conserve space. The gas reservoirs, structural elements of the resonator, and conduction elements of the cooling system are to be confined to a small space and, where possible, serve several functions.

In summary, laboratory lasers provide a base for the design of specific spacecraft lasers. Areas where development work is required before hardware will become available that can pass appropriate tests or that could be used in spacecraft for OTAES experiments are:

(1) Discharge tube life
(2) Ruggedization
(3) Cooling
(4) Controls to replace manual adjustments
(5) Integrated package.

Continue development of laser mode control and stabilization techniques. (Now underway Air Force Contract No. AF 33(615)-2884, and NASA Contract No. NAS8-20558.)

Begin 12-month design/development of space-qualified He-Ne and N_2-CO_2 lasers.

Analyze structural designs for gas lasers capable of remote alignment and tuning. Analyze the heat transfer characteristics of the various designs. Fabricate and test those designs that will withstand launch shock and give reliable, long-life performance. Investigate both dc cold cathode and RF pumping systems. Conduct shock and vibration tests on the completed designs.

Begin 24-month design/development of infrared photodetectors having high quantum efficiency at 10.6 microns, and having a frequency response extending to at least 10 MHz.

Design and fabricate high quantum efficiency IR detectors, dewars, high-frequency coupling structures, and cooled optical filters into a packaged unit that will provide the basis for field tests of optical propagation. The detector package must be self-contained, with a coolant boil-off time of at least two hours (preferably eight hours). It is anticipated that currently available semiconductor materials will be capable of adequate frequency response if properly packaged, but other newer materials or techniques must be evaluated during the design phase if they show promise of attaining the same goal.

FY 1968:

Begin 12-month ground-to-ground measurement program of atmospheric coherence diameter at 10.6 microns, and pulse distortion measurement tests at 0.6328 microns, where broad band phototubes are available.

Establish a propagation test range or ranges, preferably with portable laser transmitters and receivers, so that measurements can be made over a variety of test paths. Tests should be one-way only; no mirrors or retroreflectors should be used. A path length of at least two miles is required.

Conduct tests of two laser systems: a 10.6-micron CW and a 0.6328-micron fast-pulse system. Determine the dependence of effective receiver coherence diameter at 10.6 microns on weather conditions, site location, etc. Determine the upper limit on bandwidth of signals that can be propagated at 0.6328 microns by making pulse distortion measurements of the output of an AM-locked multimode laser. Conduct tests simultaneously at both wavelengths if possible, for more accurate comparative data.

Conduct ground-to-ground tests of a complete optical communication system of video bandwidth, transmitting two wavelengths simultaneously.

Evaluate the communication system capabilities for various modulation and detection schemes under a variety of atmospheric conditions. This program would be expected to make use of some of the results and the facilities available during the propagation test program. Collect data on fading and fading rates for comparison with theory, for the design of an electronic system to simulate the effects of the atmosphere in the laboratory, and for comparison with data to be obtained on high angle slant paths. Evaluate, in particular, the performance and reliability of the 10.6-micron receiver system.

Continue development work in laser stabilization and on wideband infrared detectors and modulators.

Improve the design and begin fabrication of prototype space-qualified modulators and detectors.

Design and fabricate ruggedized video bandwidth detectors for the visible spectrum, and video bandwidth modulators for the 10-micron band. Results of previous development efforts will be applied. The objective of this program will be the delivery of modulator and detector packages that have been rigorously tested for vulnerability to shock, vibration, temperature extremes, ionizing radiation, vacuum, etc.

Begin 30-month design and fabrication of a piggyback space-to-ground propagation experiment emphasizing pulse distortion measurements at 0.6328 microns, and coherent aperture measurements at 10.6 microns.

Carry out detailed design of an operating laser system or systems that will make atmospheric diagnostic measurements. The systems will be configured to an AAP pallet package, allowing some preliminary testing of space hardware, of atmospheric properties, and of pointing and tracking system capabilities.

The experiment should consist of laser transmitter(s) that are carried aboard the vehicle and that can be trained with sufficient accuracy to illuminate a ground receiving station.

Signal properties that have been investigated on ground-to-ground paths will be measured over high-angle, space-to-ground paths.

Begin fabrication of subsystems and components for a piggyback system as the appropriate design phase is completed.

FY 1969:

Conduct preliminary propagation tests over high-angle atmospheric paths, using high altitude balloon platforms for transmitting laser signals to the ground. Carry out such tests with satellites having usable corner reflectors at 10.6 microns.

Make use of existing laser transmitters and of balloon technology to make upper-atmosphere to ground propagation measurements. Pointing and tracking requirements will not be stringent at either end. Wavelengths of 0.6328 and 10.6 microns should be used, as well as other new laser wavelengths that may be of value for meteorology or communications.

Many of the same parameters measured in ground-to-ground tests must be measured over the long path for comparison, for verification of theory and to provide an intermediate step toward a space-to-ground experiment.

As before, the measurement of atmospheric coherence diameters at 10.6 microns and of fast pulse distortion at 0.6328 microns will be of most importance, for comparison under these conditions.

FY 1970:

Begin fabrication of some OTAES subsystems and hardware.

Fabricate prototype OTAES optical subsystems, from laser transmitter, receiver, modulator, and transmitting telescope. Fabricate the required optical ground test facilities and equipment. Conduct test and integration of subsystems with each other, and with established spacecraft design.

4.2 OPTICAL HETERODYNE DETECTION IN SPACE

4.2.1 Summary

Earth satellites have opened new areas of investigation in the atmospheric sciences. Optical technology, in applications such as planetology and large scale weather analysis and prediction, is one of the more important tools in these new investigations. Its utility can be enhanced by a more detailed understanding of the transmission properties of the atmosphere at the visible and infrared frequencies. One approach to such detailed understanding is to adapt the techniques of communication engineering to optical frequencies. A laser heterodyne receiver, for example, can distinguish fluctuations in the optical phase of the received signal. The results of such an investigation would have several potential applications such as meteorology and space geophysics data interpretation. If a spaceborne heterodyne receiver monitors a ground-based laser transmitter, the phase perturbations on the signal due to the atmosphere can be established. The scientific interest in this kind of experiment is even greater when a ground receiver is simultaneously monitoring a laser signal sent from the spacecraft.

Another, most promising, future application for laser technology is space communication, and one of the most important steps toward exploiting this possibility is the thorough examination of the communication properties of the Earth's atmosphere from bottom to top. Alternative approaches are provided in the proposed experiment. Both direct and heterodyne optical receivers will be used aboard the spacecraft for comparison under a variety of atmospheric conditions (figure 4.2-1).

This experiment can only be usefully performed in space. Data must be gathered for a long enough time to permit meaningful statistical analysis and correlation with gross measurables such as winds, temperature profiles, humidity, and seeing. Measurements will be most valuable at small zenith angles where ground-based measurements provide very limited data. Measurements from high altitude balloons can give limited but useful preliminary results incorporating much, but not all, of the sensible atmosphere in weather conditions suitable for balloon launching. Aircraft tests are not feasible because of the high vibration and turbulence environment. Heterodyne measurements made over the ground-to-space path will aid in the understanding of the detailed properties of an atmospherically limited down-link.

4.2.2 Objective

The objective of this experiment is to establish a heterodyne link from ground to spacecraft, to measure the degradation caused by the atmosphere, and to compare these results with those obtained at the same time from the down-link.

4.2.3 Justification

4.2.3.1 Contribution and Need

Heterodyne detection onboard the OTAES vehicle can be a useful tool for the evaluation of atmospheric effects. By implementing a ground to space heterodyne link it will be possible to determine scintillation spectra, optical phase fluctuations, and polarization fluctuations in the absence of significant angle of arrival effects, which are always present in space to ground measurements. By imposing various modulations it will also be possible to find the types and rates of modulation which can be supported by the atmosphere, and these can be compared with down-link measurements. Should future system designers consider adaptive optical communication from space to Earth, an optical up-link could sense the capacity of the transmission path for adaptive feedback purposes. Polarization measurements will be useful in evaluating polarized light communication techniques. Phase measurements can be used to assess optical phase or frequency modulation methods. The

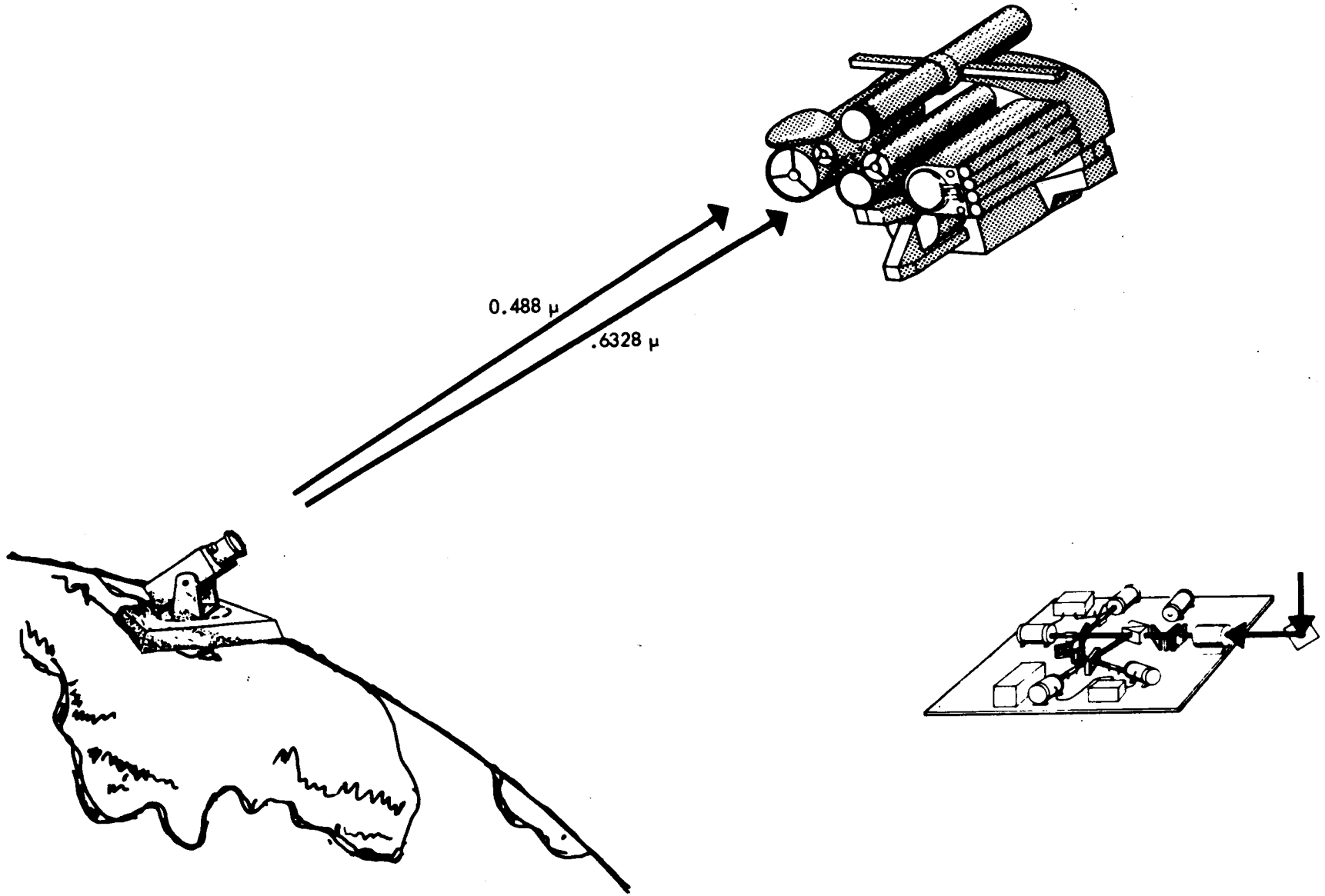

Figure 4.2-1. Heterodyne Detection in Space

transmission and S/N equations for the up-link are the same as those for the down link, which are presented in section 4.1.3.1.

Turbulence in the atmosphere can cause variations in the index of refraction. The resulting beam bending may greatly affect communication from the ground to the spacecraft. It may be necessary to sacrifice some of the aperture gain by broadening the transmitted beam to assure that some part of the deflected beam will be incident on the receiving aperture. It is not expected, however, that angle-of-arrival effects will be important at the spacecraft receiver.

Scintillation in received signal power for a ground-to-space measurement is expected to differ from that observed in a space-to-ground measurement. The data obtained from an up-link will allow the effects of the atmosphere on an earth-based beacon to be predicted for longer interplanetary path lengths. Since a heterodyne receiver can detect extremely weak signals in the presence of earthshine, it will be particularly useful in tracking a beacon which has been reduced in power to simulate Mars distances, and in analyzing atmospheric perturbations on the beam.

The performance of ground-to-space optical heterodyne communication links cannot be predicted accurately when the transmitter is immersed in the earth's atmosphere. A heterodyne receiver in space can provide the data needed to determine the types and rates of modulation that can be supported by the atmosphere. The results of this experiment can also help to establish the design choices for future laser communication systems since wavelength, modulation, and detector techniques can only be decided on the basis of a thorough knowledge of atmospheric effects. For this reason, several wavelengths will be used and various modulations will be placed on the link. The quantities to be measured in space are receiver signal power, heterodyne signal power, and fluctuations in both polarization and phase.

4.2.3.2 Need for Space Testing

The effect of transmitting a narrow beam through the whole atmosphere and to a synchronous orbit satellite cannot be determined from theoretical analyses because of the many variables and the lack of data on these variables. The beam deflection will occur in a random manner and prediction of performance can only be made after a large number of samples of beam transmissions have been made and related to the atmospheric conditions. An orbiting satellite will provide up-link performance data which may then be used to predict performance for deep space probes.

As in the case of the heterodyne down-link (4.1.3.2), measurement in the far field will ultimately be essential ($R_f = \frac{2D_t^2}{\lambda} \approx 1000$ Km), and a high elevation angle slant path is required for adequate simulation of the deep space communication situation. In addition, a stationary satellite orbit is preferred to minimize the contamination of atmospheric measurements with tracking noise.

Ground-to-balloon propagation tests are an important first step in a better understanding of the up-link properties. Aircraft tests are not feasible because of the high local turbulence and vibration environments. These effects will mask the scintillation phenomena that are of interest.

Synchronous satellite altitudes are most desirable since the scintillation observed from an aircraft or near-earth satellite would be complicated by large angular rates of the line-of-sight. In addition, measurements should be made over a sufficiently long time to obtain statistically meaningful data as well as to monitor minute-by-minute changes in atmospheric conditions with a fixed line-of-sight.

4.2.3.3 Feasibility

The development of ground based optical heterodyne receivers has advanced to a point where the design considerations can now be extrapolated for use in a satellite borne heterodyne receiver. The local oscillator laser has not yet been developed for space applications, but a reasonable design can be developed based on the present state-of-the-art of lasers and present knowledge of the space environment. Alignment of the various elements making up the heterodyne receiver can be maintained under the rigors of launch, using standard optical assembly techniques such as drilling and pinning each element in position after final alignment has been accomplished. Detectors for spacecraft application are available for all frequencies of interest, but require cooling to $30^{o}K$ or lower for the far infrared wavelengths. The ground equipment and facilities needed for this experiment are within the present state-of-the-art.

For the visible wavelengths of 0.488 microns and 0.6328 microns, critical components such as modulators, beam splitters, detectors, optical elements and their coatings have been demonstrated in environments similar to those expected for this OTAES experiment. Design and space qualification testing of lasers must be started soon since laser reliability and lifetime estimates are still low. Only the laser and the heterodyne receiver assembly remain to be space tested. However, earth-based optical heterodyne links have been demonstrated over kilometer distances. The most critical parameter is the frequency stability of the spaceborne laser local oscillators, which brings about the requirement that they be acoustically decoupled from their surroundings.

4.2.4 Implementation

4.2.4.1 Experiment Design

A ground-to-space link will be established. The spacecraft will receive 0.488 micron radiation through a one-meter aperture and 0.6328 micron radiation through a 0.3-meter aperture (figure 4.2-2). On the ground, both wavelengths should be transmitted through the same aperture.

Several parameters will be measured at each spacecraft heterodyne receiver. They are:

a. Amplitude fluctuation of heterodyne signals.

b. Frequency (or phase) fluctuations in the heterodyne signals.

c. Polarization fluctuation: Since each direct and each heterodyne receiver is sensitive to orthogonal polarizations, any differential treatment by the atmosphere can be detected.

The block diagram of the equipment required for the "Optical Heterodyne Detection on the Spacecraft" experiment is shown in figure 4.2-3. Each ground transmitter will be made up of the following subsystems: 1) super-mode laser with its power supply, mode stabilization controls, and automatic frequency control; 2) electro-optic modulator with the modulation driver, power supply, and signal source. The telescope, including secondary optics, beam deflection subsystem, and pointing and tracking controls, will be shared by both wavelengths. Each spacecraft receiver will be made up of the following subsystems: 1) spacecraft telescope, including its secondary optics, beam deflection subsystem, and pointing and tracking controls; 2) dichroic mirror; 3) optical filter; and 4) duplex heterodyne receiver.

The requirements for a ground-based laser transmitter are the same, in essence, as those for the spaceborne transmitters. Stable single-frequency operation is needed, and this will be obtained in the same way as in the spacecraft transmitter system, i.e., with a

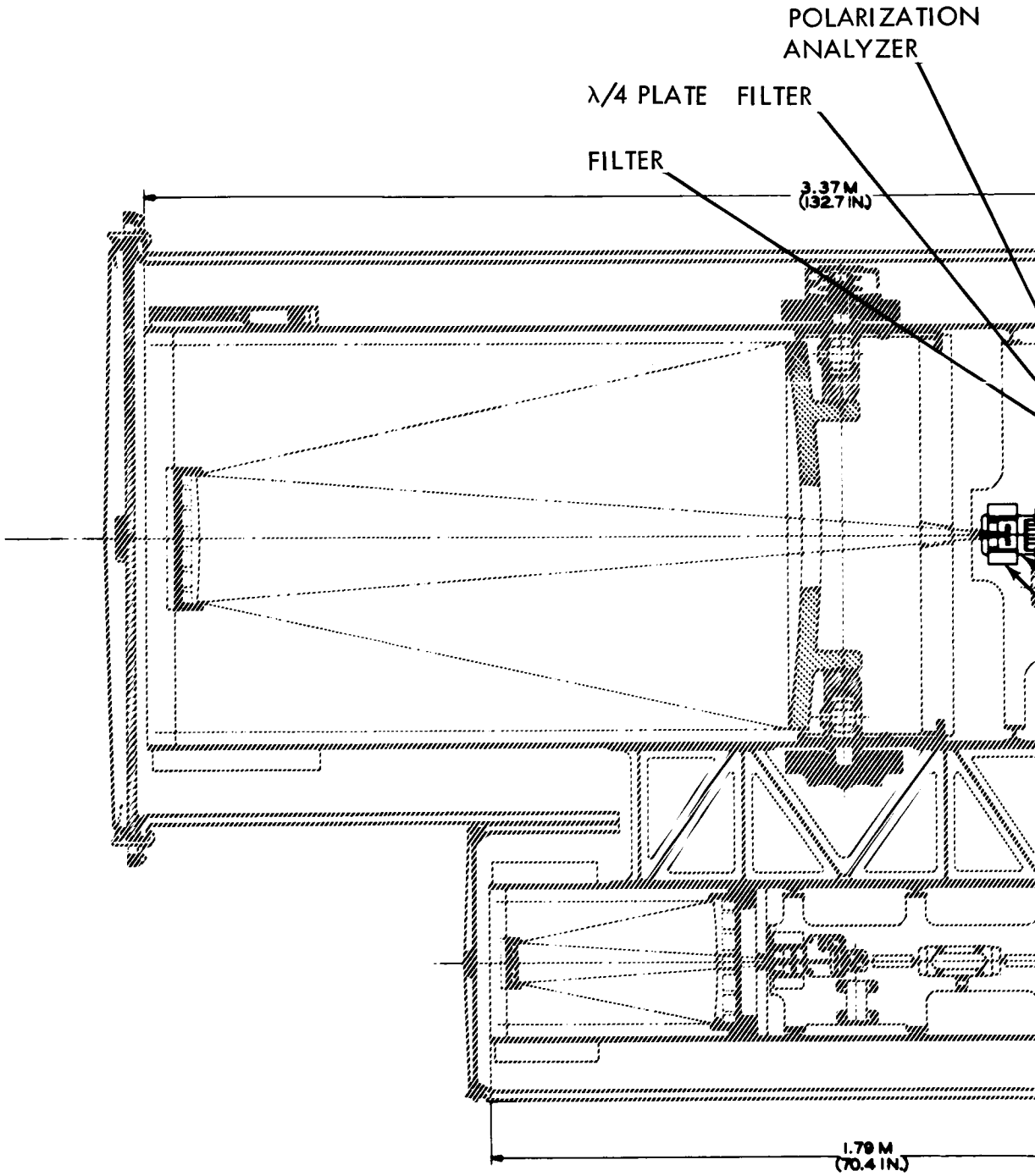
POLARIZATION
ANALYZER
λ/4 PLATE
FILTER
FILTER
3.37 M
(132.7 IN.)
1.79 M
(70.4 IN.)

1-127-1

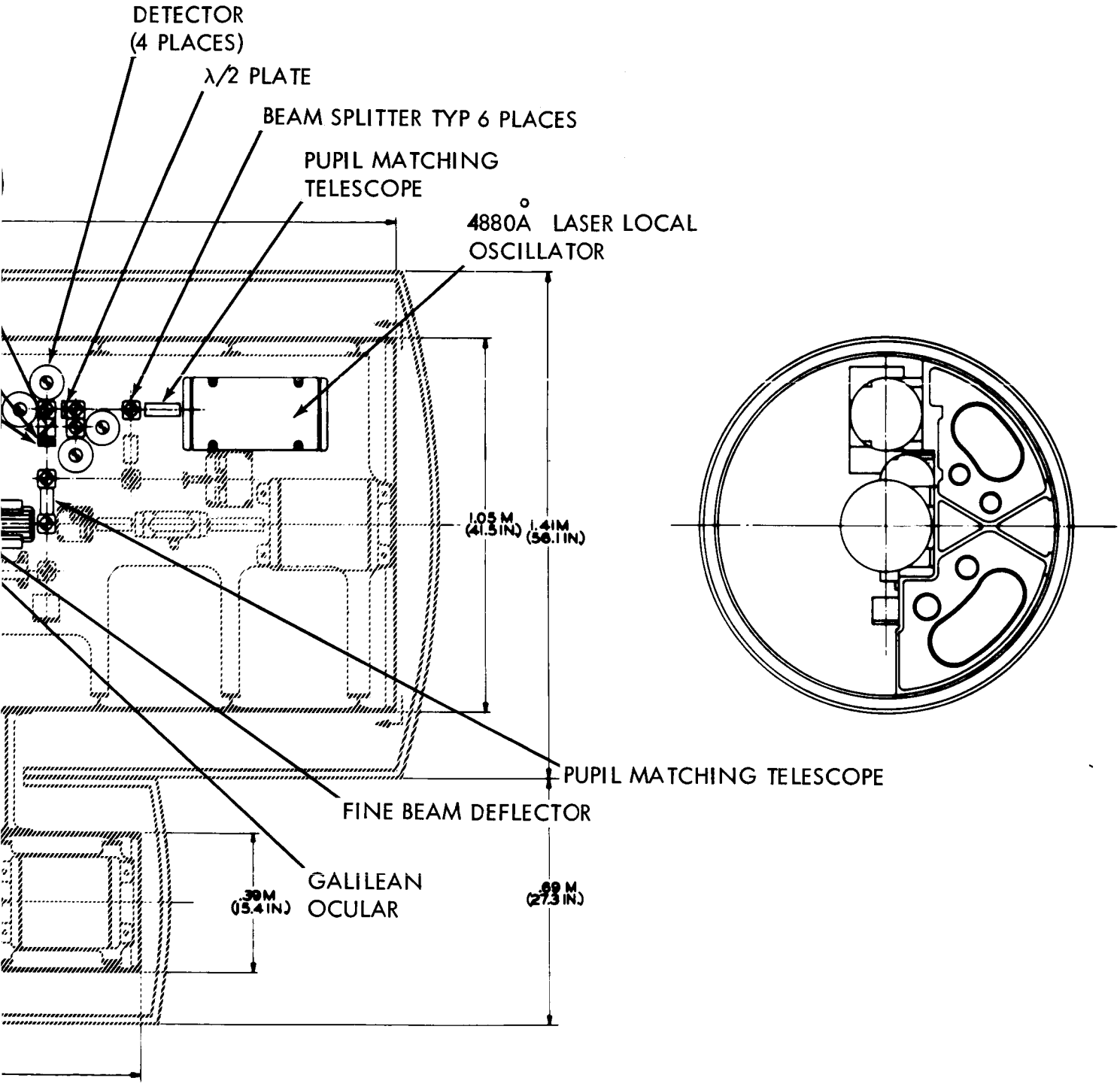

Figure 4.2-2a. Telescope Numbers 1 and 2.

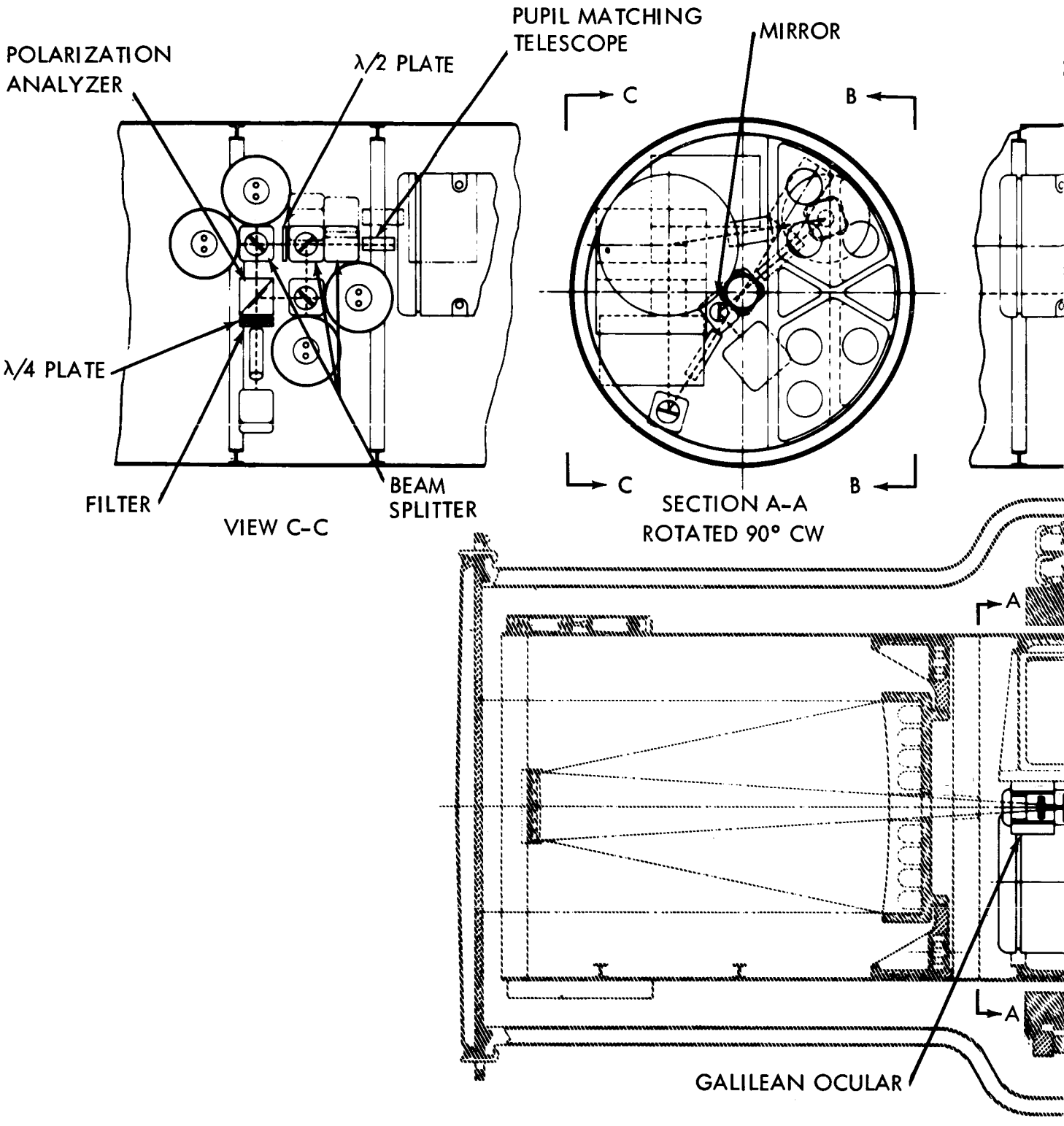
POLARIZATION ANALYZER
λ/2 PLATE
PUPIL MATCHING TELESCOPE
MIRROR
C
B
λ/4 PLATE
FILTER
BEAM SPLITTER
VIEW C-C
C
B
SECTION A-A ROTATED 90° CW
A
A
GALILEAN OCULAR

1-127 9

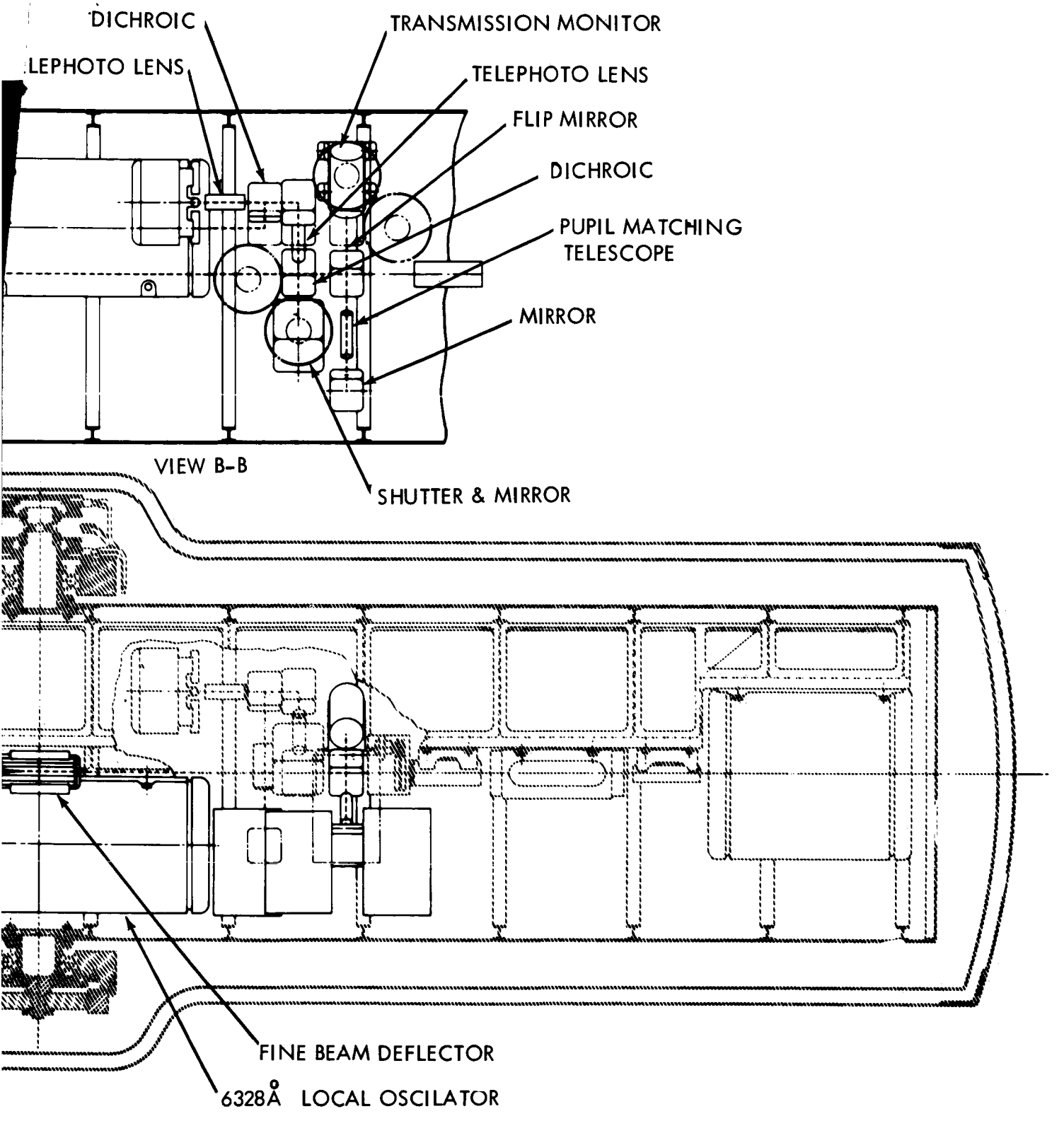

Figure 4.2-2b. Telescope Number 3

~~1-127a~~
1-128

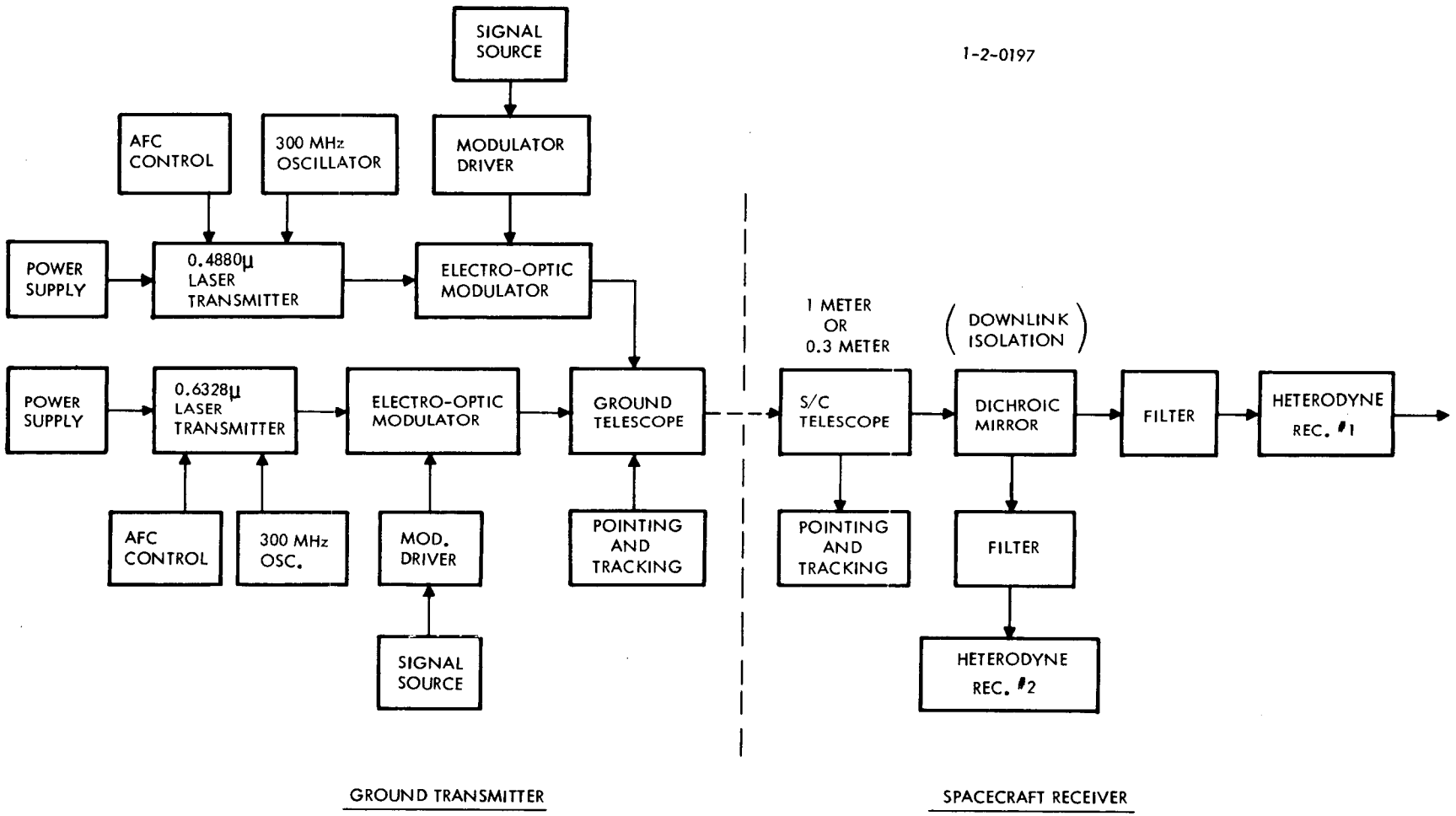

Figure 4.2-3. Block Diagram of Heterodyne Detection on the Spacecraft Experiment

combination of mode-coupling techniques and acoustic isolation. The operating wavelengths of the ground transmitters will be 0.4880 and 0.6328 microns. The difference in up-link and down-link operating wavelengths is caused by the difficulty in implementing (a) an argon laser transmitter aboard the spacecraft, and (b) a 10.6-micron receiver aboard the spacecraft. In the first case, the power drain was the limiting factor; in the second case, it was the difficulty of providing cooling to the long wavelength detectors.

The largest difference in operating conditions between the transmitters at either end of the link is caused by the atmosphere. The ground-based transmitter is immersed in the atmosphere which induces angle-of-departure fluctuations on the output beam, in exact analogy to the angle-of-arrival variations seen on an incoming beam. The consequence is that the ground transmitter must either: (a) use a very tight beam and be continually corrected with beam steering devices; or (b) broadcast into a solid angle large enough to accommodate most angle-of-departure variations - on the order of several arc seconds in diameter.

Of these alternatives only the latter is acceptable, because of path length delay in any error correcting signal that could be sent from the satellite. This means that the received power density at the satellite will be down an order of magnitude or more from the received power density on the ground from the down-link, for equal transmitted power. This is largely offset by the increased heterodyne sensitivity of the spacecraft receiver as compared to the ground-based heterodyne receiver. Thus the ground-based transmitters will use transmitted power levels about equal to the spacecraft transmitter lasers.

The super-mode laser configuration is essentially as described previously in section 4.1.4.1, as is the polarization duplex receiver to be used for heterodyne detection.

The major equipment necessary for this experiment is listed below:

a. Spaceborne Equipment

	Single-frequency laser local oscillators at 0.488 micron and 0.6328 micron.
2	High-voltage DC power supplies - 1 for each laser.
2	Cavity tuning control and stabilization circuits - 1 for each laser.
2	Laser power monitor detectors with preamplifiers.
8	Wide-band photomultiplier photodetectors - 4 for each receiver at 0.488 micron and 0.6328 micron.
8	High-voltage power supplies - 1 for each photomultiplier tube.
	Signal processing and demodulation circuits for each receiver.
2	Receiving telescopes - 1 for each wavelength, or
1	Receiving telescope for all wavelengths, having suitable beam-combining optics behind the mirror.

b. Ground-based Equipment

2	Single-frequency laser transmitters operating at 0.488 micron and 0.6328 micron having 1-watt and 100-milliwatt output power, respectively.

b. Ground-based Equipment (continued)

2 High-voltage DC power supplies - 1 for each laser.

2 Cavity tuning control and stabilization circuits for mode-locked or single-frequency operation.

2 In cavity modulators for mode-coupled operation.

2 Cavity modulator driver amplifiers.

2 Output power monitor detectors.

2 Local video detectors and preamplifiers.

1 0.1 meter transmitting telescope for both wavelengths, having suitable beam combining optics behind the mirror.

4.2.4.2 Ground Transmitters

The lasers recommended for an Earth-to-spacecraft heterodyne link include:

Ionized Argon at 0.4880 micron

Helium-Neon at 0.6328 micron

The feasibility of developing a low-power Argon laser for a spacecraft local oscillator for the OTES is being examined, with the expectation that the problems associated with its development will be resolved in time for inclusion in the OTES program (see sections 4.1.5.2 and 4.1.6).

These two wavelengths will be transmitted simultaneously through the transmitter telescope. The lasers, beam switching dichroic mirrors, and modulators will all be located on a solid foundation to maintain alignment between transmitter subsystems, and their combined output(s) will be fed to the transmitting telescope.

A transmitting aperture approximately 0.1 meter in diameter will be used. The long wavelengths may be able to use the full aperture at its diffraction limit, and the shorter wavelength must be deliberately defocused before transmission to fill a large enough angle.

Light from the lasers can be piped into the transmitting telescope via a Coude focus since the angular tolerances are not as strict as aboard the OTES spacecraft, and small misalignments between the optical beam and the rotational axes can be tolerated.

Circularly polarized light will be transmitted at each wavelength for most experiments, so that any atmospherically-induced depolarizing effects can be analyzed at the spacecraft.

Various modulators will be used, as in the spacecraft transmitter, in order to evaluate their effectiveness on an optical up-link, whose scintillation properties are not the same as a down-link. Optical AM, FM, and Polarization PCM modulation will be used in turn, under various weather conditions.

4.2.4.3 Spaceborne Receivers

The spaceborne receivers for the heterodyne detection experiments will be, like the ground receivers, polarization diversity receivers that can process orthogonal polarization states simultaneously. The spaceborne heterodyne receiver enjoys the immense advantage of being able to use the entire area of the collector efficiently because of the absence of the atmosphere. All optical components can be used at their diffraction limit.

The configuration of the spacecraft heterodyne receiver system is essentially the same as the ground-based heterodyne receiver described in section 4.1.5.3.1. Aboard the spacecraft, however, the 0.6328 micron transmitter and 0.4880 micron receivers share the one-meter-diameter collector in common, so that provisions are made for combining transmitting and receiving modes on these two frequencies.

Two laser local oscillators will be used, at 0.4880 and 0.6328 microns, for heterodyne detection at those wavelengths. The satellite can also transmit at the 0.6328 micron wavelength. Beam switching is not necessary for these wavelengths.

The signal processing electronic subsystems will operate in the same fashion as their ground-based counterparts; AM, FM, and Polarization PCM signals can be received, and the laser local oscillator will track the received signal at a fixed frequency offset, as described in section 4.1.5.3.1.

4.2.4.4 Experiments

The relationship between the up-link and down-link experiments is described in previous sections on experiment objectives, 4.1.2 and 4.2.2, and in section 4.1.5.3.3.

4.2.4.5 Operational Procedure

Tasks

a. Begin recording atmospheric condition above ground site.

b. Turn on spacecraft lasers, allow to come to thermal equilibrium with telescope and spacecraft. (Est. 4 hours)

c. Turn on ground-based laser transmitters for warm-up. (Est. 4 hours).

d. Turn on in-cavity modulators in ground transmitters. (Est. 1/2 hour)

e. Turn on ground video modulators for warm-up. (Est. 1/2 hour) (All thermal delay times depend strongly on spacecraft package design. It may be preferable to leave the lasers running all the time, if possible.)

f. Train ground transmitting telescope to satellite direction. (5 minutes)

g. Transmit 0.488 micron beacon to satellite, orient satellite, acquire and track 0.488 micron beacon, begin fine tracking, reduce spacecraft angular rates as close as possible to the tracking rates so that no corrections are needed from vibration-producing thrusters (see Time Line Diagram, figure 4.2-4).

h. Select transmitted wavelengths and begin transmitting single-frequency signals to satellite. (1 minute)

i. Tune each spacecraft local oscillator laser for correct offset from ground signal. Sweep in frequency, lock on to detected signal. (1 second)

j. Begin demodulating signals from ground transmitters and telemetering outputs (see Time Line Diagram).

4.2.5 Supporting Analyses

4.2.5.1 Optical Communication Analysis

See section 4.1.5.1.

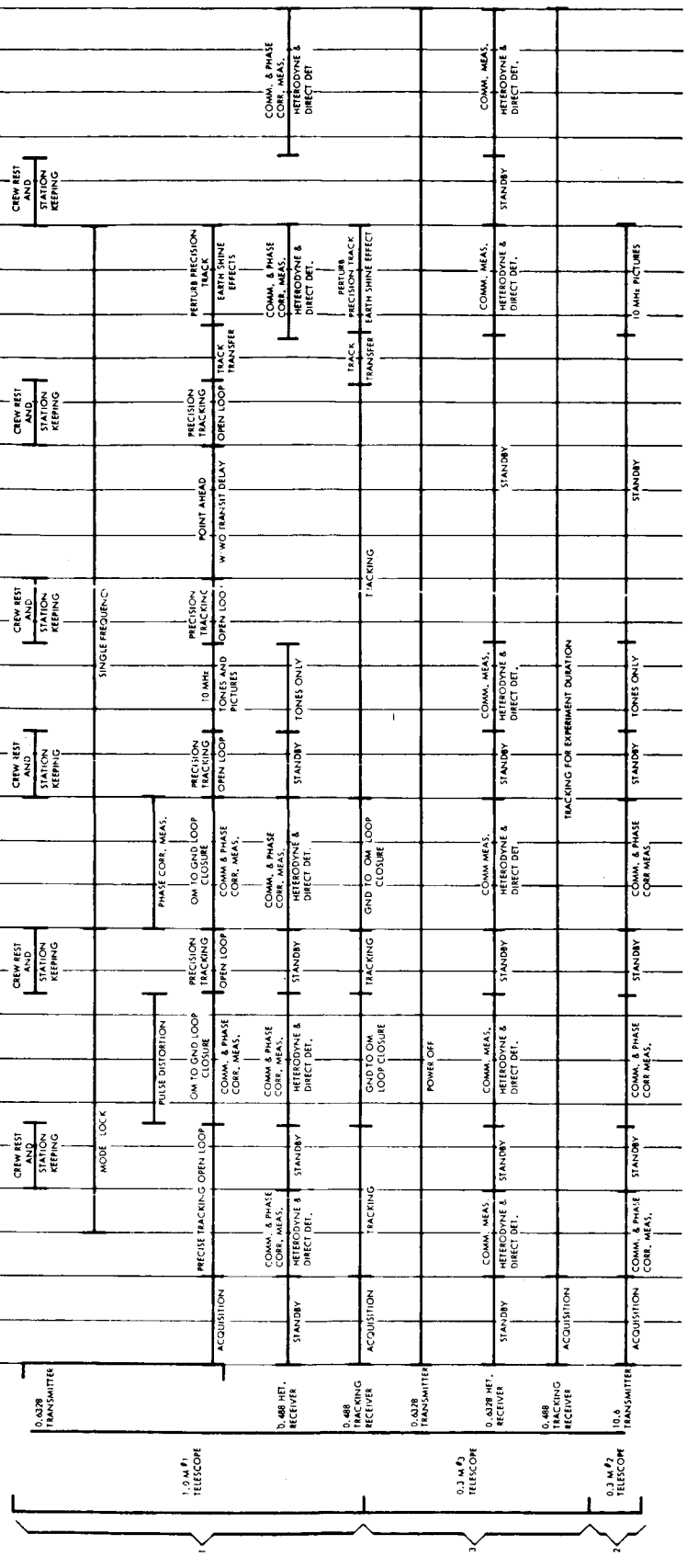

Figure 4.2-4. Time Lines for Optical Communications Telescopes

4.2.5.2 Laser Evaluation

See section 4.1.5.2

4.2.5.3 Heterodyne OTAES Link

See section 4.1.5.3.

4.2.5.4 Optical Modulation

See section 4.1.5.4.

4.2.6 Required Technology Development Schedule

Some of the required technology developments for OTAES are common to both an up-link and a down-link. In this section we will refer to only those components, techniques, or test programs that must be developed in order to carry out the portions of the heterodyne experiments that are peculiar to the up-link. Developments common to both are discussed in section 4.1.6.

FY 1967

Continue development of high-power (1-watt nominal) Argon ion lasers, for use as ground-based beacon transmitters, having a substantial fraction of their output power concentrated in a single frequency. (Now underway NASA Contract No. NAS8-20558.)

Begin a 30-month development program of a small, low-power, single-frequency Argon ion laser suitable for use as a local oscillator.

> Design and fabricate a single-frequency, single-spatial mode remotely adjustable and tunable laser. Output power of 1 milliwatt (nominal) is desired at 0.4880 micron. Incorporate design features that will minimize the input electrical power requirement as far as possible. Both dc and rf discharge pumping should be considered. Although this laser is intended for spaceborne application, weight shall be secondary to power and cooling considerations.

FY 1968

Begin a 12-month development of video bandwidth, high quantum efficiency, solid state photodetectors for the visible spectrum.

> Design and fabricate a solid state photodetector with quantum efficiency of 30%, nominal, at both 0.6328 and 0.4880 microns wavelength. Frequency response shall extend from baseband to at least 10 MHz. Sensitive area must be as large as possible consistent with the frequency response requirement and a nominal 50-ohm impedance.

FY 1969

Carry out preliminary propagation tests using high altitude balloons for receiving laser signals transmitted from the ground.

FY 1970

Begin fabrication of OTAES subsystems and hardware.

4.3 DIRECT DETECTION ON EARTH

4.3.1 Summary

One potential application for lasers is communication at very long ranges. But, before an optical communication link can be proposed as an operational tool, its efficacy must be established. A foundation of spaceborne optical communication engineering data must be obtained to allow comparison with conventional techniques. The preceding experiments have treated the optical heterodyne technique. Direct detection also applies as an alternative communication form that has planetary distance potential.

There are three salient advantages to the direct detection concept: system simplicity, lenient pointing tolerances, and an advanced state of ground-based development. In fact, direct detection system tests can be implemented on OTAES by defocusing the telescope, in the same fashion that is prerequisite to the precision tracking experiment (section 4.5), and by using the optical heterodyne transmitter. Thus, at the expense of a few logic elements in its test program sequencer, the OTAES spacecraft can be adapted for the direct detection experiment.

There is a secondary advantage to the inclusion of a direct detection link in OTAES: probability of experiment success. In the direct system, beam pointing and collimation requirements are traded off at the expense of enlarging the ground-based optical collector, thereby enhancing the reliability of the space-to-earth communication link. Since those atmospheric measurements predicated upon amplitude and polarization sensing can be accomplished with the space-borne optical transmitter in the direct detection communication mode, inclusion of the direct detection link enhances the success of that portion of the atmospheric experiments.

The one element of an optical direct detection system that remains to be developed is the large, earth-based optical collector (depicted in figure 4.3-1). For a meaningful comparison (i.e., in a planetary communication context) with alternative techniques, this aperture should be 8 meters in diameter. In this size, solar furnace technology and conventional RF antenna tracking techniques apply.

Given such an earth-based receiving system and a relaxed tolerance space-borne laser transmitter, portions of the 10 MHz communication, pulse distortion, and fading experiments can be accomplished. To be of full value to atmospheric physicists and to develop meaningful space-to-earth communication engineering data, such measurements must be made through the whole atmosphere. This atmospheric measurement requirement, and the opportunity to make exact and simultaneous comparison with an alternative communication form, constitute the justification for performing the direct detection optical communication experiment in space.

4.3.2 Experiment Objective

This experiment will provide a high-confidence link for atmospheric propagation measurements and will compare alternative optical communication forms. The specific objective is to evaluate the performance of a wide-band space-ground laser communications technique that uses state-of-the-art components, but does not require diffraction-limited optics, extreme pointing accuracy, or excessive power consumption.

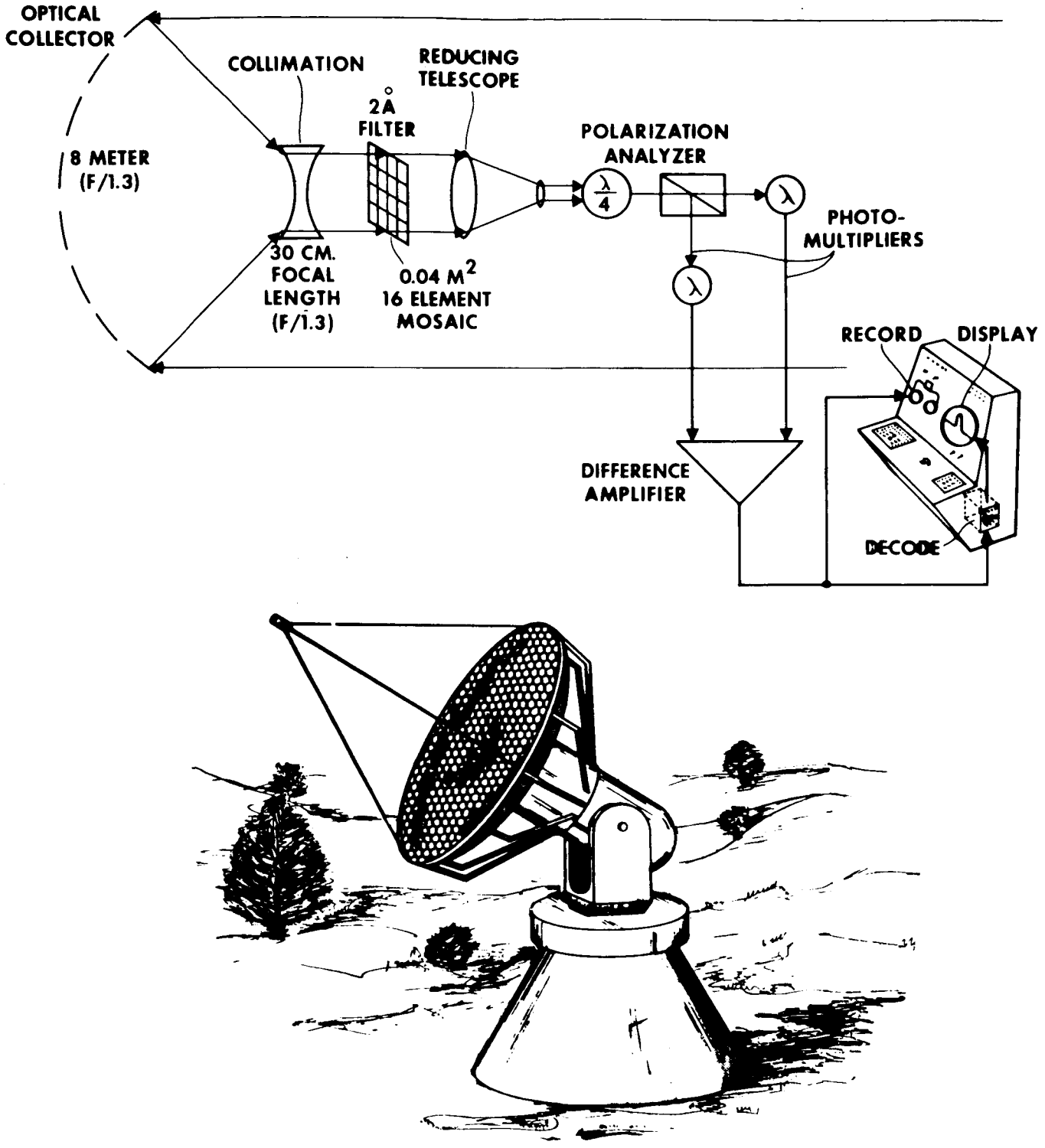

Figure 4.3-1. Direct Detection Telescope

4.3.3 Experiment Justification

4.3.3.1 Contribution and Need

The frequently expressed need[1] for television bandwidth deep space-to-earth data links suggests the use of a wide bandwidth laser communication system in which all the short wavelength optical energy can be concentrated into a very narrow diffraction-limited beam by using relatively small apertures. Assuming all other factors to be equal, the narrower the beamwidth the greater the capability of the communication system. However, the ability to transmit submicroradian beams with apertures less than a meter in diameter presents the designer with problems of precision pointing, alignment, and atmospheric refraction effects comparable in difficulty to those of the microwave communication system designer, who must construct and point massive space antennas in order to increase the present microwave systems capability.

The Direct Detection Optical Communication System concept, shown in figure 4.3-2, and 4.3-3, represents a compromise of the theoretical ultimate. In direct or energy detection, amplitude modulation on the light beam is detected directly by a photocell that is sensitive to changes in input beam power. This is analogous, in the RF spectrum, to the early crystal sets. However, since the direct detection optical communication system is independent of the atmosphere coherence diameter limitation, a large aperture collector can be used. A large receiving aperture will provide an excess of aperture gain that may be traded off to relax the pointing requirements both on the earth and in the spacecraft, preserving the capability for megahertz bandwidth communications. The direct detection system technique accepts a detector efficiency of 10^{-1}, laser efficiences of 10^{-4}, pointing accuracies of tens of microradians, and nondiffraction-limited optics. The signal-to-noise ratio for an optical communication link using direct detection, neglecting dark current in the photodetector, is[2]:

$$\frac{S}{N} = \frac{\rho P_s^2}{2e\Delta f \left| P_s + P_B \right|} \qquad (1)$$

where:

ρ = The responsivity of the photo-surface = $\frac{e\eta}{h\nu}$
P_S = The signal power received at the photomultiplier (watts)
P_B = The background power received at the photomultiplier (watts)
e = The electronic charge
Δf = The electrical noise bandwidth of the system (hertz)
η = Quantum efficiency (number of charge carriers per photon)
h = Planck's constant
ν = Optical frequency (hertz).

---

(1) M. C. Adams, Hearings before the Committee on Science and Astronautics, United States House of Representatives, Eighty-Ninth Congress, February 23, 24, 25, and 28 thru March 1, 2, 3, 7, and 8, 1966, Part 4, p. 97.

A. J. Kelley, "NASA's New Electronic Research Center", Astronautics and Aeronautics, Vol. 3, No. 5, May 1965, pp. 58-63.

H. E. Newell, Hearings before the Committee on Aeronautical and Space Sciences, United States Eighty-Ninth Congress, March 22, 23, 24, 25, and 30, 1965.

(2) G. Biernson, and R. Lucy, "Requirements of a Coherent Laser Pulse Doppler Radar", Proc. IEEE, January 1963, Vol. 51, pp. 202-213.

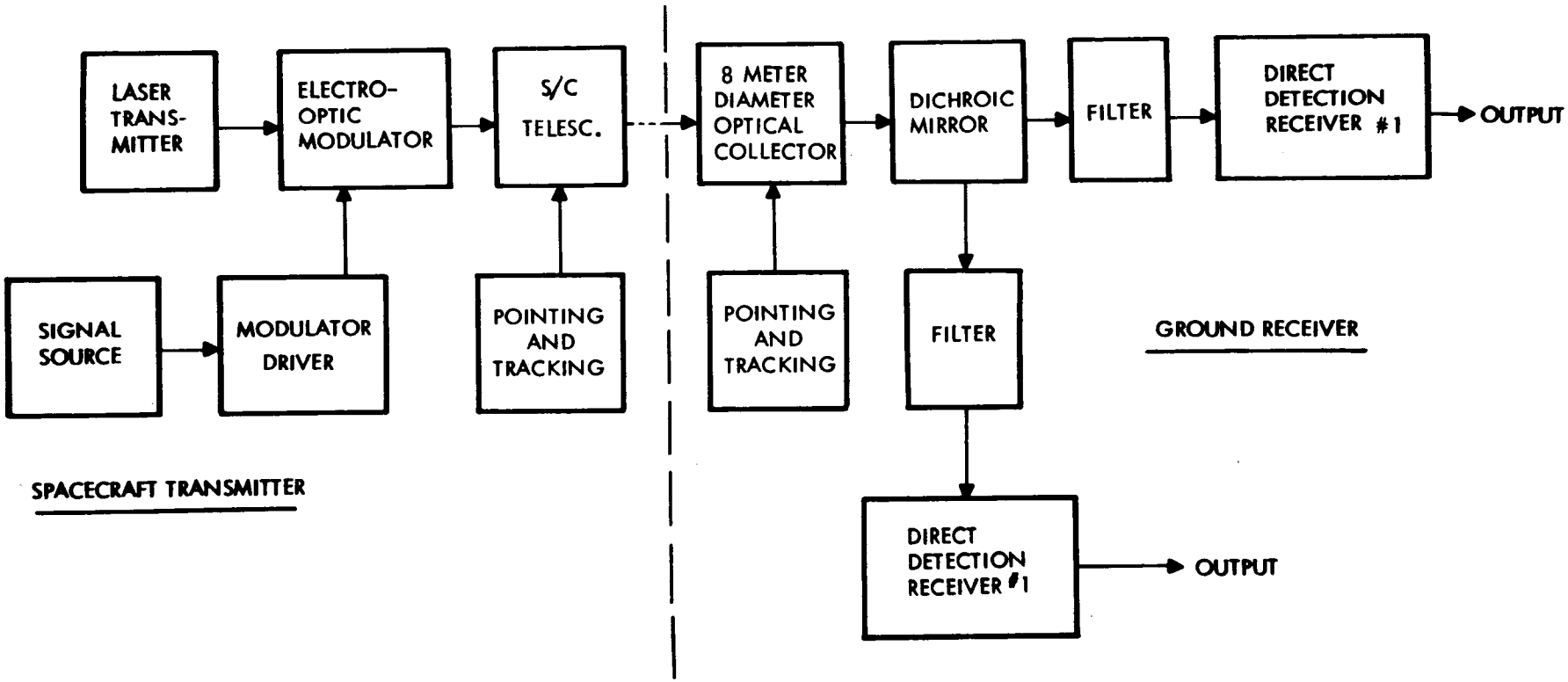

Figure 4.3-2. Direct Detection on Earth

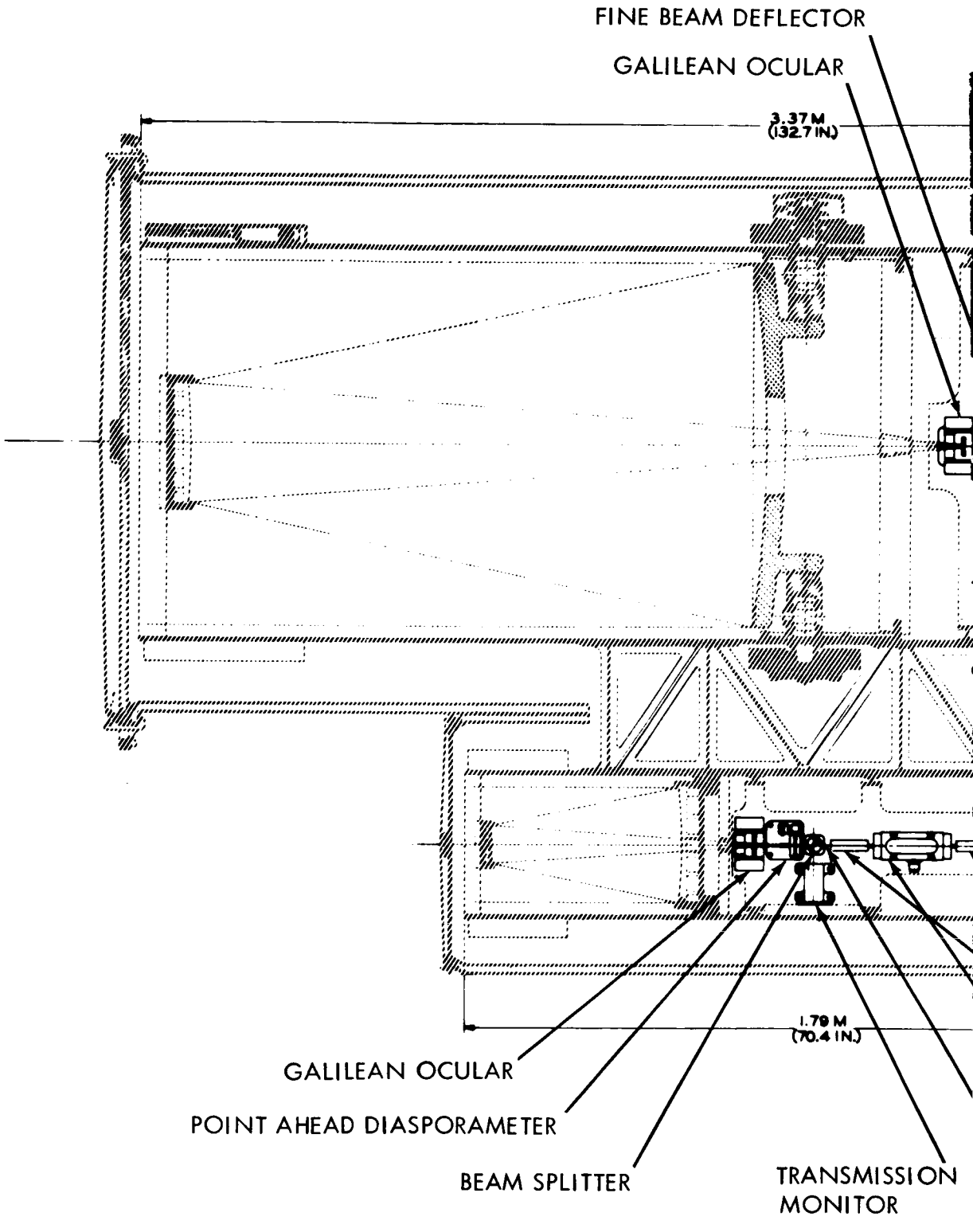
FINE BEAM DEFLECTOR
GALILEAN OCULAR
3.37 M
(132.7 IN.)
1.79 M
(70.4 IN.)
GALILEAN OCULAR
POINT AHEAD DIASPORAMETER
BEAM SPLITTER
TRANSMISSION
MONITOR

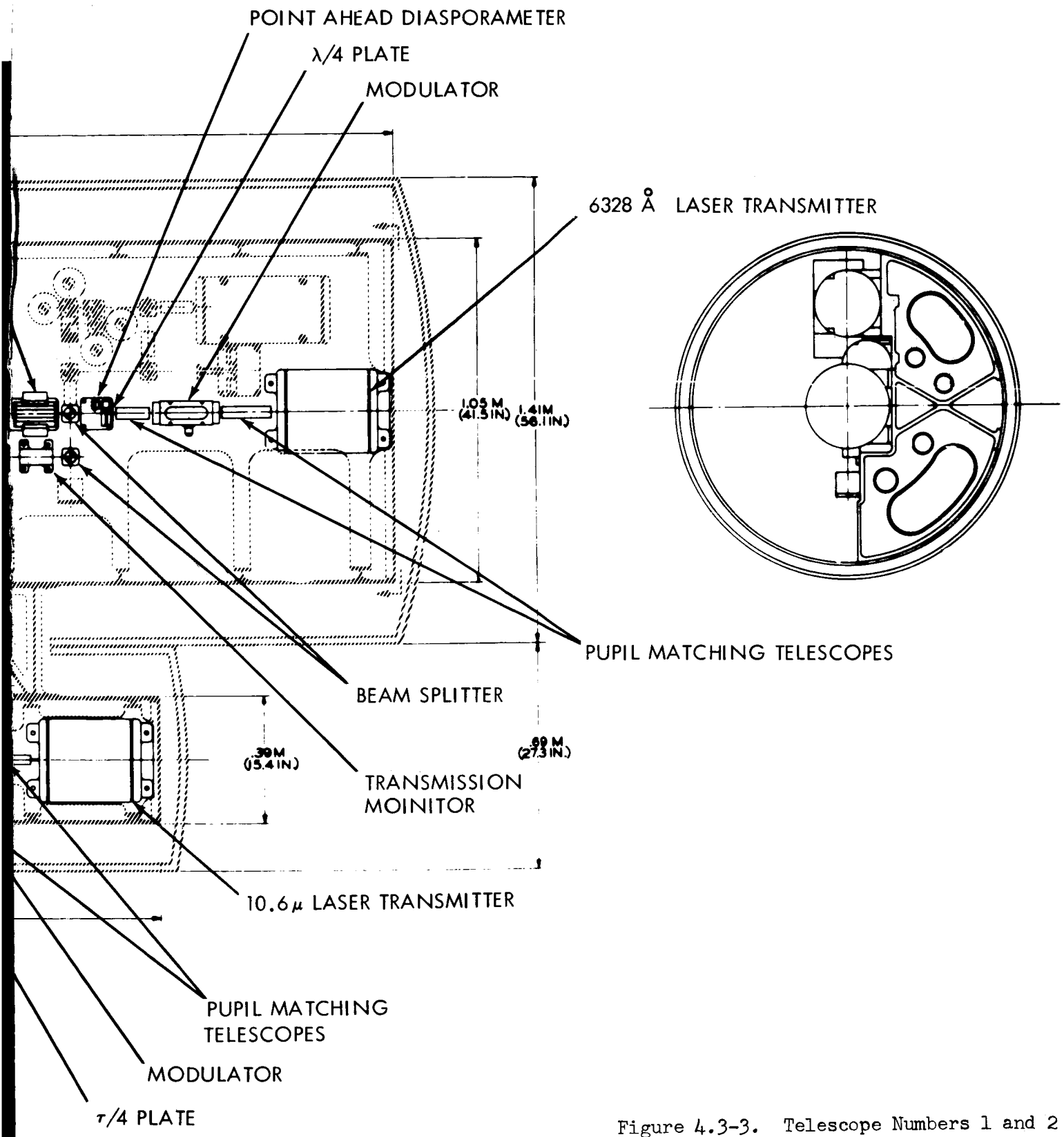

Figure 4.3-3. Telescope Numbers 1 and 2

The receiver signal power is:

$$P_s = \left(\frac{P_t}{\Omega_t}\right) \frac{A_r}{R^2} T_o T_A \tag{2}$$

where:

P_t = Transmitted power (watts)
Ω_t = Transmitter half-power solid angle beamwidth (steradians)
A_r = Effective area of the receiver collecting optics (square meters)
T_o = Optical transmission
T_A = Atmospheric transmission
R = Range (meter).

For a ground receiver, the background power due to air scattering is given by the expression:

$$\left(P_B\right)_{\text{blue sky}} = A_r T_o \Omega_r (N_\lambda)_{\text{sky}} \Delta\lambda \tag{3}$$

where:

Ω_r = The field of view of the receiver
N_λ = Average spectral radiance of the sky in the optical filter bandwidth $\Delta\lambda$, as measured at the telescope receiver aperture A_r.

Using Eqs. (1), (2), and (3), the signal-to-noise power ratio at the ground receiver system output may be written as:

$$\left(\frac{S}{N}\right)_{\text{Space to Ground}} = \left(\frac{P_t \rho A_r T_o T_A}{2e\Delta f \Omega_t R^2}\right)\left\{\frac{1}{1 + \dfrac{\Omega_r N_\lambda}{\dfrac{P_t T_A}{\Omega_t R^2}}}\right\} . \tag{4}$$

The term in the first parentheses is the expression for signal photon noise-limited operation. The term in the second parentheses represents the effect of background in reducing the signal-to-noise ratio for signal photon noise-limited operation.

Typical parameters for the system are given in table 4.3-1. A graph of the space-to-ground performance as a function of the transmitter radiant intensity is shown in figure 4.3-4.

In the curves, a typical transmitter power and beamwidth are indicated for a 30-dB signal-to-noise ratio. In this case, operation will be signal photon noise limited. Note that all the system parameters are within the state-of-the-art. Because of the high efficiency of operation ($\epsilon \cong 10^{-1}$ for CO_2-N_2 vs $\epsilon = 10^{-3}$ for HeNe) and relaxed tolerance requirements, the 10.6 microns, CO_2-N_2 laser may some day prove useful as another choice of wavelength of operation. A simple comparison of the 0.63 micron system to the 10.6 micron system may be made.

TABLE 4.3-1

TYPICAL VALUES REQUIRED FOR DIRECT DETECTION EXPERIMENT

SYSTEM PARAMETERS	SPACE-TO-GROUND NONCOHERENT
Range	3.22×10^7 meters (20,000 miles)
Laser Power(a)	10^{-3} watts
Beamwidth(a)	1.4×10^{-5} radians
Wavelength	6.328×10^{-7} meters (6328 A)
Filter Bandwidth(b)	2 A
Modulation Type	Polarization
Filter Transmission(b)	0.4
Nominal Optics Efficiency	0.75
Nominal Atmospheric Transmission(c)	0.5
Typical Background Radiance Observed by Receiver(d)	Blue Sky at Zenith(3) 2×10^1 watts/m^2-stermicron
Optical Collector Area	50 $meters^2$
Minimum Receiver Field of View	5×10^{-4} radians
Phototube Type	S-20 (C70038D)
Peak Signal to RMS Noise(a)	30 dB
System Bandwidth	10 MHz

(a) Possible system parameters as indicated on curve.
(b) Spectra lab mica interference filter.
(c) Less than standard clear atmosphere at 60^o from zenith.
(d) Angle of sun and observer neglected for simplicity.

(3) F. Moller, "Optics of the Lower Atmosphere", Applied Optics, Vol. 3, No. 2, February 1964, p. 161.

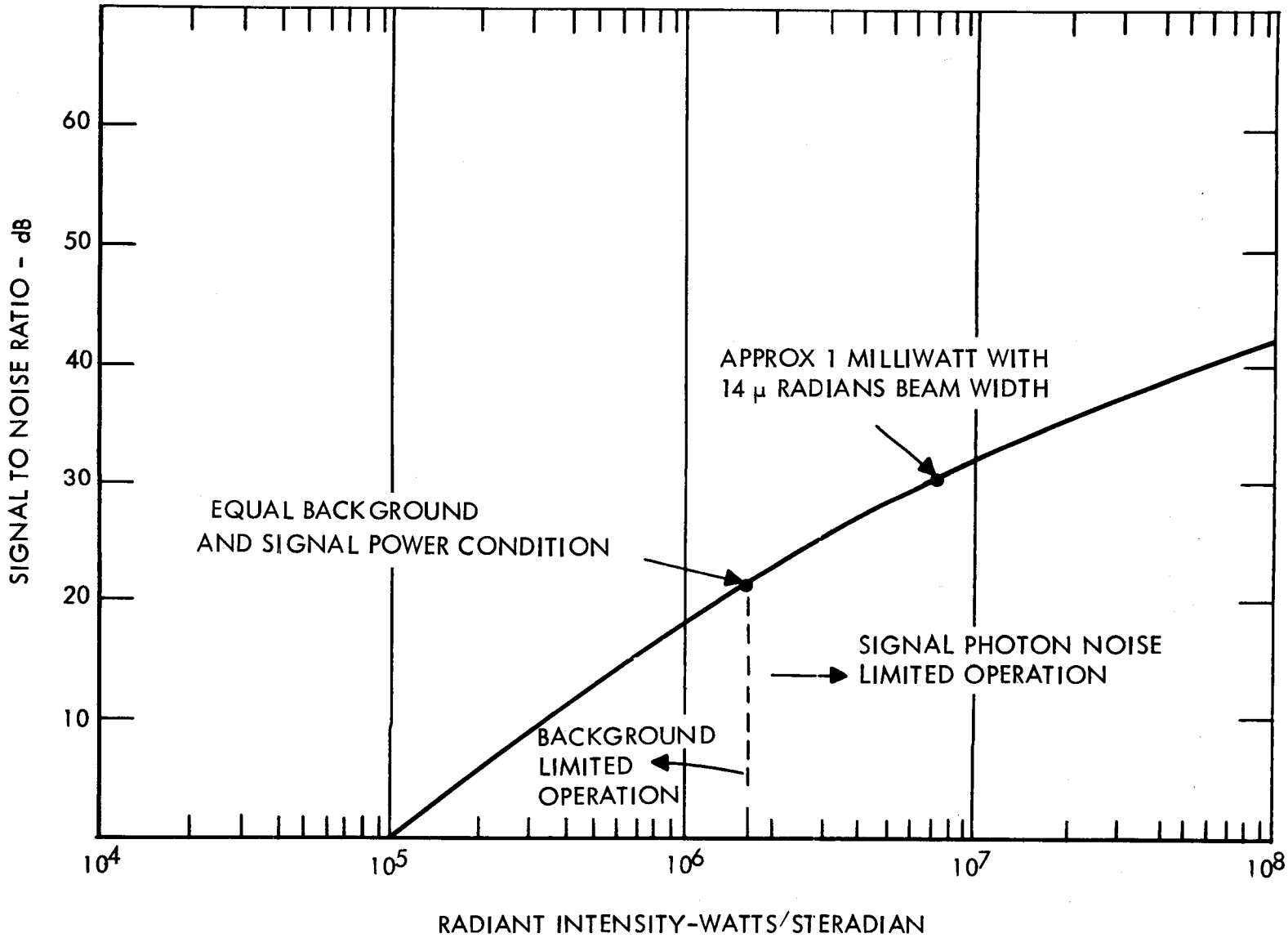

Figure 4.3-4. Performance of Direct Detection Ground-Based Receiver Against Blue Sky Background.

The background problem at 10.6 microns is less severe than at 0.63 micron. The background power incident upon the detector is:

$$P_B = N_\lambda \, \Omega_r \, \Delta\lambda \, A_r T_o T_F \quad . \tag{5}$$

A typical radiance value for clear sky at 10.6 micron is:

$$N_\lambda = 1 \text{ watt/m}^2\text{-micron-steradian}^{(4)} \quad .$$

If we assume a 2-percent bandwidth interference filter, which may be optimistic for the far infrared, and the ground-based receiver values of table 4.3-1, the background power incident upon the detector is:

$$\left(P_B\right)_{10.6} = 10^{-6} \text{ watts} \quad .$$

The responsivity at 10 volts of bias of typical Ge-Hg doped detectors at this wavelength is about 10^{-2} volts/microwatt. Thus, a steady input of 1 microwatt will produce an output voltage change across a matched load of only 10^{-2} volts. This is small compared to the 10-volt bias; consequently, the effect of the background power may be neglected in detector operation.

Neglecting background, the detectivity of a photoconductor D* is defined[5] as:

$$(D^*)_{\lambda = 10.6} = \frac{\left(\frac{S}{N}\right)_v}{P_s} \left(\Delta f \, A_c\right)^{1/2} \tag{6}$$

where:

$\left(\frac{S}{N}\right)_v$ = The voltage signal-to-noise ratio

P_s = The signal power in watts

Δf = The noise bandwidth in cps

A_c = The detector area in cm^2.

Typical D* values of Ge-Hg[4] are $3 \times 10^{10} \frac{\text{cm (cps)}^{1/2}}{\text{watt}}$.

Time constants are of the order of 10^{-7} seconds, providing they are cooled to temperatures less than 30° K. This time constant corresponds to a 2.5-MHz bandwidth and a 1.6-MHz 3-dB bandwidth. The minimum area of the detector, based upon the large array optics circle of confusion, would be 0.25 cm^2.

Substituting Eq. (2) for P_s in Eq. (6) and solving for the transmitter radiance gives:

---

(4) "Background Measurements during the Infrared Measuring Program", 1956, AFCRL-TN-60-692, November 1960, p. 149.

(5) H. Levinstein, "Extrinsic Detectors", Applied Optics, June 1965, Vol. 4, pp. 639-646.

$$\frac{P_t}{\Omega_t} = \frac{R^2 \left(\frac{S}{N}\right)_v (\Delta f A_c)^{1/2}}{D^* T_o T_A A_r} \tag{7}$$

Using the parameters from table 4.3-1 in addition to those properties of the detector, and requiring a 30-dB signal-to-noise ratio, the required transmitter radiant intensity is:

$$\frac{P_t}{\Omega_t} = 7 \times 10^7 \text{ watts/steradian} \tag{8}$$

If the results of the analysis are extended to the Mars mission distance, then the transmitted signal powers must be increased by the square of the ratio of the Mars:OTAES distances.

The purpose of the direct system for OTAES is to trade off laser power, beam-pointing accuracies, and beam-collimation requirements in the spacecraft at the expense of enlarging the ground-based optical collector. This trade-off is extremely significant because it provides a means by which spacecraft tolerances and requirements can be relaxed. It thus serves to enhance the reliability of the spacecraft-to-ground communication link.

Figure 4.3-5 shows the ground-based optics diameter plotted as a function of the spacecraft transmitter beamwidth for different laser transmitter powers. The curves are derived from Eq. (4). The system is photon noise-limited when operating against a daytime blue sky background at a distance of 32,000 km. A signal-to-noise requirement of 30 dB and a 10-MHz bandwidth have been specified. The other parameters are given in table 4.3-1.

4.3.3.2 Need for Space Testing

Extensive earth-based testing of direct detection laser systems has already been accomplished over horizontal, slant, and vertical paths within the atmosphere. A partial list of references in this field would include:

a. C. J. Peters, R. F. Lucy, K. T. Lang, E. L. McGann, and G. Ratcliffe, "Laser Television System Developed with Off-the-Shelf Components," Electronics, Feb. 8, 1965, p. 75.

b. R. F. Lucy, C. J. Peters, E. J. McGann, and K. T. Lang, "Precision Laser Automatic Tracking System," Applied Optics, Vol. 5, April 1965, p. 517.

c. Hinchman and Buck, "Fluctuations in a Laser Beam over 9 and 90 Mile Paths," Proc IEEE, March 1964, p. 305.

d. Spalding and Tomiyasu, "Laser Beam Propagation in the Atmosphere," Proceedings of the First Conference on Laser Technology, San Diego, Calif., Nov. 1963, ONR, Boston, Mass.

e. F. E. Goodwin, "Laser Propagation in the Terrectrial Atmosphere," Proceedings of the First Conference on Laser Technology, San Diego, Calif., Nov. 1963, ONR, Boston, Mass.

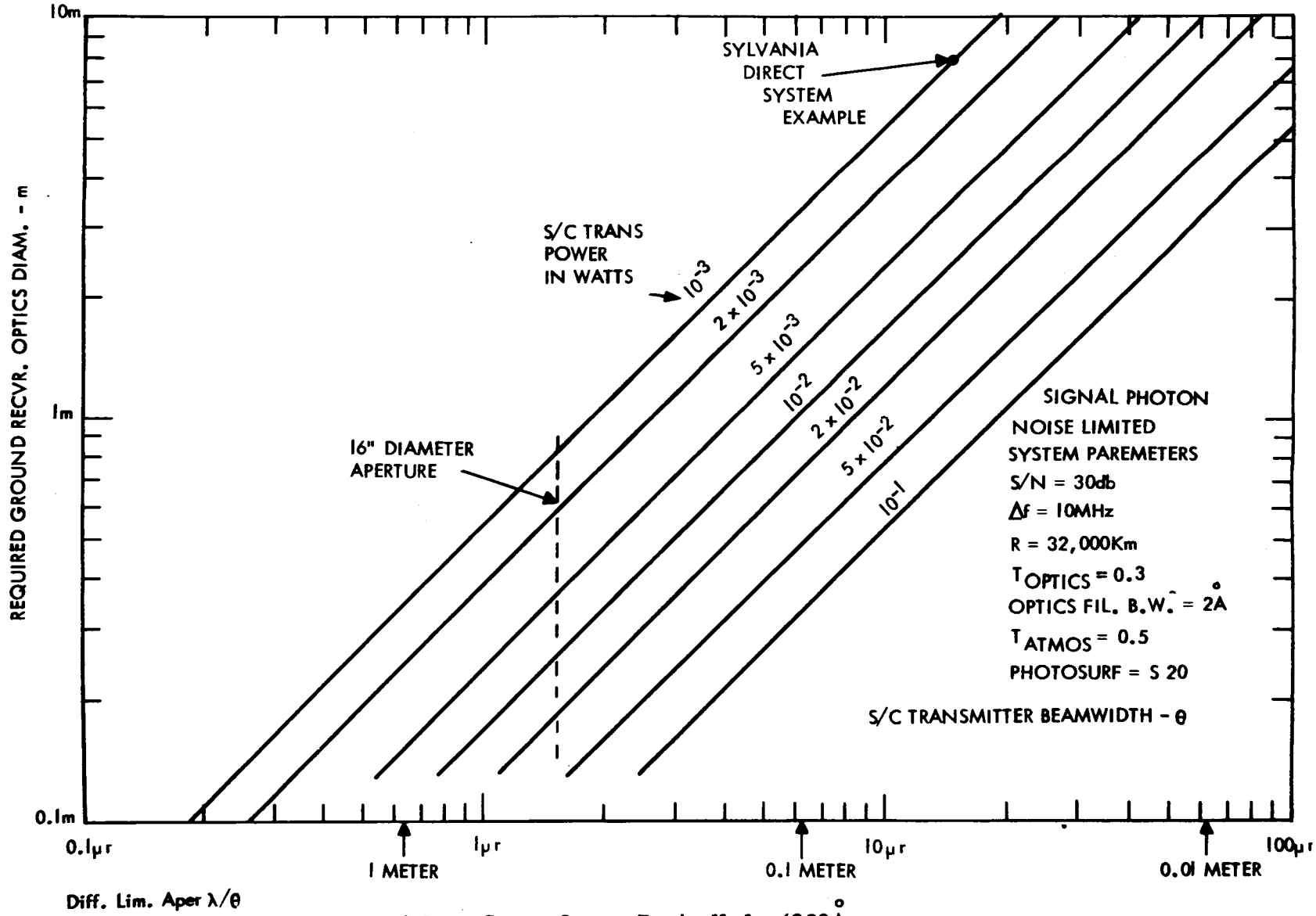

Figure 4.3-5. Direct System Tradeoffs for 6328Å

f. McDowell-Stites, "The Effect of Atmospheric Tubulence on Laser Beam Distribution," Symposium on Military Applications of Lasers.

g. Ligda, "Meteorological Observations with Pulsed Laser Radar," Proceedings of the First Conference on Laser Technology, San Diego, Calif., Nov 1963, ONR, Boston, Mass.

h. M. Subraman and J. A. Collinson, "Modulation of Laser Beams by Atmospheric Turbulence," Bell System Technical Journal, March 1965, p. 543.

i. E. J. Chatterton, "Optical Communications Employing Semi-Conductor Lasers," Lincoln Lab Tech. Report 392, 9 June 1965.

These data are applicable to predicting the direct detection system operation. In addition, a vast amount of information on optical scintillation and seeing effects is available. (J. R. Meyer-Arendt, and C. B. Emmanuel, "Optical Scintillation: A Survey of the Literature," National Bureau of Standards Technical Note 225, April 1965). These data can be used for gross predictions of direct detection system operation.

However, none of these data will provide all the information needed to determine performance of a space-to-ground optical communications system, because they have been collected on relatively short paths, often with the receiver in the near field and with the transmitter aperture located within the atmosphere. There have been no successful space to earth laser propagation tests performed which will yield quantitative data on the intensity variations of the narrow band laser transmission which are of concern to any energy detection system. These variations can be reduced by increasing the aperture size, as has long been done in astronomy. Measurements made using the wide spectrum of starlight are not applicable because the nearly monochromatic laser light can be expected to have more pronounced scintillation effects. For example, changes in color of a star due to moving "prisms" formed by the atmosphere[6] if observed with a narrow band filter-detector combination would appear as a much deeper "fade" than if it were observed with a very wide band detector. Theoretical considerations also indicated that the atmosphere effects on monochromatic light can be expected to be more serious.[7]

In principle, the amount of scintillation at a given optical frequency could be obtained by measuring starlight through very narrow band filters. Optical filters are not yet available which provide the narrow line width of a gas laser transmission. However, even if they were, the intensity of starlight is orders of magnitude less than that of laser light. For example, the spectral irradiance outside the Earth's atmosphere of one of the brightest stars in the sky, Sirius A, has been computed[8] to be approximately 10^{-11} watts cm^{-2} μ^{-1} at 0.63 micron. If it is assumed that a non-attenuating filter with a bandwidth of 0.2A could be used, the irradiance would be reduced by a factor of 2×10^{-5} to 2×10^{-16}. Using a 10-milliwatt laser with a diffraction limited beam from a 1 meter aperture at synchronous altitudes as a transmitter, the computed radiance is 1.49×10^{-9} watts cm^2, all of which would pass through a 0.2A filter.

Under these conditions the laser source is 10^7 times as bright as the star. Even with a much smaller transmitting aperture, the laser is still orders of magnitude greater than starlight. Measurements of scintillation made with the more intense laser light will be made more accurately because the "signal-to-noise" ratio will be better. The use of the

---

(6) Rudaux L. and DeVaucouleurs, Larousse "Encyclopedia of Astronomy" Prometheus Press, New York, 1959.

(7) V. I. Tatarski, "Wave Propagation in a Turbulent Medium" McGraw-Hill, New York, 1961, p. 257.

(8) Investigation of Optical Spectral Regions for Space Communications, ASD-TDR-63-185 (AD 410 537) Air Force Systems Command, Wright Patterson Air Force Base, Ohio, p. 160.

more intense light will also permit measurements at much smaller apertures than would be possible with starlight.

In addition to its monochromaticity, laser light differs from starlight in that the narrow laser beam will illuminate a relatively small volume as it passes through the atmosphere. The light scattered or refracted out of the laser beam increases the area illuminated and hence reduces the average intensity. The infinite "beam width" of the starlight refracts as much light into any area as is refracted out. It is possible that this effect will also contribute to increased scintillation of the laser light.

Although high altitude aircraft and balloon experiments are conceivable, the air supported vehicles can only approximate the desired test conditions; they cannot rise above the atmosphere and are subject to local turbulences and vehicle instabilities, all of which would cast doubt on the validity of the experiments. Essentially, aircraft and/or balloon tests are forerunners to future spacecraft tests.

The narrow band intensity scintillation data required for the design of future direct detection systems must be obtained without the necessity of allowing for near field turbulence or extracting data from very low intensity measurements, hence the need for space testing is clearly indicated. Any method of filtering of star-light which would approach the laser linewidth (and hence the time coherence properties) would result in a signal that would present grave measurement difficulties. Other natural sources are distributed sources which do not scintillate and hence are unsuitable even if they were as bright as the laser. Furthermore, the establishment of a space-to-ground communication link is essential to the OTAES atmospheric measurements. Since the direct link is clearly feasible, it offers a reliable means for measuring fading depth (multipath interference), polarization fluctuation, and communication channel bandwidth.

The implementation of a direct detection experiment in earth orbit would thus test and evaluate a simple laser communications system concept, and provide means for performing atmospheric propagation measurements. As lasers and detectors are made more efficient and as space optical and pointing problems are solved, the direct system will then become a means for high data-rate (10 MHz) optical communications at interplanetary distances.

4.3.3.3 Feasibility

The direct system has been designed to discriminate against sunlight scattering due to normal air and aerosol concentrations by the use of optical filters and by restricting the optical field of view. The design of the direct system provides a means of discrimination against seeing and scintillation effects. A primary characteristic of the direct system concept is simplicity, reliability, and low cost. At 0.6328 microns, it can be implemented with state-of-the-art components. For example, in the direct space transmitter, the laser, beam-forming optics, laser pointing, the electro-optic modulator and modulation driver have commercial counterparts in existence. A nominal 1-milliwatt laser approximately 30 cm long and 10 cm in cross-section weighing 6 kg and requiring 10 watts of prime laser tube power, such as the Spectra Physics Model 130 laser, can serve as the starting point for the design of a space-qualified laser. In addition, a modified Sylvania S2P electro-optic modulator and solid-state modulation driver requiring less than 30 watts of power are the basis for the space optical modulator. Furthermore, the beam-forming optics for the direct system do not have to be diffraction limited. Small collimating telescopes for lasers, similar to the Spectra Physics Model 331 or Tropel Model 1557-400 beam-expanding telescope, can easily form the beam required by the direct detection system.

Recent ground-to-air tracking experiments[9] have been performed using a narrow laser beam pointed at a retroreflector mounted on an aircraft. The return signal has been tracked at 14-km slant ranges with an accuracy of 25 microradians, rms. These experiments demonstrate accurate tracking and laser pointing in a turbulent atmosphere with the precision required for a direct detection optical communication link.

The 8-meter ground-based optical collector contemplated for this experiment is very similar to the 6.5-meter Narrabri Observatory multi-element optical collector[10]. This array of 252 hexagonal segments can form a 3-milliradian star image. An existing Syncom [11] microwave antenna tracking mount design could be adapted for the 8-meter optical collector. This mount has demonstrated accuracies of 50 microradians when tracking celestial objects from programmed data sources.

4.3.4 Implementation

4.3.4.1 Experiment Design

The implementation of the optical communication system for direct detection optical communication from space-to-ground was shown in the block diagram in figure 4.3-2. The laser transmitter will produce a plane-polarized output of the selected wavelength.

---

(9) R. F. Lucy, C. J. Peters, E. J. McGann, and K. T. Lang, "Precision Laser Automatic Tracking System", Applied Optics, April 1966, Vol. 5, pp. 517-524.

(10) R. H. Brown, "The Stellar Interferometer at Narrabri Observatory," Sky and Telescope, Vol. 28, No. 2, pp. 64-69.

H. Messel, and S. Butler, Space Physics and Radio Astronomy, MacMillan and Co., Ltd., London, 1964.

(11) Advent Ground Antenna Systems, Contract No. DA 36-039-SC-87365, U.S. Signal Supply Agency, Ft. Monmouth, New Jersey.

An electro-optic modulator now being developed for 100-MHz operation is shown in figure 4.3-6. Its design parameters are:

1) Physical Design

Length	:	21 cm
Diameter	:	3.5 cm
Weight	:	600 grams
Body Material	:	Aluminum
Connector	:	Mosely 301

2) Optical Design

Collimator Input Aperture	:	3 mm diameter
Collimator Power	:	2 2/3 x
Modulator Exit Aperture	:	1 mm x 1 mm
Electro-Optic Material	:	RDA

3) Electrical Design

Bandwidth	:	100 MHz
Drive Power	:	10 watts
Impedance	:	120 ohms

4) Modulator Drive Parameters

Size	:	550 cm^3 (15 x 5 x 7.5 cm)
Weight	:	1 kg
Prime Power Input	:	30 watts

5) Possible Modulation Formats

PCM/Polarization (or any similar pulse techniques)
Analogue/Polarization
FM Subcarrier/Polarization

The ground-based receiver will be an 8-meter diameter optical collector made of long focal length hexagonal mirrors approximately one foot across. Each mirror would be an f/30 parabolic or spherical surface. The overall optical collector would be a nominal, crude f/1 system. The resolution would be about 0.5 milliradians. It would be mounted on a large tracking mount to point and track the incoming signal. Pointing and tracking will be done open loop; that is, it will receive pointing and tracking data from another source, and will position itself in accordance with the data, but will not generate any error information to correct the incoming data. The data must be accurate to within 100 micro-radians. Secondary optics will provide a collimated beam about 22 mm in diameter for the direct detection receiver.

Figure 4.3-7 is a block diagram of the direct detection receiver. The dichroic mirror will be used to separate different operating wavelengths. In the 0.6328 micron receiver, the filter is used to reject much of the background radiation that would otherwise reduce the signal-to-noise ratio of the detected signal, and, under conditions of high levels of background radiation, would overload the detector.

The filter pass-band will be 0.0002 microns wide, centered at the transmitted wavelength. The quarter-wave plate will convert circularly polarized light to plane-polarized light. Light entering the polarization analyzer will contain left and right circularly polarized light. The analyzer will separate the two types of polarization. The detectors will

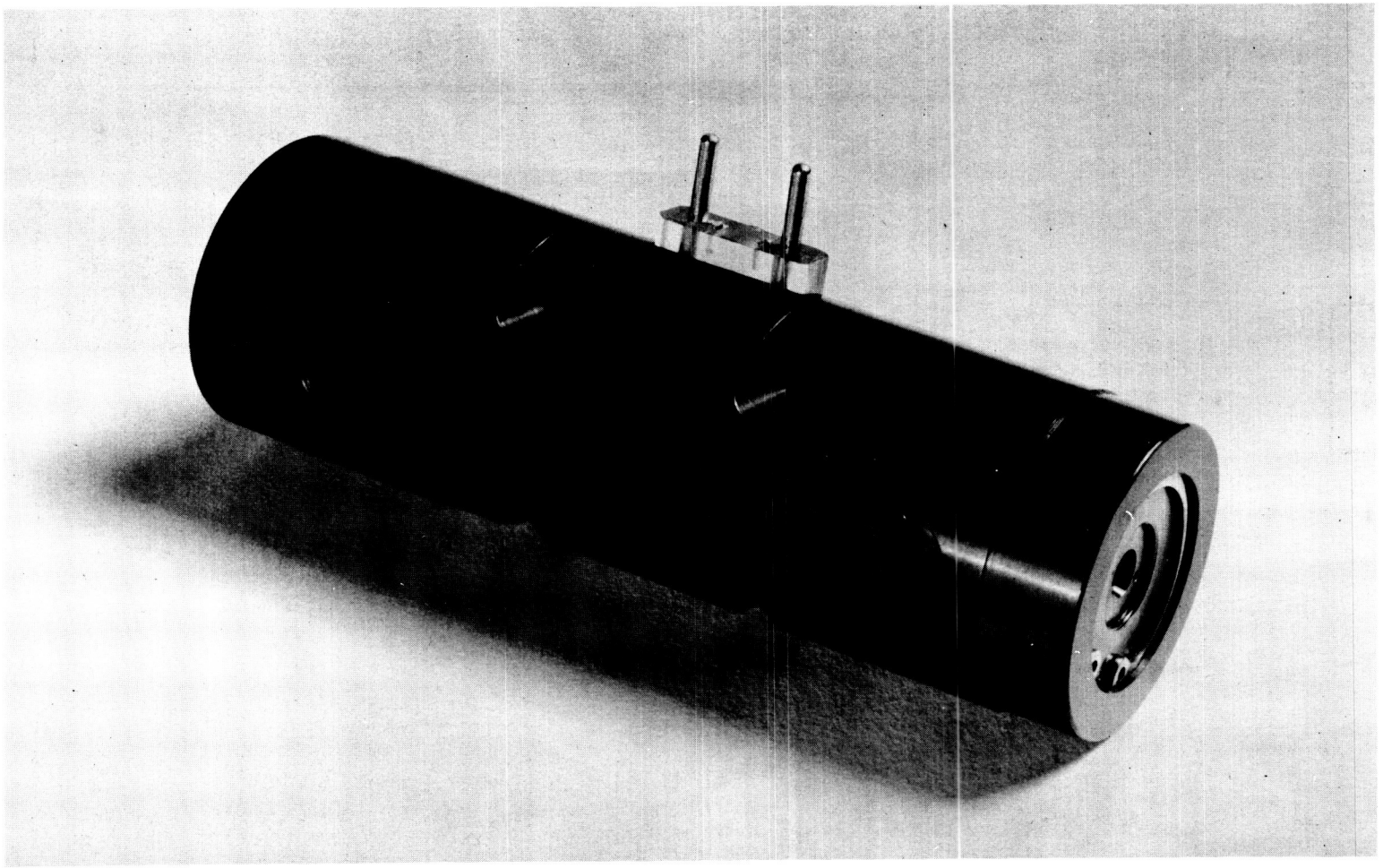

Figure 4.3-6. Experimental Low Power 100-MHz Modulation

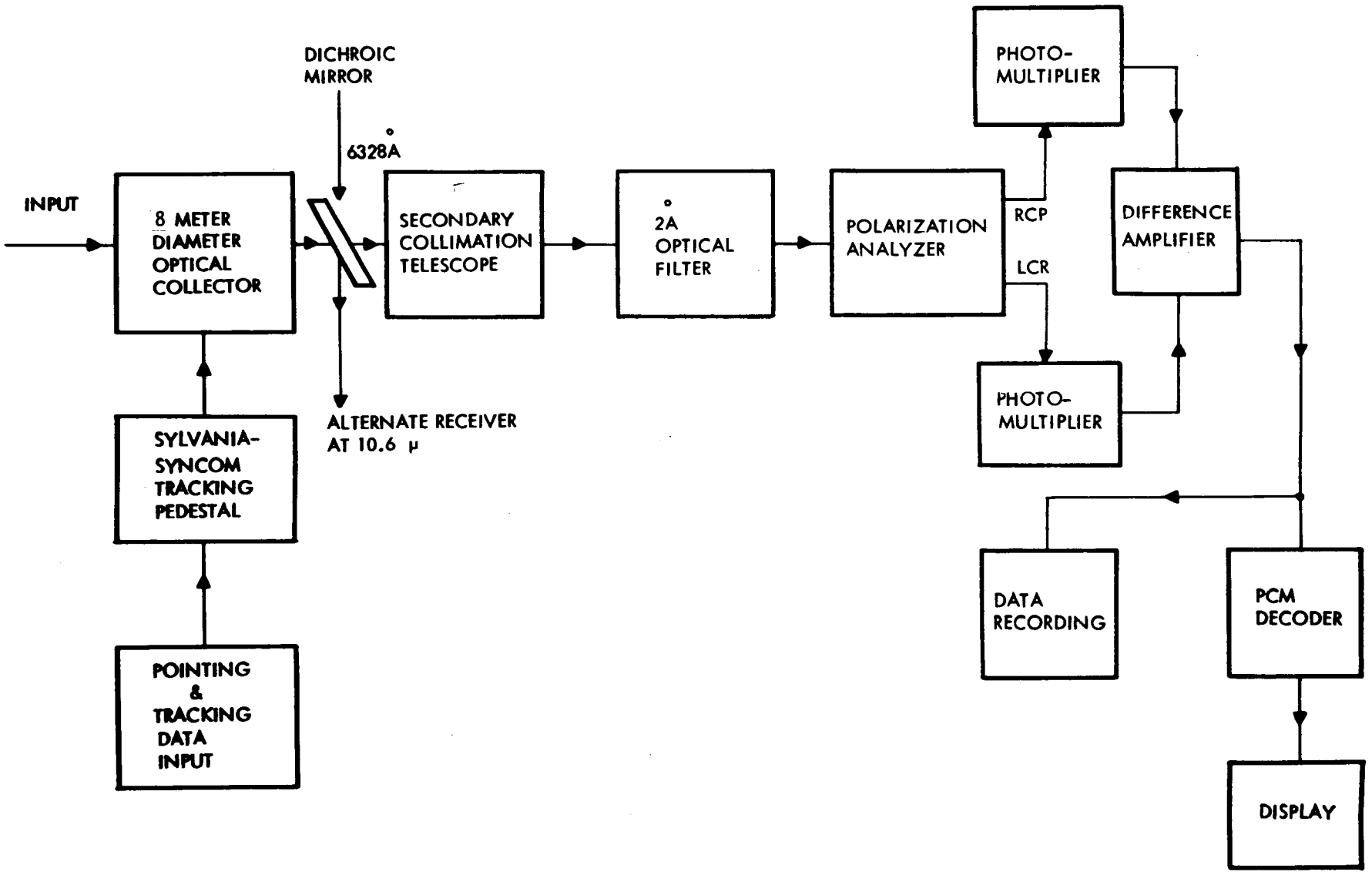

Figure 4.3-7. Ground Receiver for Direct System.

convert the light energy to electrical signals, and the output will then be processed by the data-handling electronics.

Direct system experiments must be performed and statistical data recorded under a variety of night and day conditions in order to adequately evaluate this mode of communication. Typical experiment variables, most of which are interrelated and uncontrollable, will be:

1) Meteorological conditions
2) Atmospheric path conditions
3) Background radiance
4) Angular location of sun and/or moon
5) Angular location of satellite.

In addition, it would be desirable to perform these experiments at more than one laser frequency.

Most of the optical power measurements are straightforward. Total signal power and depolarization effects are measurable with the systems detectors. Detailed examinations of portions of the input apertures can be made by scanning the post focal region with a mechanical scanner or image tube. If simultaneous measurements are made across the aperture, the aperture scan rate must be much greater than the signal fluctuation rate. Angle of arrival fluctuations can be measured by observing signal motion in the optics focal plane. Available signal power, background, and bandwidth will limit the measurements and their accuracies. The relative accuracy of measurement will be equal to $\sqrt{N/S}$.

The ground station will determine the length of each run, based upon meteorological conditions, from real-time data processing and analysis. It will be necessary to collect both short- and long-term data.

The following measurements are needed to evaluate the space-to-ground direct system. In each case, the output of photodetectors should be measured and recorded.

1a) Measure the magnitude of the received power to check losses and fading phenomena. In this experiment, the output of the photodetectors is continuously recorded to provide a chronological record of the instantaneous received power. These data can be correlated with meteorological and space-craft data to determine the intensity fading characteristics of the propagation path for the large aperture collector. This measurement should show the ability of the large aperture collector to smooth scintillation introduced by the atmosphere.

1b) Measure the signal power in the post focal image plane of the large parabola to determine the point-by-point instantaneous intensity structure of the optical signal across the input aperture. In this experiment, a scanning photomultiplier or a matrix of detectors could be used to measure the intensity fading characteristic of each section of the large collector. A comparison of small sections with large sections can be made to determine intensity fading as a function of aperture size.

2) Determine the error rate and/or overall communication channel quality. In this experiment, the various types of modulation are being evaluated. Thus, if PCM or other pulse modulation is being used, the receiver will measure the error rate. If analog modulation or FM subcarrier modulation is used, the received signal-to-noise is measured.

In addition, signal depolarization effects produced by the atmosphere will be measured during PCM/PL transmission.

3) Measure the effects of varying the transmitter beamwidth on system parameters. In this experiment, two effects are being observed. One is attributable to lateral motion of the beam on the received signal. This would introduce a modulation on the signal received by the phototubes. The modulation would be a function of the beam intensity distribution and the beam motion as it sweeps across the aperture. The second effect would involve the communication channel bandwidth. As the beam is spread, multipath scattering effects introduced primarily at the tropopause will degrade the communication channel. This effect will become pronounced as the differences in multipath transit times approach the periodicity of the laser modulation signal. Thus, large beams may have a lower bandwidth than narrow beams because they illuminate scatterers in the tropopause, which are farther from the beam center. This measurement could be performed by the pulse distortion technique at several beamwidths.

4.3.4.2 Operational Procedure

Before performing the direct detection space-to-ground experiments, the following operations must be accomplished:

1) Ground-based laser beacon acquired and tracked from the spacecraft.
2) Laser in operation.
3) Laser transmitter telescope aligned and pointed at the ground station.
4) Laser, modulator, and telescope all mutually aligned so that the ground station is illuminated by the laser beam, and the space-to-ground link is completed.

During the entire experiment program, the direct detection system will be in operation in order to monitor and record the laser transmissions from the space-craft. The first direct detection experiment (1a and 1b) will be performed during the hours 5.5-10 when a steady illumination is received from the 0.6328 micron mode-locked laser. During the hours 10-13, modulation signals will be imposed upon the laser. During this interval, the second direct detection experiment will be performed.

Finally, at hour 23.5 a third direct detection experiment will be started. This experiment would include a repetition of the first two experiments only at different beamwidths. These procedures are shown graphically on the Time Line Diagram, figure 4.3-8.

4.3.5 Supporting Analyses

The previous sections have provided system descriptions and system calculations that have defined the system performance. To assure total system performance, experiment feasibility and detailed analyses were conducted in areas such as:

a. Kinds of signal modulation.
b. Wide bandwidth modulator (see section 4.1.5.4)
c. Large receiving optical aperture.
d. Multilayer dielectric interference filters

The study of kinds of modulation was limited to a few selected types that were considered to be the most probable candidates for optical communication. The modulator study assessed the potential of obtaining a 100-MHz bandwidth modulator that would permit pulse code modulation transmission of signals having a bandwidth greater than 10 MHz. The concept of the large receiving aperture was developed from a stellar interferometer, and performance parameters were developed during the study.

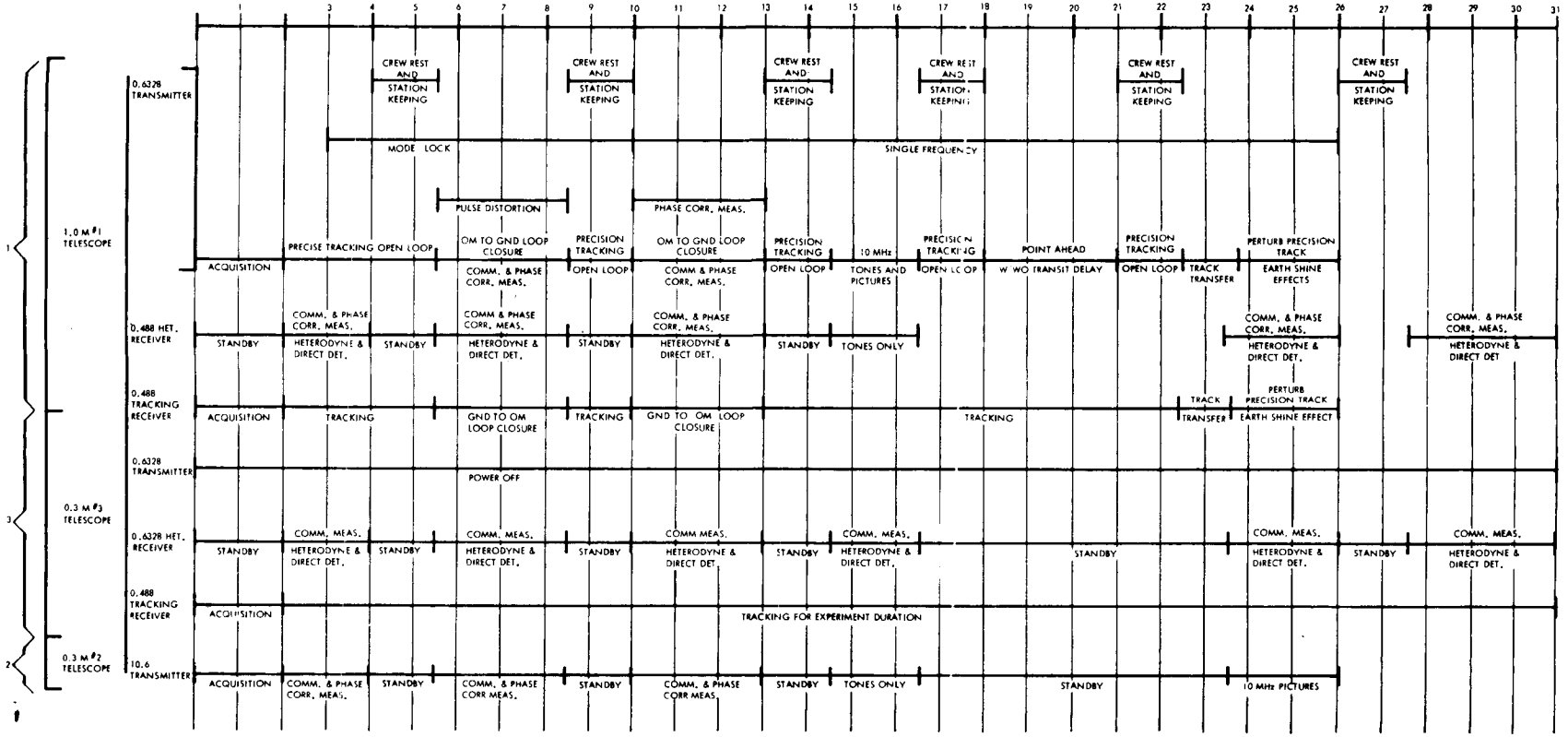

Figure 4.3-8. Time Lines for Optical Communication Telescopes.

4.3.5.1 Comparison of Modulation Techniques for Wide Bandwidth Transmission

A study of modulation techniques was performed to determine optimum forms of modulation for satellite-to-ground laser wide bandwidth links. The assumptions made for numerical comparisons of performance were that an output signal-to-noise power ratio (SNR) of 30 dB is required and that the bandwidth is 5 MHz. The optical transmitter is limited in peak power capability rather than average power capability. Background noise and photodetector noise are negligible compared to the quantum noise of the received signal, and are neglected in the analysis here. In addition, for lack of better information, it is assumed that the power spectrum of the signal is constant over the frequency range -5 MHz to 5 MHz except for a dc component and zero elsewhere, and that the probability density function of the signal is uniform in the interval 0 to 1, and zero elsewhere.

The following kinds of modulation were considered:

a. Pulsed intensity modulation.
b. Pulsed polarization modulation.
c. Direct intensity modulation.
d. Direct polarization modulation.
e. PCM intensity keying.
f. PCM polarization keying.

4.3.5.1.1 Results

Comparisons have been made strictly on the basis of output SNR, and no account has been taken of the relative subjective quality of the wide bandwidth (video) transmitted by analog and digital modulation methods. Possibly, the output SNR's required to yield equal quality for analog and digital modulation techniques will be quite different. Furthermore, it seems likely that the relative subjective quality of these techniques will depend upon the particular use to be made of the wide bandwidth output. Table 4.3-2 shows a comparison of R_o, the average number of received photons per second* at peak modulation required to obtain a 30-dB output SNR for the various types of modulation listed and assuming a 5-MHz bandwidth.

TABLE 4.3-2

COMPARISON OF MODULATION FORMS

Modulation	R_o (photons/seconds)	R_o (dB relative to PCM)
Pulsed Intensity Modulation	150×10^8	17
Pulsed Polarization Modulation	75×10^8	14
Direct Intensity Modulation	150×10^8	17
Direct Polarization Modulation	75×10^8	14
PCM - Intensity Keying	3.2×10^8	0
PCM - Polarization Keying	3.2×10^8	0
PCM - Polarization Keying with Error Correction Code	2.9×10^8	-0.4

*Only those photons that produce an output from the photodetector are considered, so detector efficiency does not enter into the results.

The results indicate that for a fixed output SNR of 30dB, the PCM modulation techniques will require substantially less peak transmitter output power than the analog techniques. On the other hand, a PCM system would be considerably more complex than an analog system and, because of the wider modulator bandwidth required, would require more modulator drive power than the analog system. These and other factors must be taken into account before a choice can be made between the various modulator systems considered herein. Only two of the assumptions made in the investigations are believed to affect critically the validity of the comparisons of the various systems. One is the assumption regarding the relative quality of analog and digital systems at equal output SNR's. The other is the assumption that an optical polarization analyzer can distinguish between two orthogonal states of polarization at extremely low photon arrival rates.

4.3.5.1.2 Discussion Pulsed Intensity Modulation

In the form of modulation considered here the signal X(t) is sampled at the Nyquist rate of 2W samples per second. Each sample is stretched (boxcarred) to a duration of $\frac{1}{2W}$ seconds, and intensity (power) modulates the optical carrier. Correspondingly, the photodetector converts light intensity into voltage pulses so that the overall transfer function of the modulator and demodulator is full-wave linear. The signal is recovered by averaging the received light intensity over each sample interval and putting the average, in the form of impulses each of whose strength is equal to its corresponding sample average, into a low-pass filter whose bandwidth is equal to the signal bandwidth. The model here is somewhat optimistic in that in practice one must sample at a rate slightly higher than the theoretical Nyquist rate in order to permit practical filters to be used. The error is negligible for the present purposes, however.

Let R_s be the average number of photons received during a sample interval when $\chi(t)$ takes on its largest value ($\chi = 1$). Assume that the gain of the photodetector is such that each photon produces a unit impulse of voltage. Let $z(t_n)$ be the number of photons received during the n-th sample interval. Then $z(t_n)$ is a Poisson random variable with average value $R_s\chi(t_n)$. The probability distribution of $z(t_n)$ is

$$P\left[z(t_n)\right] = \frac{e^{-R_s\chi(t_n)}\left[R_s\chi(t_n)\right]^k}{k!} \quad ,$$

and its variance is equal to its average value $R_s\chi(t_n)$. The output signal $\chi(t)$ is obtained by counting the number of photons received in the sample interval, and dividing by R_s. That is,

$$\hat{\chi}(t_n) = \frac{z(t_n)}{R_s} \quad .$$

The expected value of error in $\hat{\chi}(t_n)$ is zero. The variance of the estimate, given $\chi(t_n)$, is

$$\text{var}\left(\hat{\chi} \mid \chi\right) = \frac{1}{R_s^2}\,\text{var}\, z = \frac{1}{R_s^2}\left(\chi R_s\right) \quad .$$

$$= \frac{\chi}{R_s}$$

The unconditional variance is found by averaging over all possible values of $\chi(t_n)$

$$\text{var}\left(\hat{\chi}\right) = \frac{1}{R_s}\int_o^1 \chi d\chi = \frac{1}{2R_s} \quad .$$

The signal power is

$$E\left[\chi^2\left(t_n\right)\right] = \int_o^1 \chi^2\, d\chi = \frac{1}{3} \quad .$$

The SNR of the reconstituted signal $\chi(t)$ is equal to the SNR of its sample values $\chi\left(t_n\right)$, which is given by

$$SNR = \frac{E\left[\chi^2\right]}{\text{var}\left[\hat{\chi}\right]} = \frac{\frac{1}{3}}{\frac{1}{2R_s}} = \frac{2R_s}{3} \quad .$$

Finally, the required photon raton rate per second R_o is given by

$$R_o = (2W)R_s = \frac{3}{2}(2W)(SNR) \quad .$$

Taking $W = 5 \times 10^6$ and SNR = 1000, $R_o = 1.5 \times 10^{10}$ photons/second.

Pulsed Polarization Modulation

This type of modulation differs from pulsed intensity modulation as described in the previous section in that the stretched samples of the signal $\chi(t)$ are used to control the polarization of the optical carrier rather than the intensity of the optical carrier. The signal changes the relative amounts of energy transmitted in each of two orthogonal states of polarization. The two states of polarization could be right and left circular polarization or two orthogonal plane polarizations, for example.

Let $S_1(t_n)$ and $S_2(t_n)$ represent the intensity of the two polarization components of the optical carrier. Then,

$$S_1(t_n) = \left[1 - \chi(t_n)\right] S_s$$

$$S_2(t_n) = \chi(t_n)\, S_s \quad ,$$

where S_s is the total transmitted energy per Nyquist sampling interval. Any non-linearity of the polarization modulator is assumed to be compensated for by pre-distorting $\chi(t)$ to give a linear overall characteristic.

The receiver is assumed to contain a polarization analyzer and photodetector matched to each of the two states of polarization. Cross-talk between detectors is assumed negligible. Let $z_1(t_n)$ and $z_2(t_n)$ be the total number of photons detected by each of the two detectors during the n-th sample interval, and let R_s be the expected value of the sum of $z_1(t_n)$ and $z_2(t_n)$. Then $z_1(t_n)$ and $z_2(t_n)$ are independent Poisson random variables with expected values $\left[1 - \chi(t_n)\right] R_s$ and $\chi(t_n)R_s$, respectively.

The outputs samples are formed from z_1 and z_2 by the following operation

$$\hat{\chi}(t_n) = \frac{z_2(t_n) - z_1(t_n) + R_s}{2R_s} \quad .$$

The expected value of $\hat{\chi}(t_n)$ is $\hat{\chi}(t_n)$ so the expected value of the error is zero. The variance of $\hat{\chi}(t_n)$ is

$$\text{var}\left(\hat{\chi}\right) = \frac{1}{\left(2R_s\right)^2}\left[\text{var}\left(z_2\right) + \text{var}\left(z_1\right)\right] ,$$

$$= \frac{1}{\left(2R_s\right)^2}\left[\chi R_s + (1-\chi)R_s\right] ,$$

$$= \frac{1}{4R_s} \quad .$$

The expected value of $\chi^2(t_n)$ was found previously to be 1/3, so the SNR is

$$\text{SNR} = \frac{4}{3} R_s \quad ,$$

and

$$R_o = 2WR_s = \frac{3}{4}(2W)(\text{SNR}) \quad .$$

Taking $W = 5 \times 10^6$ Hz and SNR = 100 gives

$$R_o = 7.5 \times 10^9 \text{ photons/second} \quad .$$

Direct Intensity Modulation

In this case the signal is not sampled and boxcarred, but modulates the intensity of the transmitted light directly so that the average rate of photon emission is proportional to $\chi(t)$. The expected value of the rate of arrival of photons at the receiver likewise is proportional to $\chi(t)$. The receiver consists of a photodetector and a post-detection filter. The optimum filter and the performance of the system using that filter are found below.

The system can be modeled as shown in figure 4.3-9. The filter, with frequency function $H(f)$, is chosen to minimize the mean-square error of the estimate of the time-varying part of the transmitted signal, and rejects the constant part of the received signal. The mean value of $\chi(t)$ is assumed to be reinserted separately at the receiver. The process $R_1(t)$ is a sequence of unity impulses occurring at random with an average rate of $\chi(t)R_o$ impulses per second, and represents the modulated photon carrier signal.

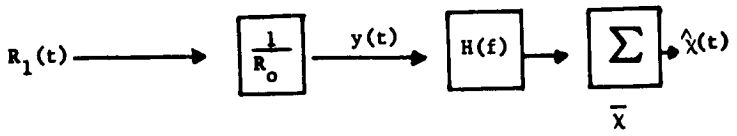

Figure 4.3-9. Model of Direct Intensity Modulation System

The optimum filter (not necessarily realizable) from the point of view of minimizing the expected value of $(\chi' - \hat{\chi}')^2$ is given by*

$$H(f) = \frac{S_{x'y}(f)}{S_y(f)} \quad ,$$

where $\chi'(t) = \chi(t) - \bar{\chi}$ is the time-varying part of $\chi(t)$, $S_y(f)$ is the power spectral density of the random process $y(t)$, and $S_{x'y}(f)$ is the cross-spectral density of $\chi'(t)$ and $y(t)$. The signal and $y(t)$ are assumed to be at least weakly stationary. The process $y(t)$ can be regarded as a sequence of impulses of strength $\frac{1}{R_o}$ occurring randomly in time with an expected rate of $\chi(t)R_o$ impulses per second. In order to obtain $S_{x'y}(f)$, and $S_y(f)$, the corresponding correlation function $R_{x'y}(\tau)$ and $F_y(\tau)$ will be calculated. This is done by first regarding each impulse of $y(t)$ as a finite pulse of width ϵ and height $\frac{1}{\epsilon R_o}$, and then letting ϵ tend to zero.

$$R_y(\tau) = E_x E_y \left\{ y \left[\chi(t + \tau)\right] y \left[\chi(t)\right] \right\}$$

*See, for example, Davenport and Root, Random Signals and Noise.

Two cases must be considered

a. $|\tau| > \epsilon$:

$$R_{y\epsilon}(\tau) = E\left\{\left[\epsilon\, R_o \chi(t)\right]\left[\epsilon\, R_o \chi(t-\tau)\right]\left(\frac{1}{\epsilon R_o}\right)^2\right\} = R_x(\tau)$$

b. $|\tau| \leq \epsilon$:

$$R_{y\epsilon}(\tau) = E\left\{\left[\epsilon\, R_o \chi(t)\right]\left(\frac{1}{R_o^2}\right)^2 (1 - |\tau|)\right\} + R_x(\tau)$$

$$R_y(\tau) = \lim_{\epsilon \to 0} R_{y\epsilon}(\tau) = \frac{\overline{\chi}}{R_o}\,\delta(\tau) + R_\chi(\tau) \ .$$

From cases a. and b. it can be seen that for all τ

$$R_y(\tau) = \frac{\overline{\chi}}{R_o}\,\delta(\tau) + R_x(\tau) \quad ,$$

from which

$$S_y(f) = \frac{\overline{\chi}}{R_o} + S_x(f) = \frac{\overline{\chi}}{R_o} + \overline{\chi}^2\,\delta(f) + S_{x'}(f) \ .$$

The cross correlation $R_{x'y}(\tau)$ is given by

$$R_{x'y}(\tau) = E\left\{\left|\epsilon\chi'(t)\right|\left[\frac{1}{\epsilon}\,\chi(t+\tau)\right]\right\} = R'_x(\tau),$$

which gives

$$S_{x'y}(f) = S_{x'}(f) \ .$$

The optimum filter is, therefore,

$$H(f) = \frac{S_{x'}(f)}{\frac{\overline{\chi}}{R_s} + S_{x'}(f) + \overline{\chi}^2\,\delta(f)}$$

If $S_{x'}(f)$ is a rectangular power spectrum of density $\frac{\sigma_x^2}{2W}$ between -W Hz and W Hz, then H(f) is a rectangular frequency function between -W Hz and W Hz except for a zero at dc.

$$H(f) = \left\{ \frac{\sigma_x^2}{\frac{2W\bar{\chi}}{R_o} + \sigma_x^2 + 2W\bar{\chi}^2\,\delta(f)} \right\}, \quad |f| < W$$

$$= 0 \qquad , \qquad |f| > W.$$

This frequency function is not strictly realizable as a practical filter, but can be approximated quite well.

The output noise power is the mean-square difference between $\chi'(t)$ and $\hat{\chi}'(t)$, and if the optimum filter is used, is given by*

$$N = \sigma_x^2 - \int_{-\infty}^{\infty} S_y(f)\, H(f)^2\, df$$

$$= \sigma_x^2 - \int_{-W}^{W} \frac{\frac{1}{2W}\,\sigma_x^4\, df}{\frac{2W\bar{\chi}}{R_o} + \sigma_x^2 + 2W\bar{\chi}^2\,\delta(f)}$$

$$= \sigma_x^2 - \frac{\sigma_x^4}{\frac{2W\bar{\chi}}{R_s} + \sigma_x^2}$$

$$= \frac{2W\bar{\chi}\sigma_x^2}{2W\bar{\chi} + R_o\,\sigma_x^2} \quad .$$

The output SNR is given by

$$SNR = \frac{\sigma_x^2 + \bar{\chi}^2}{N} = \frac{\sigma_x^2 + \bar{\chi}^2}{\sigma_x^2} + \frac{R_o\left(\sigma_x^2 + \bar{\chi}^2\right)}{2W\bar{\chi}} \quad .$$

If the signal $\chi(t)$ is uniformly distributed between 0 and 1, $\sigma_x^2 = \frac{1}{12}$ and $\bar{\chi} = \frac{1}{2}$ giving

---

*Davenport and Root, op. cit.

$$SNR = 4 + \frac{2}{3}\frac{R_o}{2W} \quad .$$

Solving for R_o, one obtains the final result

$$R_o = \frac{3}{2}(2W)(SNR-4) \approx \frac{3}{2}(2W)(SNR).$$

For high output SNR, therefore, the required photon rates for direct intensity modulation and for pulsed intensity modulation, are equal.

Direct Polarization Modulation

This form of modulation differs from pulsed polarization modulation in that the signal is not sampled and boxcarred but modulates the polarization of the optical carrier directly. The receiver continuously forms the quantity:

$$y(t) = \frac{z_2(y) - z_1(t) + R_o}{2R_o} \quad ,$$

and filters it with a filter having frequency function H(f) to obtain the best estimate of $\chi'(t)$, the time-varying part of $\chi(t)$. Here, $z_1(t)$ and $z_2(t)$ are the output signals of two photodetectors, each of which is matched to one of the two polarization components of the received signal and is assumed to consist of a random sequence of unit impulses, one impulse for each detected photon. The quantity R_o is the average number of photons per second detected by both detectors.

The analysis of the optimum filter and the performance of this case is very similar to that for the case of direct AM, and is omitted here. The optimum filter turns out to have the same frequency function (except for a gain constant) as for the direct AM case. The output SNR and required photon rates are

$$SNR = 4 + \frac{4}{3}\frac{R_o}{2W}$$

$$R_o = \frac{3}{4}(2W)(SNR-4) \approx \frac{3}{4}(2W)(SNR) \quad .$$

The photon rate required for high values of SNR is approximately equal to that required in the case of pulsed polarization modulation.

Pulse Code Modulation--Intensity Keying

In this case the signal is sampled at or above the Nyquist rate, quantized into $L = 2^M$ levels and transmitted as a series of binary numbers by on-off keying the optical carrier. "On" is assumed to correspond to a binary 1 and "off" to a binary 0. The receiver contains a photodetector and other circuitry that determine whether or not at least one photon is received during a given binary digit (bit) interval. Since background radiation and dark current have been assumed negligibly small, an error in determining the

identity of a given received bit will occur if and only if a binary 1 is transmitted and no photons are detected during the bit interval. When a binary 1 is transmitted, the number of photons detected during the bit interval is a Poisson random variable with average value R_o, and the probability of detecting exactly n photons during the bit interval is

$$P(n) = \frac{e^{-R_b} R_b^n}{n!}$$

If all L signal levels are equally likely, as assumed, then the PCM bits will take on the values 0 and 1 with equal probability. The probability of error P_b of an arbitrarily-selected received bit is, therefore,

$$P_b = \frac{1}{2} P(0) = \frac{1}{2} e^{-R_b} \quad .$$

In order to determine the required value of R_b, it is necessary to assign an allowable value for P_b. Unfortunately, no data have been found that would indicate what bit error rate is required in a PCM system to give signal quality equal to that of an analog system operating at a given output SNR. Lacking this information, it will be assumed for purposes of preliminary comparison that the quality of the two systems is equal when their output SNR's are equal.* In the case of PCM signal, the output noise consists of two parts, quantization noise and noise arising from bit errors.

The quantization noise power N_q is equal to the variance of the quantization error, which, for the assumed uniform distribution of $\chi(t)$, is

$$N_q = \frac{1}{12L^2} \quad .$$

In order to evaluate the noise N_b caused by bit transmission errors the receiver's estimate $\hat{\chi}(t_n)$ of the n-th sample value of the signal $\chi(t)$ is written as

$$\hat{\chi}(t_n) = \sum_{k=0}^{M-1} \frac{1}{L} a_k 2^k \quad ,$$

*This assumption has been made also by other investigators, including those responsible for Hughes Aircraft Company's Deep Space Optical Communications System Study.

where a_k is the value, 0 or 1, of the k-th digit of the PCM word. Now, let $\epsilon(t_n)$ be the error $\chi(t_n) - \hat{\chi}(t_n)$ in the n-th sample. Then $\epsilon(t_n)$ can be expressed as

$$\epsilon(t_n) = \sum_{k=0}^{M-1} \frac{1}{L} a_k 2^k \quad ,$$

where, since the a_k are equally likely to be 0 or 1, the probability distribution of c_k is

$$P(c_k) = \begin{cases} \frac{1}{2} P_b, & c_k = 1, -1 \\ (1 - P_b), & c_k = 0 \end{cases} .$$

The occurrence of errors in the various bits is assumed to be independent.* Since the c_k have zero mean and are independent,

$$N_b = \text{var } (\epsilon) = \sum_{k=0}^{M-1} \frac{1}{L} 2\, 4^k E\left[c_k^2\right]$$

$$= \frac{P_b}{L^2} \sum_{k=0}^{M-1} 4^k \qquad = \frac{(4^M - 1)P_b}{3L^2}$$

$$= \frac{(L^2 - 1) P_b}{3L^2} \quad .$$

The total noise power N is the sum of N_q and N_b

$$N = \frac{1}{12L^2} + \frac{L^2 - 1}{3L^2} P_b \quad ,$$

---

*This assumption is not a valid one if, for example, the signal undergoes slow fading.

and the SNR is

$$SNR = \frac{E(X^2)}{N} = \frac{\frac{1}{3}}{N} = \frac{4L^2}{1 + 4(L^2 - 1)P_b} \approx \frac{4L^2}{1 + 4L^2 P_b} \quad .$$

The error probability P_b depends upon L for any given value of R_s, the number of photons per sample, since

$$R_b = \frac{R_s}{M} = \frac{R_s}{\log_2 L} \quad .$$

Therefore, there exists an optimum value of L for each value of SNR which minimizes the required value of R_s. The last form of the immediately preceding equation gives

$$P_b \approx \frac{1}{SNR} - \frac{1}{4L^2} \quad . \tag{9}$$

A trial-and-error solution for SNR = 1000 gives the following optimum values for L, P_b, and R_b:

$L = 32$ (5 bit PCM)

$P_b = 7.5 \times 10^{-4}$

$R_b = 6.4$ photons per bit.

The required photon rate per second is

$$R_o = 6.4 \times 5 \times 10^7 = 3.2 \times 10^8 \text{ photons/second.}$$

Pulse Code Modulation-Polarization Keying

This form of modulation is similar to PCM with intensity keying except that the PCM bits are transmitted as one of two orthogonal states of polarization of the optical carrier. The receiver contains a polarization analyzer and photodetector matched to each of the two states of polarization and makes bit decisions according to which detector responds to more photons during the bit transmission interval.

There is some uncertainty as to the amount of crosstalk to be expected between the two photodetectors at low photon rates. It is not obvious whether or not a right circular polarization analyzer, for example, completely rejects left circularly polarized light when the photon rate is very low. The crosstalk will be assumed to be negligible for the present analysis. The analysis is easily modified to take crosstalk into account.

Under the assumption of no background noise or detector noise, a bit error can be made only if no photons are received by either photodetector, in which case an error will be made with probability 1/2 (assuming transmitted bits are equally likely to be 0 or 1). Let R_b be the expected number of photons received per bit. Then the probability of error per bit is, from the equation

$$P(n) = \frac{e^{-R_b} R_b^n}{n!} ,$$

$$P_b = \frac{1}{2} e^{-R_b} \tag{10}$$

as in the case of PCM with intensity keying. The analysis of output SNR and required photon rate R_0 contained in the paragraph on "Pulse Code Modulation-Intensity Keying" apply to the present case, and the numerical results obtained hold also.

Therefore, the performance of PCM with intensity keying is equal to that of PCM with polarization keying under the conditions assumed. The performance of the latter can be improved slightly by using a simple error correction technique. A parity check bit would be appended to each PCM word, making a total word length of M + 1 bits. This would permit the receiver to fill in a single omission (failure to detect any photons with either photodetector) in a (M + 1)-bit word by choosing it to yield proper parity. Although no exact analysis of this technique has been made, it is possible to estimate the effect of coding. First of all, if bit omissions are independent of each other the probability of exactly k omissions in an (M + 1)-bit word is

$$P_k = \binom{M+1}{k} P_{bo}^k \left(1 - P_{bo}\right)^{M-k+1} \qquad k = 1,2 \ldots M+1 , \tag{11}$$

where P_{bo} is the probability of bit omission. If MP_{bo} is very small, the probability of two omissions is large compared to the probability of more than two omissions. Approximately, therefore, the probability P_e that errors will remain in the M information bits at the output of the error corrector is

$$P_e \frac{3}{4} P_2 = \frac{3(M+1)M}{8} P_{bo}^2 . \tag{12}$$

The factor of 3/4 arises because a probability of 1/4 exists that a random assignment of 0 or 1 to the two bit omission would be the correct one. As a further approximation, the error in a sample that results from two PCM bit errors is taken to be equal to that which would result from a single PCM bit error. This is a reasonable approximation since most of the sample error is contributed by the highest order bit in error. Therefore, P_e of Eq. (12) can be substituted for P_b in Eq. (9) to permit P_{bo} and, subsequently, the new value of R_o to be determined. Numerical evaluation for M = 5 gives

$$R_o = 2.9 \times 10^8 \text{ photons per second.}$$

This represents a 0.4 dB deduction compared to the system without error correction.

4.3.5.2 Investigation of a Large Optical Collector for Space to Ground Communications

A large optical collecting area can be implemented by using a technique devised for a stellar interferometer.[12] The interferometer uses a large array of optical reflectors in lieu of a single large area collector. Each reflector directs the desired energy toward a common focal point for the array. Recent construction of an f/1.6, 22-foot diameter stellar intensity interferometer shows the complete practicality of this approach. This size approximates the energy collector for the ground based receiver.

A typical array would consist of a number of figured small mirrors each cut in a hexagonal shape to maximize the collecting area, and mounted on a supporting structure. The final array would approximate a large circular paraboloid. Each element would be adjusted to provide the best overall resolution. The structure would be mounted on an elevation-azimuth tracking mount. Tracking data from an outside source such as a radar would be used to point the structure. Since an optical resolution of only 0.5 milliradian is expected, the pointing accuracy would have to be of the order of 0.05 to 0.1 milliradian, which is presently obtainable.

4.3.5.2.1 Array Geometry

Figure 4.3-10 shows the geometrical layout for the large circular paraboloid in two dimensions. A single parabolic element is shown at 0'. Elemental parabolic geometry was chosen because a simple and exact analysis could be easily performed. The geometry has been adjusted so that the normal to the center of an element intersects the array's principal axis at an angle θ. The reflected ray from the center of the element as shown in the diagram intersects the array principal axis at the array focal point at an angle 2θ. Thus, the parabola geometry of the center of each element lies on a parabola with a focal length $\overline{OF}$. The array is assumed as a circular paraboloid, and the incoming signal is parallel to the OX direction within the array pointing accuracy. Because of the paraboloid-shape the rays from the center of each element in the ZY plane also intersect at the focal point F. However, the remaining area of each element does not conform to the large paraboloid, and the contribution from all the areas joins the circle of confusion of the array.

Except for the central element, the aberration in the focal plane of the array produced by each small element is caused by the incident rays arriving at an off-axis angle. Thus, each parabola focuses off its axis. The axis for a single element is denoted at X'Y'Z' in figures 4.3-10 and 4.3-11. Each parabola focuses the incoming energy into a coma-shaped image in its own focal plane. The image has its longer dimension in the Z'0'X' plane. Thus each parabola forms an elongated image inclined at an angle in ZY plane corresponding to its location in the ZY plane. Thus, at F and for a fixed angle 2θ, the rays formed by a single zone of the array form a circle. As the angle 2θ increases, the size of this circle of confusion increases. Thus, the size of the circle of confusion is a function of the angular aperture of the larger array.

When using the array as a collector for the direct communications system, the circle of confusion determines: (1) the secondary optics that will be required to focus the signal through a narrow band optical filter, which is extremely sensitive in bandwidth to the angle of passage, and thence to the photomultiplier detector, (2) the resolution or minimum angular size of background, which determines tne amount of unwanted background radiation entering the system.

---

(12) H. Messell, S. Butler, "A New Stellar Interferometer," Space Physics and Radio Astronomy, 1964, Chapter 5, MacMillan and Company, London.

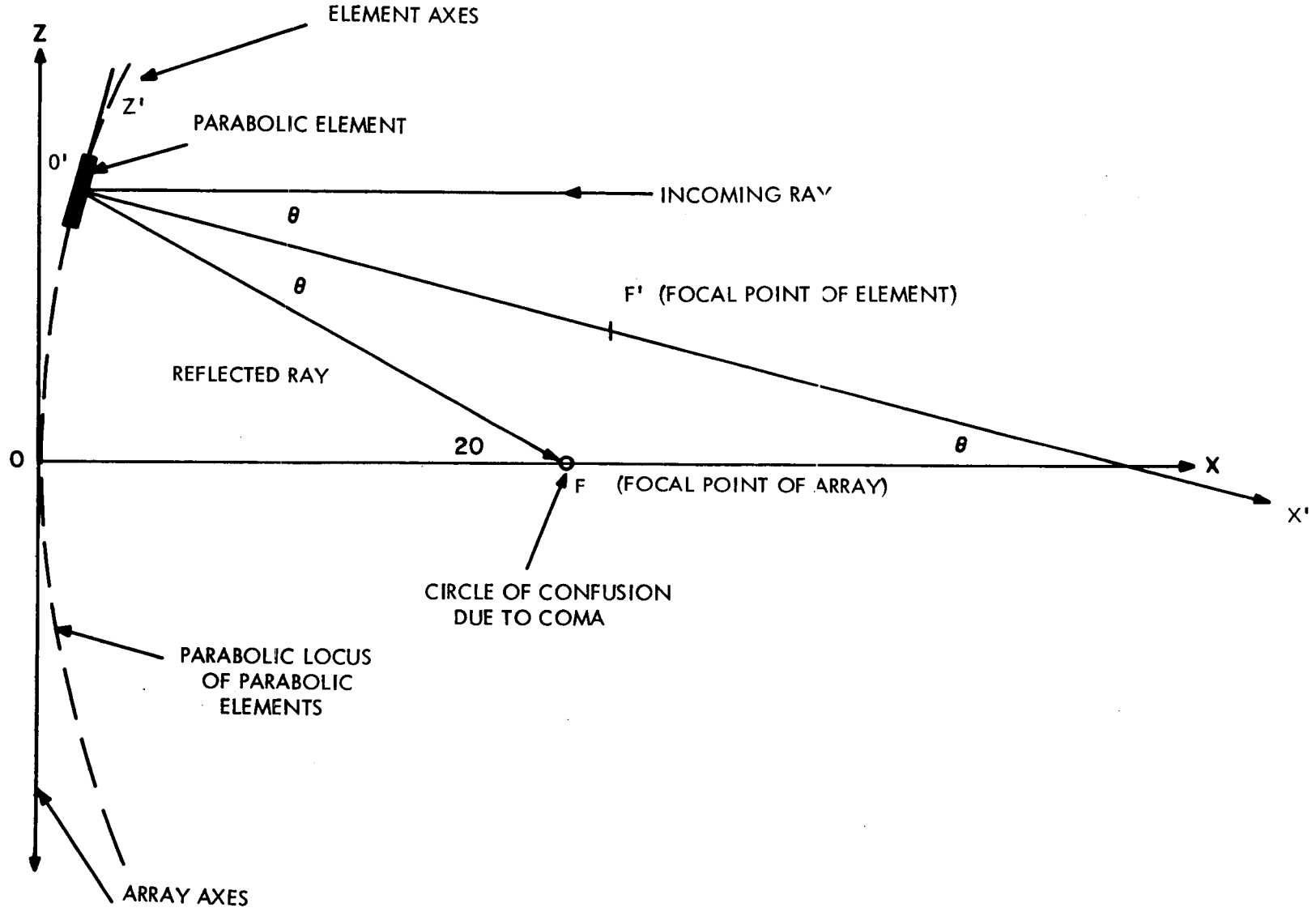

Figure 4.3-10. Array Geometry.

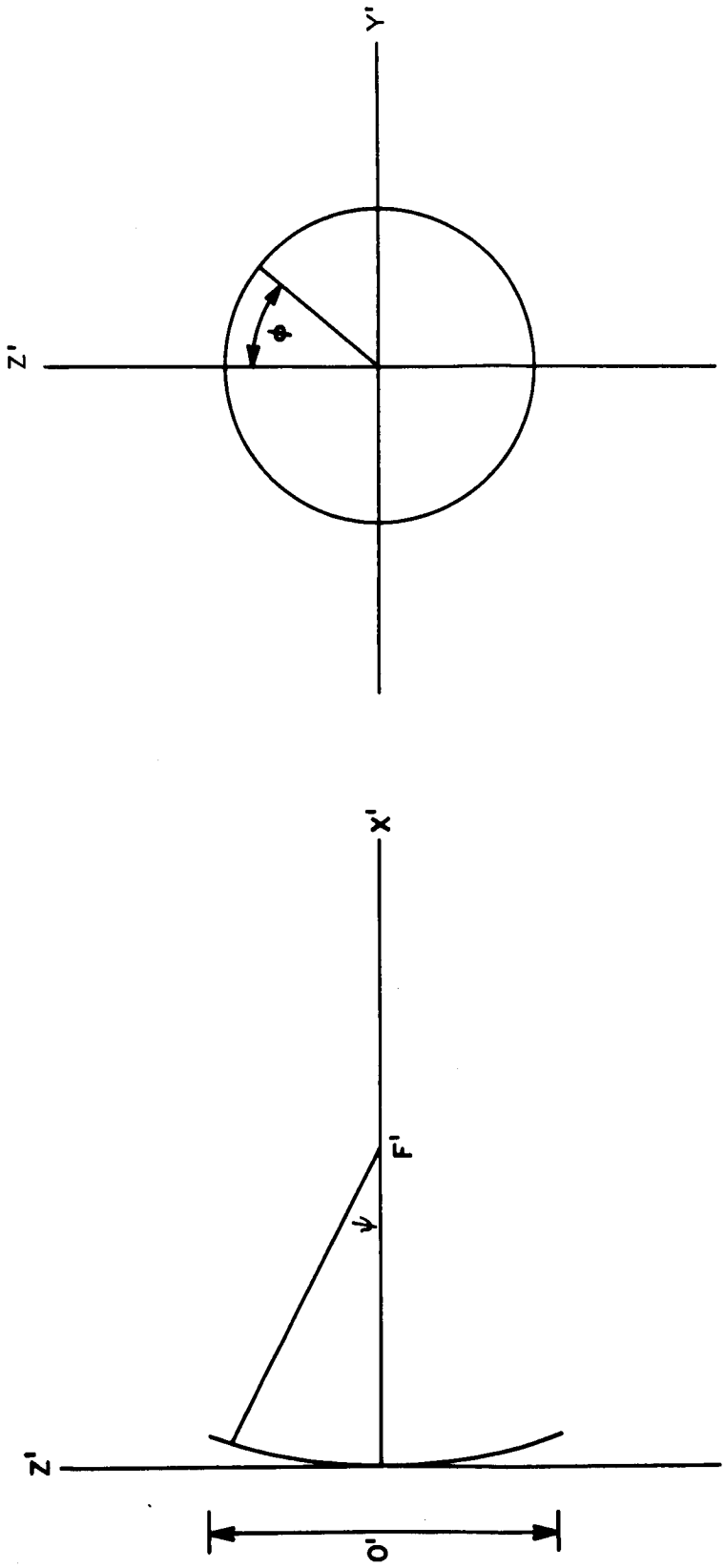

Figure 4.3-11. Parabolic Element.

4.3.5.2.2 Minimum Angular Size of Background

The geometry of a parabolic element is shown in figure 4.3-11. The Z' and Y' location of the image rays in the plane at X' = F' are given by the expression(13)

$$Y' = - \frac{\overline{O'F'} \tan \theta}{\cos \psi} \frac{\tan^2 1/2\psi \sin 2\phi}{1 - \tan \psi \tan \theta \cos \phi} \tag{13}$$

$$Z' = \frac{\overline{O'F'} \tan \theta}{\cos \psi} \frac{1 + \tan^2 1/2\ \psi \cos 2\ \phi}{1 - \tan \psi \tan \theta \cos \phi} \tag{14}$$

where

$O'F'$ = the focal length

θ = the angle of arrival of rays relative to the O'X' axis

ψ = the angular location of the ray relative to O'X' at the focal point F'

ϕ = the angular location of the ray in the Z'Y' plane.

The value of Z' is the long dimension of the coma for $\phi = 0$, and for values of ψ where small angle approximations are valid, neglecting terms in ψ^2:

$$Z' = \frac{\overline{O'F'} \tan \theta}{1 - \psi \tan \theta} \ . \tag{15}$$

The maximum length of the coma δ, which originates from the peripheral parabolas, is given by:

$$\delta_{max} = (Z')_{\psi = \psi_{max}} - (Z')_{\psi = 0}. \tag{16}$$

Substituting Eq. (15) in Eq. (16), and noting that the term $\psi_{max} \tan \theta \ll 1$, if each element has a diameter small compared to its focal length, and even for high aperture large arrays, the coma length may be approximated as:

$$\delta_{max} \approx \overline{O'F'}\ \psi_{max} \tan^2 \theta \tag{17}$$

Now:

$$\overline{O'F'}\ \psi_{max} \approx \frac{d}{2} \tag{18}$$

where d = diameter of the parabolic element. Thus Eq. (17) may be written as:

$$\delta_{max} \approx \frac{d}{2} \tan^2 \theta \tag{19}$$

(13) Plummer, "On Images Formed by a Parabolic Mirror," Astronomical Journal, Volume LXII, 5, p. 354, March 1902.

From the geometry of the parabola, it can be shown that:

$$\tan \theta = \frac{D}{4F} , \tag{20}$$

where D is the diameter and F the focal length of the large parabolic array.

Substituting Eq. (20) in Eq. (19) gives:

$$\delta_{max} \approx \frac{dD^2}{32F^2} . \tag{21}$$

The coma aberrations from any of the parabolas can be adjusted to fit within a circle in the focal plane whose diameter is given by Eq. (21) by adjusting eacn mirror individually. The angular size of δ_{max} is the resolution of the receiver, and determines the minimum background angle that the reveiver can subtend. The angular size Δ_{max} of δ_{max} is:

$$\Delta_{max} = \frac{\delta_{max}}{F} . \tag{22}$$

Substituting Eq. (21) into Eq. (22) gives:

$$\Delta_{max} = \frac{dD^2}{32F^3} . \tag{23}$$

Eq. (23) is shown plotted in figure 4.3-12 for 30-cm diameter elements. These curves show that a receiver field of view of less than 0.5 milliradians can be achieved in a large diameter high aperture ratio segmented optical collector. For example: an 8-meter diameter collector whose aperture ratio is f/1.3 views only 0.5 milliradians of background.

4.3.5.2.3 Large Aperture Segmented Mirror at Narrabri Observatory Australia

Originally the only large multi-element optical collectors were the solar furnaces. However, in recent years higher resolution arrays have been constructed at Narrabri Observatory for use in measuring star diameters. In addition diffraction limited segmented telescopes have been proposed for astronomical space observatories.

The details of the Narrabri collectors are very similar to the collector being considered for the ground-based direct detection system. A summary of the Narrabri system is presented in table 4.3-3.

The minimum star image size in this table is 3 milliradians. Private communication with Professor R. Hanbury Brown of the University of Sydney and Narrabri has revealed that because of support structure deformation only a 3-milliradian resolution was achievable. Professor Brown thought that with proper design the minimum star image size could be reduced to about 0.6 to 1.0 milliradians. This value falls within a useful range of values for application to the direct detection receiver.

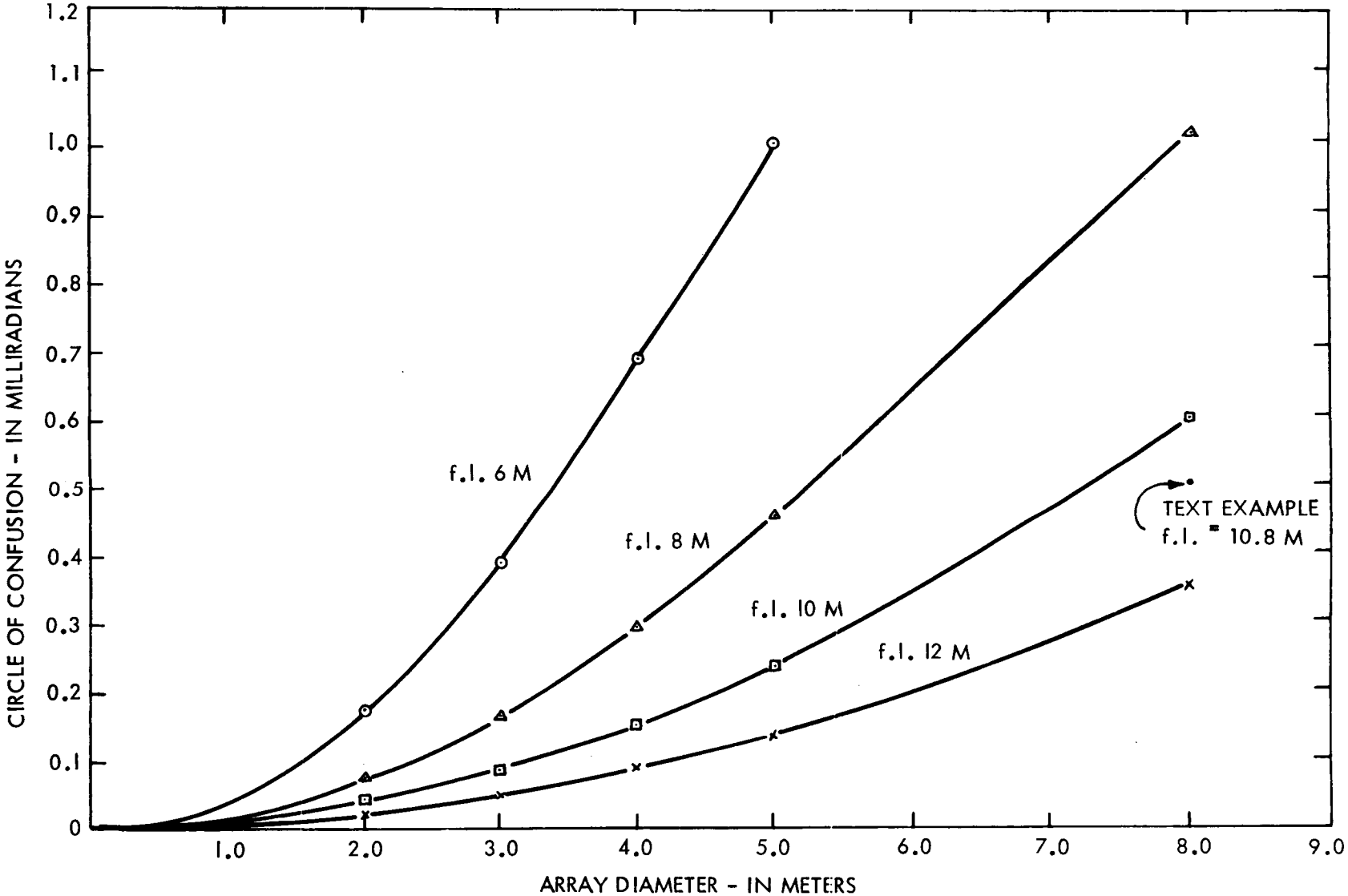

Figure 4.3-12. Array Diameter vs. Circle of Confusion for 6,8,10, and 12 Meter Focal Lengths (0.3-Meter Diameter Elements).

TABLE 4.3-3

THE LARGE APERTURE SEGMENTED MIRROR
AT NARRABRI OBSERVATORY, AUSTRALIA

Segmented Mirror Characteristics	
Aperture of array:	22 feet
Focal length of array:	36 feet
Number of elements:	252
Element Size:	hexagonal, 15 inches across flats 1 inch thick
Element Weight:	12 pounds
Element figure and tolerance:	spherical figure, 1/8 wave 72-foot R of C
Element coating:	front surface, aluminized SiO protective coat
Element mounting:	individual three-point suspension
Element heaters:	pad cemented to back of each element, 12 watts of power used for anti-dewing
Minimum image size, static:	0.5 inch
Maximum image size, including frame deflections	1.25 inches
Corresponding max angular image circle:	3.0 milliradians
Manufacturer	Mount: Dunford and Eliot Ltd., Sheffield, England Mirrors: Officine Galileo, Florence, Italy

Additional System Details:

The converging cone of light from the reflector is collimated with a 3-inch diameter, 5-inch focal length, negative lens. The collimated light is passed through a 3-inch diameter multi-layer dielectric interference filter centered at 4385 angstroms with an 80-angstrom bandwidth. An aspheric positive lens, 3 inches in diameter is used to focus the light onto the cathode of a 14-stage photomultiplier.

References:

R. Hanbury Brown, "The Stellar Interferometer at Narrabri Observatory," Sky and Telescope, Vol. 28, No. 2, pp. 64-69.

H. Messel and S. Butler, Space Physics and Radio Astronomy, MacMillan and Co., Ltd., London, 1964.

4.3.5.2.4 Tracking Mount for Large Aperture Optical Collector

Many of the large tracking radar antennas in use today can provide the design basis for the large optical collector tracking mount. The requirements placed upon the mount include: (1) the structure must support with precision the optical elements and their adjustable retaining cells; (2) the tracking mount must be capable of tracking the satellite within a fraction of the allowed optical field of view.

Optics Considerations

A typical optical design might be an 8-meter diameter f/1.3 segmented mirror. This mirror would be composed of approximately 830 hexagonal shaped molded epoxy mirrors. Each mirror would be nominally 25 cm from edge to edge and be approximately 3.2 centimeters thick in order to hold better than one wave surface figure tolerance. Each mirror would weigh approximately 0.75 Kg, and thus the optics would weigh approximately 620 Kg. Allowing about 1.0 Kg for each cell, the total weight would be about 1400 Kg. Each mirror would cost approximately $30.00. and the total mirror cost would be $25,000.

The positioning accuracy requirement of each element is determined by the minimum background angle that can be allowed. A reasonable estimate of the accuracy would be 1/10 of the allowed background angle. Thus, if the system is designed to have a circle of confusion of no more than 0.5 milliradians, the element positioning accuracy should be of the order of 0.05 milliradians. Similarly, the tracking accuracy of the entire mount should also be of this order.

Tracking Mount

An existing microwave antenna tracking mount that was developed for the Advent program[14], and is now being used for the Syncom satellite system, could be adapted to accommodate the large optical collector.

This tracking system uses a 19.5-meter diameter microwave antenna weighing 8,500 Kg. Outer rim deviation from a true surface is maintained under 56-mph wind loading. Expressed as an angular deviation, the departure from a true surface amounts to $\Delta\theta \leq 250$ microradians. Tolerances on the allowable deviation for the optical collector are $\Delta\theta \leq 50$ microradians at the rim.

Holding the optical collector structure to tolerances of this order places a premium on careful analysis of wind loading and thermal loading effects. Computer programs relating to these effects were generated and used in the development of the antenna structure, and a similar approach would be applicable to the optical collector.

The antenna tolerances were maintained with the mount completely exposed to the external environment. A reduction in the severity of structural requirements can be accomplished by sheltering the optical collector in some form of modified dome.

The performance of the tracking mount varies with the particular mode of operation. For example, as an active tracker following radio frequency sources at UHF or VHF, angular errors of 408 microradians and 970 microradians respectively are obtained. In these tests a radio frequency source was flown around the antenna at an angular velocity of 4 milliradians/sec. This rate corresponds to a satellite whose orbital characteristics are similar to Echo I. However, the pointing accuracy of the antenna was spread between 17 and 51

---

(14) Advent Ground Antenna Systems, Contract No. DA36-039-SC-87365, U.S. Signal Supply Agency, Ft. Monmouth, N.J.

microradians in the astro positioning mode, (rate-aided tracking). In this mode the mount is driven from an external program source, just as the optical collector mount will be driven by external radar data.

The indicated accuracy spread reflects the data from two different sites as well as azimuth and elevation axis differences.

Secondary Optics and Optical Filter Considerations

Each element of the multi-element array focuses the incoming energy into an image in its own focal plane. Elements positioned off the central axis of the main array form elongated, comatic images. The sum of these distorted images form the circle of confusion.

Rays entering this circle of confusion from the array must be re-directed to fall within the entrance angle limitations of the narrow bandwidth dielectric film filter. A collimation lens, (or mirror), can be used for this function.

The general requirements of the secondary optics are:

a. They must subtend all the rays that make up the circle of confusion of the large optical collector.

b. They must reduce the angular divergence of these rays such that they are passed without loss through the interference filter.

c. A field stop in the focal plane is required to restrict the field of view of the large parabolic array.

An example applicable to the direct system being considered is illustrative. The behavior of narrow-band interference filters in divergent (or convergent) light is discussed in section 4.3.5.3. Figure 4.3-13 shows the theoretical characteristics of these filters at 6328 A for a geometric mean index of refraction of 1.8. The present state of art permits application of 2Å filters for the direct detection system. From figure 4.3-13 a filter bandwidth of 2Å permits a beam divergence of 20 milliradians if maximum filter transmission is desired.

The cone angle or rays from a f/1.3 parabola is 0.77 radians; thus an angular minification of at least 39 is required.

A simple solution to this problem would be to use a collimator to form a beam of all the rays from the circle of confusion.

The angular beamwidth γ of a collimated extended source may be described by the searchlight beam spread relation,

$$\gamma = 2 \tan^{-1} \left(\frac{ds}{2f_c} \right), \qquad (24)$$

where

d_s = the source diameter

f_c = the focal length of the parabolic collimator.

The extended source diameter, which in our case is the circle of confusion, calculated from Eq. (23) using a focal length to diameter ratio of 1.3 for the array and an element

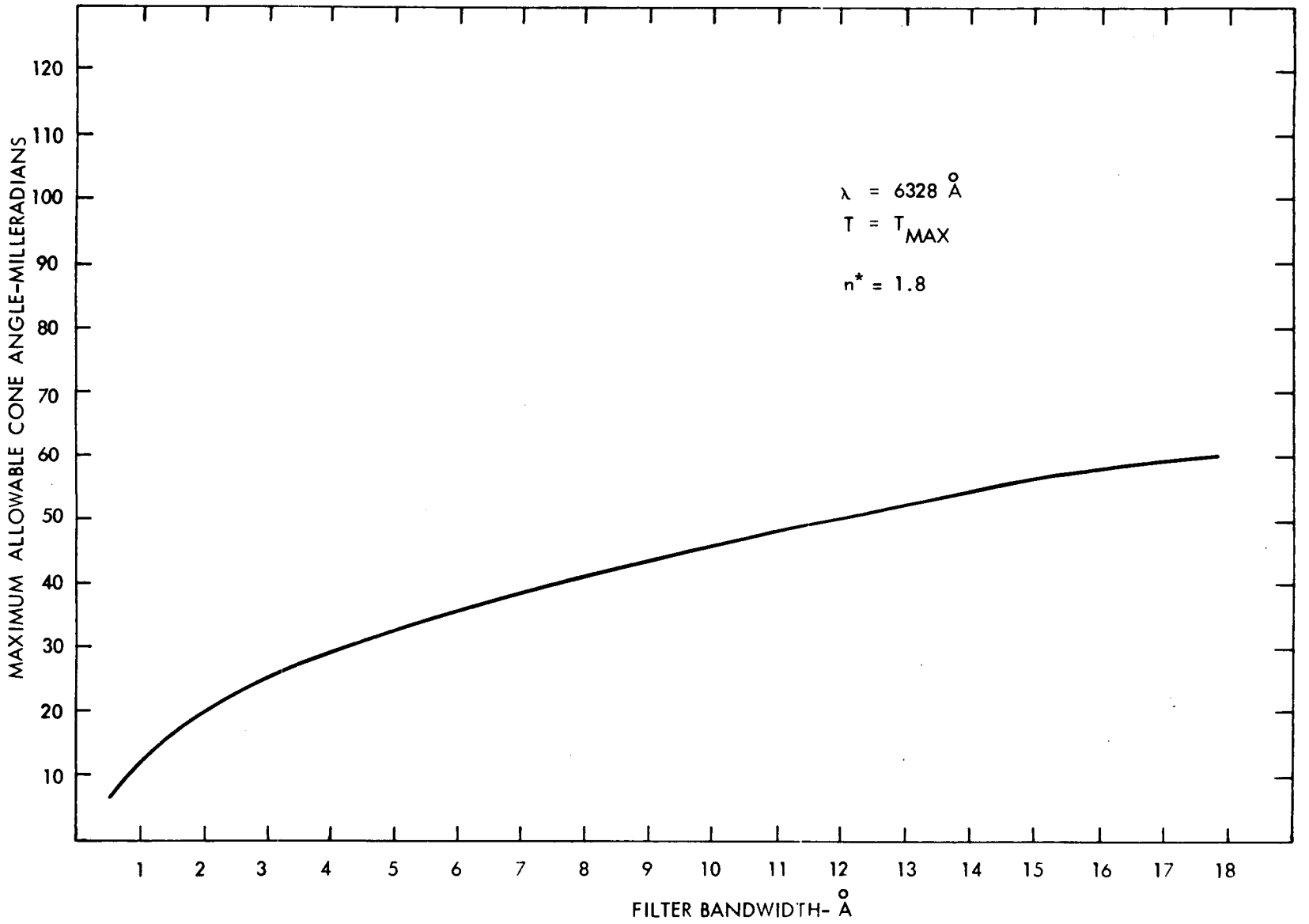

Figure 4.3-13. Maximum Allowable Secondary Optics Cone Angle.

diameter of 30-cm is 0.56 cm. Requiring $\gamma \leq 20$ milliradians, the value of f_c must be greater or equal to 28 cm. The maximum cone diameter of the rays from the circle of confusion at a distance 28 cm from the focus of the large f/1.3 parabola is 20-cm. Thus a 20-cm diameter collimator with a 28-cm focal length could be used to collimate the rays to a beam whose maximum divergence is 20 milliradians.

The minimum filter size is also 20 cm and would probably have to be constructed as an array of small, square filters. After passing through the filter, the signal rays could be reconverged at the demodulator where the optical signal would be converted to electrical signals.

If polarization modulation is used, the demodulator would consist of a polarization analyzer followed by suitable photomultiplier detectors.

Ray Tracing Analysis of Large Aperture Telescope

A ray tracing analysis for a large aperture moderate quality segmented telescope was undertaken to define the optical and mechanical parameters required for the large aperture direct detection system. In the computer program used to analyze the segmented paraboloid mirror array, it was expedient to determine the geometry of the mirror location and then tilt the individual mirror segment. In this manner the same effect was produced as if the mirror were displaced from the optical axis. The resulting data are tabulated in two separate arrangements.

In table 4.3-4, the mirror segment location is defined, together with the necessary parameters that describe the mirror tilt, the location of the centroid for the reflected image point, and also the root mean square radius of the resulting blur circle as measured on the flat image surface. Since the mirror segment tilt has been carefully calculated so that the individual image spots will have their centroids coinciding, it is merely necessary to consider that the blur circle radii for all mirror segments are completely concentric about the optical axis. In table 4.3-5, this information has been broken down further to provide the energy concentrations within the image structure as a function of varying blur circle radii. Percent energy concentrations and the separate mirror segment locations, numbers 1 through 7, are indicated. The blur circle radius recorded in each of these boxes represents the total blur circle radius.

The next step in this analysis would answer questions such as: tolerance requirements on pointing in order to provide the required half milliradian circle of confusion; pointing accuracy of each segment so as to maintain a half milliradian circle of confusion centered on the axis to within 0.05 milliradians; and, finally, the best mirror profile to use for the application.

4.3.5.3 Multilayer Dielectric Interference Filters in Parallel and Convergent Light

The purpose of this study was twofold: a) to present a survey on existing methods of calculation of all-dielectric interference filters (ADI), b) to derive simplified formulas and plots giving the behavior of ADI filters in obliquely incident and convergent light. The results of this simplified theory agree quite well with those obtainable by a more complicated analysis for the case of filters with a large number of layers (above 6); therefore, they are sufficient to provide the information necessary in engineering applications.

Dielectric Filters in Parallel Light

A multilayer dielectric filter is essentially a Fabry-Perot interferometer, in which the spacer layer is a multiple of $\frac{\lambda}{2}$ thick, and the high reflectivity is provided by alternate

TABLE 4.3-4

SYSTEM ANALYSES

Segment Location	θ Tilt	Average Y	RMS Radius
Advent #1	0.187000	-153.9074	0.1512"
Advent #2	0.165345	-136.0028	0.1174"
Advent #3	0.141558	-116.0024	0.0841"
Advent #4	0.117522	- 96.0010	0.0568"
Advent #5	0.093280	- 76.0016	0.0353"
Advent #6	0.068869	- 56.0006	0.0190"
Advent #7	0.044336	- 35.9125	0.0078"

TABLE 4.3-5

ENERGY CONCENTRATIONS AS A FUNCTION OF

BLUR CIRCLE RADIUS

Percent Energy	Segment Location→ #1	#2	#3	#4	#5	#6	#7
10	0.0515	0.0412	0.0296	0.0198	0.0128	0.0063	0.0026
20	0.0680	0.0535	0.0386	0.0263	0.0165	0.0090	0.0038
30	0.0884	0.0695	0.0495	0.0336	0.0211	0.0113	0.0046
40	0.0996	0.0786	0.0571	0.0388	0.0241	0.0130	0.0059
50	0.1268	0.0981	0.0705	0.0481	0.0298	0.0160	0.0065
60	0.1411	0.1102	0.0792	0.0538	0.0335	0.0179	0.0072
70	0.1686	0.1308	0.0936	0.0632	0.0390	0.0209	0.0085
80	0.2022	0.1565	0.1118	0.0755	0.0468	0.0249	0.0099
90	0.2342	0.1810	0.1291	0.0868	0.0534	0.0284	0.0116
100	0.2805	0.2174	0.1560	0.1059	0.0661	0.0361	0.0153

layers of dielectric of high and low refractive indices and of thickness $\frac{\lambda}{4}$. The entire filter is deposited on a glass substrate of index n, as shown in figure 4.3-14.

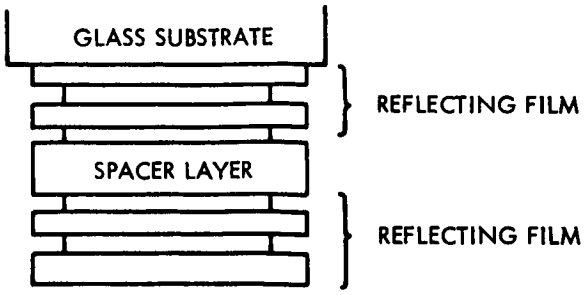

Figure 4.3-14. All Dielectric Interference Filter

The quarter-wave layers are usually denoted H for high refractive index and L for low refractive index, thus a half-wave spacer is denoted HH or LL. The materials commonly used in the visible range are zinc sulfide with $n_H = 2.35$ and cryplite with $n_L = 1.35$. The glass substrate has an index n = 1.5.

Such a system of layers is essentially a periodically stratified medium and can be treated by matrix methods(15). However, more insight into the behavior of the filter can be obtained by using an equivalent Fabry-Perot approach. Smith(22) has shown that any transparent multilayer dielectric filter can be completely represented by 4 complex parameters that describe the overall characteristics of the multilayers on the two sides of the spacer. The equivalent Fabry-Perot interferometer is shown in figure 4.3-15.

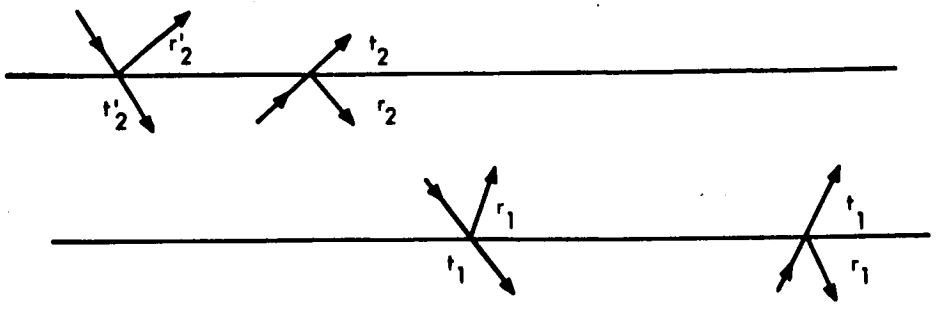

Figure 4.3-15. Representation of an ADI Filter by Two Effective Interfaces

In figure 4.3-14 we have shown 8 parameters that describe the 2 multilayers; however, only 4 of them are needed in the computation. The transmission coefficient for the electric field from medium 1 to medium 2 is given by

(15) S. D. Smith, "Design of Multi-Layer Filters by Considering Two Effective Interfaces," JOSA, January 1958, Vol. 48, No. 1, pp. 43-50.

$$t = \frac{t_1 t_2}{1 - r_1' r_2 e^{i\delta}} \tag{25}$$

where

$\delta = 2 \frac{2\pi}{\lambda} n_s d \cos \phi$

ϕ = the angle at which the wave travels between the two interfaces

t_1, t_2 = the transmission coefficients through the multilayers

r_1', r_2 = the reflection coefficients for the multilayers

n_s = the refraction index of spacer layer.

The transmissivity is then given by:

$$T = |t|^2 = \frac{|t_1 t_2|^2}{1 + |r_1' r_2|^2 - \left(r_1' r_2 e^{i\delta} + r_1'^* r_2^* e^{-i\delta}\right)} . \tag{26}$$

Let

$$r_1' = \sqrt{R_1}\, e^{-i\phi_1}$$

$$r_2 = \sqrt{R_2}\, e^{-i\phi_2}$$

$$t_1 t_2^2 = T_1 T_2$$

$$\sqrt{R_1 R_2} = R \quad .$$

Substituting into Eq. (26), we obtain

$$T = \frac{T_1 T_2}{\left(1 - \sqrt{R_1 R_2}\right)^2 + 2\sqrt{R_1 R_2}\left[1 - \cos\left(\delta - \phi_1' - \phi_2\right)\right]} \quad , \tag{27}$$

or finally

$$T(\omega) = T_o(\omega) \frac{1}{1 + F(\omega) \sin^2 \frac{\theta}{2}(\omega)} \quad , \tag{28}$$

where

$$T_o(\omega) = \frac{T_1 T_2}{(1-R)^2} \quad , \quad F(\omega) = \frac{4R}{(1-R)^2}$$

$$\theta(\omega) = -\delta + \phi_1'(\omega) + \phi_2(\omega)$$

$$\omega = \frac{\lambda_o}{\lambda} \quad .$$

Eq. (28) is analogous to the Airy formula[16] for transmission through a parallel plate; however, here all the parameters are frequency-dependent. In particular, one is interested in the behavior of the filter near the fundamental wavelength λ_o, which is given by $n_s d = \frac{\lambda_o}{2}$, at which point the transmission is maximum. Around that frequency the terms T_o and F vary slowly with ω; therefore one must only consider the variation of θ. At the wavelength λ_o, $\theta_1'(\omega)$ and $\phi_2(\omega)$ are zero, and their variation is small around $\lambda = \lambda_o$. We also note that Eq. (28) is derived under the assumptions of no loss by absorption or scattering. When these are accounted for, the maximum transmittance is given by

$$\tau_{max} = \frac{1}{\left(1 + \frac{A}{\tau}\right)^2} \quad , \tag{29}$$

where the relation A + R + T = 1 denotes the conservation of energy between reflection, absorption, and transmission.

In commercially available filters the quantity $\frac{A}{\tau_o}$ rises rapidly with R so that narrow band and high transmission are incompatible. The narrowest filters made by this method have a bandwidth (at half-transmission points) of 6 Å and a peak transmission of 25 percent, with 15 layers of dielectric film.

Recently[17, 18], high reflectivities with low absorption have been obtained in multilayer dielectric filters by a new process of deposition of the dielectric films. Reflectivities in excess of 0.995 have been obtained in mirrors having more than 30 layers. Conceivably the same technique could be used to make low-loss dielectric filters with narrow bands.

The bandwidth of the filter for parallel light at normal incidence can be found from Eq. (28). At the points at which the transmittance drops to 0.5, we must have

---

(16) M. Born and E. Wolf, "Principles of Optics," MacMillan Company, New York, 1964, pp. 55-70.

(17) D. L. Perry, "Broadband Dielectric Mirrors for Multiple Wavelength Laser Operation in the Visible," Proc. of the IEEE, Vol. 53, No. 1, January 1965, pp. 76-77.

(18) "Many Layers Add Up to Nearly Perfect Laser Mirror," IEEE Spectrum, February 1965, p. 38.

$$F \sin^2 \frac{2\pi n_s d}{\lambda} = 1 \quad . \tag{30}$$

But also at the fundamental wavelength λ_o ,

$$\sin^2 \frac{2\pi n_s d}{\lambda_o} = 0 \text{ or } n_s d = \frac{m\lambda_o}{2} \text{ , where m is an integer.}$$

Therefore condition in Eq. (30) becomes

$$F \sin^2 \pi \frac{m\lambda_o}{\lambda} = 1 \ . \tag{31}$$

Let

$$\lambda_1 = \lambda_o + \frac{\Delta\lambda}{2}$$

$$\lambda_2 = \lambda_o - \frac{\Delta\lambda}{2} \quad .$$

Then

$$F \sin^2 \pi \frac{m\Delta\lambda}{2\lambda_o} \simeq F\left(\pi \frac{m\Delta\lambda}{2\lambda_o}\right)^2 = 1 \quad .$$

The bandwidth between the half power transmission points is thus

$$\frac{\Delta\lambda}{\lambda} = \frac{2}{m\pi F} \quad . \tag{32}$$

From Eq. (32), it is seen that the bandwidth of a filter can be decreased either by increasing F (i.e. the reflectivity) or the interference or spacer order m. Since increased reflectivity reduces also the peak transmission, narrow band ADI filters use a full-wave spacer layer rather than a half-wave spacer. This also tends to reduce slightly the angular sensitivity of the filter.

Filter in Parallel Light at Oblique Incidence

To obtain the behavior of a filter in light incident at an angle, a simple problem of transmission through a parallel plate will be considered (figure 4.3-16).

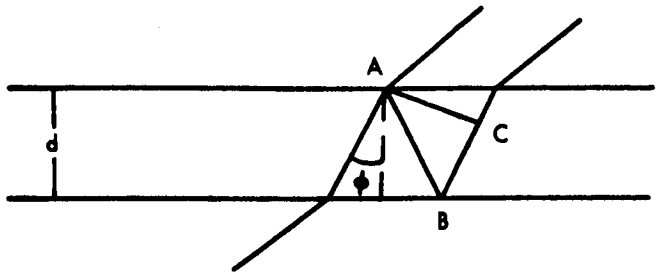

Figure 4.3-16. Transmission Through a Parallel Plate

If the light travels at an angle ϕ inside the plate, the maximum transmission occurs when the contributions from all internally reflected waves add in phase in medium 2. The difference in phase between two wavelets is given by

$$AB + BC - 2nd \cos \phi = \lambda_\phi \quad , \tag{33}$$

which must equal a full wavelength at the peak transmission. Now at normal incidence

$$AB + BC = 2nd = \lambda_o \quad .$$

Therefore, the peak wavelength λ_ϕ is given by

$$\lambda_\phi = \lambda_o \cos \phi \quad . \tag{34}$$

For a plate we can write ϕ as a function of the angle of incidence by Snell's law

$$n \sin \phi = n_{air} \sin \theta \quad ,$$

$$\frac{\lambda_\phi}{\lambda_o} = \sqrt{1 - \left(\frac{n_{air}}{n} \sin \theta\right)^2} \simeq 1 - \frac{1}{2}\left(\frac{n_{air}}{n} \sin \theta\right)^2 \quad , \tag{35}$$

or

$$\frac{\Delta\lambda_\phi}{\lambda_o} = -\frac{1}{2}\left(\frac{\theta}{n}\right)^2 \quad ,$$

for small angles of incidence.

Thus for light incident at an oblique angle, the peak transmission is shifted towards shorter wavelengths; the shift is smaller the higher the refractive index n.

We conclude that to operate a filter in oblique light with maximum transmission, the filter must be designed to peak at normal incidence at a higher wavelength as given by Eq. (35).

For multilayer dielectric filters, one can still use an expression similar to Eq. (35) if one defines an equivalent refractive index, which depends on the number of layers and the type of spacer used, n_H^* or n_L^* and which accounts also for the phase variation in the reflection coefficients.

An analysis along these lines has been carried out by Smith[19], and his results are for filters with a high index spacer

$$\left(n_H^*\right)^2 \approx \frac{n_H^2}{n_r} \qquad \text{where } n_r = \frac{n_H}{n_L} \tag{36}$$

for filters with a low index spacer

$$\left(n_L^*\right)^2 \approx n_L^2 \Big/ \left(1 - \frac{1}{n_r} + \frac{1}{n_r^2}\right) . \tag{37}$$

For zinc-cryolite filters we have

$$n_H^* \approx 1.78 \text{ and } n_L^* \approx 1.52 .$$

Thus, in general, $n_H^* > n_L^*$, which means that filters with high index spacers are less sensitive to angle variations. The above results hold for $n_r^x > 15$ where x is the number of layers. For zinc sulfide, the cryolite filters $x_{min} = 5$, a condition satisfied by all narrow band filters. The analysis confirms a well known experimental fact that filters with a high index spacer always have an effective index lower than the spacer index, and vice-versa, for low index spacers.

Filters in Convergent Light

When convergent light is incident on an interference filter (figure 4.3-17), the effective transmission coefficient can be found by integrating the contributions from all rays forming the cone of the semi-angle α.

(19) C. R. Pidgeon and S. D. Smith, "Resolving Power of Multi-Layer Filters in Nonparallel Light," JOSA, Vol. 54, No. 12, December 1964, pp. 1459-1466.

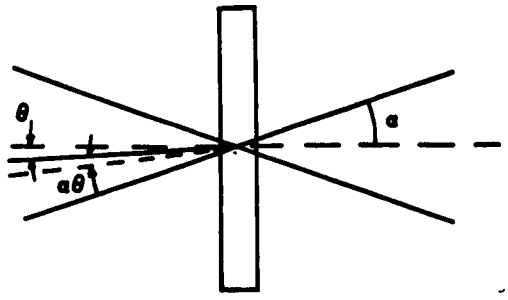

Figure 4.3-17. Filter in Convergent Light

The transmission is given (neglecting the phase variations) by

$$\tau_{\theta,\,\lambda} = \frac{\tau_{max}}{1 + F \sin^2\left(\frac{2\pi nd}{\lambda} \cos \phi\right)}$$

for a ray incident at an angle θ and traveling at angle ϕ in the spacer. The effective transmission is then

$$\frac{T}{\tau_{max}} = \frac{\int_0^{\alpha} \frac{\sin \theta d\theta}{1 + F \sin^2\left(\frac{2\pi nd}{\lambda} \cos \phi\right)}}{\int_0^{\alpha} \sin \theta d\theta} \quad . \tag{38}$$

The purpose of our analysis is to obtain the wavelength λ_o at which the filter must peak in parallel light at normal incidence in order to obtain maximum transmission in convergent light of wavelength λ and angle α.

We note that for small angles θ,

$$\cos \phi = \sqrt{1 - \left(\frac{n}{n^*} \sin \theta\right)^2} = 1 - \frac{1}{2}\left(\frac{n}{n^*}\right)^2 \sin^2 \theta \quad , \tag{39}$$

and also $\cos \theta \simeq 1$ up to angles of $\theta = 5^o$. This enables us to write Eq. (38) in the form

$$\frac{T}{\tau_{max}} = \frac{\int_0^{\alpha} \frac{\sin \theta \cos \theta \, d\theta}{1 + F \sin^2 \frac{\pi \lambda_o}{\lambda}\left[1 - \frac{1}{2}\left(\frac{n}{n^*} \sin \theta\right)^2\right]}}{\int_0^{\alpha} \sin \theta \, d\theta} \quad . \tag{40}$$

Let

$$\frac{\pi\lambda_o}{\lambda}\left[1 - \frac{1}{2}\left(\frac{n}{n^*}\sin\theta\right)^2\right] = v$$

$$v_1 = \frac{\pi\lambda_o}{\lambda}\ ;\ v_2 = \frac{\pi\lambda_o}{\lambda}\left[1 - \frac{1}{2}\left(\frac{n}{n^*}\sin\theta\right)^2\right]\ .$$

With these substitutions the integral in Eq. (40) becomes

$$\frac{T}{\tau_{max}} \geq \left(\frac{n^*}{n}\right)\frac{\lambda}{2\lambda_o\pi\sin^2\frac{\alpha}{2}}\int_{\frac{\pi\lambda_o}{\lambda}}^{\frac{\pi\lambda_o}{\lambda}\left[1-\frac{1}{2}\left(\frac{n}{n^*}\right)^2\sin^2\alpha\right]}\frac{dv}{1 + F\sin^2 v}\ . \tag{41}$$

The integral in Eq. (41) can be integrated by further substitution

$$\tan v = t \qquad \sin v = \frac{t}{\sqrt{1+t^2}} \qquad dv = \frac{dt}{1+t^2}$$

$$\frac{T}{\tau_{max}} \geq \frac{\frac{1}{\pi}\left(\frac{n^*}{n}\right)^2\frac{\lambda}{\lambda_o}}{2\sin^2\frac{\alpha}{2}}\left\{\frac{\tan^{-1}\left(\sqrt{1+F}\tan\frac{\pi\lambda_o}{\lambda}\right) - \tan^{-1}\left(\sqrt{1+F}\tan\frac{\pi\lambda_o}{\lambda}\left(1-\frac{1}{2}\left(\frac{n}{n^*}\right)^2\sin^2\alpha\right)\right)}{\sqrt{1+F}}\right\}. \tag{42}$$

To simplify Eq. (42), we rewrite everything in terms of the angle ϕ_{max}, which corresponds to α, as

$$\frac{T}{\tau_{max}} \geq \frac{1}{\pi}\ \frac{\lambda_o}{\lambda}\frac{\cos^2\frac{\alpha}{2}}{1-\cos\phi_{max}}\frac{\tan^{-1}\left(\sqrt{1+F}\tan\frac{\pi\lambda_o}{\lambda}\right) - \tan^{-1}\left(\sqrt{1+F}\tan\frac{\pi\lambda_o}{\lambda}\cos\phi_{max}\right)}{\sqrt{1+F}}\ . \tag{43}$$

We wish now to maximize the expression Eq. (43), and find a relation between α and $\frac{\lambda_o}{\lambda}$.

We now use the trigonometric identify

$$\tan (u-v) = \frac{\tan u - \tan v}{1 + \tan u \tan v} \text{ or } u - v = \tan^{-1} \frac{\tan u - \tan v}{1 + \tan u \tan v}$$

to transform Eq. (43) into

$$\frac{T}{\tau_{max}} = \frac{1}{\pi} \frac{\lambda_o}{\lambda} \frac{1}{\sqrt{1+F}} \frac{\cos^2 \frac{\alpha}{2}}{1 - \cos \phi_{max}} \left\{ \tan^{-1} \frac{\sqrt{1+F} \left(\tan \frac{\pi\lambda_o}{\lambda} - \tan \frac{\pi\lambda_o}{\lambda} \cos \phi_{max} \right)}{1 + (1+F) \tan \frac{\pi\lambda_o}{\lambda} \tan \frac{\pi\lambda_o}{\lambda} \cos \phi_{max}} \right\} . \quad (44)$$

To maximize Eq. (44) with respect to $\frac{\lambda_o}{\lambda}$ we anticipate the fact that $\frac{\lambda_o}{\lambda} \approx 1$.
Therefore we will only take a derivative with respect to the second term in Eq. (44).

$$\frac{\partial \left(\frac{T}{\tau_{max}} \right)}{\partial \left(\frac{\lambda_o}{\lambda} \right)} = \frac{\partial}{\partial \frac{\lambda_o}{\lambda}} \left[\frac{\tan \frac{\pi\lambda_o}{\lambda} - \tan \frac{\pi\lambda_o}{\lambda} \cos \phi_{max}}{1 + (1+F) \tan \frac{\pi\lambda_o}{\lambda} \tan \frac{\pi\lambda_o}{\lambda} \cos \phi_{max}} \right] = 0 . \quad (45)$$

Taking derivatives we obtain

$$\frac{\frac{\pi}{\cos^2 \frac{\pi\lambda_o}{\lambda}} - \frac{\pi \cos \phi_{max}}{\cos^2 \frac{\pi\lambda_o}{\lambda} \cos^2 \frac{\pi\lambda_o}{\lambda} \cos \phi_{max}}}{1 + (1+F) \tan \frac{\pi\lambda_o}{\lambda} \tan \frac{\pi\lambda_o}{\lambda} \cos \phi_{max}}$$

$$- \frac{\pi (1+F) \left(\tan \frac{\pi\lambda_o}{\lambda} - \tan \frac{\pi\lambda_o}{\lambda} \cos \phi_{max} \right) \left(\frac{\tan \frac{\pi\lambda_o}{\lambda} \cos \phi_{max}}{\cos \frac{\pi\lambda_o}{\lambda}} - \frac{\cos \phi_{max} \tan \frac{\lambda_o}{\lambda}}{\cos^2 \frac{\pi\lambda_o}{\lambda} \cos \phi_{max}} \right)}{\left[1 + (1+F) \tan \frac{\pi\lambda_o}{\lambda} \tan \frac{\pi\lambda_o}{\lambda} \cos \phi_{max} \right]^2} = 0 . \quad (46)$$

Simplifying Eq. (46), we obtain:

$$\frac{1}{1 + F \sin^2 \frac{\pi\lambda_o}{\lambda}} = \frac{\cos \phi_{max}}{1 + F \sin^2 \left(\frac{\pi\lambda_o}{\lambda} \cos \phi_{max} \right)} \tag{47}$$

as the maximum transmission condition. The condition in Eq. (47) can be interpreted easily if we recall that

$$T_{o,\lambda} = \frac{1}{1 + F \sin^2 \frac{\pi\lambda_o}{\lambda}} \quad \text{and} \quad T_{\substack{\phi,\lambda \\ max}} = \frac{1}{1 + F \sin^2 \frac{\pi\lambda_o}{\lambda} \cos \phi_{max}}$$

are the transmissions at normal incidence and maximum angle ϕ_{max} respectively. Eq. (47) then becomes:

$$T_{o,\lambda} = \cos \phi_{max} \, T_{\substack{\phi,\lambda \\ max}} \quad . \tag{48}$$

Thus the filter peak frequency λ_o must be chosen such that the transmission at the maximum incidence ϕ_{max} must exceed the transmission at normal incidence by a factor $\frac{1}{\cos \phi_{max}}$.

Frequency Shift

A more explicit relation between $\frac{\lambda_o}{\lambda}$ and ϕ will now be obtained. We use the notation $\frac{\lambda_o}{\lambda} = 1 + \frac{\delta\lambda}{\lambda}$, and the series expansions

$$\cos \phi \approx 1 - \frac{\phi^2}{2} \, , \quad \sin^2 \frac{\pi\lambda_o}{\lambda} \approx \left(\pi \frac{\delta\lambda}{\lambda} \right)^2 \, ,$$

with the above Eq. (47) to obtain:

$$\frac{1}{1 + F\pi^2 \left(\frac{\delta\lambda}{\lambda} \right)^2} = \frac{1 - \frac{\phi^2}{2}}{1 + F\pi^2 \left(\frac{d\lambda}{\lambda} - \frac{\phi^2}{2} \right)^2} \quad . \tag{49}$$

Multiplying out in Eq. (49), we obtain

$$\frac{\delta\lambda}{\lambda} = \frac{\phi^2}{4} \, , \tag{50}$$

or recalling that $\cos \phi = 1 - \frac{1}{2}\left(\frac{\sin}{n^*}\right)^2 = 1 - \frac{\phi^2}{2}$,

we have

$$\frac{\delta\lambda}{\lambda} = \frac{1}{4}\left(\frac{\alpha}{n^*}\right)^2 . \tag{51}$$

Eq. (51) is accurate only for angles less than 5^o under which assumptions it was derived. It is seen by comparing Eq. (35) with Eq. (51) that the necessary wavelength shift in convergent light is half the shift in collimated light incident obliquely at the cone semi-angle α.

Transmission

We can now compute the maximum transmission in convergent light. At a maximum we have by Eq. (50).

$$\frac{\lambda_o}{\lambda} = 1 + \frac{\delta\lambda}{\lambda} = 1 + \frac{\phi^2}{4}$$

Therefore in relation in Eq. (44) we have

$$\tan \frac{\pi\lambda_o}{\lambda} = \tan \frac{\pi^2_\phi}{4} \approx \frac{\pi^2_\phi}{4}$$

$$\tan \frac{\pi\lambda_o}{\lambda} \cos \phi = \tan \pi \left(1 + \frac{\phi^2}{4}\right)\left(1 - \frac{\phi^2}{2}\right) = \tan \pi \left(1 - \frac{\phi^2}{4}\right) \approx - \frac{\phi^2}{4}$$

Therefore

$$\frac{T_{max}}{max} = \frac{1}{\pi}\frac{\lambda_o}{\lambda} \frac{1}{\sqrt{1 + F}} \frac{\cos^2 \frac{\alpha}{2}}{1 - \cos \phi_{max}} \tan^{-1} \left\{ \frac{1 + F \frac{2\pi\phi^2}{4}}{1 - (1+F)\left(\frac{\pi\phi^2}{4}\right)^2} \right\} \tag{52}$$

Now $\sqrt{1 + F} \approx \sqrt{F} = \frac{2}{\pi} \frac{\lambda}{\Delta\lambda}$ for large F (narrow band filters).

Let

$$\sqrt{F} \frac{\pi\phi^2}{4} = \frac{\lambda}{\Delta\lambda} \frac{\phi^2}{2} = \tan v,$$

$$\tan^{-1}\left\{\frac{\sqrt{1+F} \quad \frac{2\pi\phi^2}{4}}{1 - (1+F)\left(\frac{\pi\phi^2}{4}\right)^2}\right\} = 2v = 2 \tan^{-1} \frac{\lambda}{\Delta\lambda} \frac{\phi^2}{2} \quad .$$

Finally we obtain:

$$\frac{T_{max}}{\tau_{max}} = \frac{1}{\frac{\lambda}{\Delta\lambda} \frac{\phi^2}{2}} \tan^{-1} \frac{\lambda}{\Delta\lambda} \frac{\phi^2}{2} \quad . \tag{53}$$

From Eq. (53), we can compute the maximum transmission of a filter in convergent light as a function of cone angle. For example, let $n^* = n_L \, n_H = 1.35 \times 2.35 \approx 1.8$ for a (ZnS), and a Cryolite filter with a ZnS spacer. We obtain at $\alpha = 0.1$ and $\frac{\Delta\lambda}{\lambda} = 0.002$ from Eq. (53).

$$\frac{T_{max}}{\tau_{max}} = \frac{\tan^{-1} 0.77}{0.77} = 0.85 \quad .$$

Thus, there is relatively little deterioration in transmission as compared to normally incident light if the filter is properly offset.

In figure 4.3-18 we have plotted Eq. (53) in terms of the dimensionless quantity

$$x = \frac{\phi^2_{max}}{2 \frac{\Delta\lambda}{\lambda}} = \frac{1}{2} \left(\frac{\alpha}{n^*}\right)^2 \Big/ \frac{\Delta\lambda}{\lambda} \quad .$$

From that graph, one can determine the transmission of a filter of bandwidth $\frac{\Delta\lambda}{\lambda}$ in convergent light of angle α; or, vice-versa, given a transmission coefficient, the maximum tolerable cone angle can be determined.

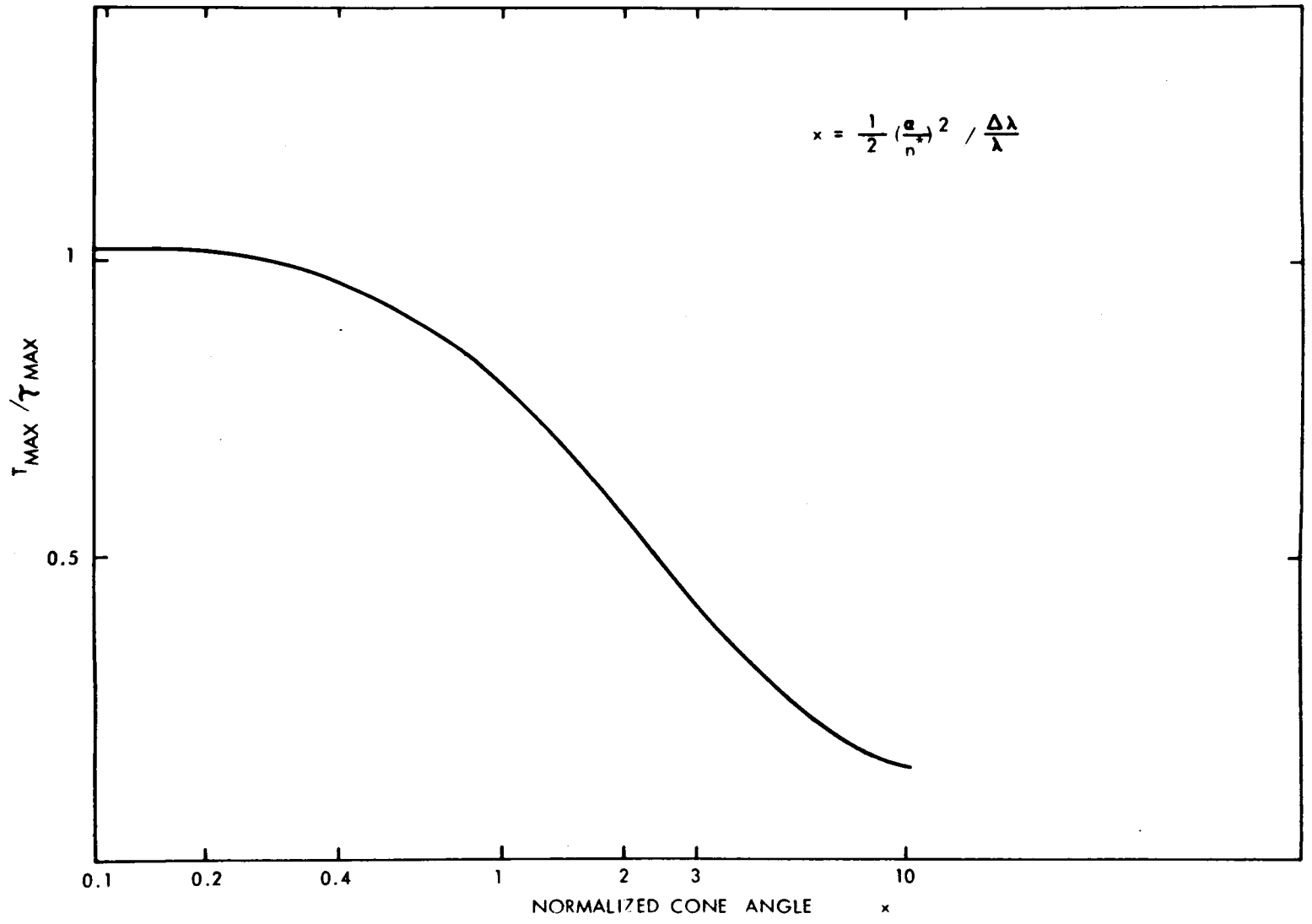

Figure 4.3-18. Maximum Transmission vs. Normalized Angle of Convergent Light.

Bandwidth Broadening

Finally we wish to calculate the bandwidth of the filter in convergent light, that is we wish to find the points at which $T = \frac{1}{2} T_{max}$. For large F we can write the condition from Eq. (44) and Eq. (53) as

$$\frac{1}{2} \frac{1}{\frac{\lambda}{\Delta\lambda} \frac{\phi^2}{2}} \tan^{-1} \frac{\lambda}{\Delta\lambda} \frac{\phi^2}{2} = \frac{1}{\frac{\lambda}{\Delta\lambda} \phi^2} \tan^{-1} \frac{\sqrt{F}\left(\tan \frac{\pi\lambda_o}{\lambda} - \tan \frac{\pi\lambda_o}{\lambda} \cos \phi\right)}{1 + F \tan \frac{\pi\lambda_o}{\lambda} \tan \frac{\pi\lambda_o}{\lambda} \cos \phi} , \tag{54}$$

or

$$\frac{\lambda}{\Delta\lambda} \frac{\phi^2}{2} = \sqrt{F} \frac{\tan \frac{\pi\lambda_o}{\lambda} - \tan \frac{\pi\lambda_o}{\lambda} \cos \phi}{1 + F \tan \frac{\pi\lambda_o}{\lambda} \tan \frac{\pi\lambda_o}{\lambda} \cos \phi} . \tag{55}$$

Let

$$\lambda_1 = \lambda_2 + \Delta\lambda_1$$

$$\lambda_2 = \lambda_o + \Delta\lambda_2$$

be the wavelengths at half power transmission. The bandwidth of the filter in convergent light is

$$\Delta\lambda_a = \left|\Delta\lambda_1 - \Delta\lambda_2\right| .$$

Now

$$\tan \frac{\pi\lambda_o}{\lambda} - \tan \frac{\pi\lambda_o}{\lambda} \cos \phi = \tan \pi \frac{\Delta\lambda_{1,2}}{\lambda} - \tan \pi \left(1 + \frac{\Delta\lambda_{1,2}}{\lambda}\right)\left(1 - \frac{\phi^2}{2}\right) \approx \frac{\pi\phi^2}{2} .$$

Also

$$F = \frac{4}{\pi 2}\left(\frac{\lambda}{\Delta\lambda}\right)^2 \quad \text{for a half-wave spacer .}$$

Therefore, Eq. (55) becomes

$$1 + F \tan \frac{\pi\lambda_o}{\lambda} \tan \frac{\pi\lambda_o}{\lambda} \cos \phi = 2 \ , \tag{56}$$

or

$$\left(\pi \frac{\Delta\pi_{1,2}}{\lambda}\right)\left[\pi\left(\frac{\Delta\lambda_{1,2}}{\lambda} - \frac{\phi^2}{2}\right)\right] = \frac{\pi^2}{4}\left(\frac{\Delta\lambda}{\lambda}\right)^2 \ . \tag{57}$$

We are interested only in the difference $\left|\Delta\lambda_1 - \Delta\lambda_2\right|$ which is given from Eq. (57) by

$$\left(\frac{\Delta\lambda_a}{\lambda}\right)^2 = \left(\frac{\phi^2}{2}\right)^2 + \left(\frac{\Delta\lambda}{\lambda}\right)^2 \ . \tag{58}$$

The broadening of the filter is a function of both cone angle and filter bandwidth as can be seen from Eq. (58)

$$B = \frac{\frac{\Delta\lambda_a}{\lambda}}{\frac{\Delta\lambda}{\lambda}} = \sqrt{1 + \left(\frac{\lambda}{\Delta\lambda}\frac{\phi^2}{2}\right)^2} \tag{59}$$

For the filter with $\alpha = 0.1$,

$$\frac{\Delta\lambda}{\lambda} = 0.002$$

$$n^* = 1.8 \ .$$

We have

$$B = \sqrt{1 + \left(\frac{0.01}{1.82} \times \frac{1}{0.002 \times 2}\right)^2} = 1.26 \ .$$

We note that the broadening of the filter B can be written in terms of the dimensionless quantity x:

$$B = \sqrt{1 + x^2} \ . \tag{60}$$

The deterioration in signal-to-noise ratio in an incoherent detector in convergent light as compared with the same detector in parallel light is given by

$$D = \frac{\frac{T_{max}}{\tau_{max}}}{\sqrt{B}} = \frac{\tan^{-1} x}{x^4 \sqrt{1 + x^2}} \qquad (61)$$

For example, if one tolerates a factor D = 0.46, one obtains x = 2, which corresponds to $\alpha_{max} = 6^{\circ}$ for a filter with $n^* = 1.8$. Eq. (61) is plotted in figure 4.3-19.

The above calculations are based on a half-wave spacer; however, Lissberger[20] has shown that the angular sensitivity decreases as the order of the spacer layer is increased. In fact, for a very large order layer, the effective index of refraction n^* simply becomes the index of refraction of that layer itself, which, for a high index spacer, is larger than n^*. $\left(n_H > n_H^*\right)$.

Temperature Dependence of ADI Filters

Little has been published about the temperature dependence of interference filters. Basically the peak wavelength of a filter shifts with increase in temperature towards longer wavelengths. This is due to two factors:

a. Thermal expansion of the reflecting layers and spacer layer

b. Change of index of refraction with temperature.

From one manufacturer's data (Thin Films Products Company, Cambridge, Mass.) a filter centered at 0.6328 microns exhibits a shift of about 2.5×10^{-5} micron/$^{\circ}$C. Thus temperature stabilization is very important in narrow-band filters. Temperature-tuned filters are possible, although the range of tuning is rather limited.

Mica Interference Filters

It has been noted in connection with Eq. (32) that the bandwidth of an interference filter can be reduced by using a thick spacer layer. The mica interference filter[21] makes use of this property, and has as spacer a mica sheet several hundred wavelengths thick on which the dielectric layers are deposited. Such a filter combines narrow bandwidth with high transmission which is generally impossible to obtain in ordinary multilayer dielectric filters. Mica filters with a bandwidth of 0.0002 micron in the visible range and transmission as high as 50 - 60 percent have been reported.[22]

---

(20) P. H. Lissberger, "Properties of All-Dielectric Interference Filters, I. A New Method of Calculation,"

P. H. Lissberger and W. L. Wilcock, II. "Filters in Parallel Beams of Light Incident Obliquely and in Convergent Beams," both in JOSA, February 1959, Vol. 49, No. 2, pp. 212-230.

(21) J. A. Dombrowolski, "Mica Interference Filters with Transmission Bands of Very Narrow Half-Widths," JOSA, August 1959, Vol. 49, pp. 794-806.

(22) "Design and Fabrication of Optical Filters for Laser Frequencies," Technical Documentary Report No. AFAL-TR-64-26, October 1964, Spectra-Lab Sylmar, California.

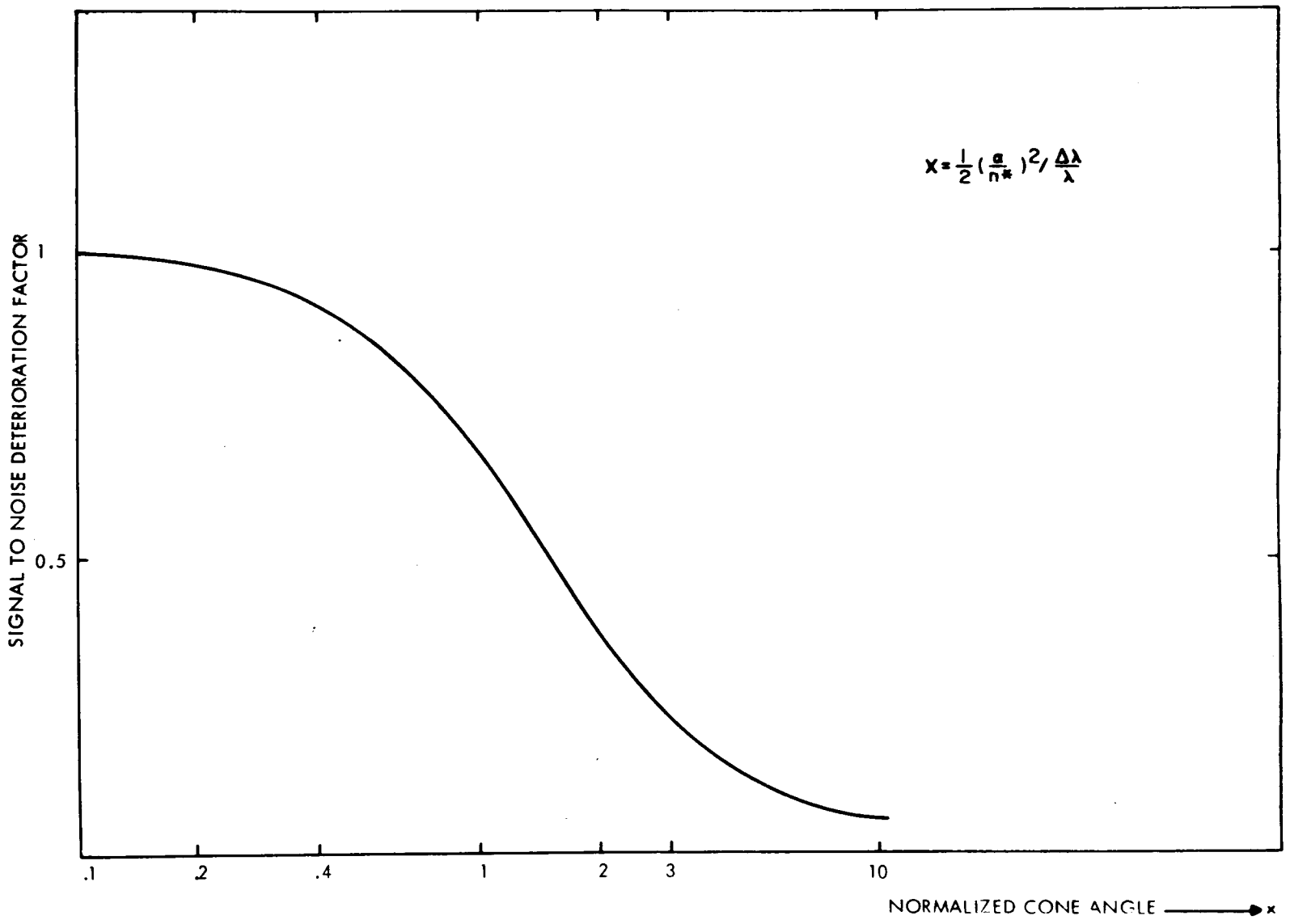

Figure 4.3-19. Signal-To-Noise Deterioration vs. Normalized Angle of Convergent Light.

The transmission of the filter is given by the Airy formula Eq. (28)

$$\tau(\omega) = \tau_o(\omega) \frac{1}{1 + F(\omega) \sin^2 \frac{\theta}{2}(\omega)} .$$

At normal incidence, neglecting phase changes upon reflection we have at peak transmission,

$$\frac{\theta}{2} = \frac{2\pi nd}{\lambda} = p\pi \quad , \quad \text{where p is an integer}$$

or

$$nd = \frac{p\lambda}{2} .$$

Thus the filter will peak at wavelengths given by

$$P_1 \frac{\lambda_1}{2} = \frac{P_2\lambda_2}{2} = nd .$$

The separation between adjacent peaks is found by making

$$P_2 = P_1 + 1$$

$$\lambda_2 = \lambda_1 - \Delta\lambda$$

$$P_1\lambda_1 = (P_1 + 1)(\lambda_1 - \Delta\lambda)$$

or

$$\Delta\lambda = \frac{\lambda_1}{P_1 + 1} \approx \frac{\lambda_1}{P_1} , \quad \text{for p very large .}$$

Thus adjacent transmission peaks are quite closely spaced and auxiliary filters must be used to eliminate unwanted wavelengths. However, these filters can be made much wider than the mica filter and affect but little the overall transmission characteristic.

Mica presents some additional problems because it is birefringent. Thus different transmission peaks occur for the two polarizations of light. The problem can be overcome by making the mica spacer layer to act as a half-wave plate; then, by additional coating with a material with the same index of refraction as mica, the thickness is adjusted to an integral number of half-wavelengths.

Mica filters are somewhat less temperature sensitive than ordinary ADI filters. Shifts of about 5×10^{-6} micron/^{o}C have been measured.[22] For narrow band applications such a variation might still prove to be too large, making necessary temperature stabilization.

At the present, mica interference filters are not available commercially, but are undergoing extensive development work in view of their application to future laser systems.

4.3.6 Required Technology Development

4.3.6.1 Large Aperture Direct Detection Receiver

The technological advance required to implement a direct detection system is the development of the large aperture, segmented, moderate quality telescope. The initial study of this receiver telescope is presented in section 4.3.5.2. Further ray-tracing analysis can produce the design requirements that will define the optics supporting structure and servo controlled mount. In addition, the secondary optics, filter, and other receiver components must be integrated with the large collecting aperture.

An artist's concept and a schematic of the receiver is shown in figure 4.3-1. The required technological development can be achieved by first constructing a prototype model of a scaled-down receiver. This prototype would prove feasibility, provide test data, and thus ensure that the later full-scale receiver would perform according to the direct detection system requirements. The program recommended is:

a. Prototype Model of Direct Detection Receiver (Estimated cost - $300,000; estimated time - 2 years).

   (1) Design and construct a 3 meter diameter optical collector with a 0.5 milliradian or less field of view.

   (2) The collector should be installed on a servo controlled mount capable of tracking a laser source to less than one-half the field of view at a nominal angular rate of 4 milliradians/sec. This will provide a means for evaluation tests to be conducted using air vehicles or possibly spacecraft piggy-back experiments performed under the Apollo Applications Program.

   (3) Design, construct, and install the remaining direct detection system elements including:

      (a) secondary optics
      (b) narrow-band interference filters
      (c) optical demodulators,
      (d) photodetectors, and
      (e) associated electronics.

   (4) Design and construct an auxiliary optical angle error sensing system to be mounted on the large receiver capable of providing the tracking error input to the servo-controlled mount.

   (5) Provide an auxiliary manual control system and sighting telescope, coupled to the mount servo, to provide a means of acquiring the remote laser transmitter.

   (6) Provide an auxiliary pointing and tracking data input to provide either radar control or computer program control of the system.

   (7) Conduct air-to-ground tests to show feasibility, and to develop design parameters for a full scale OTAES model.

b. Full Scale Direct Detection Receiver (Estimated cost $1,500,000; estimated time 2 years)

Design and construct 8-meter direct detection receiver based upon prototype tests and experience. Install receiver at predetermined NASA-OTAES ground station site.

c. Data Recording, Display and Reduction System (Estimated cost $600,000; estimated time 2 years)

(1) Design and construct display and recording facilities for direct detection experiment and other atmospheric experiments performed with direct system.

(2) Design and construct real data processing equipment to provide signal fading information for experiment control.

(3) Integrate data system with other OTAES experiment data and control systems.

4.3.6.2 Modulation Systems

The recommended programs are:

a. Development of Space-Qualified 0.6328 Micron Modulator (Estimated Cost $200,000; estimated time 2 years)

(1) Develop and deliver two space-qualified service test models of a 0.6328-micron modulator and solid-state driver with 100-MHz video bandwidth developing 100 percent modulation with 10 watts signal power. This development should be based on the recently developed laboratory models of this system.

(2) Conduct a thorough trade-off analysis of the several electro-optic crystal materials available as to their applicability to the OTAES space requirements. Two very important characteristics to be included in this analysis are (1) crystal optical damageability and (2) optical surface quality characteristics and their retention.

(3) Emphasis will be placed upon the transmittance characteristics of the optical components in the modulator as well as optimizing the anti-reflection coating techniques to minimize internal heating. This is a critical design consideration for the modulators that will be eventually used under the high optical power conditions of planetary communications.

(4) A specific design feature of the modulators supplied will be an optimized thermal design. Transverse and longitudinal temperature gradients in the crystal will be minimized to meet the requirements of the space environment. The methods used to minimize the thermal birefringence of these modulators is to be applicable to the design of those used for planetary communications.

(5) The impact upon the modulator design and the crystal characteristics (conductivity, tan δ, dielectric breakdown, etc.) will be reviewed and summarized for various communication modulation formats (FM, FM-subcarrier, pulsed intensity modulation, pulsed polarization modulation, etc.)

(6) The mechanical design will emphasize: (1) launch survival and (2) alignment retention in the space environment. Deflection and decollimation of the output beam shall be as small as possible.

(7) As a specific output of this program, the phase distortion of the emergent beam will be measured across its diameter.

b. Development of 10.6-micron Modulators (Estimated Cost $300,000 for two phases: Phase I - Laboratory Model(s), Phase II - Space-Qualified Model(s); estimated time 2.5 years)

(1) Under Phase I, design/deliver laboratory modulators and associated solid-state drive amplifiers to operate at 10.6 microns, and demonstrate a video bandwidth capability of 100 MHz. A particular goal of this development will be trade-off analysis of the several electro-optic materials in a planetary communication context. Characteristics of the materials used become extremely important in light of the large optical power levels anticipated for this device. The more important characteristics include: conductivity, thermally induced birefringence, transmittance, and optical surface qualities and coatings and their retention characteristics. The modulator will be capable of demonstrating 100 percent modulation with minimum drive power.

(2) Under Phase II, design and deliver service test models of space-qualified 10.6-micron modulators and their associated solid-state drivers. This program is to be based upon the work in Phase I, hence will be initiated subsequent to satisfactory completion of Phase I.

4.4 COMMUNICATION WITH 10 MEGAHERTZ BANDWIDTH

4.4.1 Summary

The rapidly increasing data gathering capabilities of deep space probes have made necessary the development of techniques for transmitting data at maximum rates using a minimum of spacecraft power. The rate at which data can be transmitted varies directly as the bandwidth of the communication channel. Optical communication, using wide bandwidth modulation and detection techniques, offers a potential solution for this need. Very narrow beamwidths are obtainable at optical wavelengths using nominal apertures, providing high energy density in the beam for reasonable amounts of transmitted power. The high energy density will support wide bandwidth communication with high signal-to-noise ratio.

Performance of wide bandwidth optical communication systems can be analytically determined by making assumptions about the propagation path and assuming mathematically ideal system components. However, it can be expected that a communication system placed in orbit will depart from this mathematical ideal. Determination of the effect of these departures on system performance can only be measured by placing them in the orbital environment. Because the atmosphere is neither homogeneous nor isotropic, and because the applicable theory is not developed for the general case, it is necessary that the measurements be made along actual transmission paths through the entire atmosphere. The few measurements made to date have been over relatively short, nearly horizontal paths which cannot be considered representative of an actual space-to-ground transmission path. Present knowledge of the atmosphere does not permit accurate estimates to be extrapolated from measurements made along these horizontal paths. This can only be accomplished from an orbiting satellite (figure 4.4-1). Variations of the atmosphere and its effect on the system bandwidth performance must be measured over a long time period to obtain statistical data. These measurements will be made simultaneously at different wavelengths. Different forms of modulation with several types of signals will be used. The atmospheric characteristics at several altitudes will be recorded during the measuring period for correlation with the communication data.

Much of the hardware needed for these tests has been developed as laboratory or industrial equipment, but no major items have been space qualified. Wide bandwidth modulators and detectors operating at the 10.6-micron wavelength must be developed; and all equipment will have to be designed and built for space application.

4.4.2 Experiment Objective

This experiment will gather engineering data on alternative optical communication system forms having bandwidths of 10 MHz using several types of modulation on the transmitted laser beams. Measurements will be made to determine the signal-to-noise ratio and data error rates as functions of types of modulation and atmospheric conditions. This information will be compared to the theoretically determined values. Deviations will be analyzed to determine reasons for their occurrence and to predict performance of operational systems. Engineering performance data will be developed for key system components in a variety of simulated operational environments.

4.4.3 Experiment Justification

4.4.3.1 Contribution and Need

All deep space probes, present and planned, have a very limited communication rate. For example, Mariner 2 provided communication at 33-1/3 bits per second for the first part of the mission and then switched to 8-1/2 bits per second during its encounter with Venus. Similarly, Mariner 4 also required a reduction in bit-rate transmission when it was

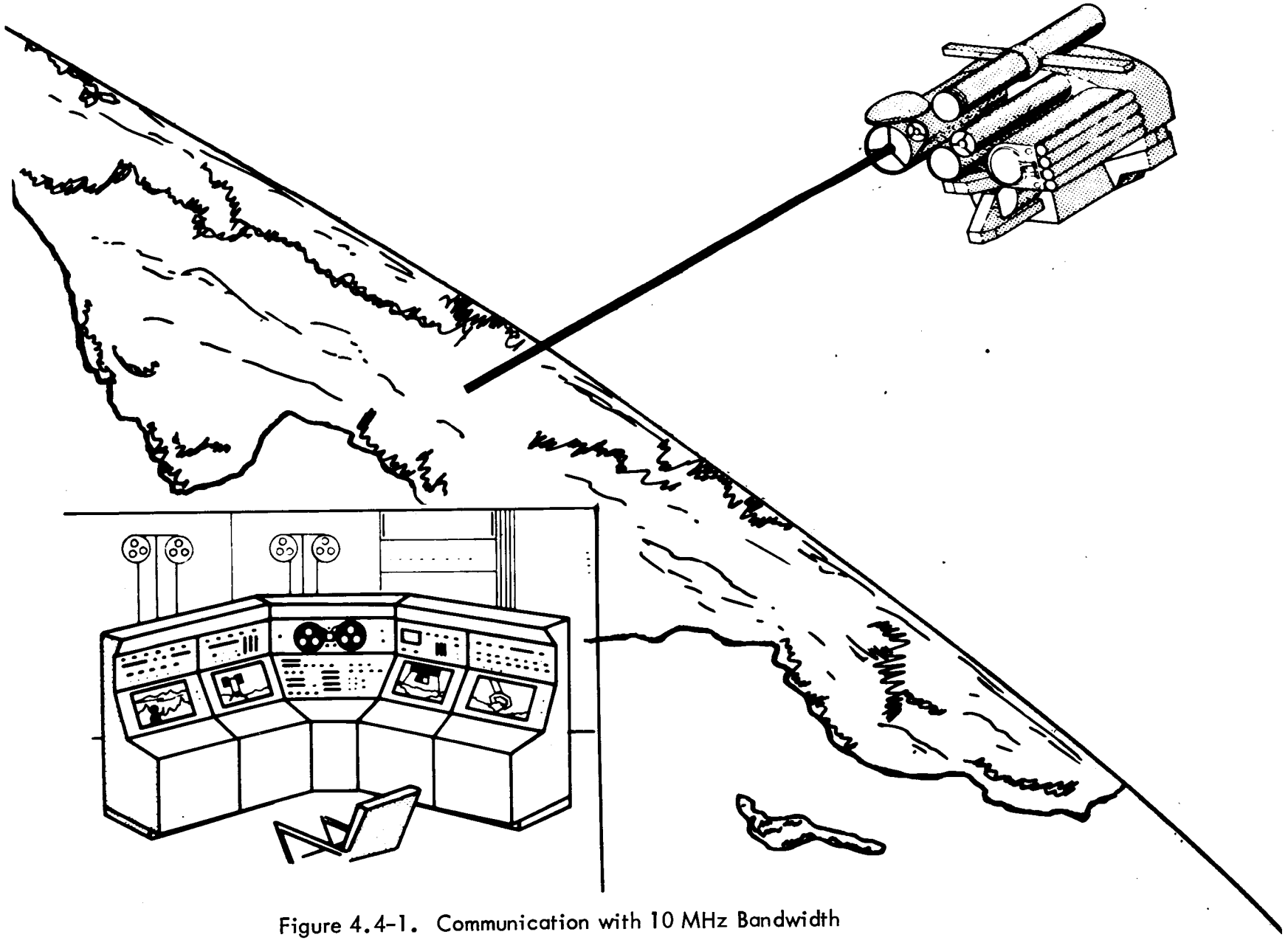

Figure 4.4-1. Communication with 10 MHz Bandwidth

approximately 35 x 10^6 kilometers from the Earth. In his congressional testimony, Newell[1] pointed out that approval of the Voyager program had to be delayed until a minimum communication capability of 8000 bits per second could be assured. The data error rates associated with these bit rates are of the order of 5 x 10^{-3}. Reduced error rates can be obtained at the expense of bandwidth. Conversely, increased bandwidth can be obtained at the cost of greater error rates. It has been estimated by Kelley[2] that in the 1970-71 period, data needs for exploration of the near planets will require 10^7 bits per second system capacity.

The energy density in the beam is controlled not only by available spacecraft power but also by the beam-forming capability of the radiating aperture and the energy conversion efficiency of the transmitter. Space probes are presently communicating at radio frequencies, and the beam-forming capabilities of the maximum apertures available at these wavelengths are relatively poor in comparison to the narrow beams and corresponding higher energy density obtainable at optical wavelengths. Pointing requirements are a direct function of beamwidth. Trade-offs can be made of transmitter efficiency, energy density, pointing requirements, aperture size, and wavelength to optimize optical communication system performance for a given spacecraft prime power.

Various combinational modulation forms have been used at radio frequencies to optimize satellite system performance for its analog and digital communication needs. Future space missions using optical communications will also have special characteristics, requiring a particular modulation form to optimize the performance for each mission. Development of performance data for the various optical modulation methods will provide communication system engineers a basis for optimizing the modulation form for each mission.

If it can be proven that an optical communication system can provide 10 MHz bandwidths at planetary ranges, the system performance of future space probes can be greatly enhanced.

4.4.3.2 Need for Space Testing

The success of the United States space program (over 90 percent in spacecraft launches) has been attributed to a careful evolution of equipment designs. Key elements in the present Ranger and Surveyor vehicles have been developed from prototype test data obtained on earlier flights. Development of wide bandwidth communication systems for deep space missions should follow a similar pattern, obtaining a broad range of data on all characteristics and components of potential systems. Using these data, system designers will then be able to select and optimize for particular applications.

The bandwidth performance of an optical communication system is determined from evaluation of the following equations:

$$\frac{S}{N} \times \Delta f = \frac{\eta_q}{4h\nu}\left(\frac{P_s^2}{P_s + P_b}\right)$$

(1) H. E. Newell, Hearings before the Committee on Aeronautical and Space Sciences - United States Senate - Eighty-ninth Congress, March 22, 23, 24, 25, and 30, 1965.

(2) A. J. Kelley, "NASA's New Electronics Research Center," Astronautics and Aeronautics, Vol. 3, No. 5, May 1965, pp. 58-63.

where:

$$P_s = P_t \frac{A_r T_A T_o}{R^2 \theta_t^2} = \text{Received signal power} \quad (3)$$

and:

$\frac{S}{N}$ = Signal-to-noise power ratio
η_q = Detector quantum efficiency
h = Plancks constant
ν = Optical frequency
P_b = Background power
P_t = Transmitted power
A_r = Area of receiver
T_A = Transmission of the atmosphere
T_o = Transmission of the optical systems
R = Transmission path length
θ_t = Transmitter beamwidth

Many of these factors are established by system conditions in which bandwidth is a secondary consideration. Most component performance data can be obtained by testing on Earth using a simulated space environment. Some system characteristics may also be determined by using an Earth-based transmitter and receiver. However, the transmission of the atmosphere (T_A) is a nonlinear factor over which the system designer has no control; and at this time, he has little data on its effect on bandwidth.

It is known that there is turbulence just below the stratosphere that contributes to stellar scintillation and will also affect the transmission of optical signals. Thus, a signal source well above this altitude is indicated. In fact, data should be gathered from tests of propagation through the whole atmosphere. This can only be done from an orbiting spacecraft. The characteristics of the whole atmosphere, including turbulence, temperature, and other effects, and the effect on bandwidth for transmission each way, must be measured using satellite-borne equipment. The effects of the narrow beamwidth (θ_t) on signal-to-noise ratio $\left(\frac{S}{N}\right)$ and bandwidths (Δf) must be determined as the beam passes through the varying density of the atmosphere so that the system designer can optimize these tradeoffs. Since all tests will be performed using several types of modulation, further data will be obtained on the system performance as a function of modulation technique.

Another factor requiring space testing is the need to operate in the far field of the optical aperture. This requires that the receiver be located a distance (R) from the transmitting aperture D_t according to the following expression:

$$R = \frac{2 D_t^2}{\lambda}$$

(3) H. T. Friis, W. D. Lewis, B.S.T.J., Vol. 26, September 1947, p. 227.

For 10.6-micron wavelength and a 0.3-meter aperture, this is 18 KM; and for 0.63-micron wavelength and a 1.0-meter aperture, this is about 1×10^6 meters. Operation in the near field will not provide a proper simulation of the deep space mission.

Short duration tests could be performed using rocket-borne equipment to operate through the whole atmosphere. However, long duration tests to obtain statistically significant data will require satellite-borne equipment.

4.4.3.3 Feasibility

This experiment is planned to be performed at several optical wavelengths. The degree of perfection of the several critical elements required for communication at these wavelengths varies markedly with the wavelength under consideration. For visible wavelengths, 0.488 micron and 0.6328 micron, all critical components such as lasers, modulators, beam splitters, and optical elements and their coatings have reached a state of development where some items such as optical elements, beam splitters, and detectors have demonstrated reliable performance on rockets and satellites; other items such as lasers and modulators have been operated in experimental communication links carrying television signals over distances of 2 kilometers.(4) Reliability and lifetime estimates are still low for OTAES applications and will need to be improved.

At the 10.6-micron wavelength of the CO_2 - N_2 laser, operation of most component parts in the space environment is relatively unknown. The number of transmission materials available for selection is limited, and suitable reflection and anti-reflection coatings are also limited. Until the recent availability of the CO_2 - N_2 laser, work in the infrared region was spread over the band; but it can be expected that considerable effort will be concentrated at the 10.6-micron wavelength because of the availability of a coherent source of high energy and the great need of materials to be used with this source. Development of devices for operation at this wavelength can also be expected to keep pace with material development. Detectors for operation at 10.6 microns are limited to the photodetectors such as gold- or mercury-doped germanium, and they require cooling to liquid nitrogen or liquid helium temperatures for proper operation. Present devices can be operated at bandwidths of 1 MHz. Further development will be required to obtain 10 MHz bandwidths with long life and high reliability. Modulators have not yet been developed for 10.6 microns, but studies(5) show that suitable materials are available that can be operated as modulators in the same configuration as the presently available visible light modulators. Drive power requirements will be about the same as that required for the visible light modulators, for a given modulation bandwidth. The modulator and the detector for 10.6-micron performance are the primary high risk components for this experiment.

4.4.4 Implementation

4.4.4.1 Experiment Design

A comparison of communication alternatives at bandwidths of 10 MHz will be performed to determine limiting or critical perturbations and their source when communicating from space to ground, and to gather data on system characteristics. This experiment will also be performed in the ground-to-space configuration although the projected requirements for the

---

(4) C. J. Peters, et al, "Laser-Television System Developed with Off-the-Shelf Equipment," Electronics, February 8, 1965, pp. 75-78.

(5) G. McDowell and W. E. Bicknell, "Design Considerations for Near and Mid-Infrared Modulators," Sylvania Electronic Systems, ARL Departmental Note No. 21, June 1966.

up-link are not as great as for the down-link. The parameters to be measured will include transmitted signal strength, modulation characteristics, received signal strength, received noise level, and received signal error rate. These parameters will be used to determine signal-to-noise ratio and data error rate.

The equipment used for this experiment will be the same equipment used for demonstrating heterodyne detection on the ground, heterodyne detection in space, and direct detection on the ground. The spaceborne equipment will use three telescopes, one having an aperture of 1.0 meter and the other two having apertures of 0.3 meter. Telescope #1 will be used for transmission of the 0.6328-micron wavelength and reception of the 0.4880-micron wavelength as shown in figures 4.4-2 and 4.4-3. Telescope #2 has a 0.3-meter aperture and will be used only for transmission of the 10.6-micron wavelength as shown in figures 4.4-3 and 4.4-4. Telescope #3 has a 0.3-meter aperture and will be used for reception of the 0.6328-micron wavelength as shown in figures 4.4-3 and 4.4-5. The 0.6328-micron transmitter in telescope #3 is redundant. It is included for experiment reliability, hence, will not be used in the normal experiment procedure.

These concepts have been synthesized with an emphasis on minimizing moving parts. Where possible, dichroic mirrors have been designed into the system providing high efficiency transmission at one wavelength and high reflection efficiency at another wavelength. On telescope #1, the 0.6328-micron laser transmits on a direct line through to the telescope. This signal passes through the pupil matching telescope, the modulator, another pupil matching telescope, the point-ahead beam deflector, a quarter-wave plate, the dichroic mirror which transmits the 0.6328-micron wavelength efficiently, the fine beam deflector, and finally through the diverging lens to illuminate the primary mirror.

Using the dichroic mirror, it will be possible to perform an experiment where transmission can be accomplished at one wavelength and reception may be performed at another wavelength, simultaneously. In the receiver, the 0.488-micron wavelength signal from the ground-based argon transmitter passes through the fine beam deflector, is reflected by the dichroic mirror to the beam splitter where half the energy will be transmitted to the heterodyne receiver and the remainder will be diverted to the tracking sensor.

The dichroic mirror, although an efficient reflector for 0.488-micron wavelength and an efficient transmitter for the 0.6328-micron signal, is not absolutely effective in these modes. A small amount of the 0.6328-micron energy will be reflected to the transmission monitor.

For this experiment, the modulator is extremely important. The transmission modulator (Pockels Cell) such as the Sylvania type S2 can be operated to provide several forms of modulation of the transmitted beam. This modulator works on the principle of inducing a phase shift between two components of the electric field of the light wave. By appropriate control of the input signal amplitude, the plane of polarization can be rotated by 90^{o} to give vertical polarization for zero signal and horizontal polarization for full signal, providing polarized light modulation. Analog signals will give continually varying polarization of the beam whereas digital signals will provide one or the other plane of polarization depending on whether a "one" or a "zero" is present. In the digital case, a quarter-wave plate may be inserted in the beam with its optical axis oriented at 45^{o} to the vertical plane of polarization. The beam will then be circularly polarized, right-hand circular polarization for one plane of polarization and left-hand polarization for the other plane. The angle of rotation of the satellite around the telescope-to-ground line of sight will have no effect in the detection of the signals in this case. However, a quarter-wave plate will be required in the receiver to convert the circularly polarized light to plane-polarized light; and an analyzer will be required in the receiver to separate each plane of polarization. A narrow-band filter will also be used in the receiver optical path to eliminate the background radiation that might otherwise overload the detectors.

In the transmitter, if a plane polarizer is inserted immediately following the modulator, the output beam will be intensity modulated. If the polarizing axis of the plane polarizer is at right angles to the zero-signal plane of polarization, a zero signal will give

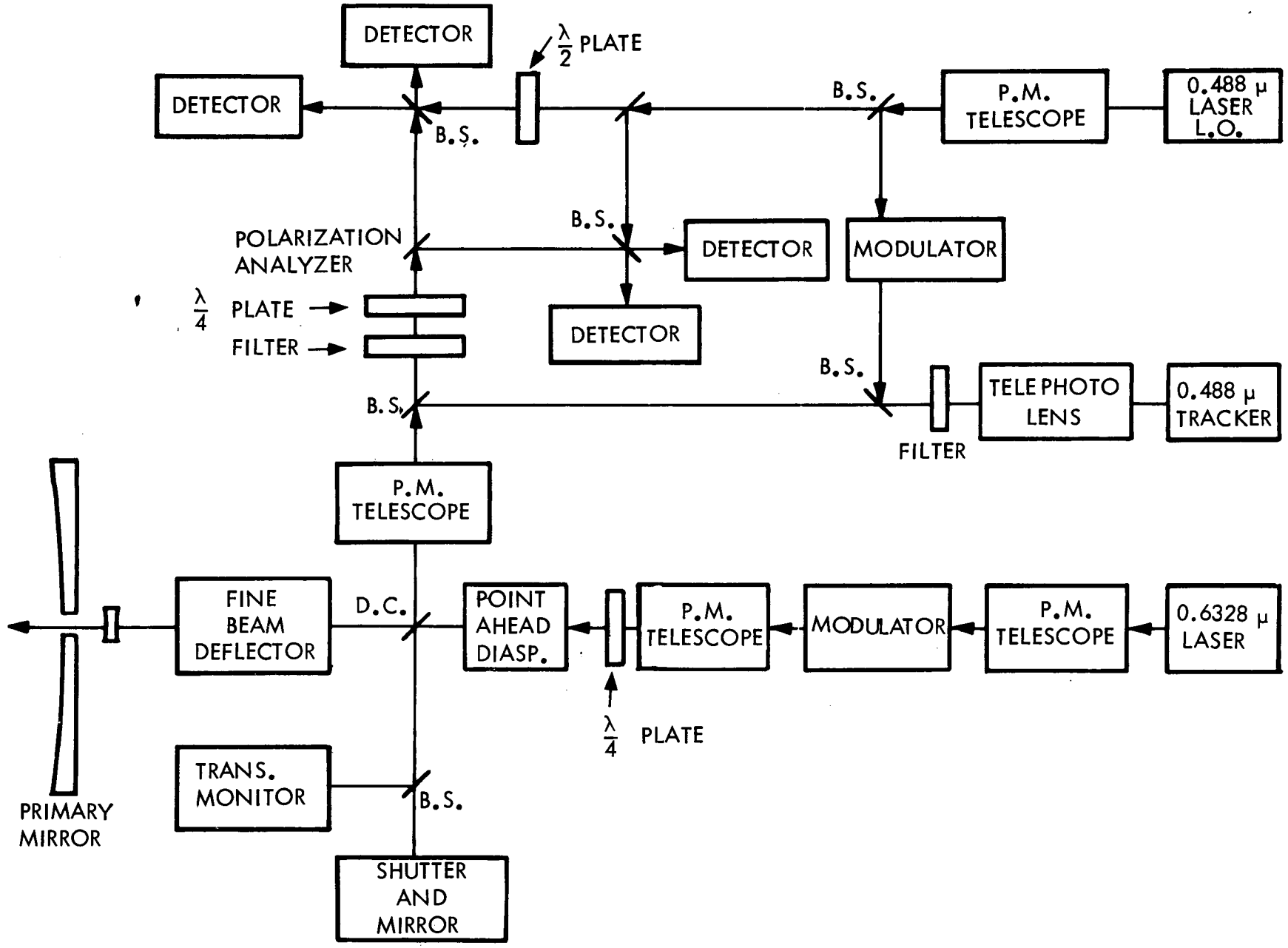

Figure 4.4-2. Block Diagram of Telescope #1: 1.0 Meter - Gimbaled.

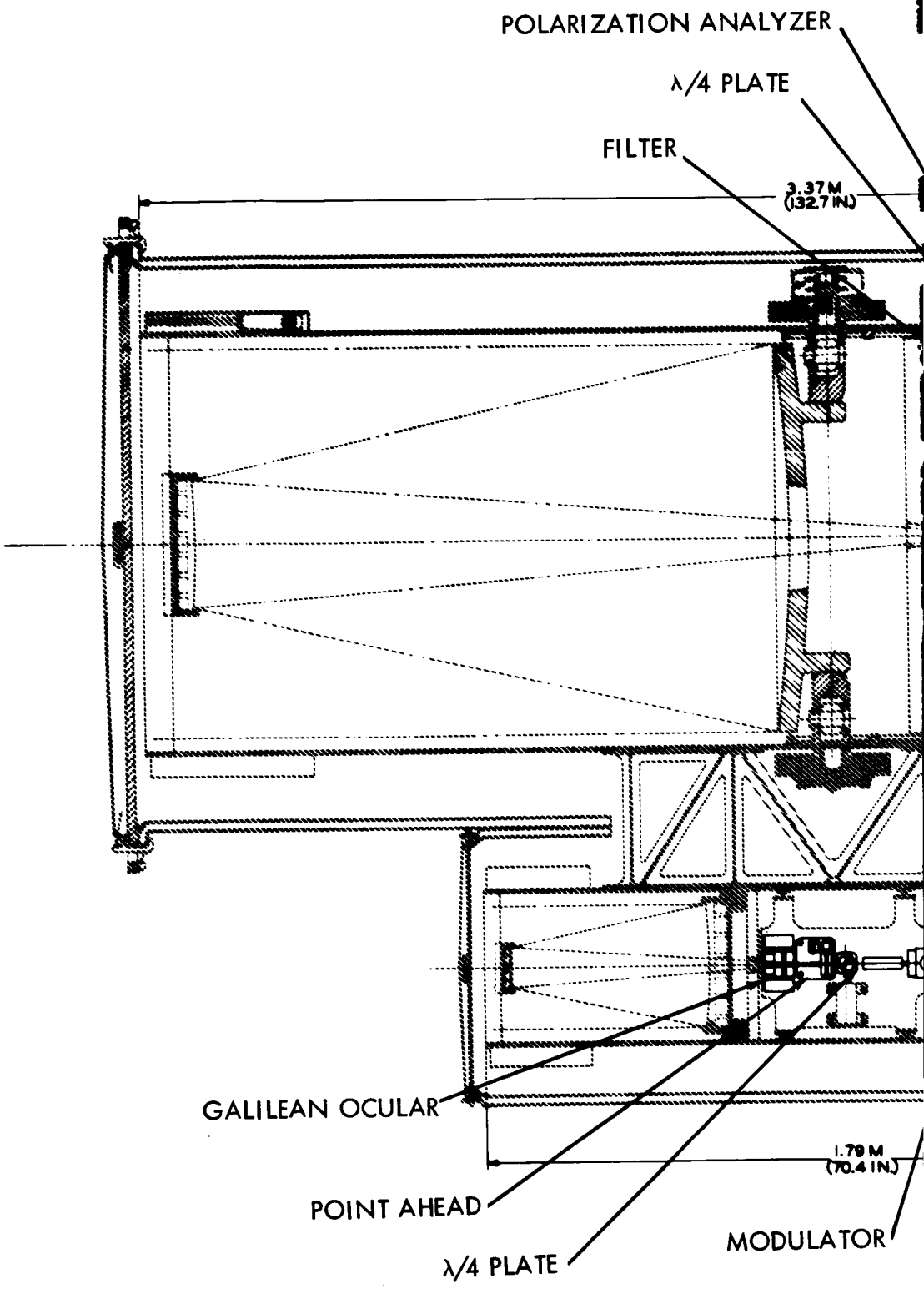

1-209

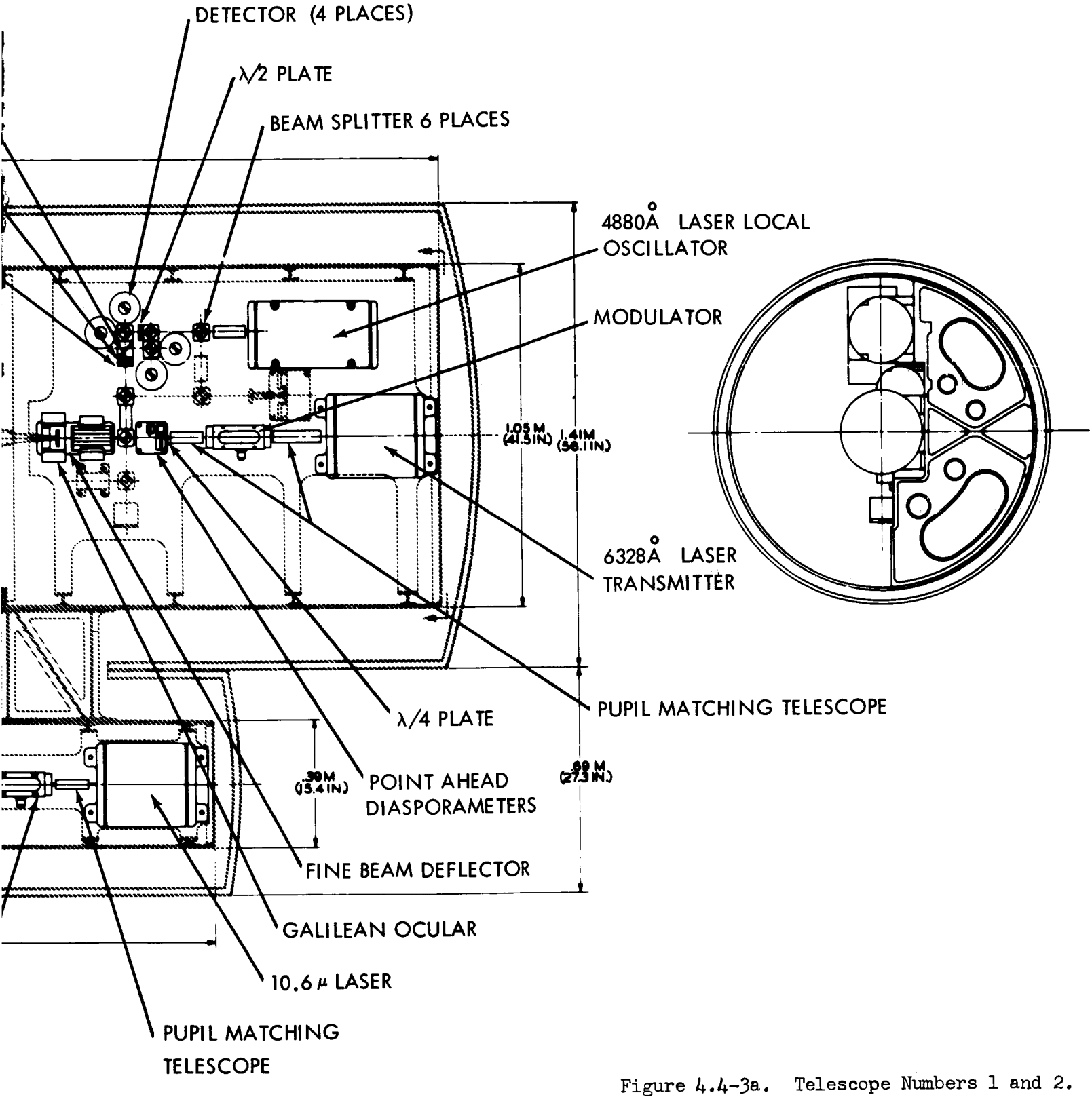

Figure 4.4-3a. Telescope Numbers 1 and 2.

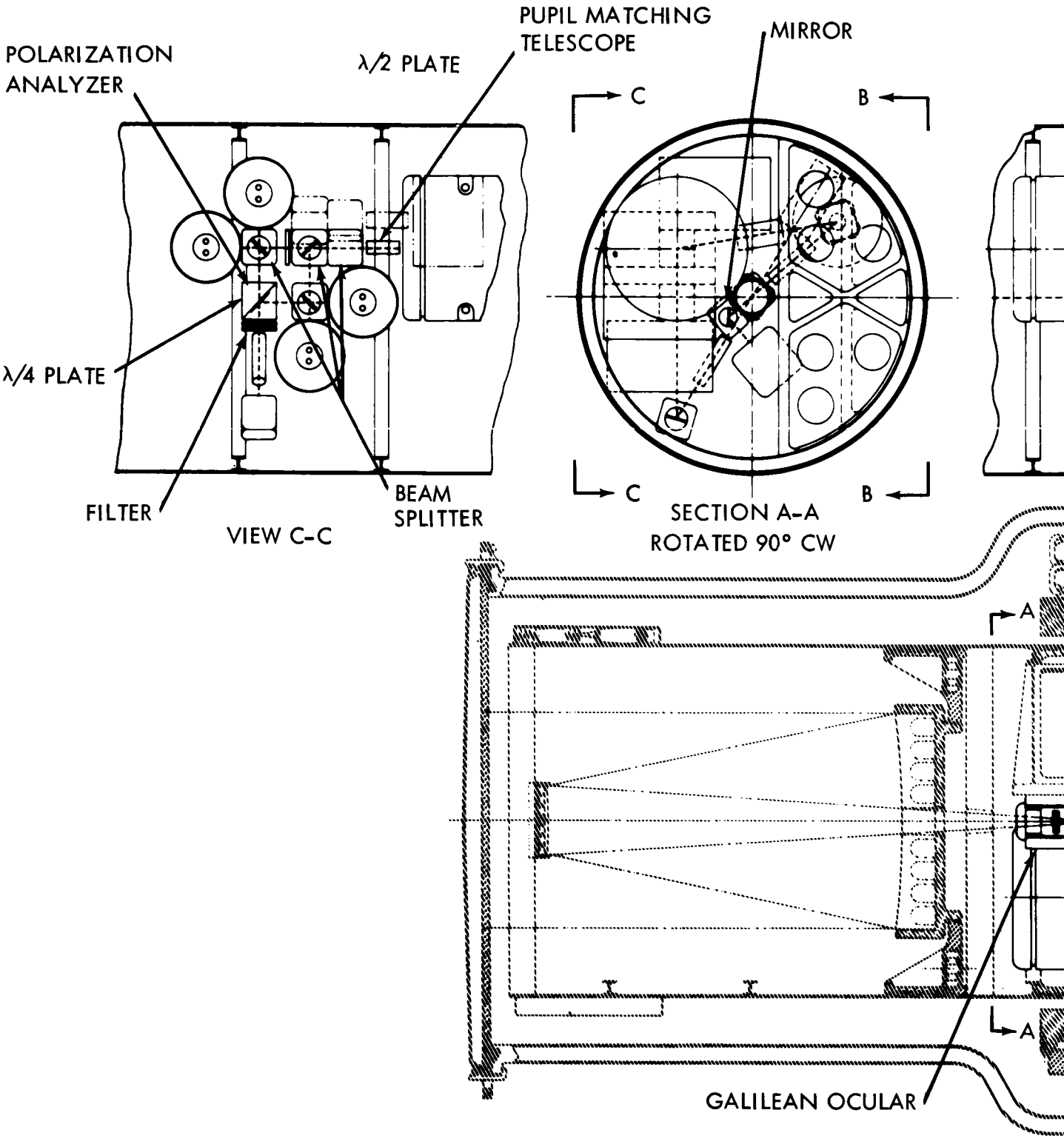
POLARIZATION ANALYZER
λ/2 PLATE
PUPIL MATCHING TELESCOPE
MIRROR
C
B
λ/4 PLATE
FILTER
BEAM SPLITTER
VIEW C-C
SECTION A-A ROTATED 90° CW
A
GALILEAN OCULAR

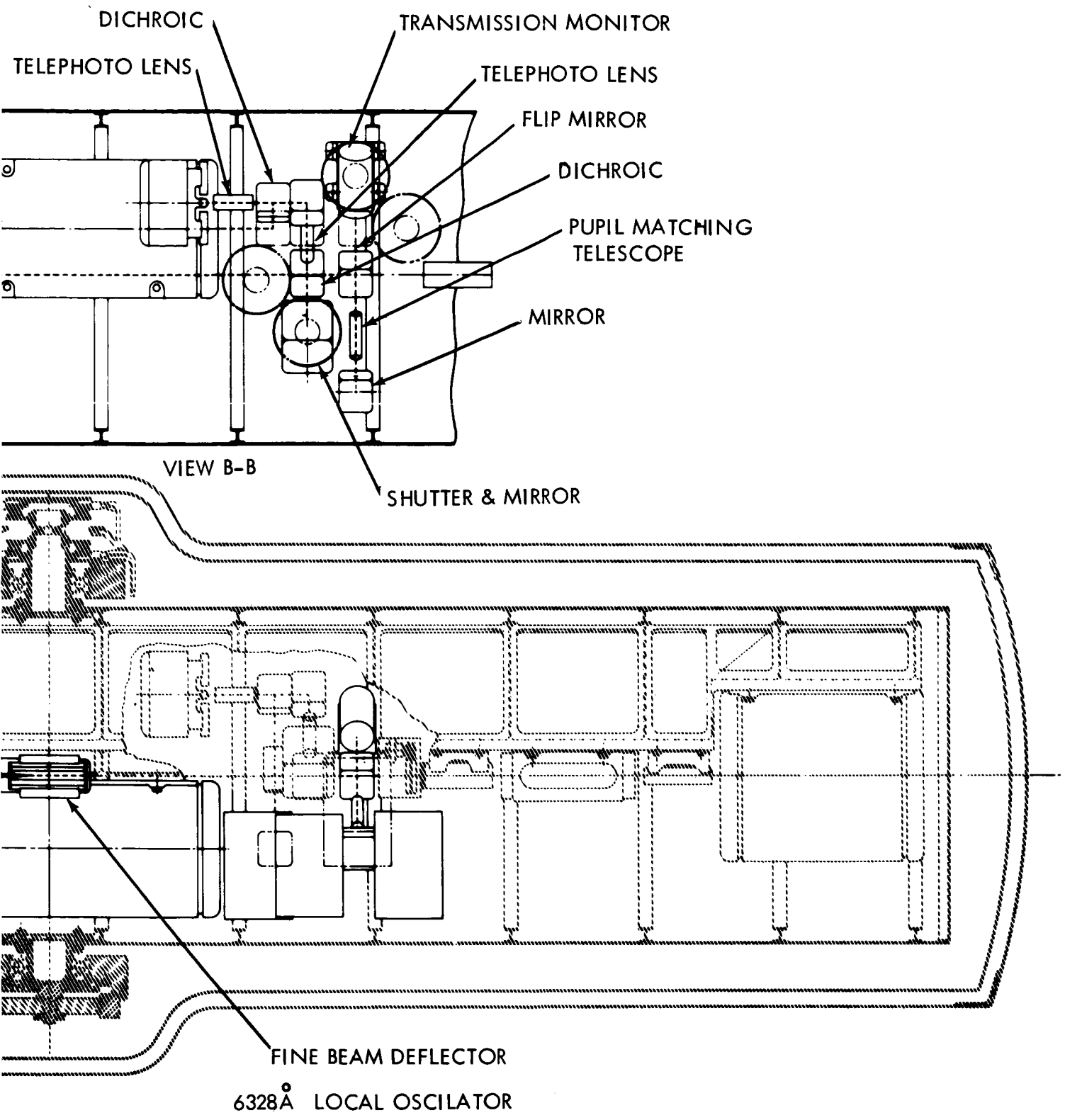

Figure 4.4-3b. Telescope Number 3

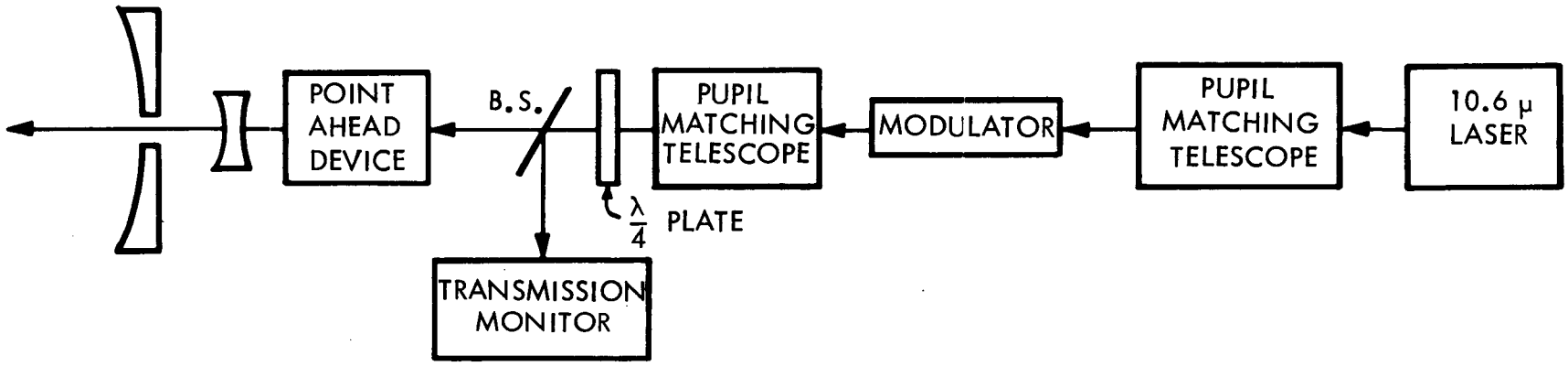

Figure 4.4-4. Block Diagram of Telescope #2: 0.3 Meter-Strap-On

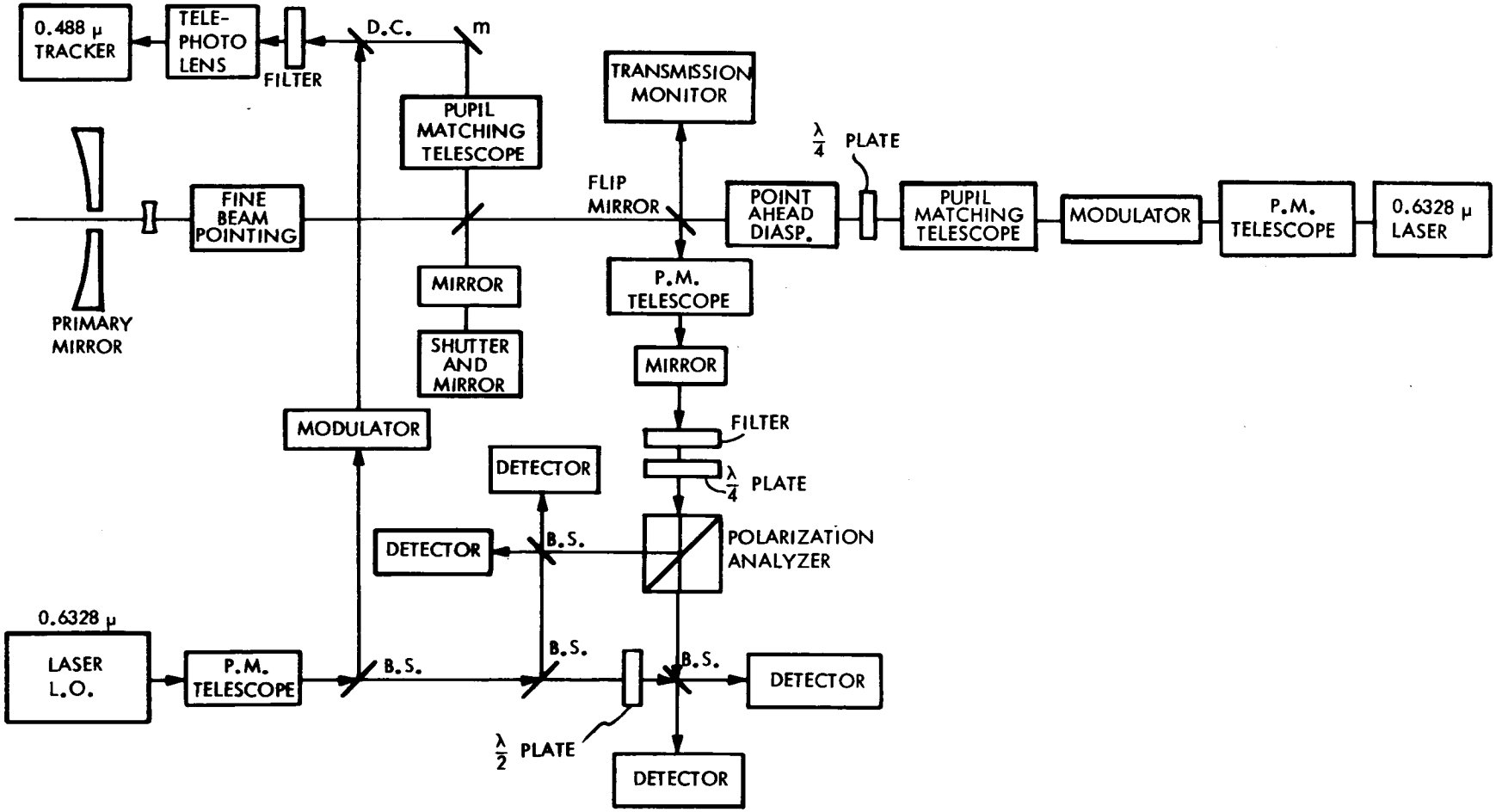

Figure 4.4-5. Block Diagram of Telescope #3: 0.3 Meter-Separately Gimbaled.

maximum intensity. If the polarizing axis is aligned with the zero-signal output plane of polarization, the intensity will be a maximum for zero signal and will go to zero for maximum signal.

The modulator may be used to obtain phase modulation of the output beam. In this case, the plane of polarization of the input beam is oriented at right angles to the modulator electric field. The modulation input causes the phase of the electric field of the light beam to be retarded in proportion to the applied field, giving phase modulation as a function of input signal amplitude.

If the applied signal amplitude is held constant and the modulation is applied as a varying frequency, the optical signal will be frequency modulated.

The design of these modulators varies for each application as shown in figure 4.4-6. The possibility of using one modulator and altering the added parts will require study during the design detailing. At most, three different modulators could be required; and a means for placing each in the light beam must be developed.

Input power measurements to the lasers and to the modulator driver will be measured with conventional voltage and current sensors to determine total power input for each element. The output power will be measured using the transmission monitors, which will have been calibrated prior to launch. The heterodyne receivers will also have been calibrated prior to launch so that received signal measurements can be made. Simultaneous operation of a transmitter on one wavelength and reception on a different wavelength can be accomplished. This will provide a means of comparing received data which, through proper analysis, will identify effects that are common to both wavelengths, such as pointing errors, and evaluate effects which are wavelength dependent, such as absorption characteristics.

Telescope #2 has been designed to transmit the 10.6-micron laser beam. The laser will transmit through the pupil matching telescope, the modulator, another pupil matching telescope, the beam splitter plate, the quarter-wave plate, the point-ahead device, and then out the telescope. A small part of the energy from the 10.6-micron laser will be reflected by beam splitter to the transmission monitor which will be calibrated prior to launch for measurement of laser output performance. At the present stage of development, the receiver for the 10.6-micron laser requires cryogenic cooling for efficient operation of the detectors. For this reason, reception of the 10.6-micron wavelength on the spacecraft is not planned.

Telescope #3 has been designed as a back-up for the #1 telescope transmitter. It contains a redundant 0.6328-micron laser transmitter and receivers for heterodyne detection of the 0.6328-micron wavelength and tracking of the 0.488-micron wavelength. When the transmitter is in use, the flip mirror rotates out of the optical path, disabling the 0.6328-micron receiver. This same rotation will position a beam splitter to divert a small amount of energy to the transmission monitor. The major portion of the beam, however, passes through the pupil matching telescope, the modulator, another pupil matching telescope, the circular polarizer, the point-ahead beam deflector, the beam splitter, the dichroic mirror, through the fine beam deflector, and out through the telescope aperture. For receiving the 0.6328-micron wavelength signal, the entering beam will be reflected to the receiver by the flip mirror in its normal position. The 0.488-micron wavelength will be reflected by the dichroic mirror to the tracking receiver. Although the #3 telescope will not have as narrow a beamwidth as the #1 telescope, most of the experiments planned for the #1 telescope can be performed with it, in the event that the #1 telescope suffers a major failure.

The optical communication system's needs for space, weight, and mounting within the spacecraft are as follows. The space requirements behind the one-meter telescope primary, exclusive of thermal shielding between lasers and primary, will be a volume 1.3 m deep behind the mirror and one meter in diameter. This assembly is estimated to have a mass of

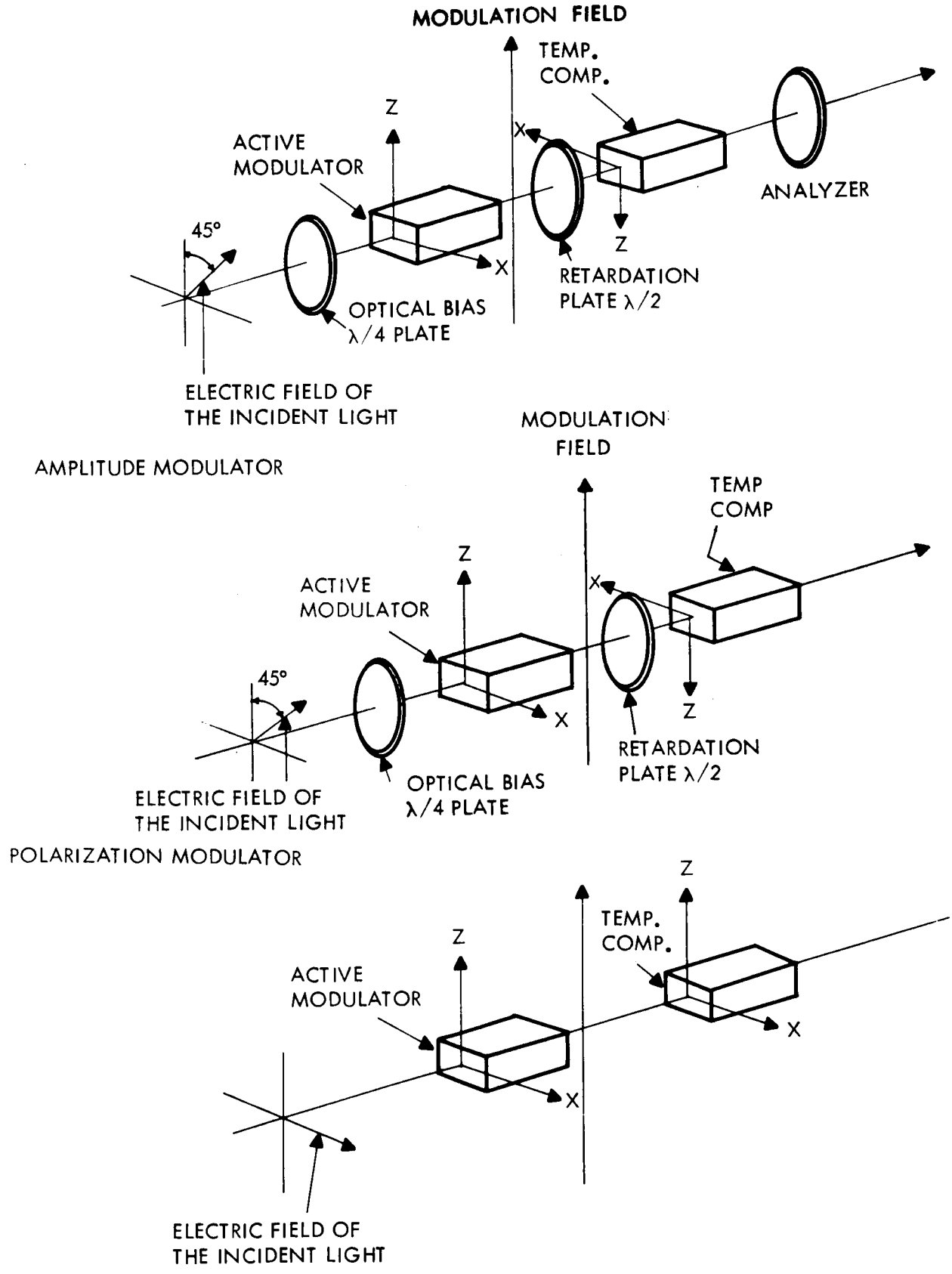

Figure 4.4-6. Amplitude Modulator/Polarization Modulator/Phase Modulator

100 Kg. For telescope #2, the space requirement will be a volume 1.0 m deep behind the primary and 0.35 m in diameter. The assembly mass is estimated to be 35 Kg. For telescope #3, the space will be a volume behind the primary 2.3 m deep and 0.35 m in diameter. Estimated assembly mass is 120 Kg.

4.4.4.2 Operational Procedure

The wide-band communication experiments are planned to be operated as an extension of the Heterodyne Detection on Earth experiment, the Heterodyne Detection on the Spacecraft experiment, and the Direct Detection experiment. That is, measurements for wide bandwidth communications will be made using heterodyne and direct detection techniques. The first experiment that is expected to be performed will be the direct detection experiment. When it has been determined that the direct detection experiment on earth is operating satisfactorily, the modulator will be supplied a wide-band signal from the signal source.

The signal will be encoded with one of several available modulation sources. These will be: 1) tones, 2) voice, 3) TV test pattern, 4) TV picture, and 5) digital code words. These sources will be used directly and to encode a carrier to drive the modulator. The drive source may be Pulse Code, Phase, Frequency, or Amplitude modulated. For example, the optical signal can be polarized light modulated, the polarization can be pulse code modulated, and the pulse code will be generated by sampling and quantizing voice (PL/PCM/voice).

For the direct detection system, the following combinations will be used:

Optical	Carrier	Signal Source
Intensity Modulation	Direct	1-5
	FM	1-5
	PCM	1-5
Polarized Light Modulation	PCM	1-5

The tones, TV test pattern, and digital words will be used to make quantitative measurements of the system performance; and the voice and TV picture will be used for subjective evaluation of the system. The tones spaced at decade intervals will provide a number of points for measurement on a frequency response plot. The TV test pattern will provide another means of determining system performance by correlation of many received signals, and the digital code words in a known format will provide a means of measuring error rate of the received signal with a minimum of data processing. During each transmission, transmitter output power, modulator power, received signal power, and signal characteristics will be measured.

Transmissions will be made over extended periods of time to obtain signal characteristics and error rate information as a function of atmospheric characteristics, pointing accuracy, and receiver aperture size. This experiment may also be performed by varying other functions such as the receiver optical filter bandwidth.

The direct detection wide bandwidth experiment is planned to be performed initially with a 0.6328-micron transmission. Simultaneously, experiments may be performed using the 10.6-micron laser. The simultaneity of these experiments is dependent on the ground receiver design and the problems associated with reception of infrared signals. In all cases, prime power to the laser transmitter will be monitored, prime power to the modulator

will be monitored, and the transmitted energy will be monitored and all data telemetered to the Earth.

Following the completion of the direct detection experiments, the Optical Heterodyne Detection on Earth experiment will be performed (section 4.1). This done, the heterodyne portion of the wide bandwidth communication experiment will be performed. (The laser stabilization circuits required for the heterodyne operation will remain activated, and the procedure will then be the same as for the wide bandwidth direct detection portion.)

For the wide-band heterodyne detection tests, the following combinations will be used:

Optical	Carrier	Signal Source
Intensity Modulation	Direct	1-5
	FM	1-5
	PCM	1-5
Polarized Light Modulation	PCM	1-5
Frequency Modulation	FM	1-5
Phase Modulation	AM	1-5
	PCM	1-5

The heterodyne experiments will be performed at each wavelength over an extended period of time to obtain information regarding the temporal effects on the transmitted signal. This will facilitate separation of the various atmospheric effects on the received signal. Variation of reception aperture and measurements of angle of arrival will enable determination of the effects of close-in turbulence and turbulon size versus distance. These measurements will be compared to measurements made at narrow bandwidths during the heterodyne detection on earth experiment to determine the effects of the atmosphere as a function of bandwidth.

Upon completion of the heterodyne detection on the spacecraft experiment, using narrow-band signals, the wide bandwidth experiment will be performed using heterodyne detection. The ground-based equipment will be modulated in the same way that the spacecraft equipment is modulated, that is, Intensity, Polarized Light, Frequency, and Phase modulated. The signal source will use: 1) tones and 2) digital codes. These can be readily processed on the spacecraft with minimum data processing equipment. The first signal to be used will be the 0.6328-micron wavelength. The received signal will be analyzed by on-board data processing equipment to determine error rate and frequency response. The performance of the heterodyne receiver will be determined on the ground prior to launch; the effect of this receiver on wide bandwidth performance will have been determined and its limiting effect upon the received signal analyzed. The reduced data will be transmitted via the telemetry link to the ground station for comparison to the transmitted signal and for analysis of the effect of the atmospheric conditions on the spacecraft received signal.

A direct detection ground-to-space link has not been planned as a specific experiment. However, wide bandwidth performance for direct detection transmissions can be determined with the equipment that will be used for heterodyne reception on the spacecraft.

It is not anticipated that a man will be required for performance of the various experiments, although the initial alignment of the optical systems after they have been placed in orbit may need to be verified.

The time planned for performing the wide bandwidth communication experiment is shown in figure 4.4-7 for the first 31-hour operational period. This is a standard operational routine that will be repeated from time to time, depending on weather conditions and system performance. Based on data obtained during this routine, selected experiments will be performed to take advantage of the conditions present. Operation of wide bandwidth communication at these times may be needed for extended periods to gather data during varying conditions.

4.4.5 Supporting Analyses

In the preceding experiment sections, 4.1 and 4.3, there are presented several analyses relating to optical communications. All of these are pertinent to wide bandwidth communication.

Subsection 4.1.5.2, Laser Evaluation, discusses the basis of laser selection, including the laser characteristics essential to this experiment.

Subsection 4.1.3.1, Contribution and Need, analyzes the performance of the heterodyne detection communication system used for this wide bandwidth experiment.

Subsection 4.1.5.4, Optical Modulation, discusses the design study of two modulator types for use at 100 MHz: a lumped capacitor design and a traveling-wave design. (A wide bandwidth modulator is one of the most important elements in the wide bandwidth experiment.)

Subsection 4.1.5.1, Optical Propagation Measurements, reviews the optical communication equations for direct and heterodyne communication. It presents trade-off curves comparing spacecraft prime power, bandwidth, and signal-to-noise ratio at distances equal to Earth synchronous orbit and Mars maximum distance.

Subsection 4.3.5.1, Comparison of Modulation Techniques for Wide Bandwidth Communication, mathematically compares the forms of modulation suitable for a satellite-borne optical communication system. The comparisons are made on the basis of relative signal-to-noise ratios. The mathematical analysis does not, however, give weight to the relative complexity of implementation of such systems.

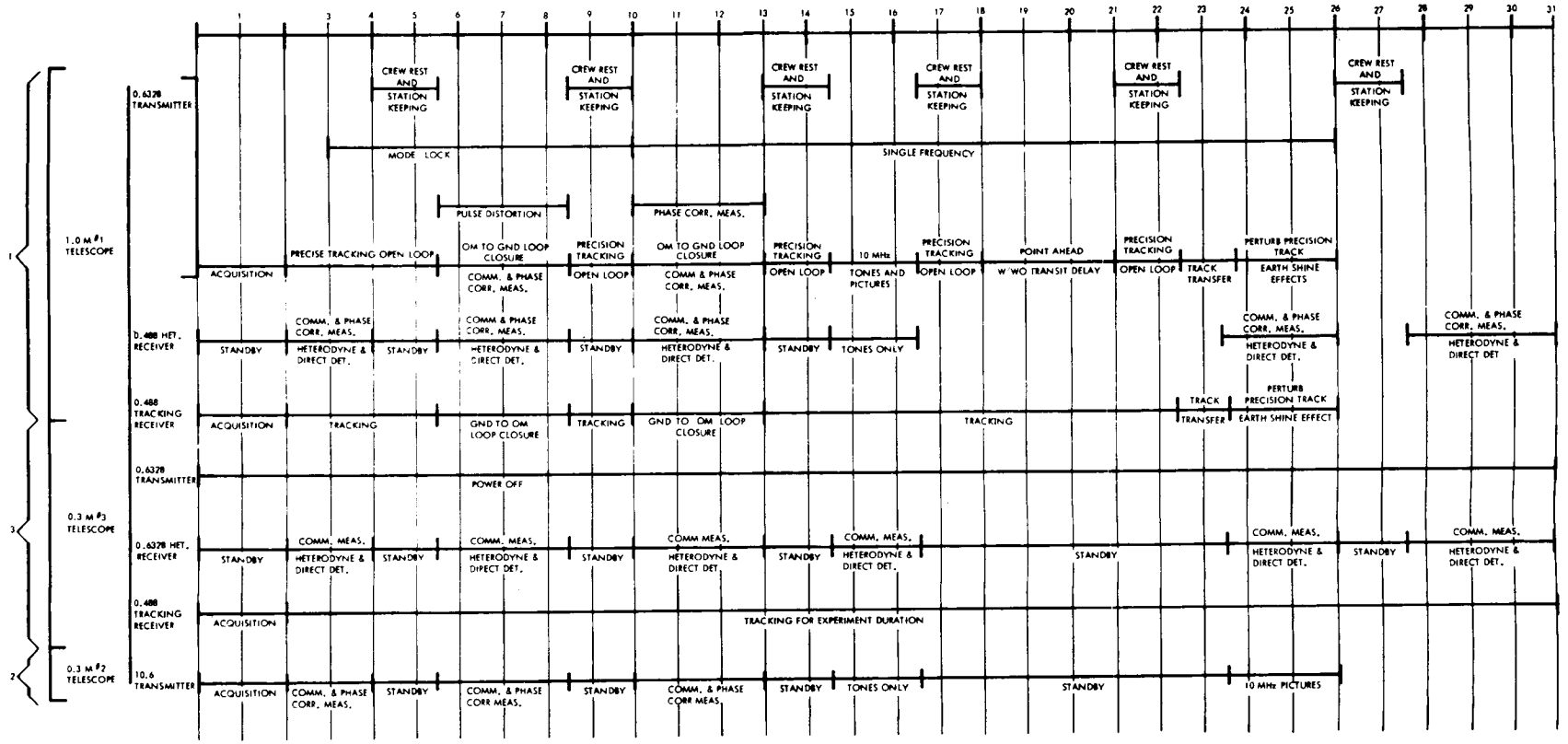

Figure 4.4-7. Time Lines for Communication at 10 MHz

4.5 PRECISION TRACKING OF A GROUND BEACON

4.5.1 Summary

Two way wide bandwidth laser communication links for space application will require that the laser power be concentrated in very narrow beam widths due to power limitations, especially in the spacecraft. In order to utilize narrow beams (divergence of 0.14 arc second at the 3 db power points) a pointing capability commensurate with the beam angular divergence is required. Pointing a laser to this accuracy from the spacecraft to a ground site would be virtually impossible without a reference line of sight from the ground. In this experiment, performed at synchronous altitude, this reference line of sight will be provided by an earth laser beacon whose angular beam spread can be considerably larger than the spacecraft's due to the greater power available at the ground site. The Deep Space Information Facility (DSIF) microwave link can establish the spacecraft's position to an accuracy of $\pm$ 22.5 sec. Thus, a 45 sec beam from the earth will insure illumination at the space vehicle initially and can be narrowed down after the spacecraft has acquired the beacon. Due to atmospheric turbulence the ground based beacons image in the spacecraft telescope moves laterally (image dancing). In the spacecraft this motion gives rise to tracking error signals which, after being fed to an image motion compensation (fine beam deflection) system, would cause the spacecraft line of sight to erroneously follow the image dancing. For a given apparent motion the angle through which the tracker has to move decreases with altitude. The minimum altitude at which the fluctuation is reduced to an acceptable .01 arc second (1/10 the Airy disc of the proposed 1.0 meter telescope) is 2000 miles.

In order to establish contact with a co-located transmitter-receiver on the ground, the relative velocities of the spacecraft and the earth require that a lead angle be maintained between the spacecraft tracker - beacon transmitter (reference) line of sight and the spacecraft transmitter - ground receiver line of sight. For a Mars probe this lead angle can reach 40 arc seconds; for the synchronous orbit it is less than 2 arc seconds. In this experiment lead angles are inserted on an open-loop basis, however to realize the best precision tracking requires closed loop operation between the spacecraft and the ground complex. (This is the subject of the experiment POINT AHEAD AND SPACE-TO-GROUND-TO-SPACE LOOP CLOSURE.)

Due to earth's rotation, a systematic transfer of the tracking and transmitting operation must be performed at time intervals determined by the separation of the earth stations. A capability of non-systematic handover will also be required in the event that weather conditions at a particular ground site will deter maintaining the laser communications link.

The acquisition and tracking function at the spacecraft must take into account the varying earth shine conditions present at earth for different illumination phases of earth as seen from Mars. This requires that the tracking and acquisition procedures will be performed under different light levels. Thus acquisition and tracking will be performed under the varying earth shine conditions which will be naturally present in synchronous orbit over a diurnal cycle.

4.5.2 EXPERIMENT OBJECTIVE

The purpose of this experiment is to investigate the practicability of tracking a ground based laser to an accuracy of 0.1 arc-seconds from the space vehicle. Overall tracking conditions will be simulated from synchronous orbit. Tests will be performed in a manner such that results can be extrapolated to obtain expected tracking performance for a deep-space mission.

4.5.3 EXPERIMENT JUSTIFICATION

4.5.3.1 Contribution and Need

The requirement for narrow beam widths to compensate for the relatively small transmitter power foreseen for future deep space laser communication systems establishes a need to point the laser beam at an earth based receiver with an accuracy commensurate with the angular divergence of the transmitted laser beam. The long transit time of light, traversing path lengths of the order of 1 AU requires that the transmitter beam be pointed ahead of the receiver station in order to compensate for the relative angular changes of the earth and space vehicle. The accuracy with which this pointing is effected is very much dependent upon the precision of establishing a tracking line of sight from the vehicle to the earth station. The ability to track the ground beacon accurately is a paramount prerequisite for the beam-pointing demonstration, as well as for all the communication and atmospheric experiments utilizing laser light transmission.

4.5.3.2 Need for Space Testing

4.5.3.2.1 Isolation of System From Effect of Image Dancing

Perturbations of the space borne laser transmitter line of sight arising from mechanical disturbances in the vehicle may result in angular fluctuations which exceed the transmitted beam widths and thereby prevent the beam from illuminating the earth receiver. In order to correct these perturbations by image motion compensation techniques, it is necessary to test the system at sufficient altitude to isolate the system from atmospheric induced image dancing.

As the laser light traverses the turbulent atmospheric layers, beam collimation and position are perturbed. For example, the effective motion of a "turbulon" (gas lens), h ϕ, may be inferred from the angular fluctuation it imparts to a stellar image, see figure 4.5-1a. The phenomena which give rise to image dancing occur at an altitude up to about 10^4 ft., and image dancing may be on the order of $\pm$ 5 arc seconds to $\pm$ 10 arc seconds as observed on the ground. The Airy-Disk in a 1.0 meter telescope is of the order of 0.1 arc sec and lateral shifts of 1/10 the Airy Disk or .01 arc second, are observable. The satellite range at which the fluctuation is reduced to .01 arc-second is 2×10^3 miles, and if the satellite is injected at a range in excess of this value, the input angle to the tracker is essentially noise free.

4.5.3.2.2 Determination of Minimum Beamwidth for Earth to Space Link

Angular fluctuations in the laser beam which arise from atmospheric turbulence, unlike lateral beam shifts, cannot be reduced by increasing the distance from the disturbance. The observed effect in the telescope image plane will be amplitude fluctuation or "scintillation". The laser beam must have sufficient angular divergence to insure that the space vehicle will always be illuminated since in extreme cases angling can cause the beam to miss the space vehicle. The determination of the optimum beam width for the laser uplink is more important with increase in vehicle range: At close range (up to 0.1 Astronomical Unit, AU) adequate light signal power densities to provide high tracking signal-to-noise ratio can be maintained with high powered, diverging laser beams, however, at distances greater than .1 AU, it will be necessary to narrow the laser beam divergence considerably. Using star scintillation data, it is anticipated, that angular beam divergences can be optimized in the range of 3 to 6 arc-second. By measuring the amplitude fluctuations of the space tracker signals, and analyzing the data, the optimum beam width in the space directed laser can be determined.

4.5.3.2.3 Testing of Acquisition Techniques

Acquisition of the ground laser beacon by the space borne receiver requires a fairly complex set of maneuvers which involve initial locking on several celestial targets. Varying earth shine conditions in which the earth laser must be acquired will affect the acquisition probability due to increase in false alarm rate and non-signal recognition as a result of background noise increase.

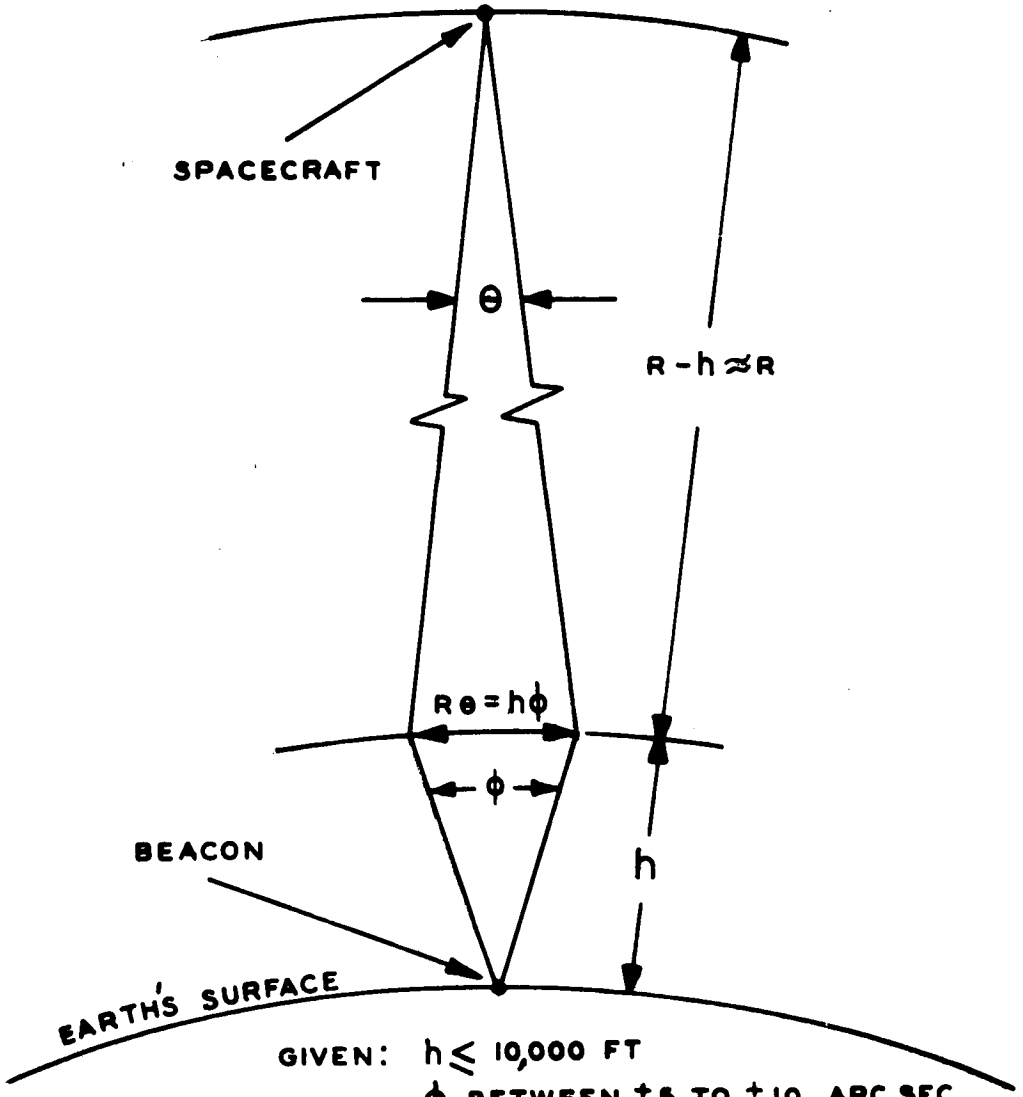

GIVEN: $h \leq 10{,}000$ FT

ϕ BETWEEN ± 5 TO ± 10 ARC SEC.

SPECIFIED: $\theta \leq .01$ ARC SEC

$R\theta = h\phi$

THEREFORE, $R = \frac{h\phi}{\theta} \approx$ 2000 STATUTE MILES (FOR $\phi = 10$ ARC SEC)

Figure 4.5-1a. Image Dancing

4.5.4 Implementation

4.5.4.1 Experiment Design

4.5.4.1.1 Experiment Concept

A ground station laser transmitter (beacon) beam is pointed at the spacecraft. The Deep Space Information Facility, DSIF, which tracks the spacecraft, furnishes the pointing information. In the spacecraft, telescopes with laser transmitting and receiving equipment must also track the earth laser beacon. Initial telescope pointing will require assistance from an on-board microwave tracking system, and from star trackers or planet trackers needed for complete determination of special orientation of the telescope. Of course, the spacecraft's attitude control system must initially orient the spacecraft so that the gimballed telescopes will be able to acquire the earth's beacon. Because of the importance of successful beacon tracking to other experiments, two independently gimballed telescopes, of differing fields of view and performance characteristics, are being proposed for this experiment. (See subsection 8.1 for further discussion on the selection of the number of laser telescopes.)

The laser communication link is not complete until spacecraft transmission is received at an earth station. Because of the relative velocity between the spacecraft and the ground station, the spacecraft transmission must not be beamed coaxially with the upcoming transmission; rather the downgoing beacon must be "pointed ahead". The manner in which this is done in a closed-loop feedback manner is the subject of another experiment, POINT AHEAD AND SPACE-TO-GROUND-TO-SPACE LOOP CLOSURE, subsection 4.6. The initial point-ahead is commanded from an earth station.

Since the processed signal at the ground can be used in evaluating the tracking performance of the experiment being discussed, the open loop insertion of point-ahead angles is considered a part of this experiment. The following subsections elaborate on the various phases of the experiment and consider alternatives as they arise. Details of current practice in spacecraft attitude control and microwave-link operation are important to the success of the experiment. However, in the remaining discussion much of this will be taken for granted and emphasis will be placed on the new frontier of laser space telescope tracking technology.

The experiment is to be conducted from synchronous orbit, which is high enough to eliminate the effects of image dancing, and where this experiment requires only one ground station. Consequently, there will not be any systematic slewing or reacquisition requirements, as would be the case for lower orbits. Reacquisition will be investigated, and slew is a part of the TRANSFER TRACKING FROM ONE GROUND STATION TO ANOTHER experiment, subsection 4.7.

4.5.4.1.2 Illumination of Spacecraft by a Ground Station

Using DSIF information, which is good to ± 22.5 arc seconds, a pulsed argon laser beacon beam of 45 arc second half-power width is directed at the vehicle. This beam width will insure that the spacecraft is illuminated. After initial acquisition has been achieved, the ground beacon's beam width can be reduced to increase the illumination at the laser telescope aperture.

4.5.4.1.3 Acquisition & Tracking of Ground Beacon

4.5.4.1.3.1 Spacecraft Orientation

The spacecraft and its telescopes must be properly oriented for the latter to receive the illuminating beacon signal. The spacecraft attitude will be referenced to both a line of sight to the sun and to the star Canopus. Two alternative means of acquiring Canopus are being considered: One is to orient the spacecraft in roll by having an on-board microwave tracker track a ground beacon and then issue gimbal commands to a star tracker to search for and acquire Canopus. The second method is to issue gimbal commands to the star tracker such that it will acquire Canopus if the correct roll attitude exists and then program a spacecraft roll as in the recent Mars-Mariner flight or as had been planned for the Advanced Orbiting Solar Observatory. For discussion of receiver line of sight stabilization for separate star and beacon tracker gimbals, refer to OTAES Interim Progress Report, Vol. IV, Appendix I-2.2.

4.5.4.1.3.2 Coarse Pointing of 0.3 Meter Telescope

The on-board microwave tracker establishes the direction to the ground station complex and provides the initial direction for the 0.3 meter telescope. The 0.5 degree half-angle cone of uncertainty in this information is too large for the limited field of view (1.5 arc minutes) of the telescope. Therefore, a planet tracker, boresighted and strapped to the telescope would search the cone of uncertainty and acquire the earth's disc (in a Mar's mission) or a simulated earth (white light beacon for a synchronous orbit mission). The planet tracker accuracy is ± 10 arc seconds. The 0.3 meter gimballed telescope is shown in figure 4.5-1b.

The telescope's transmitting laser beam spread, which can be controlled by longitudinally positioning the galilean collimating ocular located behind the primary mirror (see subsection 8.4), is 3 arc-seconds to insure illumination of the ground receiver. A point ahead angle of 1.85 arc seconds for a synchronous orbit must be commanded; this is accomplished with internal optics. Now the acquisition procedure for the 0.3 meter telescope is essentially complete. At the appropriate time in the experiment the beam width can be reduced in steps to 0.5 arc seconds when a tracking accuracy of ± 0.15 arc second is realized. The ground beacon's beam width must be reduced from the initial 45 arc seconds to 6 arc seconds in order to achieve such tracking accuracies. The ground beacon

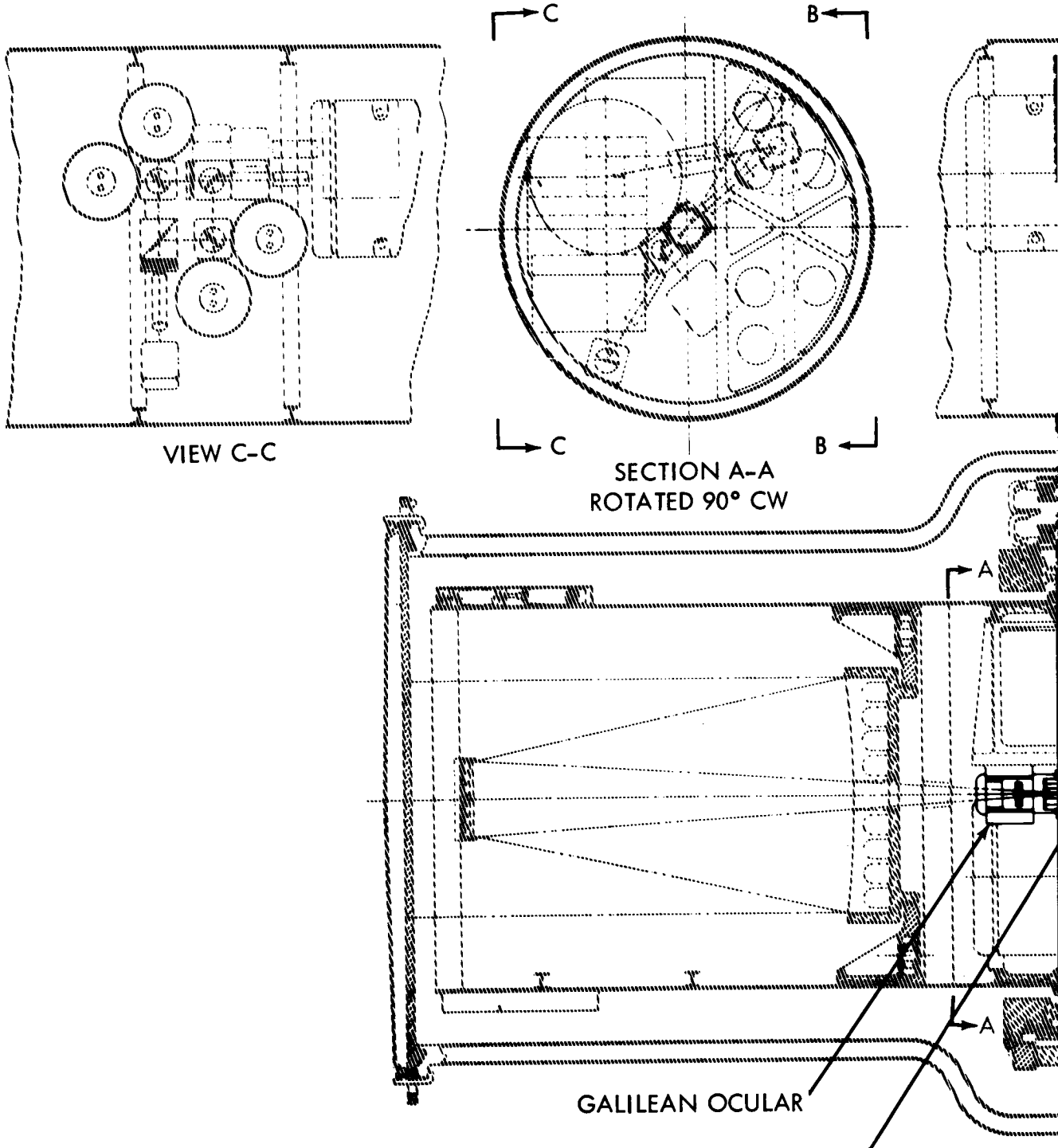
C
B
C
B
A
A
VIEW C-C
SECTION A-A
ROTATED 90° CW
GALILEAN OCULAR
FINE BEAM DEFLECTOR

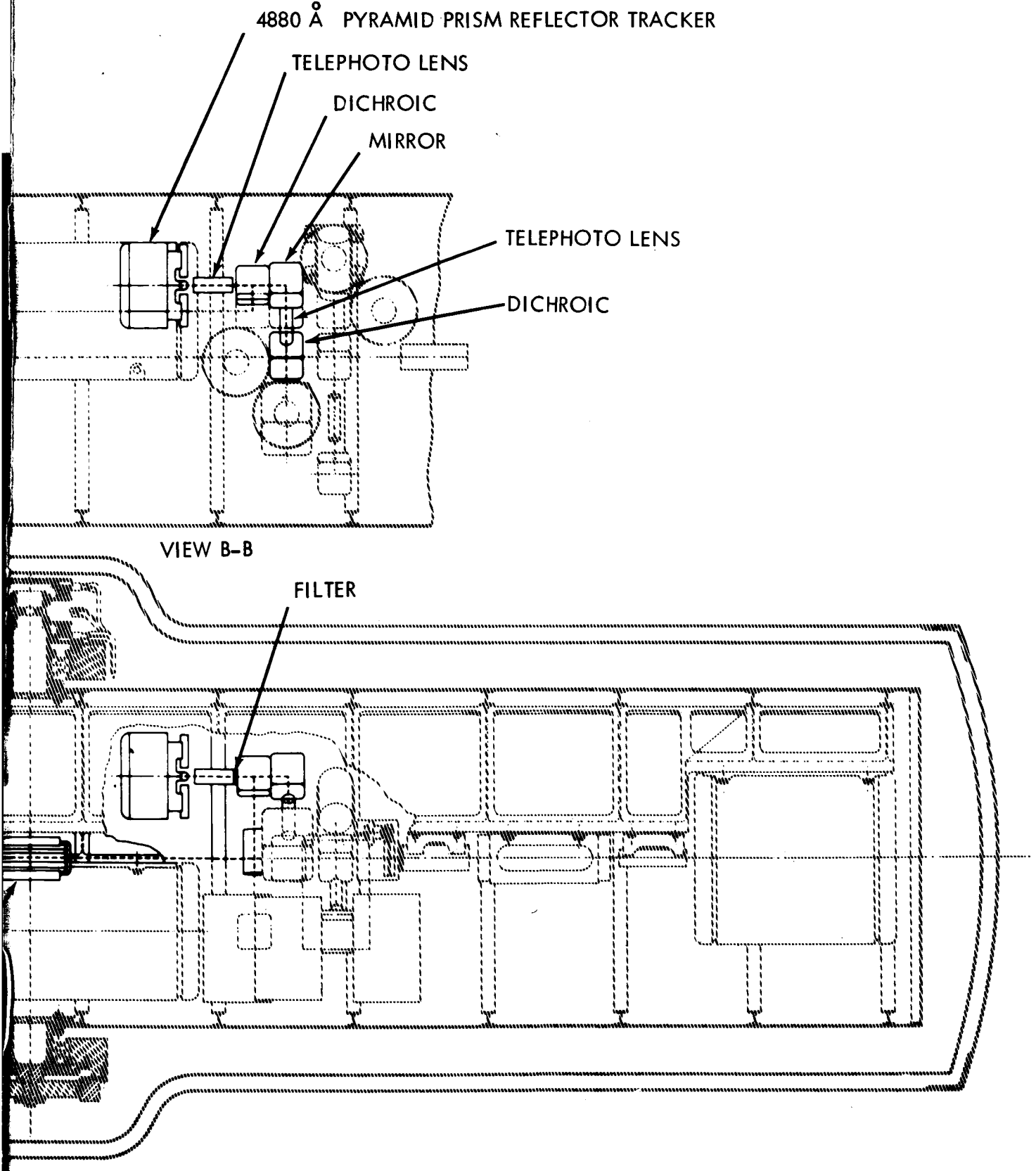

Figure 4.5-1b. 0.3 Meter Gimbaled Telescope Tracking Section

~~1-227~~
1-228

can be narrowed upon receipt of the spacecraft laser transmission, which establishes the necessary tracking LOS to the spacecraft. This implied loop closure is part of the experiment in subsection 4.6.

4.5.4.1.3.3 Coarse Pointing of 1.0 Meter Telescope

The 1.0 meter telescope operation will be analogous to that of the 0.3 meter gimballed telescope, however, the 1.0 meter unit has a smaller field of view (30 arc-seconds) and inherently better tracking and beam pointing accuracies (on the order of 0.1 arc second). See figure 4.5-1c.

For the purpose of improved reliability the 1.0 meter and the gimballed 0.3 meter telescopes can duplicate each other's functions; however, it is quite probable that detailed analysis of operational procedures would dictate that some differences be instituted. For example, the 1.0 meter unit could be slaved to the 0.3 meter unit to within 30 arc-seconds and the planet tracking procedure on the former eliminated.

4.5.4.1.4 Fine Tracking and Pointing of the 1.0 and 0.3 Meter Telescopes

Coarse tracking will take the form of gimbal drive to the telescopes. Electro-optical fine beam deflectors will respond to high frequency disturbances of the tracker line of sight. (See subsection 8.2 and 8.4 for hardware details.) Since spacecraft vibrations would affect both the upcoming and down going transmissions, the fine beam deflector corrects both in the manner of image motion compensation. This approach to compensating for high frequency spacecraft perturbations could not be considered if the proposed orbit were not high enough to eliminate the effects of image dancing (See Subsection 4.5.3.2).

The laser tracker is designed to detect the spectrum of perturbations due to spacecraft jitter as well as the slower occurring misalignments of the overall telescope line-of-sight to the earth beacon. Since the quadrant photomultiplier does not utilize image plane modulation, which for the present purposes would degrade available signal to noise (see subsection 4.5.5.1) a monitoring system has been designed which will provide continuous automatic gain control for nulling out differential photomultiplier drift (see subsection 4.5.5.2). The problem of slow drifts occuring in the boresighting between the tracker and the transmitter axis requires boresighting calibration (see subsection 4.5.5.3).

4.5.4.1.5 Acquisition and Tracking in Varying Earth Shine Conditions

The acquisition and tracking function at the spacecraft must take into account the varying earth shine conditions present at earth for different illumination phases of earth as seen from Mars. This requires that the tracking and acquisition procedures will be performed under different

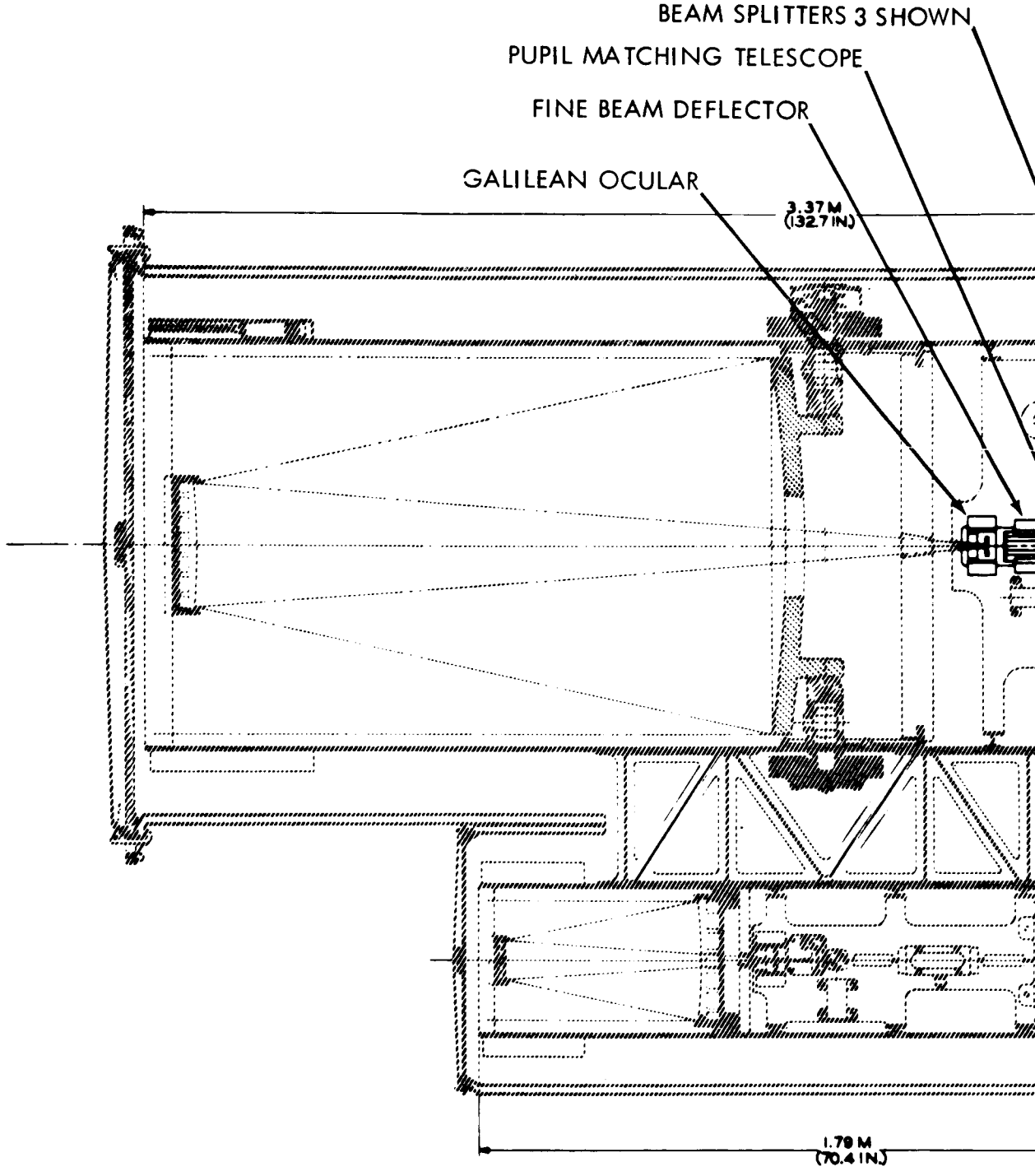
BEAM SPLITTERS 3 SHOWN
PUPIL MATCHING TELESCOPE
FINE BEAM DEFLECTOR
GALILEAN OCULAR
3.37 M
(132.7 IN.)
1.79 M
(70.4 IN.)

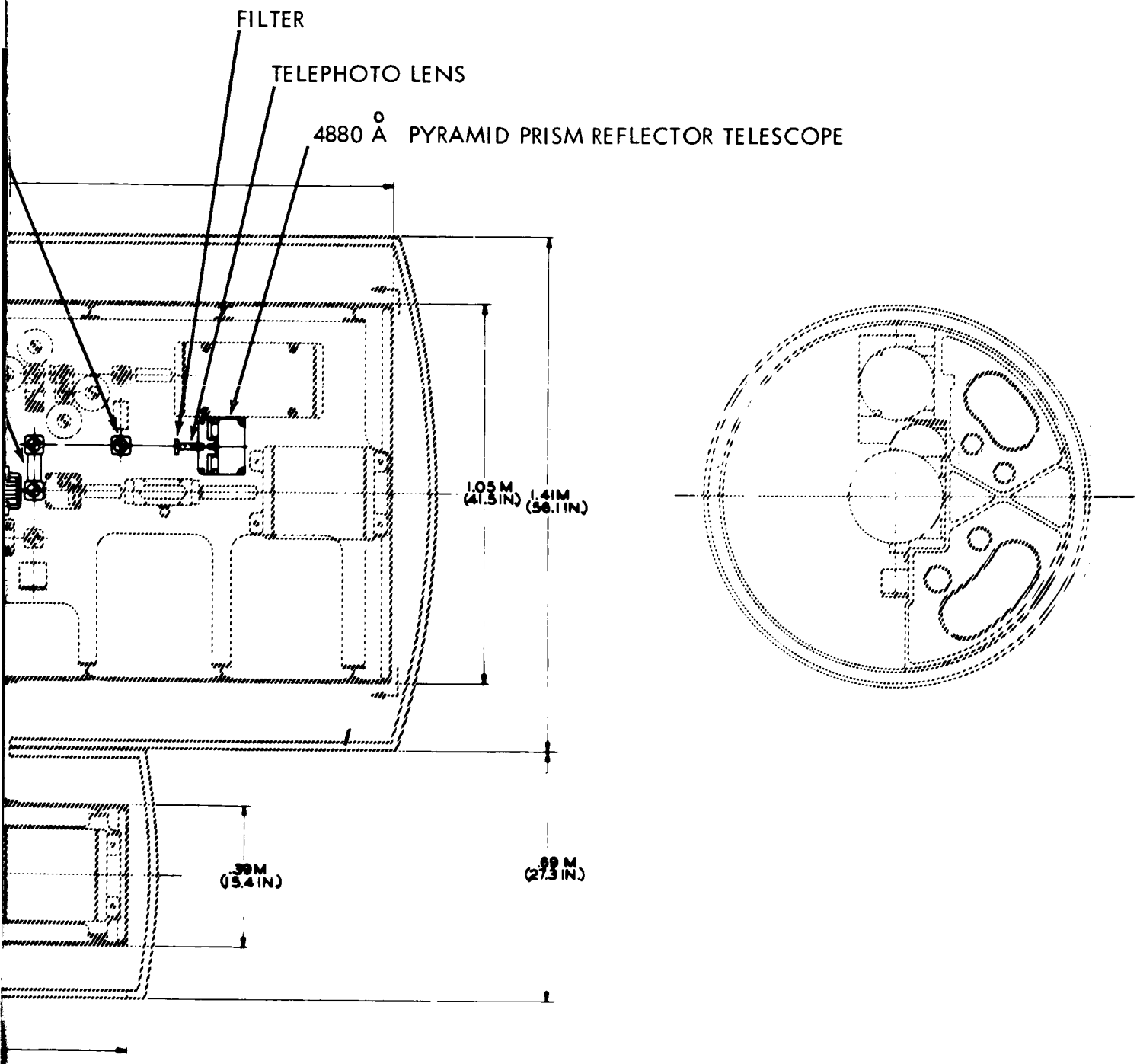

Figure 4.5-1c. 1.0 Meter Telescope Tracking Section

~~1-231~~

1-232

light levels. Thus acquisition and tracking will be performed under the varying earth shine conditions which will be naturally present in synchronous orbit over a diurnal cycle. A numerical analysis of the effects of earth shine on acquisition and tracking is presented in section 4.5.5.1.

4.5.4.2 Operational Procedure

4.5.4.2.1 Tasks

a. Earth station argon beamed up (45 arc seconds divergence).

b. Vehicle Roll Axis is aligned to sun.

c. Initial stabilization of vehicle is achieved by sun line of sight and microwave tracker.

d. Star tracker gimbals are commanded to search for Canopus.

e. Canopus is acquired and tracked.

f. The 0.3 meter telescope gimbal commands place the boresight axis of the telescope within the $\pm 0.5°$ cone of uncertainty established by the microwave tracker.

g. The planet tracker, boresighted to the telescope, acquires and tracks the white light beacon (simulated earth). The planet tracker accuracy is $\pm$ 10 sec. The telescope is positioned by the planet tracker error signals so that its fine field of view intercepts the earth laser beacon.

h. The 0.3 meter telescope tracks the earth laser to an accuracy of $\pm$ 3 seconds and beams a wide laser (6 $\widehat{\text{sec}}$) to the ground station. The earth station tracks the space vehicle laser and narrows down its own transmitter laser to 6 arc seconds in order to upgrade the space vehicle tracking performance.

i. The point ahead beam deflector is set at a value which will result in the beam being intercepted at the ground receiver which is co-located with the ground transmitter. The required bias angle to achieve this is a function of the differential tangential velocity vector of the space vehicle in synchronous orbit and the earth station at a particular latitude. The divergence of the spacecraft laser beam is initially 3 seconds to insure contact with the ground array. The beam spread can be controlled by longitudinally positioning the galilean collimating ocular located behind the primary mirror.

Tracking is evaluated at the space vehicle by monitoring the differential photomultiplier outputs on each axis of the .4880 micron beacon tracker. Monitoring the beam deflector inputs as well as the telescope gimbal positions will provide necessary data to determine the average beam direction.

j. An open loop beam pointing evaluation will also be part of the experiment. The overall acquisition involves the earth array receiving the spacecraft laser beam in addition to the spacecraft telescope receiving the earth laser beam.

Internal boresight alignment of tracker and transmitter is performed just prior to transmission of the laser beam from the spacecraft, thus this error can be effectively nulled. The accuracy of the initial bias offset will be somewhat more difficult to account for. The theoretical sensitivity of beam pointing measurements at the ground site will be within one tenth of the beam array width.

k. After pointing the 6 arc sec beam at the receiver array, the beam is narrowed to 0.5 arc second in several intermediate steps.

l. The 1.0 meter telescope gimbals are pointed within $\pm$ 15 sec from commands read from the 0.3 meter telescope gimbals. The deflection voltages from the fine beam deflector are read out and transferred to the fine beam deflectors of the 1.0 meter telescope to insure that the laser beacon falls within field of view of the telescope.

m. The 1.0 meter telescope acquires and tracks the earth laser beacon and points a 1.0 arc second laser beam at the earth array. The beam is narrowed down from 1.0 to 0.1 arc second by positioning the galilean ocular. Step "j" is repeated to evaluate the tracking performance of the 1.0 meter telescope.

n. After the heterodyne communication and atmospheric experiments have been performed, acquisition and tracking will be tried for deep space simulated conditions. Ground laser and space laser power will be reduced to simulate realistic deep space conditions.

4.5.4.2.2 Tracking Loop Test Steps (See figure 4.5.2)

a. With $E_a = E_b = 0$, $\theta_a = 0$, receiver-transmitter boresight loop operating, test combined receiver-transmitter zero-offset, using the Earth Station's beam-pointing error detection apparatus.

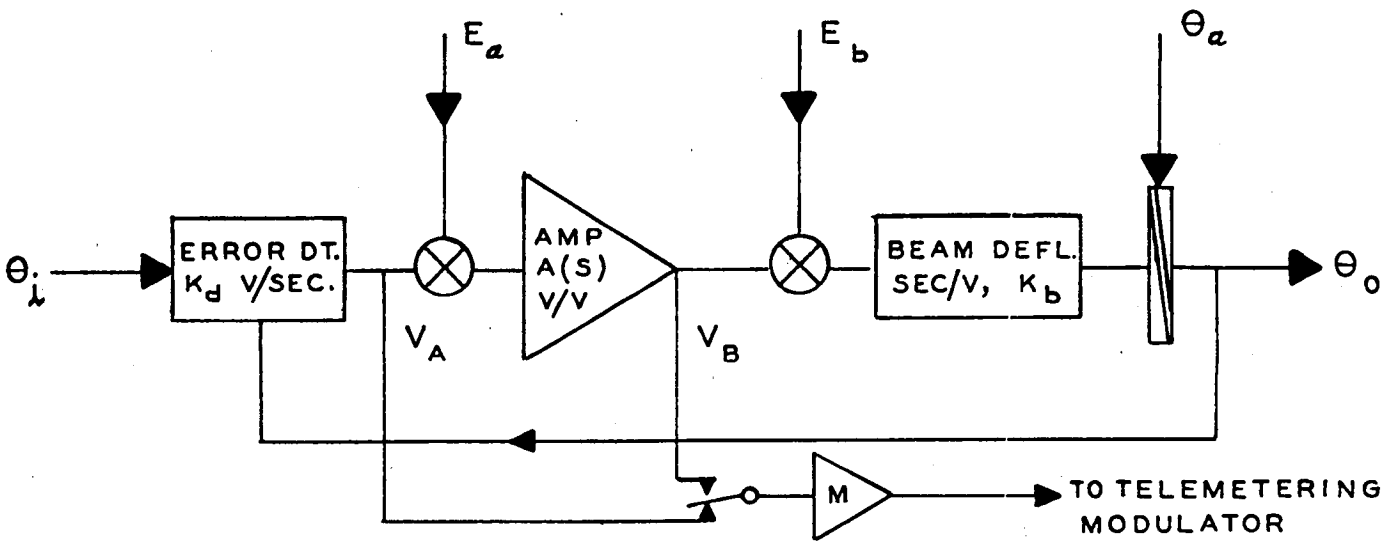

Figure 4.5-2 Block Diagram for Tracking Loop Performance Test

The spacecraft's lead (point-ahead) angle mechanism is set to zero. The overall (Space-to-Ground-to-Space) feedback loop is not closed.

b. With $E_b = 0$, $\theta_a = 0$, vary E_a through programmed range of amplitudes and frequencies (not exceeding the normal operating range of the feedback loop); monitor and telemeter to Earth Station E_a, V_a and V_b. Monitor variation of transmitter beam.

c. With $E_a = 0$, $\theta_a = 0$, vary E_b through programmed range of amplitudes and frequencies (not exceeding the normal operating range of the feedback loop); monitor and telemeter to Earth Station E_b, V_a and V_b. Monitor variation of transmitter beam.

d. With $E_a = E_b = 0$, vary θ_a through programmed range of amplitudes and frequencies (not exceeding the normal operating range of the feedback loop); monitor and telemeter to Earth Station θ_a, V_a and V_b. Monitor variation of transmitter beam.

e. With $E_a = E_b = 0$, $\theta_a = 0$, increase beacon transmitter power from the value heretofore used (which simulates the power density available for deep-space operation).

4.5.5 SUPPORTING ANALYSIS

4.5.5.1 Space Vehicle Acquisition and Tracking of Earth-Station Laser

4.5.5.1.1. Abstract

Numerical values for acquisition and tracking signal-to-noise ratios are presented for a Deep-Space Probe operating against an Earth-based laser beacon, and criteria for simulating conditions from synchronous satellite range are established. Pulse modulation of the beacon may be advisable for acquisition in the deep space case. A discussion of the relative merits of a quadrant photomultiplier tracker versus an image dissector tracker is presented.

4.5.5.1.2 Earth Station Laser Beacon

Operating conditions for the Deep-Space Probe, to be simulated at the synchronous satellite altitude, are based on the assumption that argon laser sources capable of average power output of several hundred watts to 1 KW will become available. The limitation upon the power output is due to heating; thus, if the laser is pulse-modulated, the available peak power is in inverse proportion to the duty cycle.

4.5.5.1.3 Quadrant Photomultiplier Detector Vs. Image Dissector

The relative merits of the image dissector and quadrant photomultiplier will be discussed for the spacecraft laser tracker. Operation of the image dissector is briefly described as follows. Laser light is brought to a focus on the cathode of the image dissector. An electron analog image of the laser is then relayed to the anode. The focused electron image is electrostatically scanned by means of a pair of deflection plates in the x and y directions.

Consider the scan signals along a single axis when a sinusoidal signal is impressed on one pair of deflection plates. When the laser beam is imaged at the center of the scan oscillation, a null signal is present at twice the frequency of scan.

For an offset condition, the signal harmonic content shifts to the fundamental of the scan frequency, and the offset direction can be detected by synchronous phase detection. A serious problem exists however due to a number of tracking conditions which make the image dissector very difficult to implement. As will be shown in subsection 4.5.5.1.6, the levels of earth shine will be highly competitive with the laser signal even after limiting the spectral bandwidth to 1 Å for the deep space case. In fact the earth will be imaged in the focal plane of the detector which will cause an offset balance for the quadrant photomultiplier detection system, especially for a partially illuminated earth. By modulating the laser signal on the ground, the problem of

quadrant unbalance can be overcome. For example, the quadrant photomultiplier signals are processed by a narrow band filter whose center frequency is at the laser modulation frequency and thereby the unbalanced dc earth image is made ineffective. The filter is made wide enough to pass the spectrum of angular disturbances that are to be tracked. As the image is jittered about in the focal plane due to the mechanical disturbances, each detector of the quadrant will "see" an AM signal, provided the carrier frequency is widely separated from that of the spectrum of mechanical disturbances and frequency modulation does not become a problem.

The signal processing techniques ordinarily used for the image dissector trackers will be quite complicated since there will be frequency modulation of the carrier as the image dissector aperture scans across the ground modulated laser image. The signal will require additional multiplexing down from the ground modulated laser frequency to the image dissector scan frequency before standard synchronous detection techniques can be employed. A second difficulty arises as a result of the image dissector scanning across the Earth's limb and terminator as it will appear in the image dissector focal plane. The resulting step signal containing higher harmonics may be confused with the laser signal itself.

A third difficulty arises from the use of pulsing and gating techniques, whereby the laser power is increased inversely as the duty cycle pulse is decreased for the purpose of background suppression. Although a gated mode might be used in acquisition, it could not be used in the image dissector tracking mode since another source of signal modulation would add further to the confusion of the overall signal spectrum.

4.5.5.1.4 Quadrant Photomultiplier Tracker

Assuming that, in a photomultiplier detector, load resistor noise is rendered negligible in comparison with noise due to light background, dark current and noise-in-signal (owing to the intervening dynode gain), the signal-to-noise ratio is given by

$$\frac{s}{n} = \frac{P_s \times S}{\left\{\left[(P_S+P_B)\ S+id\right]\ 2e\,\Delta f\right\}^{\frac{1}{2}}} \qquad (1)$$

where:

P_s is the light signal power striking the photocathode of each of the four photomultipliers at servo null

P_b is the background light power on each of the four photocathodes

i_d is photomultiplier cathode dark current

S is the cathode sensitivity in amperes per watt at the wavelength of interest

e is the charge of the electron

Δf is the bandwidth.

Figure 4.5-3 is a schematic of the quadrant photomultiplier tracker arrangement.

4.5.5.1.5 Acquisition, Deep Space Case

At the start of the acquisition process, the Deep-Space vehicle's angular position is known to the Earth Station to a 3 sigma error of about $\pm$ 22.5 arc-seconds.(1) A beam with divergence of 45 arc-seconds is therefore used at the Earth-Station, to insure illumination. The total power received by the space vehicle at range R, using a telescope with aperture diameter D is

$$P_r = P_t \cdot \frac{4}{\pi (R\theta)^2} \cdot \frac{\pi D^2}{4} \cdot A = P_t A \left[\frac{D}{R\theta}\right]^2 \qquad (2)$$

where:

θ is the divergence of the transmitted beam

A is atmospheric transmission.

for:

$P_t = 10^3$ watts

$R = 1$ AU $= 150 \times 10^9$ meter

$D = 38" = .965$ meters

$\theta = 45$ arc sec $= 0.218 \times 10^{-3}$ rad

A = atmospheric transmission for 4880 Å laser $\approx .7$

$P_r = 6.15 \times 10^{-13}$ watts

(1) G. Strauss, "Study of Laser Beam Pointing Problems", Fourth Bi-monthly Technical Report, No. 000162-4, NASA Contract No. NASw-929, Kollsman Instrument Corp., Elmhurst, N.Y., 15 April, 1965, sec IIa.

The tracking system analyzed here will be a quadrant photomultiplier utilizing a tetrahedral reflecting prism shown schematically in Figure 4.5-3.

Each of the 4 detectors in the quadrant photomultiplier tracker receive the following signal power

$$P_s = M_t \, P_r/_4 \tag{3}$$

where:

M_t = optical transmission factor, includes transmission of tracker optics, collimating optics, 1 Å filter, fine beam deflector and obscuration losses to secondary mirror.

$$M_t = M_{1\text{Å}} \; M_B \; M_P \; M_O$$

where:

$M_{1\text{Å}}$ = transmission of 1 Å filter $\approx .5$
M_B = transmission of fine beam deflector $\approx .75$
M_P = transmission of primary and secondary optics including secondary obscuration $\approx .85$
M_o = optical transmission of refractive elements in galilean ocular, tracker telescope $\approx .8$
$M_t = 5 \times .75 \times .85 \times .8 = .25$

The signal power on each quadrant is

$$P_s = 3.85 \times 10^{-14} \text{ watts}$$

4.5.5.1.6 Background Noise Due to Earthshine

The noise contribution due to background light is evaluated on the basis of Earthshine alone, because the amount of starlight which will appear in the restricted field of view does not begin to compete with the light reflected from Earth. The maximum irradiance from the Earth at the Moon is a function of wavelength.(2) In the vicinity of 4,800 Å, the wavelength

(2) R.A. Rollins, Jr., "Investigation of Optical Spectral Regions for Space Communications", University of Michigan, ASD Technical Documentary Report No. 63-185, May, 1963, figure 54.

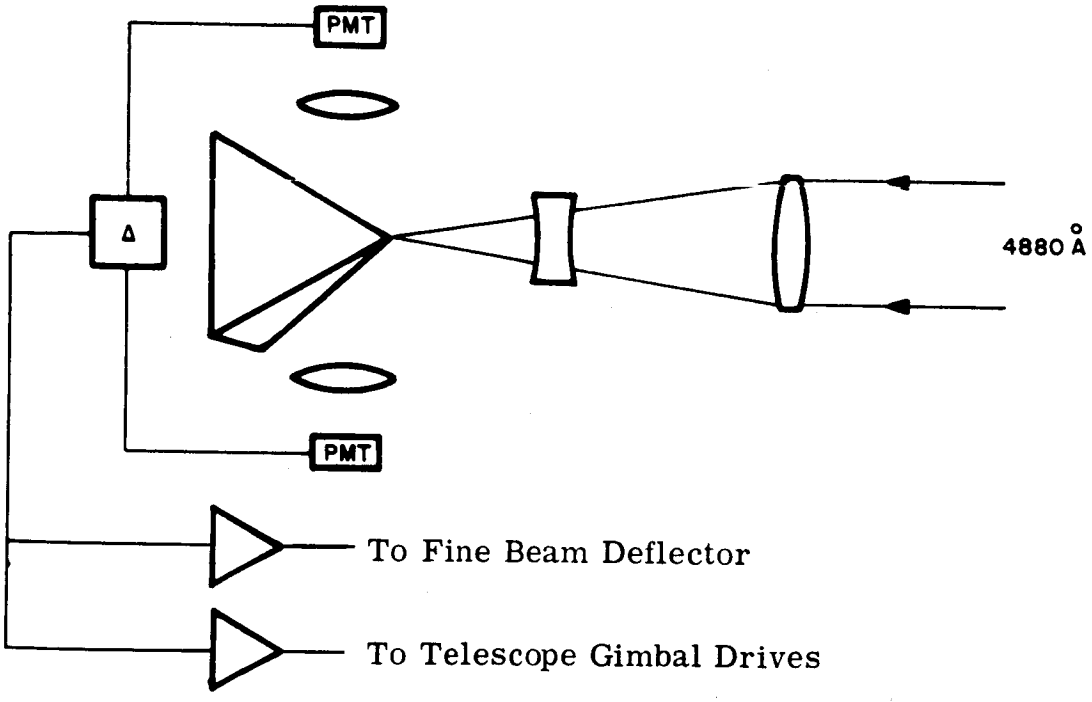

Figure 4.5-3 Quadrant Photomultiplier Space Tracker Configuration

of Argon, it is 2×10^{-5} W/cm^2 - $\mu = 2 \times 10^{-5}$ W/m^2-Å. At the vehicle range of 1 AU, this reduces by the square of the range ratio, $(384 \times 10^6 \text{m}/150 \times 10^9 \text{m})^2$ to 13×10^{-11} W/m^2 -Å. In the case of a Mars mission the vehicle will not view a fully illuminated Earth. In a typical situation, as there pointed out, the angle between space-vehicle, Earth and Sun might be $\beta = 68^\circ$, and the amount of light will be proportional to $\left[(\pi - \beta)\cos\beta + \sin\beta\right]/\pi = 0.516$ times the value calculated above, assuming Earth to be a Lambertian reflector. Each of the four detectors will thus receive.

$$P_b = \frac{13 \times 10^{-11} \text{ Watts}}{\text{m}^2 \text{ Å}} \times \frac{\pi}{4} \times (0.96\ 5\text{m})^2 \times 1\ \text{Å} \times .25 \times \frac{1}{4} \times 0.516 \qquad (4)$$

$$P_b = 2.30 \times 10^{-12} \text{ Watts.}$$

Dark current for the new RCA C 70038D photomultiplier tube (high quantum efficiency) is given as 2×10^{-9} amperes at the anode, with dynode gain of 5×10^4. The corresponding cathode dark current is $i_d = 4 \times 10^{-14}$ amperes. Quantum efficiency at 4,800 Å is 22% and the cathode sensitivity $S = \eta\, e/h\nu$; $e = 1.6 \times 10^{-19}$ coulombs and $h\nu$ at 4,800 Å, is 4.15×10^{-19} Joules; hence S = 0.085 amperes cathode current per watt incident power. The dark current contribution to the noise is $i_d/S = P_d = 4.7 \times 10^{-13}$ Watts.

Using eq (1) with the values calculated above and ΔF = 10 hz, S/N = 0.85. This value is not sufficient for tracking and an earth laser mode with synchronous gating on the space craft may be necessary for the initial acquisition. Reduction of the bandwidth to 1 cps would increase the S/N to approximately 2, which will be sufficient for initial tracking if the mechanical disturbances on board the spacecraft at 1 cps can be restricted to a value less than the initial transmitted laser 1 arc sec beam divergence.

The 1 arc second beam width laser must be received by the earth station, thereby providing a tracking line of sight to the space vehicle, and thus permitting the ground laser to be narrowed down to 6 arc-seconds.

If the Earth Beacon were to use pulse modulation during the acquisition phase, one might, e.g., specify 10 pulses of 1 msec. width per second, for 1% duty cycle, and 100 KW peak power. The error detectors would operate in a gated mode, so as to exclude background noise in the absence of signal; gating signals could be derived by sending a synchronous pulse train up over the microwave system, with pulse sharpening in the vehicle.

The error detector (photomultiplier) circuit would have to have reasonable fidelity, commensurate with the relatively easy accuracy requirements during this stage. Assuming that the 1 msec. pulse width corresponds to twice the circuit rise-time, 10^{-3} sec. = 2 x 2.2 rC, and the bandwidth $\Delta f = 1/2\,\pi rC$ = $4400/2\,\pi$ $\sec^{-1}$ = 700 $\sec^{-1}$. The power received during the pulse is now 100 times the cw power of the previous calculation, and the signal to noise ratio becomes s/n = 9.9, i.e., for the background limited condition (where the noise power in the denominator of eq.1 is essentially due to background noise), increase of peakpower is helpful, since the numerator sees the full effect, while the denominator sees only the square root of the required increase in bandwidth.

This example of pulsed operation does not represent a specific design recommendation; in the event that pulsing must be used, the data rate will have to be made commensurate with the servo bandwidth, in order for the operation to be optimized.

4.5.5.1.7 Tracking, Deep-Space Case

During tracking, the Earth Station will use a transmitter beam with a 3 arc-second beam divergence, and the power density of the vehicle will be multiplied by a factor of 225, assuming the worst case. The signal to noise ratio, when reverting back to the cw laser mode, and increasing the servo bandwidth to 100 hz for ± .05 arc sec tracking, becomes 99. This will be more than adequate for the 0.1 arc second tracking

4.5.5.1.8 Acquisition, Synchronous Satellite Case

At synchronous satellite range, approximately 22 x 10^3 miles, the spectral irradiance due to Earthshine is (3),

$$\frac{2 \times 10^{-5}\ \text{W}}{\text{m}^2\ \text{Å}} \times \left[\frac{238 \times 10^3\ \text{mi}}{22 \times 10^3}\right]^{-2} = 2.34 \times 10^{-3}\ \text{W/m}^2\text{-Å}$$

At the range of the synchronous satellite, 22 x 10^3 mi, Earth (radius = 3.96 x 10^3 mi) subtends 2 $\sin^{-1}$ (3.96/22.0) = 20.8° = 0.364 Radians. The solid angle is $\frac{\pi}{4}$ $(0.364)^2$ = 0.104 Steradian and the irradiance, in terms of spectral power density per unit of solid angle is

$$\frac{2.34 \times 10^{-3}\ \text{Watt}}{\text{m}^2\text{-Å} \times 0.104\ \text{ster.}} = 22.5 \times 10^{-3}\ \text{Watts/m}^2\text{/Å / steradian.}$$

(3) G. Strauss, Ibid.

The amount of earth shine which will illuminate one of the quadrant detectors at the synchronous satellite range with the tracker field of view of 30 $\widehat{sec}$ is

$$P_b = \frac{22.5 \times 10^{-3} W}{m^2 \, \mathring{A} \, ster.} \times \left(\frac{\text{Telescope Rcvg. area}}{\pi/4 \times (.965)^2} \right) \times \left(\frac{\text{Filter Bdwdth} \times \text{Xmission}}{1 \, \mathring{A} \times .25 \times 1/4} \right) \times \frac{\text{Solid angle FOV}}{\pi/4 \times (2.25 \times 10^{-4})^2}$$

$$= 1.1 \times 10^{-11} \text{ watts.}$$

Earthshine simulation from synchronous orbit could be controlled by reducing the field of view of the telescope, but this would require adjusting a diaphragm in the Field of View of the telescope. Rather than introduce a mechanical adjustable stop in the telescope, the laser power on the ground will be boosted in order to simulate the signal to noise ratio rather than the absolute amount of earthshine. A 1 watt argon laser beacon will be available on the ground and during the acquisition mode deep space simulated power density at the space craft would require considerable attenuation by means of reducing the operating power and introduction of neutral density filters at the ground transmission site.

4.5.5.1.9 Tracking, Synchronous Satellite Case

As discussed previously the fine tracking mode of operation requires the ground laser beam to be narrowed down to 6 arc seconds. The attenuation scale factor used for deep space simulation would carry over to the tracking case while the ground laser narrows its beam divergence from 45 $\widehat{sec}$ to 6 $\widehat{sec}$.

4.5.5.2 Continuous Boresighting for Space Vehicle Photomultiplier Differential Gain Control

The quadrant photomultiplier tracker on board the spacecraft is essentially a light balancing device which will track to the center of illumination of the incoming laser light. The quadrant photomultiplier arrangement is a highly efficient device when operating with the low signal levels which will be present for a deep space laser tracking and communications link. Image plane modulation involves interrupting the light by means of an oscillating aperture and then using synchronous phase detection of various harmonic components of the signal as generated by this modulation. Tracking by photometric balancing techniques are usually avoided because of serious problems which arise from detector bias imbalances and photosensor cathode sensitivity non-uniformities. However, the unique optical arrangement of the transmitter-receiver telescope allows for a continuous boresight monitoring mode whereby a feed back loop is implemented to control the overall gain factors in a balanced quadrant photomultiplier arrangement.

A portion of light from the 4880 Å laser used for the spacecraft heterodyne detection scheme is tapped off for utilization in the quadrant photomultiplier gain control feed back loop. Referring to the block diagram of Figure 4.5-4, the laser light is reflected to the tracker optics by means of the pair of beam splitters. The center of the laser image must be precisely positioned on the center of the tetrahedron so that a light null balance is obtained. Thus, error signals which arise in a quadrant pair of detectors, develop as a result of electronic imbalances in the amplification train. The laser beam is amplitude modulated by means of a Sylvania S-2 type polarization modulator. The sinusoidal driving signal on the modulator serves as a reference signal to a synchronous detector whose output will be positive or negative depending on the polarity of gain drift. The dc error out of the synchronous detector, controls the gain of the high voltage supply to one of the bridged pairs of photomultipliers.

The accuracy of centering the laser beam on the pyramidal reflector must be within a 0.1 $\widehat{\text{sec}}$ tolerance as viewed from object space. The effective focal length of the telescope as viewed from the tracker optics to object space is 3450 in. The beam centering accuracy corresponding to 0.1 $\widehat{\text{sec}}$ is 1.7×10^{-3} inches. The angular accuracy of the various components of the boresighting system is not very critical due to the large magnification of the tracking optics. The focal length of the tracker optics separately is 7.15". A beam centering of 1.7×10^{-3} inches provides an overall error tolerance of 50 arc seconds for the auxilliary optical components.

4.5.5.3 Boresighting of Spacecraft Transmitter Laser to the Receiver Optical Axis

4.5.5.3.1 Introduction

A method is described for maintaining accurate parallelism between transmitter zero-lead and receiver optic axes (in terms of the beam pointing configuration) which features separate corrective fine beam deflectors for transmitter and receiver. Use is made of the on-board laser transmitter and the quadrant photomultiplier tracker operating in an intermittent look-through mode. A tracking offset error is developed as a result of misalignment between the tracker and transmitter axes. A feedback loop is closed around the point ahead beam deflector which is initially set to its null position. Offset errors resulting from mechanical misalignments are fed back to the point ahead beam deflector in order to drive the tracker error signal to null. The look-through boresight operation will normally operate prior to the space to earth laser link since a zero point ahead angle is required for this operation.

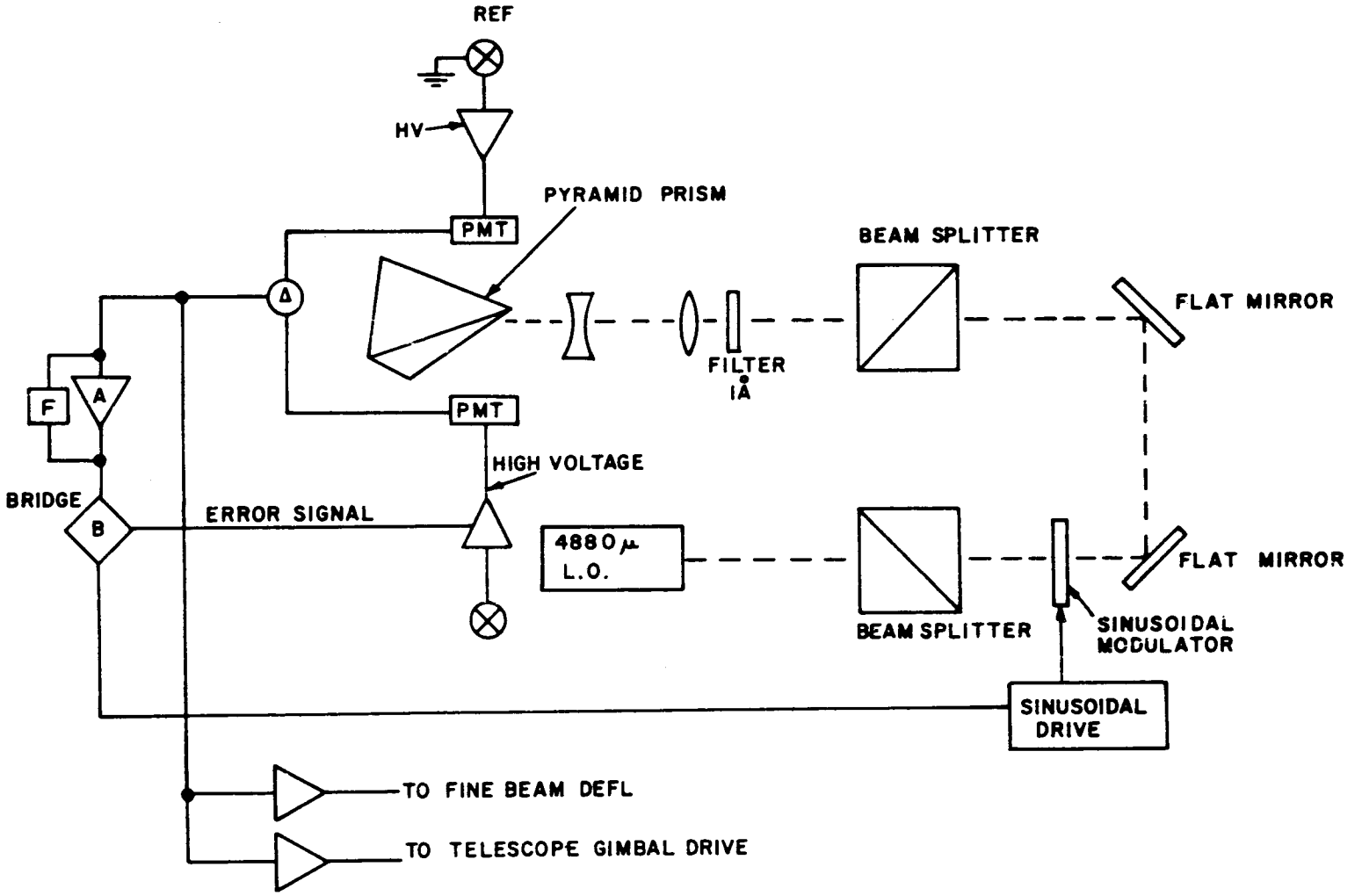

Figure 4.5-4 Continuous Boresighting for Space Vehicle Photomultiplier Differential Gain Control

4.5.5.3.2 Detailed Discussion

Figure 4.5-5 is a block diagram of the transmitter-receiver boresight alignment technique. With the diasporameter set to null, laser light is directed to the flat mirror via the dichroic filter and beam splitter arrangement. The dichroic filter is designed to transmit at 6328 Å, but a small portion ($\sim$.005) of the light will be reflected. When the shutter is opened, the light is directed to the quadrant photomultiplier tracker. The narrow 1 Å filter designed to transmit at 4880 Å will have some tramsmission at 6328 Å, to allow enough light to be detected by the photomultipliers at a single modulated frequency as obtained from the modulator driver. The signal is passed through the narrow band filter-amplifier combination and then synchronously demodulated by means of the bridge and reference signal. The resulting dc signal will be used to servo the lead angle position of the diasporameter, thereby providing null compensation to the respective transmitter and receiver line of sights.

4.5.5.3.3 Available Signal for Boresight Monitoring

A 10 milliwatt 6328 Å laser will be used for the boresight mode. Assuming that a power of 10^{-11} watts per quadrant is sufficient, the required transmission of the 1 Å filter at 6328 Å is to be determined. The optical losses up to the 1 Å filter are,

$$10^{-11} \text{ watts} = \frac{10}{4} \times 10^{-3} \quad w \times T_p \times T_D \times T_{BS}^{3} \times T_{(1\text{Å})}$$

where:

T_P = transmission of polarizer modulator = 0.5

T_D = reflectivity of dichroic in transmission mode = 5×10^{-3}

T_{BS} = .5

$T_{(1\text{Å})}$ = transmission of 1 Å filter at 6328

thus,

$$T_{(1\text{Å})} = 10^{-5}$$

The secondary transmission of the 1 Å filter should be very low with an optical density in the range of 4 or 5.

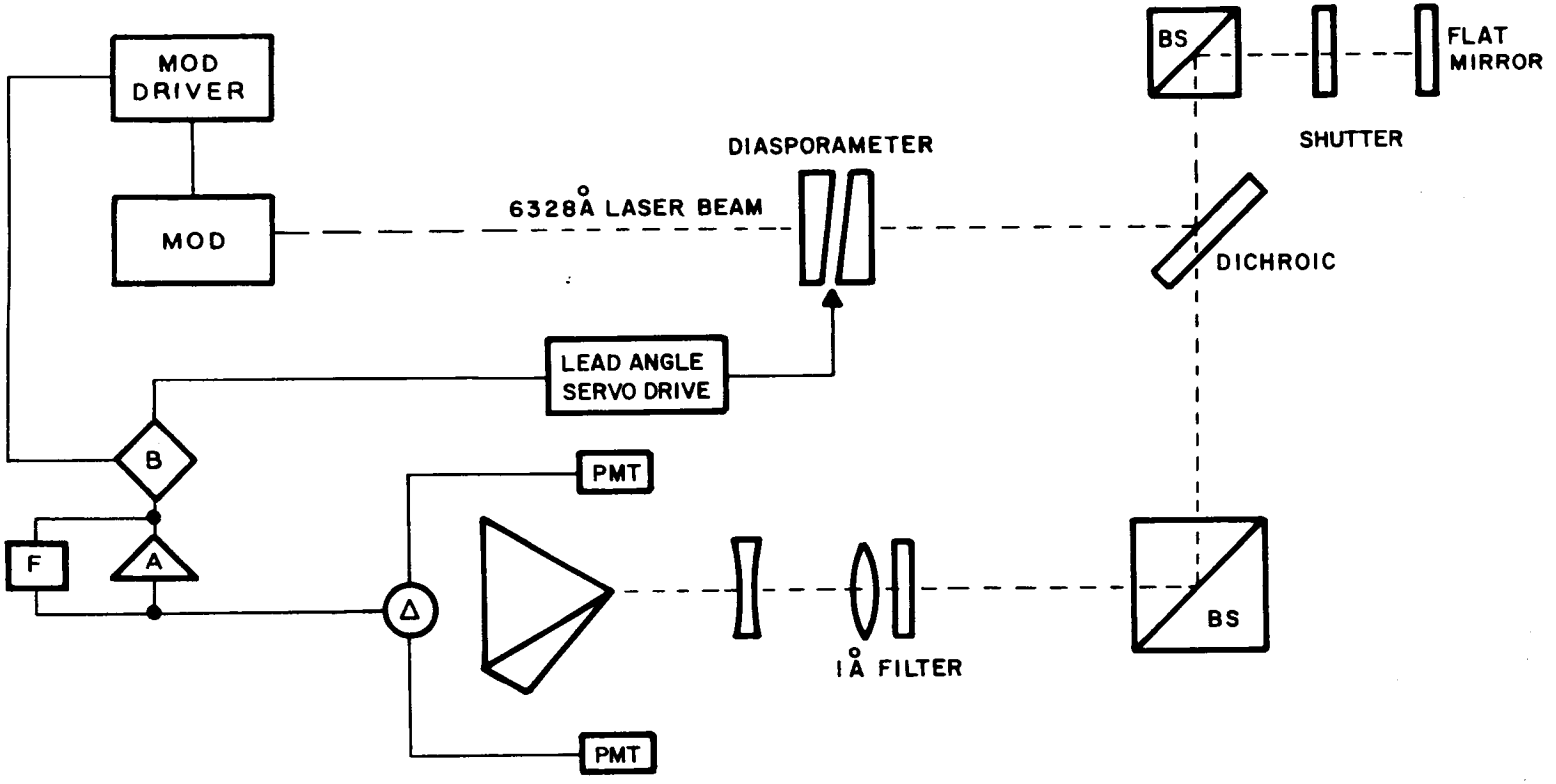

Figure 4.5-5 Intermittent Boresighting for Transmitter Null Lead Angle Control

4.6 POINT AHEAD AND SPACE-TO-GROUND-TO-SPACE LOOP CLOSURE

4.6.1 Summary

In a two-way communications link for deep space missions the relative orbital velocity between the space vehicle and earth, coupled with the long signal transit delays, require that the spacecraft transmitter "point ahead" of the apparent spacecraft-ground transmitter line-of-sight in order that the ground receiver receive the spacecraft transmission. For a typical Mars fly by the lead angle will be on the order of 40 arc-seconds near the terminal phase. Continuous and accurate reception from the spacecraft requires that the point ahead be referenced to the coordinate reference frame established in the Precision Tracking of a Ground Beacon experiment. The "point ahead" precision requires that control be effected through a closed space-to-ground-to-space feedback loop. Perturbations due to spacecraft disturbances must be compensated: low frequency disturbances by spacecraft and telescopic control; high-frequency disturbances by beam (deflector) control within the telescope.

Several types of optical detection at the ground receiver will be investigated. Heterodyne detection involves use of a matrix of small telescopes and a local laser oscillator signal beating against the incoming signal in each telescope. Direct detection methods, one using a 4 photon bucket arrangement and a second using a single photon bucket with a conically scanned laser beam, are being considered. Image dancing due to atmospheric disturbances operating in a manner analogous to that discussed in the summary of the Precision Tracking of a Ground Beacon experiment, impose the need for testing "point ahead" under the actual condition of a space mission, here proposed at synchronous altitude.

4.6.2 Experiment Objective

The purpose of this experiment is to close the loop around the equipment in the Precision Tracking of a Ground Beacon experiment (subsection 4.5) and to evaluate the effect of the space-to-ground-to-space loop closure on overall tracking and pointing performance. Transit time delays corresponding to ranges of 1 astronomical unit are to be simulated; the effects of Earthshine are to be evaluated.

4.6.3 Experiment Justification

4.6.3.1 Contribution and Need

The trajectories of interplanetary missions exhibit relative displacements and velocities between the spacecraft and the Earth based ground station such that the difference in angle between the apparent line of sight from the spacecraft to Earth and the direction of the axis of the communication beam becomes appreciable. That is, to have the down beam from the spacecraft received at the ground station requires that the axis of the down beam must be pointed ahead of the apparent ground station position. The angle between the apparent line of sight to the ground

station and the down beam axis will be on the order of forty arc seconds when the spacecraft is near Mars. With laser beam divergences ranging from 0.1 arc seconds to 2.5 arc seconds, depending on choice of wavelength and transmitting aperture, the need for accurate point ahead prediction and implementation becomes manifest.

The advantages of laser communications cannot be adequately utilized in interplanetary space programs unless the point ahead capability can be attained to the required accuracy. The required accuracy is that which will maintain the space transmitted laser beam within the half power points of the Earth receiver array. The experimental investigation of this point ahead capability is an essential complement to the Precision Tracking of a Ground Beacon experiment.

4.6.3.2 Need for Space Testing

The point ahead capability is dependent upon the accurate instantaneous determination of the relative motion and orientation between the spacecraft and the ground station. Perturbations of the apparent line of sight and the direction of the down beam will be produced by atmospheric fluctuation and mechanical disturbances of the spacecraft/telescope structure. Atmospheric effects will superimpose perturbations on the upcoming laser beam. It would appear to be impossible to achieve accurate pointing for altitudes less than approximately 2,000 miles because atmospheric fluctuations produce, at lower altitudes, unacceptably large amounts of noise in the apparent line of sight. See also subsection 4.5.3.2.

4.6.3.3 Feasibility

The environment of a synchronous Earth orbit appears to be highly suitable for the subject experiment and to realistically exercise the deep space communications capability of laser communication systems. The methods proposed for the performance of the experiment are common and well within the state-of-the-art. Though the magnitudes of each of the many factors contributing to the inaccuracy in point ahead control may not be isolated, it is feasible that the overall capability in pointing control over a suitable range of operability be investigated.

4.6.4 Implementation

4.6.4.1 Experiment Design

4.6.4.1.1 Experiment Concept

A laser communications link between a spacecraft and an earth station (s), using narrow beamwidth transmission and directionally sensitive receivers (telescopes), requires very accurate tracking and pointing. Because of the relative motion between spacecraft and earth at large distances (1 AU), the lines of sight between spacecraft and a ground beacon transmitter and between spacecraft and ground receiver can differ by as much as 40 arc

seconds. The spacecraft reference line is established by having the beacon illuminate the spacecraft and then having the spacecraft track the beacon. PRECISION TRACKING OF A GROUND BASED BEACON is another experiment (subsection 4.5); and, although reference to specific subsections of that experiment presentation will be made here, that experiment must be performed before implementing the point ahead operation.

For the ground based receiver system three possible detection techniques will be discussed which use signal intensity (gradient) measurements to determine the pointing error (with respect to the receiver) of the spacecraft laser beam. A pointing correction will be telemetered to the spacecraft in the form of digitized altitude, azimuth angular commands.

4.6.4.1.2 Acquisition & Tracking of Ground Beacon

Initially the ground beacon directs its transmission at the spacecraft in accordance with Deep Space Information Facility (DSIF). The spacecraft telescope images the beacon signal and tracks the beacon. A planet tracker will assist the telescope in acquiring the beacon. Two spacecraft telescopes with different fields of view and tracking precision are proposed. These units are independently gimballed to the spacecraft. A .3 meter telescope with a field of view of 1.5 arc minutes will track to $\pm$ .15 arc seconds, provided the beacon beamwidth is in the neighborhood of 3-6 arc seconds. A 1.0 meter telescope with a field of view of .5 arc minutes will track to $\pm$ .05 arc seconds. (See subsection 4.5.4.1.3) Fine tracking and pointing of these telescopes requires that high frequency perturbations be compensated by elements internal to the telescope, (see subsection 4.5.4.1.4).

The beacon tracking system on board the spacecraft consists of a coarse and a fine servo system. The coarse system is a low frequency response system which controls the pointing direction of the gimballed telescopes. The fine system is a relatively high frequency response system which controls the placement of the beacon image on the image plane of each telescope. Deviation of the beacon image from the center of the image plane will produce an error signal, which after passing through a differential amplifier, will be used to drive two orthogonal sets of beam deflectors in such a way as to center the image. The driving signal will be a measure of the displacement of the line of sight from the telescope axis. This driving signal will represent closely the mean direction and the perturbations of the line of sight produced by atmospherics and structural flexure and vibration.

4.6.4.1.3 Closed Loop Pointing Control of Spacecraft

To simulate the point ahead situation of a Mars fly-by (40 arc seconds) from synchronous orbit requires a 4 mile separation between the ground based beacon and the ground receiver. In an actual fly-by the two would be co-located. Initial point ahead angles on the spacecraft will be

derived through telemetered commands from the ground station. The spacecraft laser beam must be received by the earth station before initiation of the space-to-ground-to-space feedback loop. Figure 4.6-1a depicts the 1.0 meter telescope with the transmission components highlighted.

A second major servo loop in this experiment provides for correction of the direction of the down beam by means of transmitting the error in beam pointing, as measured at the ground station, up to the spacecraft. Closing this correction loop through the ground station provides simultaneous correction in the up beam, as well as the down beam. This space-to-ground-to-space loop closure provides a measure of the error in prediction and control of the down beam (and up beam) pointing. Operation of this feedback loop with its inherent delay of several minutes when operating at Earth-Mars distances, the ability to detect beam pointing error on the order of a small fraction of the beamwidth and the realizable degree of error control are prime items of interest. Since the actual delay to the satellite in synchronous orbit is only a fraction of a second, tape recorders with controllable separation between write and read heads can be used to simulate transmission delays of up to eight minutes one way.

Appendix I-1 in the OTAES Interim Report (1) indicates the effect of this delay upon realizable feedback loop performance. One of these delays would be inserted between the error encoder and the telemetering modulator, and would, consequently, affect the forward transfer as well as the overall loop, simulating the transmission delay of the error command. The other would simulate the delayed effect of the correction (from the satellite down) by storing the error measurement for eight minutes before utilization. The validity of this implementation must be verified by further analysis. The major advantage of this method lies in the fact that it permits (if valid) the testing of a realistic embodiment of the space-to-ground-to-space feedback loop, as a future interplanetary probe might see it.

4.6.4.1.4 Beam Pointing Error Detection

Three possible methods of beam pointing error detection are being investigated.

4.6.4.1.4.1 Distributed Telescope Array

A distributed telescope array type of detector, described in subsection 4.6.5.3 and shown in Figure 4.6.5.3-1 consists of a suitable mosaic of small telescopes, typically 5-inch diameter, consistent with the largest aperture permitting reception of coherent optical signal through the atmosphere without degradation of wavefront. Each of the telescopes thus will permit coherent reception (using local oscillator power from a

(1) Interim Progress Report, Optical Technology Apollo Extension System, CCSD, March 8, 1966, Vol. IV

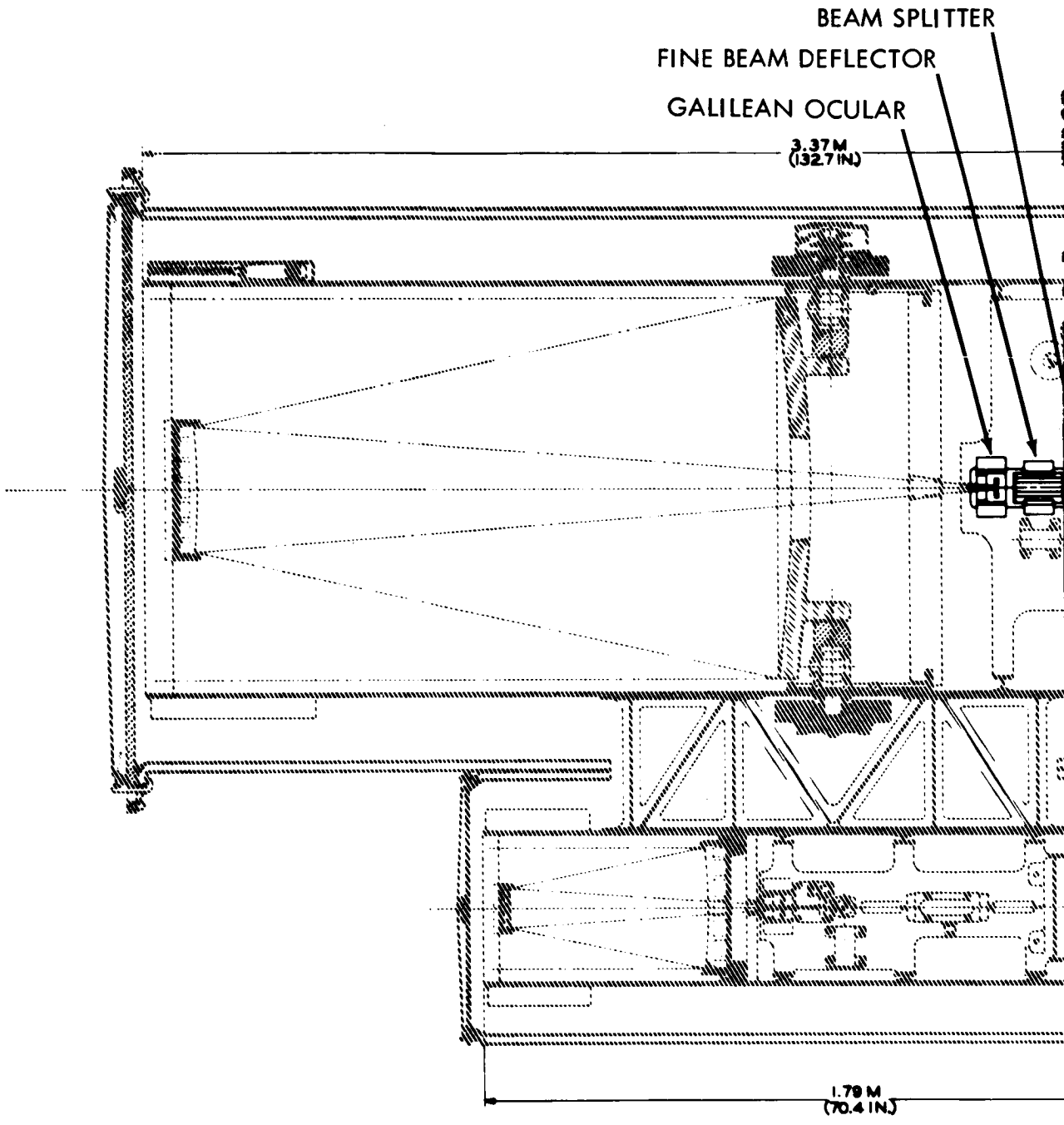
BEAM SPLITTER
FINE BEAM DEFLECTOR
GALILEAN OCULAR
3.37 M
(132.7 IN.)
1.79 M
(70.4 IN.)

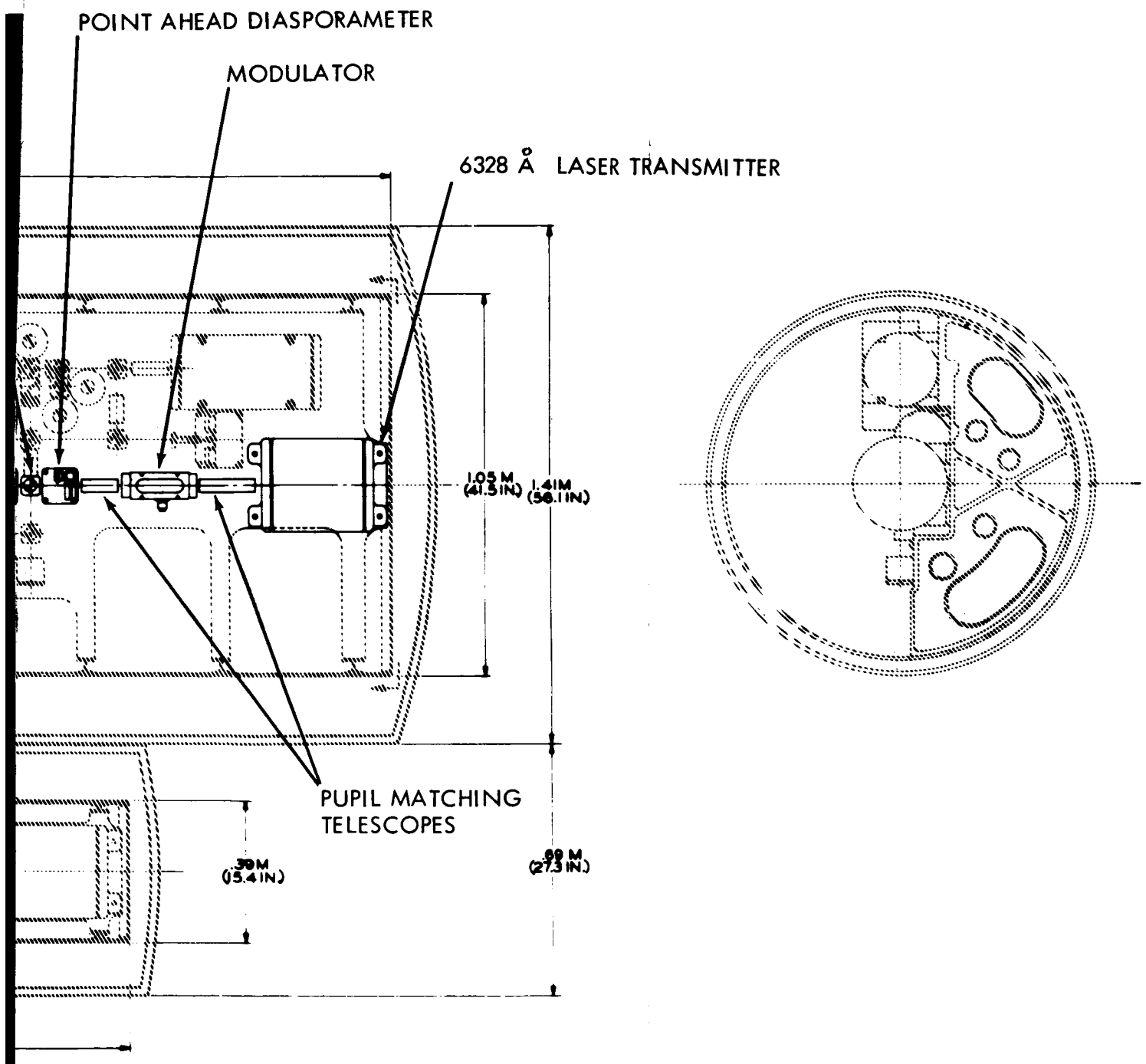

Figure 4.6-1a. 1.0 Meter Telescope Transmission Section

~~1-259~~

1-254

common supply) of signals from a deep-space-craft, or, for the purpose of the proposed test, from the satellite. Two axis signal-splitting behind each telescope permits angle tracking, with error measurements of the 100 (typically, for a full-dress, deep-space link) averaged over the entire aperture. The angular uncertainty of the spacecraft's (or satellite's) position due to atmospheric fluctuation, typically about 2 arc seconds for a 5-inch aperture and reasonable zenith angle, is thus reduced by the square root of the number of individual measurements. Temporal smoothing can be used to reduce the error further. Beam pointing error is detected by comparing sum signals received in top and bottom halves, as well as left and right halves of the array. Although the slope of signal strength versus distance does not develop much error signal across the (typically) 5-foot width of the array, the analysis in subsection 4.6.5.3 shows that, by use of 5-second time integration, a 1/10 beamwidth pointing error can be measured with about 50 per cent confidence for a typical 0.1 arc-second beam.

4.6.4.1.4.2 Multiple Large Aperture Array

The second candidate configuration for the beam pointing error measurement features an array of four to five relatively large receiving apertures, not necessarily of astronomical quality, arranged on a square whose size corresponds to the subtense of the 3-db beamwidth (about 50 feet, for a 0.1 arc-second beam coming from 22,000 miles). The larger horizontal extent permits appreciably higher error sensitivity then the 5-foot array promises, but subtle differences in sky overcast over a relatively large area may cause spurious error measurement. Pointing here, is again found by comparing signal levels across diagonals of the square, top to bottom and left to right. Use of the larger telescope offers no improvement in coherent reception over the same number of small telescope apertures.

4.6.4.1.4.3 Single Large Photon Collector

The third candidate configuration uses a single large (non-astronomical quality) telescope as a photon collector. Angular modulation of the satellite's beam must be used to generate error information, such as the conical scan familiar from tracking radar. Depending upon the value of nutation angle used (the angle between the axis of the cone and the locus of instantaneous beam position centers), the error sensitivity may be fairly high, because the slope of signal intensity versus unit distance at the ground now corresponds to the skirt rather than the peak of the beam, but signal power is also sacrificed, by the same token. Error signals are, in this case, sinusoids at the frequency of the conical scan, whose phase is compared with that of a reference oscillator used to control the scan. Beam pointing measurement by detection of a conically scanned laser beam is discussed in subsection 4.6.5.4.

4.6.4.1.5 Implementation of Point Ahead

The actual lead angle required, about forty seconds of arc, can readily be simulated from a synchronous equatorial satellite, by physical separation of the Earth's transmitting and receiving installations of approximately four miles. The receiving installation, which maintains angle-track on the satellite, must, of course, communicate accurate angle information to the transmitter, in order to enable it to keep the satellite illuminated.

It is anticipated that the point ahead experiment will be conducted after tracking capability has been tested and verified. In order to co-locate the earth station receiver and transmitter, the initial point ahead bias must be maintained to allow for the tangential velocity difference at synchronous orbit and ground. At the start of the point ahead test, the Earth station will command the point ahead mechanism to slew over the amount required to hit the new receiver, some four miles away.

It can be seen that, for the proposed mechanization, the overall loop is inextricably interwoven with the point ahead operation; the space-to-ground-to-space loop closure thus represents an integral part of the point ahead experiment, rather than a separate demonstration. Nevertheless, it would be of interest to open the feedback loop during the test (for periods that would have to be determined experimentally, gradually increasing), to see how far and how fast the transmitter beam will wander off the target without the benefit of correction.

The idea underlying the major portion of loop testing is the same one as in the PRECISION TRACKING experiment, namely that of introducing calibrated disturbances at several points of the loop. Amplitude and frequency of the disturbance, as well as that of the response are either metered on the ground, or monitored in the satelite and relayed back to the ground station. Overall loop performance, as well as the functioning of individual blocks, will be considered. It should also be possible to adjust the loop gain by controlling the sensitivity of the error detector (volts per arc second), the scale factor of the analog-to-digital converter (pulses per second per volt) at the ground station, or the scale factor of the digital-to-analog converter, via telemeter control (Figure 4.6-1b).

4.6.4.2 Operational Procedure

The nature of this experiment is such that it is anticipated that little or no benefit may accrue from manual operation or intervention. Except for the functions of equipment monitoring, replacement and possibly repair, it may be said that this experiment is designed to show a capability in pointing which must be attained in spite of man produced disturbances rather than because of the presence of spacecraft occupants. The magnitudes and spectral characteristics of the control functions are largely beyond the response capabilities of the human operator. The operational procedure may be outlined by the following ordered sequence of tasks.

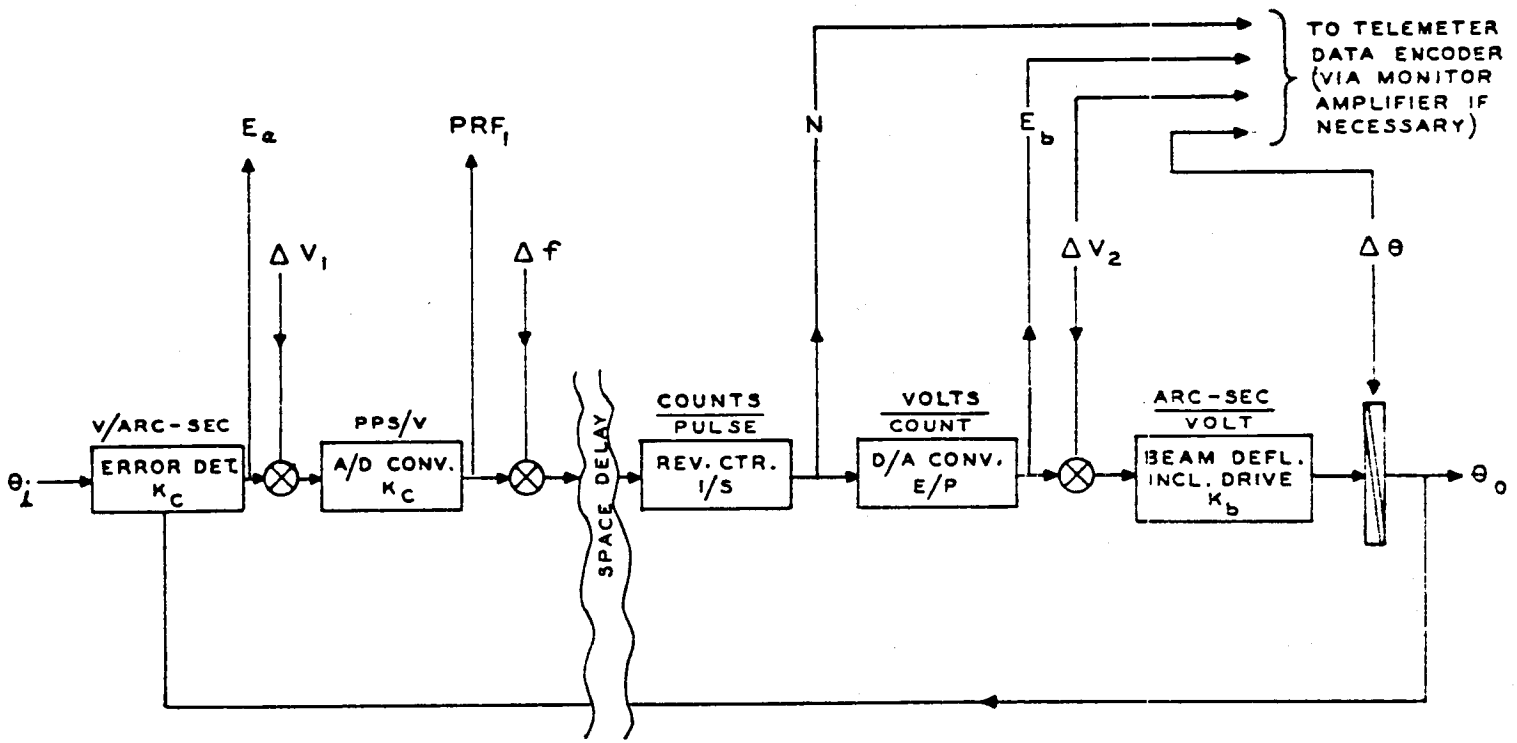

Figure 4.6-1b. Analytical Model Space-To-Ground-To-Space Feedback Loop for Point-Ahead Experiment

a. After acquisition of the beacon and stabilization of the spacecraft, and upon command by ground control, via the beacon or microwave link, the diasporameter is actuated so as to point the down beam ahead by the appropriate pre-calculated amount.

b. The error in down beam pointing angle is measured at the ground based receiver complex both with and without vibration compensation on the down beam and with and without suspension of normal movement of the spacecraft occupants.

c. With the space-to-ground-to-space loop closed, task b is repeated and the difference between calculated point ahead angle and error controlled point ahead angle is measured for one way time delays ranging from the actual transit time between ground station and the spacecraft up to 8 minutes.

d. With the space-to-ground-to-space loop open, task b is repeated with the addition of the introduction of controlled disturbances into the variously indicated functional blocks of the point ahead control system to determine what combination of factors define the domain of adequate pointing performance.

e. With the space-to-ground-to-space loop closed, task c is repeated with the introduction of controlled disturbances as indicated in task d to define the domain of adequate pointing cycle.

4.6.5 Supporting Analyses

4.6.5.1 Accuracy Requirements for Reference Axes

The mathematical analysis of lead angle computation for aberration and transit time corrections is given here with numerical values corresponding to a Mars Fly-By trajectory.

Typical values range from about 10 arc seconds at the beginning of the mission to about 40 arc seconds at fly-by.

The space vehicle is stabilized by means of the Sun Sensor and the Canopus Tracker. Assume that the initial Search-Acquisition process as previously described has been carried out using the DSIF, the Earth Station beacon, and the space vehicle beam pointing system. It is further necessary to use a precision celestial sensor to provide half of the Reference Axes, tracking on Canopus, for example, with the other half provided by the space vehicle track to Earth.

A preliminary analysis of the precision needed for the Reference Axes' celestial sensor may be derived as follows, see Figure 4.6.5.1-1. The space vehicle track to Earth Station coincides with the Y-axis, and the X-Z plane is the plane at right angles to the tracker LOS to Earth (established by the closed loop). The space vehicle transmitter beam is directed along vector OP at an azimuth angle α and an elevation angle β (in spherical polar coordinates). These angles represent the components of the space vehicle to Earth transmission lead angle, and for $r = 10^8$ miles, $\alpha = 40$ arc second, $\beta = 0.2$ arc second, approximately.

The precision celestial sensor is used to determine the X-Y plane (i.e., the Z-axis). This might be the projection of the LOS to Canopus on the X-Z plane perpendicular to the LOS to Earth (Y-axis). It is assumed for this analysis that the LOS to Earth is errorless.

The analysis below shows that a 50 arc second error about the other reference axis (i.e., the Z-axis) is equivalent to a coordinate rotation about the Y axis. At a range of 100 million miles, the azimuth error is 5×10^{-8} radians which is one tenth of the 0.1 second laser beam width. The elevation angle is negligible. These error angles are small because the lead angles themselves are small, yielding small displacements of the radius vector OP at Earth.

It is clear that the geometry of the closed loop tracking to Earth dilutes the requirement for extreme precision in celestial sensors which might otherwise be required for an open-cycle system. This analysis will eventually be modified to include the effects of "In Vivo" atmospheric propagation in the loop, but it is not expected that the results for the space vehicle configuration will be significantly affected.

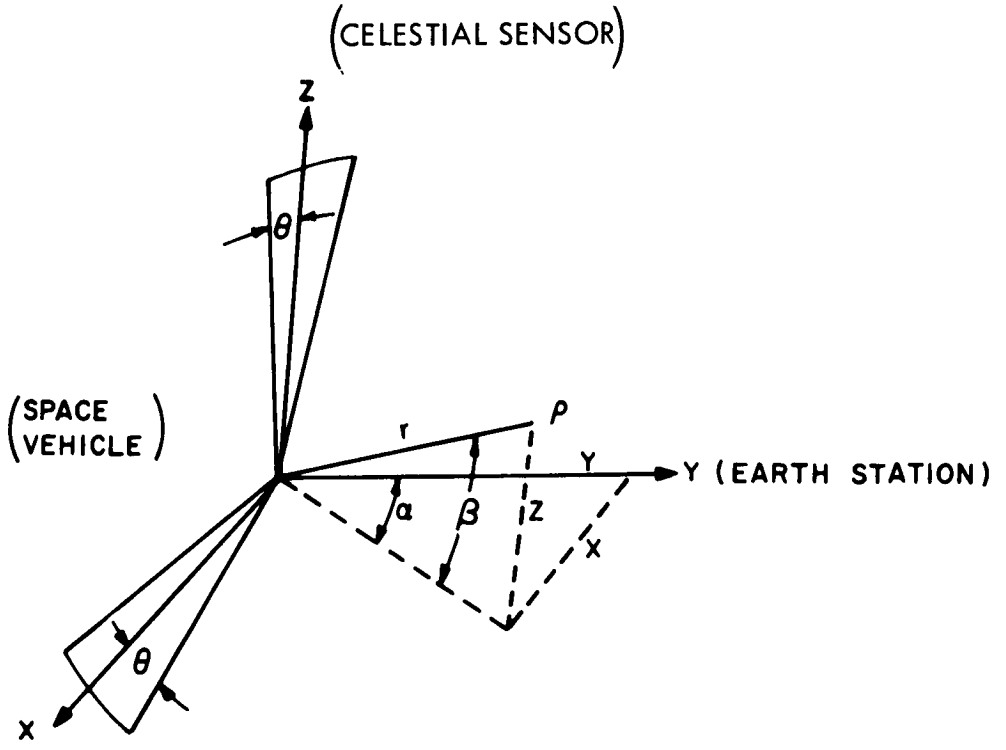

Figure 4.6.5.1-1 Reference Axes

Coordinates

$r = 10^8$ miles (Range)

$\alpha = 40\widehat{\text{sec.}} = 2 \times 10^{-4}$ rad. (Lead angle)

$\beta = 0.2\widehat{\text{sec.}} = 10^{-6}$ rad. (Lead angle)

$x = r \cos \beta \quad \sin \alpha = r\,\alpha = 2 \times 10^4$ miles

$y = r \cos \beta \quad \cos \alpha = r = 10^8$ miles

$z = r \sin \beta = r\,\beta = 10^2$ miles

Coordinate Rotation

$z^1 = z \cos \theta - x \sin \theta = z - x\,\theta,$

$x^1 = z \sin \theta + x \cos \theta = z\,\theta + x,$

thus:

$z^1 - z = -x\,\theta.$ Therefore, $\Delta Z = -x\theta$

$x^1 - x = z\,\theta.$ Therefore, $\Delta x = z\theta$

x is the equivalent displacement of the beam along the Z axis as projected to earth and for α = 40 arc seconds, $x = 2 \times 10^4$ miles.

$x \cdot \theta$ will be the error displacement of the beam in miles for the perturbation about the Z axis. For a perturbation of the lead angle corresponding to one-tenth of the beam width $d\alpha = 5 \times 10^{-8}$ rad, the permitted error in θ is as follows:

$$x \cdot \theta = r\,d\alpha$$

$$\theta = \frac{10^8 \times 5 \times 10^{-8}}{2 \times 10^4} = 2.5 \times 10^{-4} \text{ rad.}$$

$$\theta \approx 50\widehat{\text{sec.}}$$

4.6.5.2 Heterodyne Detection of Spacecraft Laser

4.6.5.2.1 Basic Analysis

Superheterodyne detection makes it possible to realize the optimum signal-to-noise ratio (corresponding to noise-in-signal alone) by lifting a weak signal above locally generated noise arising from background light, photodetector dark current and thermal agitation in the resistive load circuit of the detector. Post-detection signal power and the component of noise due to the local oscillator current are both proportional to the local oscillator power.

The signal to noise ratio for optical heterodyne detection is developed as follows:

$$\overline{i_{ac}^2} = 2 \left[\frac{P''^2_r}{P_{LO}}\right] i_{dc}^2 = 2 P_r'' P_{LO} \left[\frac{\eta e}{h\nu}\right]^2 \quad (1)$$

where:

i_{ac} = average ac current
P_r'' = received signal power
i_{dc} = dc current
P_{LO} = power in local oscillator

The relationship between dc current and power on the detector assuming $P_{LO} \gg P_r''$ is

$$i_{dc} = \frac{\eta e \ P_{LO}}{h \nu}$$

where:

η = quantum efficiency of photodetector
h = Planck's constant = 6.63×10^{-34} joule - sec
ν = frequency of light = 4.74×10^{14} hz for 6328 Å helium-neon laser
e = charge of electron = 1.6×10^{-19} coulombs

The noise current arising from various local sources is given by:

$$\overline{i_n^2} = \overline{i_{dc}^2} + \overline{i_{dk}^2} + \overline{i_{th}^2} + \overline{i_B^2}$$

where:

$\overline{i_{dc}^2} = 2 e i_{dc} \Delta F$ (Local oscillator current noise)

$\overline{i_{dk}^2} = 2 e i_d \Delta F$ (phototube dark current noise)

$\overline{i_{th}^2} = 4 KT \Delta F/r$ (thermal current noise)

K = 1.374×10^{-23} joules/^oK

T = absolute temperature ^oK

r = load resistor

$\overline{i_B^2} = 2e i_b \Delta F$ (current noise generated by background induced current, i_b)

In the numerical example given in the following subsection it will be shown that local oscillator induced photo current $i_{dc} >> i_{dk} + i_{th} + i_b$ and signal to noise reduces to:

$$S/N = \frac{\overline{i_{ac}^2}}{i_N^2} = \frac{N P_r''}{h \nu \Lambda F}$$

which is the post-detection signal-to-noise power ratio corresponding to noise-in-signal alone.

Signal to noise ratios will be calculated for a 1 AU deep space mission. The attenuation factor for simulation of the deep space case from synchronous orbit will be given.

4.6.5.2.2 Signal Power

The signal power incident at the receiving aperture of diameter D centimeters, efficiency M from a source at range R, with P_t watts peak power and beam cross-section 0 is

$$P_r = P_t \, MD^2 / (R\Theta)^2 \text{ watts}$$

Atmospheric attenuation reduces this amount of power to

$$P_r' = \eta \, P_r$$

The factor η is largely a function of zenith angle for a specific wavelength. Quantity P_r' is divided into four parts by a pyramidal prism of optical efficiency M and the amount of light power available for each of the four photo-detectors is $1/4 \, P_r$

$$P_r'' = 1/4 \, M\eta \, P_t \, D^2 / (R\Theta)^2$$

The numerical values for the above equation are:

$M = \eta = .5$
$P_t = 1$ watt
$D = 5" = 12.7$ cm
$R = 1$ AU $= 150 \times 10^{11}$ cm
$\Theta = 0.1$ arc sec $= 0.485 \times 10^{-6}$ rad.

Thus,

$$P_r'' = 1.85 \times 10^{-13} \text{ watts}$$

With optical heterodyning, the energy is divided by a factor of m' = 0.5

$$m' \, P_r'' = .93 \times 10^{-13} \text{ watts}$$

4.6.5.2.3 Noise Contributions

Local oscillator power is $P_{LO} = 5 \times 10^{-3}$ watts, resulting in

$$i_{dc} = \eta \, e \, P_{LO}/h\nu = 1.28 \times 10^{-3} \text{ amperes}$$

The dark current for the L4501-L4504 series of (Philco) photo mixer photodetector diodes is several orders of magnitude smaller than the dc current due to the local oscillator and can be neglected.

The background power is given by

$$P_b = \beta_d \, \Delta \lambda \, \Omega \, \pi D^2/4 \, mm'/4$$

where:

$\beta_d = 16 \times 10^{-8}$ watts/CM^2- ster-Å
$\Delta \lambda = 132 \times 10^{-6}$ Å
$\Omega = 25 \times 10^{-10}$ sterad (10 arc-sec FOV) and
$m = m' = 0.5$.

Thus, the background power is $P_b = 1.7 \times 10^{-18}$ watts

Compared with the $h\nu\Delta F$ term of the local oscillator which is

$$31.5 \times 10^{-20} \text{ Joules} \times 10^7 \text{ cps} = 3.15 \times 10^{-12} \text{ watts}$$

the background contribution to noise can indeed be neglected.

4.6.5.2.4 Post Detection Signal-to-Noise Power Ratio

The post detection signal-to-noise power ratio is

$$S/N = \frac{\eta P_r''}{h\nu\Delta_F} = \frac{0.5 \times .93 \times 10^{-13} \text{ watts}}{3.15 \times 10^{-12} \text{ watts}} = .015 \text{ for each individual telescope.}$$

Use of 100 telescope apertures multiplies the available signal power and the post-detection power signal-to-noise ratio by 100; for tracking purposes, a further improvement accrues from the reduction in bandwidth, 10^7 cps (at the IF level) to 10 cps (at the servo level), bringing S/N up by another factor of $\sqrt{\Delta f / \Delta f \text{ (servo)}}$ or 1,000. The tracking signal-to-noise ratio for the individual 5" telescope is therefore 0.015 x 1,000 = 15, at R = 1 AU.

4.6.5.2.5 Signal-to-Noise Simulation from Synchronous Orbit

The laser power on board the spacecraft is 10 m watt at 6328 Å. Optical losses are mainly due to the dichroic filter, the fine beam deflector and the obscuration from the secondary mirror. Through optical design the distribution of light across the laser beam can be changed from a gaussian intensity profile to a uniform profile, thereby reducing the loss arising from secondary obscuration. An optical transmission factor of 0.75 will allow 7.5 mw of laser power with a beam spread of 0.1 arc seconds from the 1.0 meter telescope. With atmospheric attenuation of 0.5, the power density on the receiving aperture is

$$P_r'' = 1/4\ m\ \eta\ P_t\ D^2/(R\theta)^2$$

where:

$P_t = 7.5 \times 10^{-3}$ watts
η = atmospheric attenuation = 0.5
$R = 3.84 \times 10^8$ meters
$\theta = 5 \times 10^{-7}$ rad.
$m = 0.5$
$D = .125$ meters

The power incident on each photodetector is

$$P_r'' = 2.16 \times 10^{-10} \text{ watts}$$

The incident power available is approximately a factor of 1,200 greater than for the deep-space case. Since 16 telescopes will be used for spatial averaging as opposed to 100 telescopes for the deep-space case, the alteration factor for proper simulation is .16 x 1200 = 192

4.6.5.3 Earth Station Beam Pointing and Angle Tracking by Use of a Distributed Telescope Array

4.6.5.3.1 Telescope Array

A pictorial representation of the earth station array is shown in Figure 4.6.5.3-1. The total array comprises 16 telescopes, each 5" in diameter. For tracking a deep space vehicle the array would be mounted on an equatorial mount in order to compensate for earth rotation. In the case of tracking a synchronous orbiting satellite, it will be necessary to correct for earth's rotation on the space vehicle telescope and the ground array needs only a limited angular gimbal mount. Each of the 5" telescopes acts as a coherent receiver by virtue of mixing the incoming signal with that of a local oscillator to provide superheterodyning. The coherent receivers function as spectral filters to eliminate background radiation.

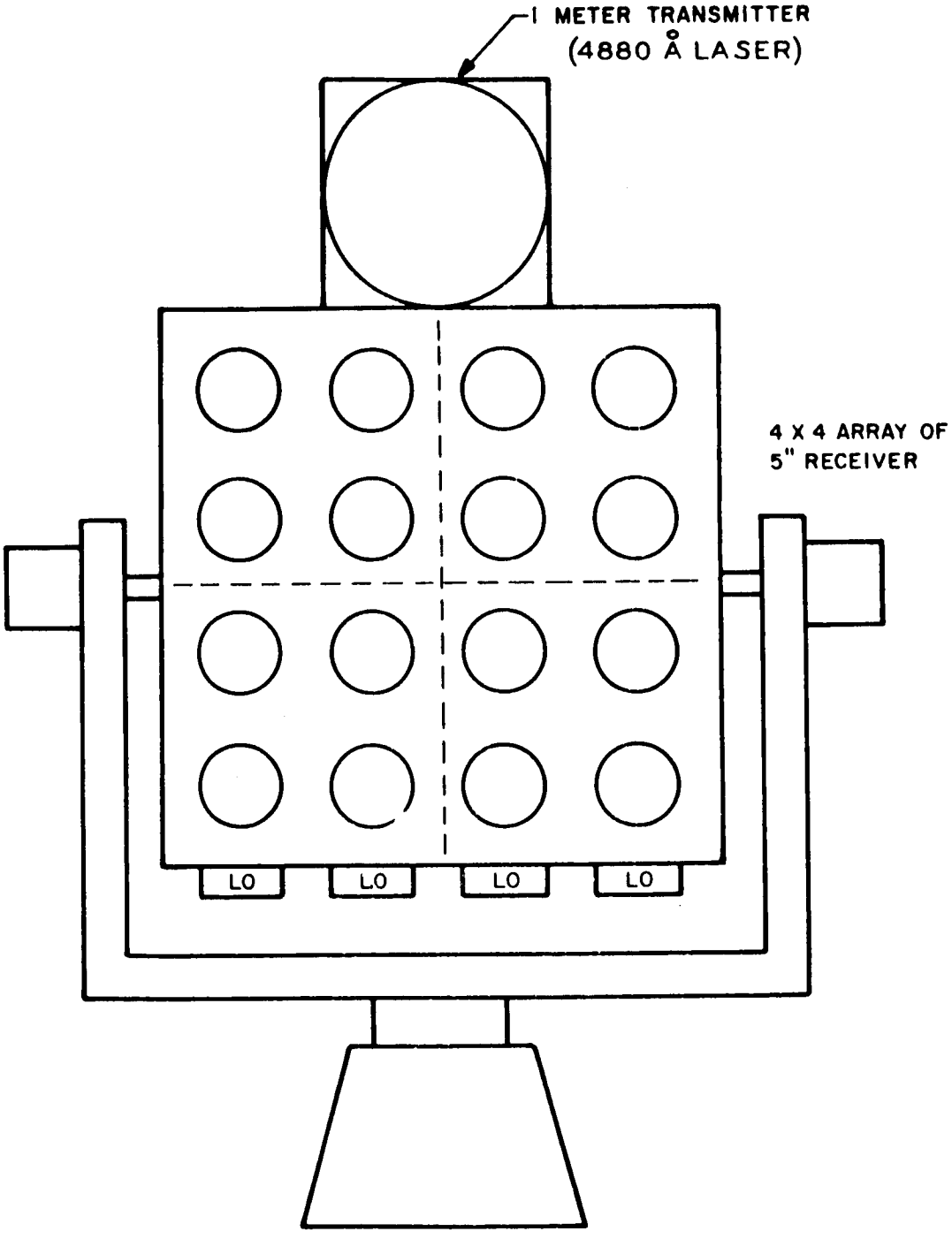

Figure 4.6.5.3-1 Earth Station Distributed Receiver-Tracker Array and Transmitter

The distributed array provides a dual capability in the pointing and tracking experiments. Angle tracking the incoming wave front is essentially aligning the optical axis of the tracker to the nearly plane wavefronts. This is essentially accomplished in a single 5" telescope and the array of telescopes serves to obtain a better spatial average by averaging the tracking data of the 16 telescopes. The second important function of the array is to evaluate the down coming beam position and thus the space vehicles tracking performance. This information is derived by a reconstruction of the beam profile taking into account the spatial and temporal fluctuations imparted by atmospheric turbulence. Beam profile measurements are accomplished by sampling the diagonal elements of the telescope matrix and estimating the spacecraft beam pointing error in an alt-azimuth reference. This information is utilized in the ground-to-space feed back loop which is closed around the point ahead beam deflector in the space vehicle.

4.6.5.3.2 Angle Tracking

A schematic of a single 5" telescope channel is shown in Figure 4.6.5.3-2. Light is collected by a 5" objective and is focussed at the apex of a tetrahedron which is shown in one plane for illustrative purposes. The positions at which the local oscillator signal is injected are shown on both sides of the axis for convenience. The azimuth error in angle tracking is obtained by differential measurements of the average laser power as it impinges on opposite pairs of the tetrahedron reflecting surface. The rms angular jitter for a five inch aperture is $\theta_{rms} = 1.75$ arc seconds for zero zenith angle and 2.08 arc seconds for 45° zenith angle. Assuming that the principal frequency components of fluctuations are below 10 cps, the smoothing due to the spatial averaging unit (See Figure 4.6.5.3-3) is

$$\theta_{sav} = \frac{\theta_{rms}}{\sqrt{n}} = \frac{1.75}{\sqrt{16}} = .44 \text{ arc second}$$

The additional smoothing can be obtained from the temporal averaging unit by sampling many points separated in time by much less than $1/B_n$ seconds (B_n = servo noise bandwidth, cps) over a period of time $t \gg \frac{1}{B_n}$ seconds. For a 5 second smoothing time

$$\theta_{tav} = \frac{\theta_{sav}}{\sqrt{2B_n t}} = \frac{.44}{\sqrt{2x10x5}} = .044 \widehat{\text{sec.}}$$

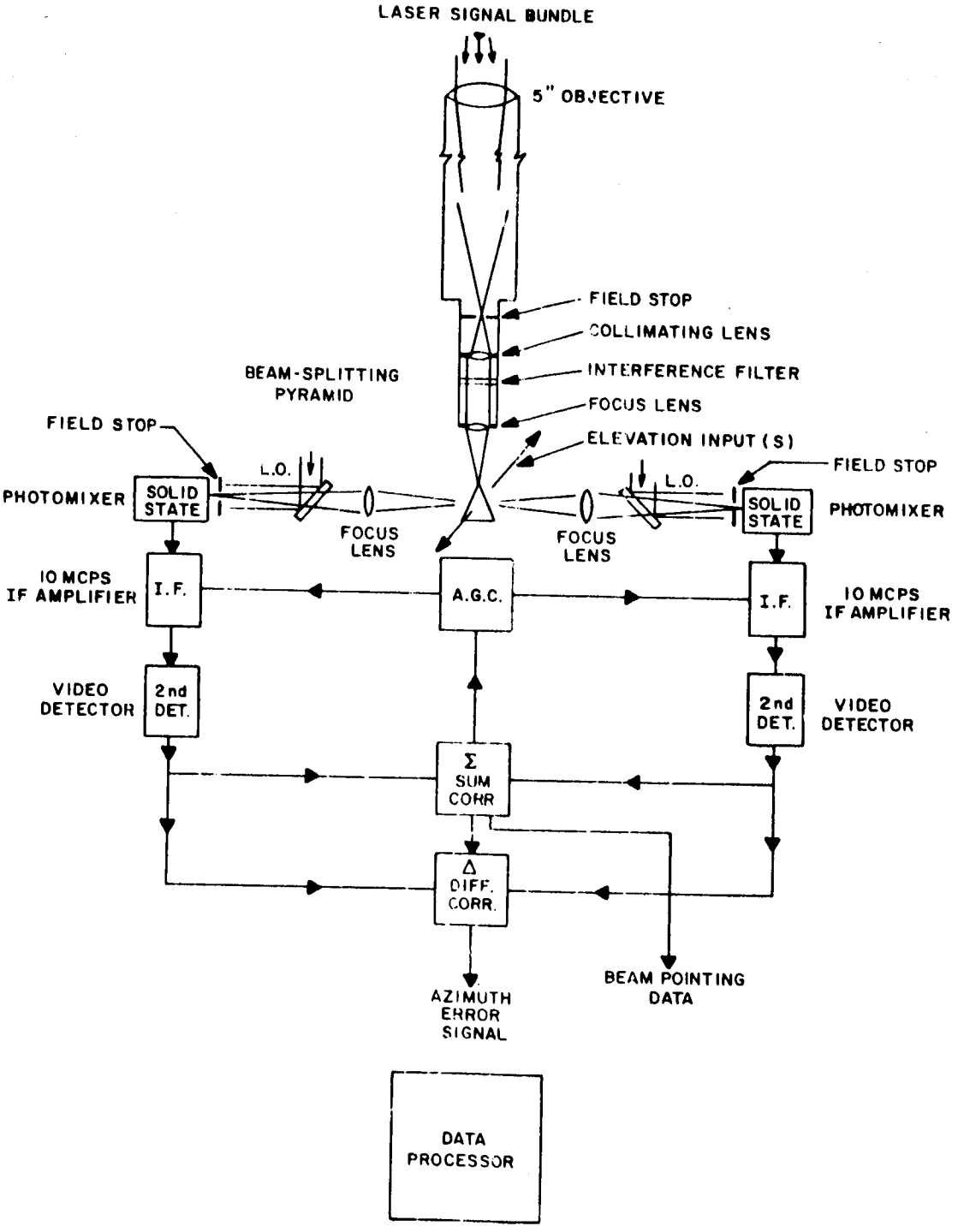

Figure 4.6.5.3-2 Single Channel Receiver-Tracker and Azimuth Error Channel

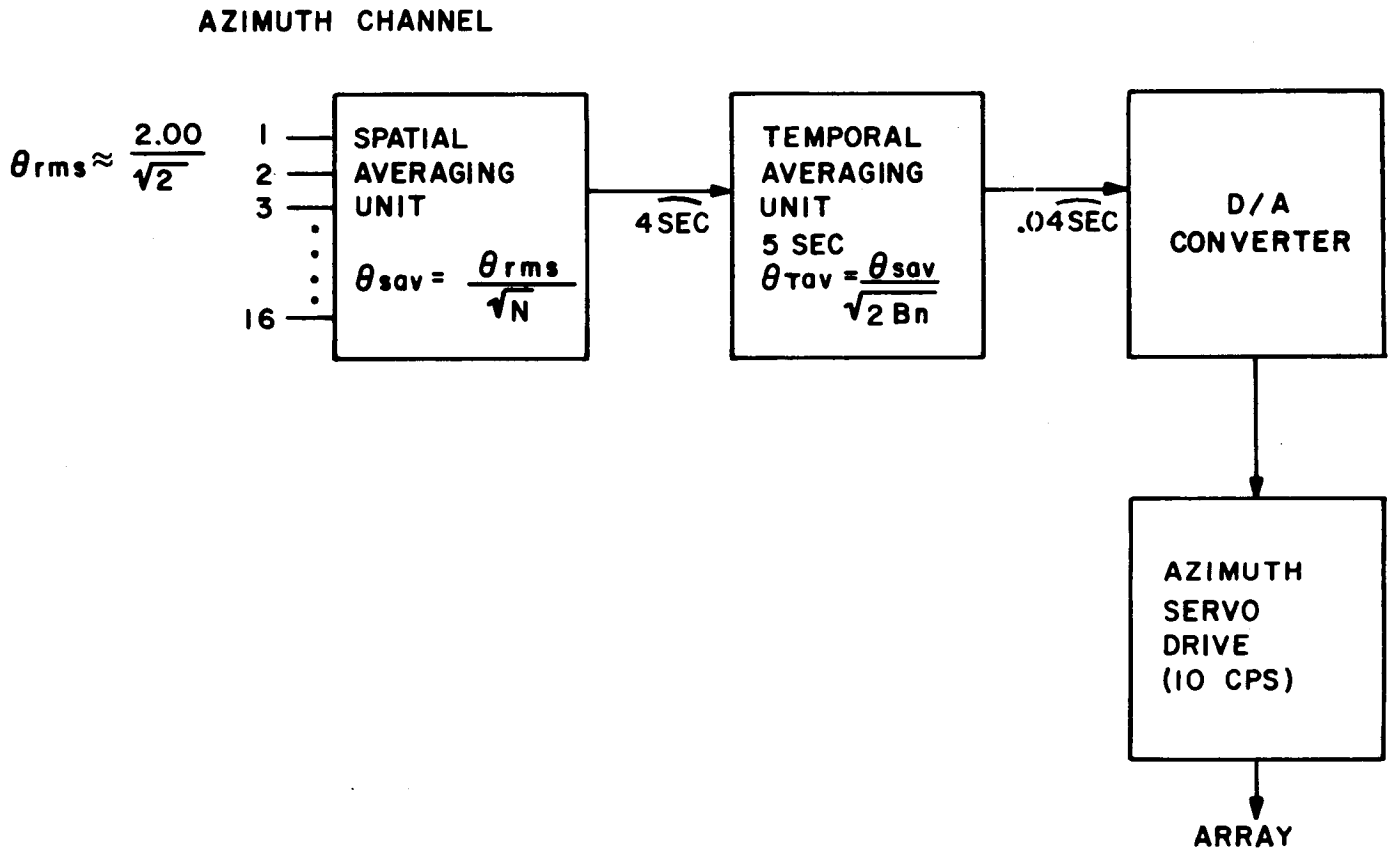

Figure 4.6.5.3-3 Angle Tracking

4.6.5.3.3 Earth Station Beam Pointing Sensitivity

The amplitude comparison detection technique provides error signal feedback to the space vehicle to correct its beam pointing operation. Since the Earth Station array cross-section intercepts only a small fraction of the space vehicle beam, it is clear that the error signals are small fractions of the impinging signal power. Nevertheless, the use of coherent detection and non-coherent video summation coupled with correlation data processing techniques provides adequate signal-to-noise ratios to permit differential amplitude comparison.

4.6.5.3.3.1 Pointing Control Analysis

A pointing analysis will be made for the 0.1 sec, 1 watt, 6328 Å laser-beam transmitted from synchronous orbit as it is received by a distributed array consisting of 16 telescopes, each of 5" diameter aperture.

In antenna practice, the one-way power antenna pattern is approximated by a Gaussian equation,

$$I = I_o e^{-(a^2\ \theta^2)}, \qquad (1)$$

Where θ is the angle measured from the center of the beam.

The constant a^2 is given by

$$a^2 = \frac{2.776}{\theta_B^{\ 2}}, \qquad (2)$$

where θ_B is the bandwidth measured between half-power points. This Gaussian distribution represents the Fraunhofer far-field region off diffraction theory, and is valid in the vicinity of the beam center.

The cosine distribution used in the latter analysis may be derived as follows:

For small values of the exponent,

$$e = 2.776\ \theta^2/\theta_R^{\ 2} \qquad = 1 - 2.776\ \frac{\theta^2}{\theta_B} =$$

$$1 - \frac{2.776}{2 \times 2.776}\left(\frac{(5.55)^{1/2}\ \theta\ )^2}{\theta_B}\right) \approx \cos\left(\sqrt{\frac{5.55}{\theta_B}}\ \theta\right) \qquad (3)$$

Therefore equation (1) becomes

$$I = I_o \cos\left(\sqrt{\frac{5.55}{\theta_B}}\ \theta\right) \qquad (4)$$

At $\theta = \theta_B/_2$, the angle is 1/2 $\sqrt{5.55}$ = 1.18 rad or 67.6°, whose cosine is 0.38, instead of 0.5. However, for the purposes of this analysis, the agreement is close enough to allow the simpler cosine distribution to be used (See Figure 4.6.5.3-4)

$$I = I_o \cos \theta_e = I_o \cos (K \theta_s)$$

where

θ_e = electrical angle $\leq \pm 60^o$ ($\pm \pi/3$ rad)

θ_s = space angle $\leq \pm 0.05$ sec ($\pm 2.5 \times 10^{-7}$ rad)

$$k = \frac{\theta_e}{\theta_s} = \frac{\pi/3}{2.5 \times 10^{-7}} = 0.42 \times 10^7$$

It will be assumed that this value of "k" is satisfactory near the center of the beam,

$\theta_e = \pm 12^o$, $\theta_s = \pm 0.01$ arc sec

The following analysis is done to determine the appropriate expressions for the slope of the beam intensity gradient vs. a function of spatial angle.

$$\frac{dI}{d\theta_s} = -k I_o \sin (k\theta_s) = -(0.42 \times 10^7) I_o \sin (12^o)$$

$$= -0.87 \times 10^6 I_o$$

$$\delta I \quad \frac{dI}{d\theta_s} \quad \theta_s = -k I_o \sin (k \theta_s) \delta \theta_s$$

$$= -0.87 \times 10^6 \quad I_o \quad \delta \theta_s$$

4.6.5.3.3.2 Sensitivity For Synchronous Orbit

The difference δI is the difference magnitude corresponding to the beam slope across half of the array whose width is δS = 1.5 ft

$$S = r \theta_s; \quad \frac{dS}{d\theta_s} = r;$$

$$\frac{dI}{d\theta_s} = \frac{dI}{dS} \quad \frac{dS}{d\theta_s} = r \quad \frac{dI}{dS}$$

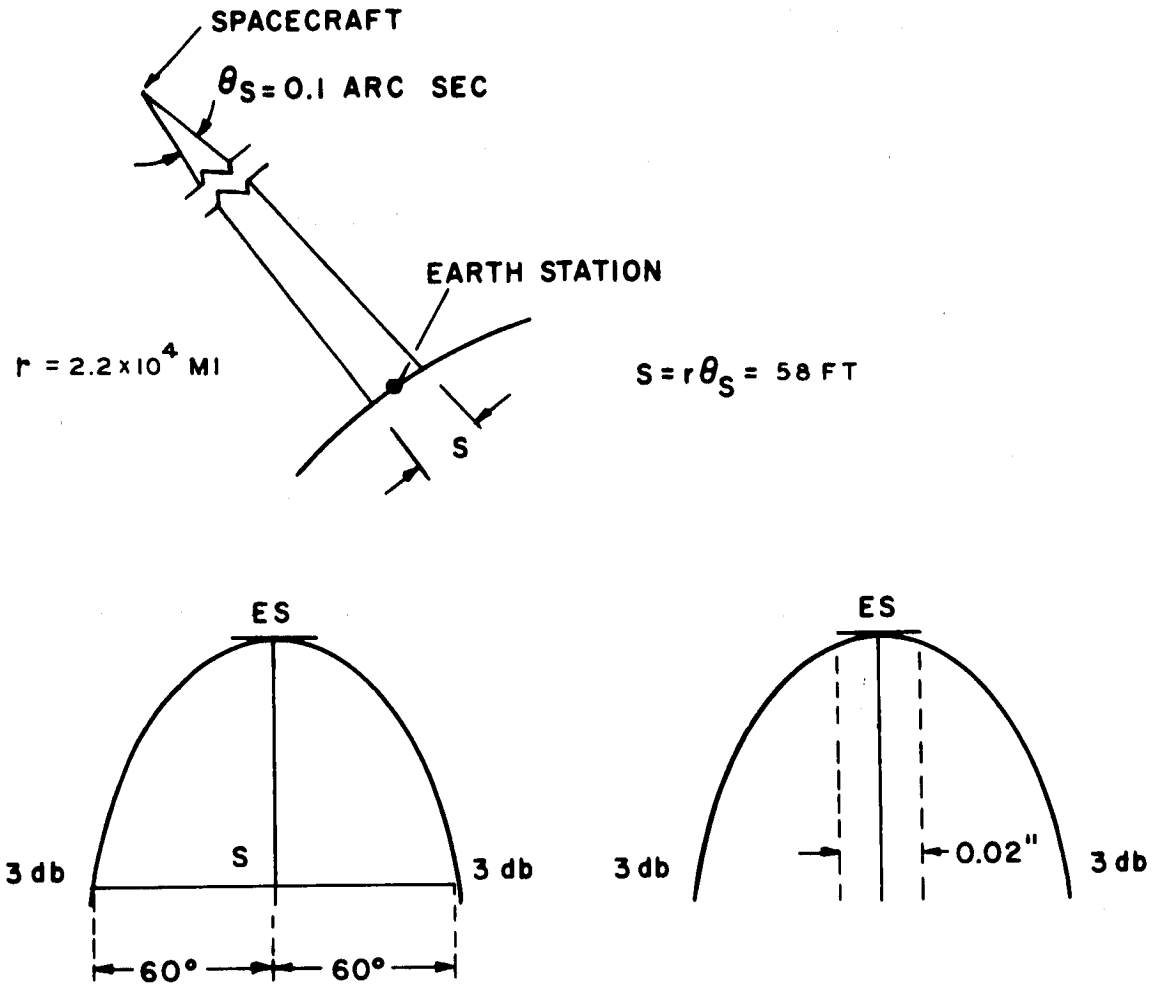

Figure 4.6.5.3-4 Earth Station Beam Pointing Sensitivity from Synchronous Orbit

$$\frac{dI}{dS} = \frac{1}{r}\,\frac{dI}{d\theta_s} \quad ; \quad \delta I \left(\frac{dI}{d\theta_s}\right)\left(\delta\theta_s\right) = \frac{(dI)}{dS} \qquad \delta S$$

For $r = 2.2 \times 10^4$ miles, a beam width of 0.1 sec subtends

$$S = 2.2 \times 10^4 \times 5.28 \times 10^3 \times 5.0 \times 10^{-7} \text{ rad} = 58 \text{ Ft.}$$

For $\delta S = 1.5$ Ft.

$$\delta\theta_s = \frac{1.5 \times 5 \times 10^{-7}}{58} = 1.28 \times 10^{-8} \text{ rad}$$

Therefore $\delta I = -0.87 \times 10^6 \text{ Io } (1.28 \times 10^{-8}) = -1.1 \times 10^{-2} \text{ Io}$

The mechanics of the measuring process are as follows:

Very small changes of beam intensity are stated as

$$\frac{\delta I}{I} = \frac{-k\, I_o \sin(k\theta_s)\ \delta\theta_s}{I_o \cos(k\theta_s)}$$

$$= -k \tan(k\,\theta_s)\ \delta\theta_s$$

$$\theta_s = \frac{1}{k}\tan^{-1}\left(\frac{-\delta I}{Ik\,\delta\theta_s}\right)$$

which is the required departure angle from boresight. For small departure angles, $\theta_e \leq \pm 30^\circ$ (10%) $k\theta_s \approx (k\theta_s)$

$$\frac{\delta I}{I} \approx -k^2\theta_s\delta\theta_s \text{ and } \theta_s{}^2 \cong -\frac{1}{k^2\delta\theta_s}\ \frac{(\delta I)}{I}$$

$(\theta_s \leq -30^\circ)$

The change δI with respect to θ_s is

$$\frac{d}{d\theta_s}\ (\delta I) = \frac{d}{d\theta_s}\left(\frac{dI}{d\theta_s}\ \delta\theta_s\right) = k^2 Io \cos(k\theta_s)\,\delta\ \theta_s$$

$$= (.42 \times 10^7)^2\ (\cos 12^\circ \text{ el.})\ (1.28 \times 10^{-8})\ Io$$

$$= (.176 \times 10^{14}) \quad (.978) \quad (1.28 \times 10^{-8})\ I_o$$

$$= 2.2 \times 10^{5}\ I_o$$

$$\Delta(\delta I) = \frac{d}{d\theta_s} \quad (\delta I)\ \Delta\theta_s$$

let $\Delta(\delta I) = 1.1 \times 10^{-2}\ I_o$

Therefore

$$= 2.2 \times 10^{5}\ I_o \quad \Delta\theta_s = 1.1 \times 10^{-2}\ Io$$

$$\Delta\theta_s = \frac{1.1 \times 10^{-2}}{2.2 \times 10^{5}} = 5 \times 10^{-8}$$

$$= .01 \text{ arc sec}$$

Hence a 0.01 arc second beam displacement at θ_s = 0.01 arc second doubles the magnitude difference.

4.6.5.3.3.3 Sensitivity For Deep Space

For range r = 10^8 miles = 6×10^{11} ft., the beam width θ_s = 0.1 arc-sec subtends

$$s = 6 \times 10^{11} \times 5 \times 10^{-7} \text{ rad} = 3 \times 10^{5} \text{ ft.}$$

The half array width is δs = 3 ft.

$$\delta\theta_s = \frac{3}{6 \times 10^{11}} = 0.5 \times 10^{-11} \text{ rad}$$

Therefore:

$$\delta I = 0.87 \times 10^{6}\ I_o\ (0.5 \times 10^{-11})$$

$$= 0.435 \times 10^{-5}\ I_o$$

The amplitude sensitivity values for the deep space and synchronous orbit cases to be used for beam pointing noise analysis are restated below:

$$\delta I = 0.435 \times 10^{-5}\ I_o \quad \text{(Deep Space)}$$

and

$$\delta I = 1.1 \times 10^{-2}\ I_o \quad \text{(Synchronous Orbit)}$$

4.6.5.3.4 Earth Station Beam Pointing Noise Analysis

The beam pointing measurement described in subsection 4.6.4.1.3 is subject to error due to the noise with which the incoming signal must compete; reduction of this error is accomplished by means of temporal integration. Beam pointing error of 0.01 arc-second (1/10 of a beam width) can be measured to 58 percent accuracy (or about 0.006 arc seconds) at a vehicle range of 10^8 mi. by allowing the signal to integrate for five seconds.

4.6.5.3.4.1 Error Integration for Deep Space

The nature of the time integration process may be deduced by a photon counting process. Each five inch telescope collects 3.8×10^{-13} watt for a five megacycle video bandwidth. The half array is composed of 50 telescopes and the total power is

$$P_{50} = 19 \times 10^{-12} \text{ watt}$$

For $\lambda = 6328$ Å $\nu = 4.75 \times 10^{14}$ cps, the energy per photon is $h\nu = 3.14 \times 10^{-19}$ joule. The period corresponding to a single modulation cycle is

$$T_F = \frac{1}{f} = \frac{1}{5 \times 10^6} = 0.2 \times 10^{-6} \text{ sec}$$

The number of photons received per telescope in one period is

$$E_{(T_F)} = \frac{3.8 \times 10^{-13} \times 0.2 \times 10^{-6}}{3.14 \times 10^{-19}} = 0.242 \quad h\nu/\text{cycle}$$

and in 1 second

$$E_{(1 \text{ sec})} = 0.242 \times 5 \times 10^6 = 1.21 \times 10^6 \quad h\nu/\text{sec}$$

For 50 telescopes in the half array

$$E_{(50 \text{ sec})} = 50 \times 1.21 \times 10^6 = 6.05 \times 10^7 \ h\nu/\text{sec}$$

The quantum noise corresponding to this signal is

$$N_{(50 \text{ sec})} = \sqrt{E_{(50 \text{ sec})}} = \sqrt{6.05 \times 10^7} = 7.79 \times 10^3 \ h\nu/\text{sec}$$

with a relative error

$$\epsilon(50\ \text{sec})\ \frac{N}{E}\ (50\ \text{sec}) = \frac{1}{\sqrt{E(50,\text{sec})}}$$

$$1.28 \times 10^{-4} \cong 0.013 \text{ percent}$$

Hence the noise error is $N = 1.28 \times 10^{-4}$ Io per 3 feet (half array width) compared to the required value derived in section 4.6.5.3.3.3 given as

$$\delta I = 4.35 \times 10^{-6} \text{ Io per 3 feet}$$

For the half array, $\Delta S = 3$ ft, a $\delta I = 4.35 \times 10^{-6}$ Io corresponds to 1 part in 230,000. Hence, we define the receit of 230,000 photons as one measurement interval, Δm. In one second, there are

$$\eta \Delta m = \frac{E_{(50,\text{sec})}}{2.30 \times 10^5} = \frac{6.05 \times 10^7}{2.30 \times 10^5} = 264 \Delta m \text{ interval/sec}$$

The time for each Δ m interval is

$$\tau = \frac{1}{n\Delta m} = \frac{1}{0.264 \times 10^3 \Delta m} = 3.79 \times 10^{-3} \text{ sec}/\Delta m$$

The relative error on the basis of integration for a Δ m period is

$$\epsilon' = \epsilon \tau^{1/2} = 1.28 \times 10^{-4} \times (3.79 \times 10^{-3})^{1/2} \quad 7.88 \times 10^{-6}$$

which shows that the integration period of 1 second is sufficient to detect the required difference, by a factor of $4.35/7.88 = 0.55$

In other words, a signal-to-noise ratio of unity (1 noise electron for every photoelectron) for the ΔI measurement is achieved about one time every 2 seconds.

Increasing the integration period to 5 seconds results in the following accuracy improvement.

$$E_{(50\ ,\ 5\ \text{sec})} = 5 \times 6.05 \times 10^7 = 3.25 \times 10^8 \text{ h } \nu/\text{sec}$$

$$N_{(50\ ,\ 5\ \text{sec})} = \sqrt{3.25 \times 10^8} = 1.8 \times 10^4 \text{ h } \nu/\text{sec}$$

$$\epsilon\ (50\ ,\ 5\ \text{sec}) = \frac{1}{N_{(50\ \ 5\ \text{sec})}} = \frac{1}{1.8 \times 10^{4}} = 0.55 \times 10^{-4}$$

$$\eta \Delta m\ (5\ \text{secs},) \quad \frac{E_{(50\ ,\ 5\ \text{sec})}}{2.30 \times 10^{5}} = \frac{3.25 \times 10^{8}}{2.30 \times 10^{5}} = 1.42 \times 10^{3}\ \Delta\ m_{\text{interval/5sec}}$$

The relative error is now

$$\epsilon'(5\ \text{sec}) = \frac{E_{(50\ ,\ 5\ \text{sec})}}{\sqrt{N_{\Delta m}\ (5\ \text{sec})}} = \frac{0.55 \times 10^{-4}}{\sqrt{1.42 \times 10^{3}}} = \frac{0.55 \times 10^{-4}}{37.7}$$

$$= 1.46 \times 10^{-6}$$

The error reduction factor now becomes

$$F = \frac{4.35 \times 10^{-6}}{1.46 \times 10^{-6}} = 3\ \text{(signal-to-noise = I for mean)}$$

Hence the measurement is accomplished with an accuracy of

$$\left(\sqrt{F}\right)^{-1} = \left(\sqrt{3}\right)^{-1} = \left(1.73\right)^{-1} \qquad \text{or } 58\%$$

That is a 0.1 beam width displacement is measurable with an accuracy of about 58%. The presence of other system losses and noise sources may decrease the accuracy, but what has been shown is that a sensitivity of a small fraction of a beam width detection can theoretically be achieved.

4.6.5.3.4.2 Error Integration for Synchronous Orbit

For the deep space simulation performed at synchronous altitude the total coherent power into the half array which is composed of 8 telescopes is to be maintained at the expected value from deep space; i.e.,

$$P_8 = 19 \times 10^{-12}\ \text{watt}$$

The integration time is to be determined. For the half array, $\Delta S = 1.5$ ft, a $\delta I = 1.1 \times 10^{-2}$ Io corresponds to 1 part in 90. Thus the receipt of 90 photons constitutes one measurement interval, Δ m in this instance.

The number of Δm intervals in one second is

$$\eta \Delta m = \frac{E\ (8\ \text{sec})}{\delta I} = \frac{6.05 \times 10^{7}}{9.0 \times 10^{1}} = 6.7 \times 10^{5}/\text{sec}$$

The relative error E can be calculated from

$$\epsilon' = E\,T^{1/2} \qquad \text{where } T^{1/2} = \frac{1}{\sqrt{n\Delta m}}$$

From the previous deep space calculation

$$\epsilon' = 7.88 \times 10^{-6}$$

$$E = \frac{\epsilon'}{T^{1/2}} = 7.88 \times 10^{-6} \times \sqrt{.67 \times 10^{6}}$$

$$= 7.88 \times 10^{-6} \times .82 \times 10^{3}$$

$$= 6.45 \times 10^{-3}$$

The no. of photons needed for the measurement is

$$N = \frac{1}{E^2} = \frac{1}{42 \times 10^{-6}} = 240{,}000$$

The number of photons per sec was given as

$$6.05 \times 10^{7}\ h\upsilon/\text{sec}$$

The integration time is thus

$$T = \frac{2.4 \times 10^{5}}{6.05 \times 10^{7}} = .38 \times 10^{-2}\ \text{sec}$$

4.6.5.4 Beam Pointing Measurement by Detection of Conically Scanned Laser Beam

Lobe detection of a conically scanned laser beam by means of a single photon bucket can be employed in the beam pointing measurement for the Space - to - Ground - to - Space feedback loop. This technique was developed for tracking radars whereby the transmitting antenna was mechanically nutated about a central axis and the target (usually a moving one) was tracked by means of

synchronous detection of the return beam.[1] When the antenna is on target the line of sight to the target and rotation axis coincide and the null condition is obtained. For non-coincidence of the rotation axis and target line of sight an AM modulated signal is generated at the conical scan frequency. A directly analagous scan method can be implemented with a spacecraft laser and ground receiver in the form of a large optically segmented telescope or "photon bucket." In this instance, the measurement is not made with a co-located transmitter and receiver since the target is the earth receiver which will detect the conically scanned laser beam. The conical scan can be produced by a rotating optical wedge placed in front of the laser transmitter. The cone or "squint" angle will be a function of the wedge angle and the refractive index of the rotating optical wedge.

The antenna pattern of the laser beam is approximated by the Gaussion function

$$G(t) = G_o \exp(-a^2\theta^2)$$

where:

θ = angle between antenna beam axis and target axis

G_o = Value of $G(\theta)$ at $t = 0$

a^2 = constant = $2.776/\theta_B^2$

where θ_B = angular width of antenna pattern

Mathematical analysis of radar conical beam scanning was given by Skolnik[1] and Develet [2]. An equation was derived by Develet which gives the rms angular noise jitter for a coherent detection system as follows:

(1) Skolnik, Merrill I. "Introduction to Radar Systems" McGraw-Hill, 1962, pp 166-175.

(2) Develet, Jean A. Jr., Thermal-Noise errors in Simultaneous Loping and coincal-Scan angle tracking systems, IRE Transaction on space Electronic and Telemetry, June 1961.

$$\theta^2_{rms} = \left\{ \frac{5\alpha^2}{DB_c \ln 2 \ln 10 \sum_{K=0}^{N} \pi J_o (\phi_K)^2} \right\} \left(\frac{\phi B_N}{S} \right) \text{ radian}^2$$

where:

α = 3 db width of beam

DB_c = number of decibles below maximum the beam crosses the boresight axis

$\phi = KT_o (F-1)$ where $KT_o = 10^{-20.4}$ watts/cps

F = noise figure of the preamplifier system

ϕ_K = The K modulation indeces of the information phase or frequency modulation in radians

B_n = servo noise bandwidth (cps)

S = Total received power on boresight consistent with ϕ.

The above relationship which was derived for radar applications will need little modification in order to apply to the laser conical scan detection. The ϕ term, however, is the thermal antenna noise, which for the laser application would be dwarfed by the shot noise arising from the photon flux from signal and background. Thus, a modification of the analysis would primarily be one of properly defining the noise source.

The implication of coherent detection in the context of beam scanning is different than that as discussed for the heterodyne detection case for the distributed telescope array.

Since the beam is scanned in a cone, the scan frequency can be used for synchronous phase detection with the a prior-knowledge of frequency and phase at the earth station. If the laser beam is modulated at a carrier frequency in the IF spectrum, a detection process will needed in order to remove the carrier frequency. This can be accomplished by either a square law detector or a preliminary stage of coherent detection in the IF spectral region. Coherent detection at the IF and scan frequencies will improve signal to noise but will have no effect on reducing the background noise in the manner of laser heterodyning which effectively restricts the optical bandwidth.

The general implementation of the conically scanned beam is shown in Figure 4.6.5.4-1. The phase and frequency of the reference generator must be regularly updated by the microwave downlink from the spacecraft. Beam mispointing in the form of altitude and azimuth angles are relayed up to the spacecraft thereby closing the overall space-to-ground-to-space feedback loop. A numerical analysis of this type of system will be undertaken in the next OTES work phase.

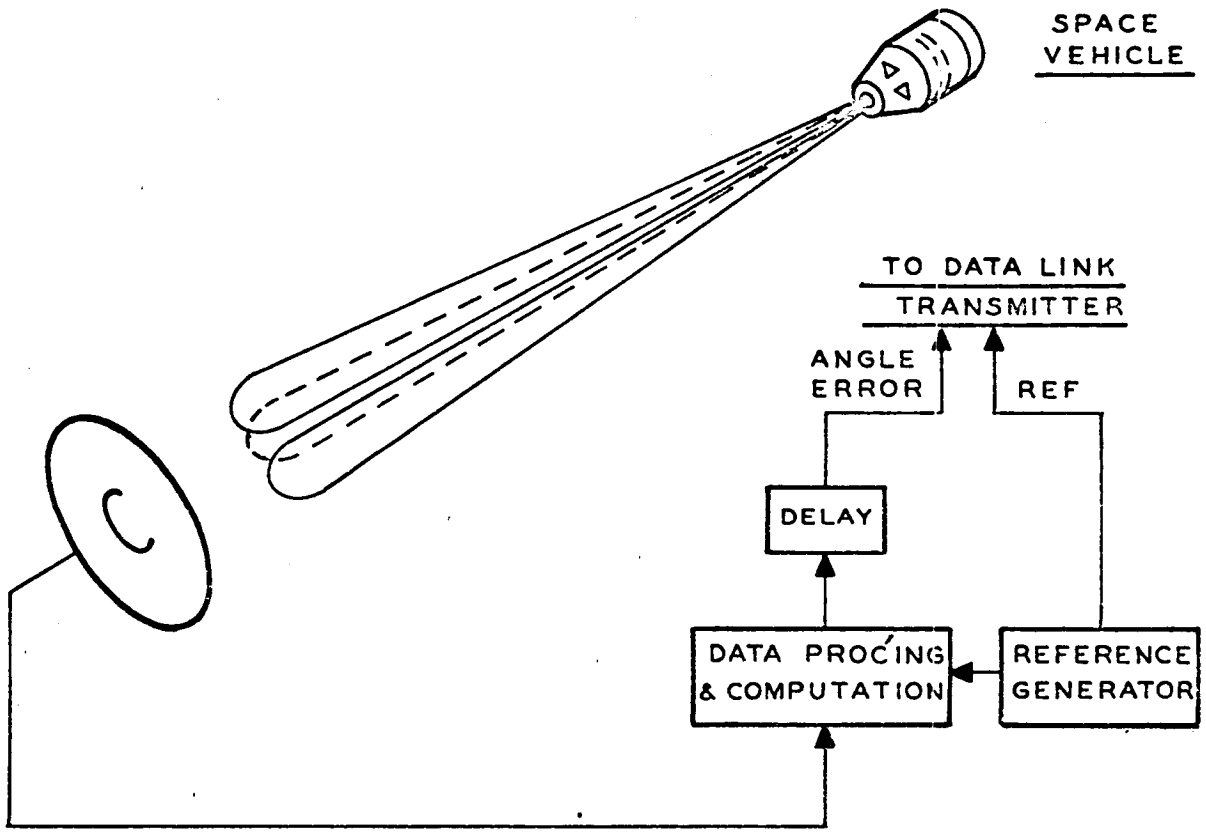

Figure 4.6.5.4-1 Single "Photon Bucket" and Conically Scanned Beam Scheme

4.7 TRANSFER TRACKING FROM ONE GROUND STATION TO ANOTHER

4.7.1 Summary

A deep space vehicle in optical communication with earth must possess the capability of transferring track between earth stations in order to maintain continuity of operation despite cloud overcast and the Earth's rotation. The acquisition and tracking between a spacecraft and a ground complex (beacon transmitter and ground receiver), which naturally precedes transfer tracking, is discussed in subsection 4.5 and 4.6. A chain of earth stations must be established and so located that a minimum of two stations with reasonable zenith angles and high probability of clear weather will have a direct line of sight to the vehicle. Meaningful experimentation with precision tracking of a ground beacon can only be conducted from altitudes above 2000 miles. The transfer tracking demonstration is predicated upon accurate tracking, and consequently also requires such space testing.

The station spacing required to demonstrate the 11 arc-second tracking transfer from synchronous altitude - which is the altitude proposed for Precision Tracking and Point Ahead experiment - is one mile, however, a four mile separation is required for the POINT AHEAD AND SPACE-TO-GROUND-TO-SPACE LOOP CLOSURE experiment. Consequently the transfer will be performed at a four mile separation. Both stations at a 4 mile separation will have co-located receivers and transmitters for the tracking transfer demonstration. The function is nearly identical to the "point-ahead" except that the transfer commands will be given to the coarse-fine beam deflection control system. The transit time delays of 8 minutes at 1 AU distance must be simulated for this experiment.

4.7.2 Experiment Objective

The purpose of this experiment is to investigate transfer tracking between earth stations and a spaceborne laser telescope simulating the conditions of a deep space probe (Mars fly-by).

4.7.3 Experiment Justification

4.7.3.1 Contribution and Need

A deep-space vehicle in optical communication with earth must possess the capability of transferring track between earth stations in order to maintain continuity of operation despite cloud overcast and Earth's rotation. Hand-over operation must be initiated when meteorological conditions (clouds) threaten to interrupt communication between the station presently receiving and the spacecraft. On a regular, cyclic basis, hand-over operation must be conducted when the zenith angle from the station presently receiving becomes

excessively high. Increasing zenith angle aggravates the effects of atmospheric attenuation and fluctuation, as well as the steady-state part of the deflection. (1) (2)

4.7.3.2 Need For Space Testing

Investigation of laser communication system and hand-over performance affected by atmospheric degradations, vehicle pertubations, and point-ahead requirements, indicates the need for space testing. As discussed in some detail in the Precision Tracking of a Ground Beacon experiment, accurate tracking and meaningful experimentation with the tracker can be conducted only from altitudes above 2000 miles. See Subsection 4.5.3.2. The tracking transfer demonstration is predicated upon accurate tracking, and consequently also requires such space testing.

4.7.3.3 Feasibility

The equipment requirements for this experiment over and above that which is required for the PRECISION TRACKING and the POINT AHEAD experiments consists of a microwave link and ground based computational facilities. These are associated with the navigation and information transfer requirements of transfer tracking and present no foreseeable problems beyond the state-of-the-art.

4.7.4 Implementation

4.7.4.1 Experiment Design

Adequate hand-over techniques must be developed before wide band-width laser communications can be utilized for either earth orbit or deep space vehicles which require uninterrupted communication. Certainly a function required for deep-space optical communication must be proved out before actually undertaking such a mission. In order to make this possible, a chain of earth stations must be established, so located that a minimum of two, and preferably more stations will have direct line of sight to the vehicle, with reasonable zenith angles and high probability of clear weather.

---

(1) A. Wallace, Study of Laser Beam Pointing Problems, First Bi-monthly technical Report No. KIC-RD-000162-1, Kollsman Instrument Corporation, Elmhurst, N.Y., 15 October, 1964, Tables VIII and X.

(2) F.V. McCanless, "A Systems Approach to Star Trackers", IEEE Transactions on Aerospace and Navigational Electronics, Vol. ANE 10, Sept., 1963, No. 3, p. 184.

One study,[3] resulted in the recommendation for using a total of eight stations around the globe, with probability of clear reception greater than 90 percent for the full rotation of the earth (if one site location in Red China is assumed to be accessible), and greater than 95 percent for a very large portion of the diurnal cycle. This study is, however, based on communication down to zenith angles of 70 percent which may be excessive for high-quality optical contact; it may be necessary to provide more stations to reduce required elevation coverage. For the sites listed in Ref. (3), the largest spacing is that between sites at 19°N - 156°W and 20°S - 113°E, a chord length of some 5200 statute miles, which may subtend as much as 11 arc-seconds at vehicle range of 1 AU.

In the realistic deep-space case, such methods as characteristic codes for the two Earth Stations may be used, to allow the vehicle to differentiate between them; this may not be necessary, if the "new" station begins transmission the instant at which the "old" station stops. In any event, the active field of view of the telescope is likely to be larger than the maximum of 11 arc-seconds angular separation between Earth Stations, so that there should be no difficulty in tracking on to the new station. The process of hand-over can be aided by commanding the space vehicle tracker to slew over to the new station's coordinates. The appropriate angle commands can be computed on Earth, using the known coordinate frame of the vehicle attitude with respect to the stellar coordinates and earth line of sight. Both the coarse and the fine portions of the vehicle tracking system may be involved in this operation. Presumably, the fine tracking system operates reasonably close to the center of its range; a relatively large step, such as 11 seconds, should preferably be carried out by the telescope gimballing system to prevent the fine beam deflector from running off the edge of its range. Although the state of the fine beam deflectors may very well be known at the earth station, the relative staleness of this information (due to the telemetering space delay) is likely to be comparable with the spectrum of beam deflector motion.

The point-ahead angle requirement may change by as much as 0.7 arc second or several beamwidths, between two Earth Stations. Corresponding commands must also be computed and telemetered to the vehicle, so that the transmitter beam can be laid on to the new station with a minimum of delay. The timing of the tracking and pointing transfer commands should be such that switchover of transmission from the old to the new station will occur immediately after the tracking transfer instructions have been issued, thus allowing the vehicle to track the new station. Reception must, however, continue at the old station for one transmission delay interval. The transmitter telescope

---

(3) Kenneth L. Brinkman et al, Study on Optical Communication From Deep Space, Hughes Aircraft Company, Aerospace Group, Interim Progress Report, No. SSD 3166 R, NASA Document No. N64-16770.

at the new station must be directed by data radioed over from the old station and corrected for the angular difference. The new station's receiver, which will not begin operation until one transmission delay later, can also be slewed into position upon the basis of such data.

On the basis of the protracted tracking and angle smoothing operation preceding the optical communication process, and the refined tracking permitted by it, the angular computations required for the above should certainly be feasible. The exact form of the computations, as well as that of the commands remains to be investigated.

It is anticipated that the realistic spatial situation of the lead angle requirement in the point ahead demonstration, using a synchronous satellite requires a four mile separation of receiver and transmitter stations. Ordinarily, the station spacing required to demonstrate tracking transfer from synchronous altitude would be one mile. Since the stations required for the point ahead demonstration would be available, these stations can be used to demonstrate tracking transfer. Obviously, a system that can transfer tracking between stations four miles apart will more than satisfy the normal requirement of one mile separation. In the demonstration, one station would normally receive and the other transmit, with necessary data communication between the two for transmitter antenna direction. Realistic space transmission delay can be simulated by means of tape recorders.

The synchronous satellite should be equipped with an optical receiving-tracking system and transmitter (at two different wavelengths). The satellite-based command-control receiving system (microwave) should include provisions for handling tracking-offset commands, as must the tracking and pointing system.

Two separate earth-stations are required, each capable of transmission at the satellite receiver frequency, receiving at satellite transmitter frequency, as well as containing beam-pointing error measurement apparatus. Computing facilities must be available for the calculation of tracking angle and lead angle offset commands. Microwave link facilities must include provisions for proper encoding of these commands to the space vehicle. Tape recorder delay provisions must exist.

4.7.4.2 Operational Procedure

In view of the extremely tight tracking requirements and the small angular increments used in tracking and pointing transfer, man is not likely to be of direct assistance except with peripheral functions such as atmosphere monitoring. The operational procedures may be outlined by the following sequence of tasks:

a. Compute the required angular offsets x and y in the line of sight referred to the spacecraft in order to transfer the tracking LOS from earth station B to earth station A.

b. Transmit commands to satellite to offset telescope tracker and lead angle deflectors by amounts computed under a.

c. Simultaneously command earth station transmitter B to start transmitting to satellite, using computed lead angle and tracking information still available to it (since B has been receiving up until now).

d. Receiver drive at A to be prepointed toward vehicle, to be ready to receive communication one space delay interval later.